Nearshore Surficial Geology, Heavy Minerals and Geochemistry, Northern Juan de Fuca Strait

by

Caleen Elaine Kilby
B.Sc., University of Alberta, 1977

A Thesis Submitted in Partial Fulfillment of the Requirements for the Degree of

MASTER OF SCIENCE

in the Department of Geography

We accept this thesis as conforming to the required standard

[redacted]
Dr. B.D. Bornhold, Supervisor (Department of Geography)

[redacted]
Dr. E. Van der Flier-Keller, Co-Supervisor (Dept. of Geog.)

[redacted]
Dr. L.A. Hobson, Outside Member (Department of Biology)

[redacted]
Dr. J.V. Barrie, Additional Member (Department of Geography)

[redacted]
Dr. P. Bobrowsky, External Examiner (B.C. Geol. Survey)

Supervisor: Dr. Brian D. Bornhold

ABSTRACT

The nearshore surficial geology, heavy mineral distribution and geochemistry of northern Juan de Fuca Strait is examined in this study. Surficial sediments were mapped using analyses of 150 offshore samples along with 382 km of geophysical records including sidescan sonar and high-resolution seismic profiling. Grain-size and geochemical analyses were performed on sediment less than 2 mm in size. Heavy mineral separations and heavy mineral identification were performed on the sand fraction of selected samples. Beach and river samples were collected and analysed for heavy mineral content and to trace mineral provenance.

Seabed surface samples reveal sediments which are texturally and mineralogically immature. A series of shallow (above 30 m depth) nearshore terraces are covered with a thin veneer (few metres or less) of relict glacial gravel and boulders along with medium to fine sand. Below approximately 80 m depth a muddy sand veneer covers a sediment wedge which thickens towards the centre of the strait. Recent sediments are derived from reworked underlying and adjacent glacial material, erosion of the coastal sandstone facies of the Carmanah Group, and river influx reflecting the adjacent terrigenous lithologies. Sediments are subsequently winnowed and reworked into

bedforms such as flow-transverse dunes and oscillation ripples.

Comparatively high amounts of heavy minerals, averaging 7%, are found in the sand fraction of the sediments. These concentrations are over twice the levels found in sands of Barkley Sound and five times higher than in sands of the continental shelf northwest of the study area. Heavy minerals consist primarily of amphiboles (hornblende), epidote and lithic fragments. The Metchosin Igneous Complex is the most likely source of the heavy minerals. Magnetite/ilmenite are the predominant opaque minerals.

Trace metals show low background levels in the surface sediments in both mud and sand fractions in the offshore and beach sands. Only Ti shows significantly high background levels (0.7%). Enriched Cu, Fe, Mn, V, Ti and Cr values are in evidence between China Beach and Sheringham Point. Between these two points a small nearshore heavy mineral placer is identified along Sandcut Beach extending to at least 800 m from shore. The placer has heavy mineral concentrations from 15% up to 45%, and enriched Ti values from 0.75% to as high as 1.4%. Source of the placer is believed to be from former mine tailings dumped at, or below tide-water. Formation of shallow marine or beach placers

along the northern strait are most likely limited due to mineral and textural immaturity of the sediments. However, locally beaches may experience sufficient hydraulic reworking and seasonal recycling to create heavy mineral placers.

[redacted]

Dr. B.D. Bornhold, Supervisor (Department of Geography)

[redacted]

Dr. E. Van der Flier-Keller, Co-Supervisor (Dept. of Geog.)

[redacted]

Dr. L.A. Hobson, Outside Member (Department of Biology)

[redacted]

Dr. J.V. Barrie, Additional Member (Department of Geography)

[redacted]

Dr. P. Bobrowsky, External Examiner (B.C. Geol. Survey)

TABLE OF CONTENTS

LIST OF TABLES

LIST OF FIGURES

LIST OF PLATES

ACKNOWLEDGEMENTS

The author is grateful to Dr. Brian Bornhold for his guidance and criticism throughout this study and to Drs. Vaughn Barrie and Eileen Van der Flier-Keller for their advice and suggestions. The author is indebted to Dr. Chris Yorath and Mr. Ralph Currie for their friendly discussions and their availability for numerous consultations. Thanks are extended to the staff at Pacific Geoscience Centre and in particular to T.Forbes, T. Hamilton, B. Sawyer, K. Conway, G. L'Esperance and C. Spindler. Thanks are also extended to P. Matysek for his helpful suggestions.

The author would like to thank the crews of the CSS *Parizeau* (July 1989) and CSS *Tully* (February 1988, March 1989) for their assistance at sea. Laboratory assistance supplied by L. Sheehan, and field assistance supplied by Dr. V. Preto and N. Carawan is gratefully acknowledged. The Geological Survey of Canada paid the author's salary during the summers of 1988 to 1990, other financial support being supplied by (1) the University of Victoria in the form of graduate grants, (2) the National Science and Engineering Research Council in the form of a grant to Dr. Bornhold and (3) the British Columbia Geological Survey Branch in the form of a research grant to Dr. Van der Flier-Keller.

The author is deeply grateful for the assistance, advice and endurance of W. Kilby and S. Kilby throughout this study.

I. Introduction

Today's ever-growing demands on land use suggest there will be a greater focus on the offshore for exploitation of resources in the future. Among these resources are sand for beach maintenance, building and roadway aggregate, and placer materials as a source of metals.

This study describes the distribution and texture of materials on the seafloor in the nearshore areas of northern Juan de Fuca Strait. Observed bedforms and other seafloor features are described. Geochemistry, heavy mineral concentrations and mineralogy are considered in an initial effort to evaluate the potential of nearshore placer formation along the northern strait and to determine sediment provenance. This study provides a framework upon which decisions for further studies may be made, particularly the viability of the area for future placer evaluation.

In addition to providing information about mineral resources, studies of nearshore sediments contribute valuable information for environmental, ecological and engineering work. An increase in the population of the southwestern coast of Vancouver Island, along with increased marine traffic in Juan de Fuca Strait, provide compelling reasons to acquire better knowledge of the sediments of the coastal area of the northern strait.

A knowledge of the seabed sediments, their texture and

thickness, is necessary to evaluate the environmental consequences of oil spills or pollution due to contamination of nearshore waters by urban or industrial waste. The nature of the sediments and the coastal energy regime will determine the degree of environmental damage which may be incurred and the ability of an area to recover from such events.

The sediments which cover the continental shelf, and their stability, are important factors in the variability and abundance of marine food resources. In addition, recreational uses of the nearshore waters and beaches, construction and channel maintenance all require a knowledge of the coastal substrate.

1. Overview of the Study

This study examines the nearshore surficial geology and heavy mineral deposits of northern Juan de Fuca Strait between Sooke Bay and San Juan Point. This includes the area from the beach seaward to the edge of the prominent platform, designated as the 100 m isobath (Figure 1).

Various field and analytical techniques are employed to determine the grain size characteristics of the sediments, their distribution, and heavy mineral content. These include offshore dredging and grab sampling, textural analyses and mineralogical determinations. Nearshore geology and seabed morphology have been mapped using sidescan sonar, high-resolution seismic profiling and

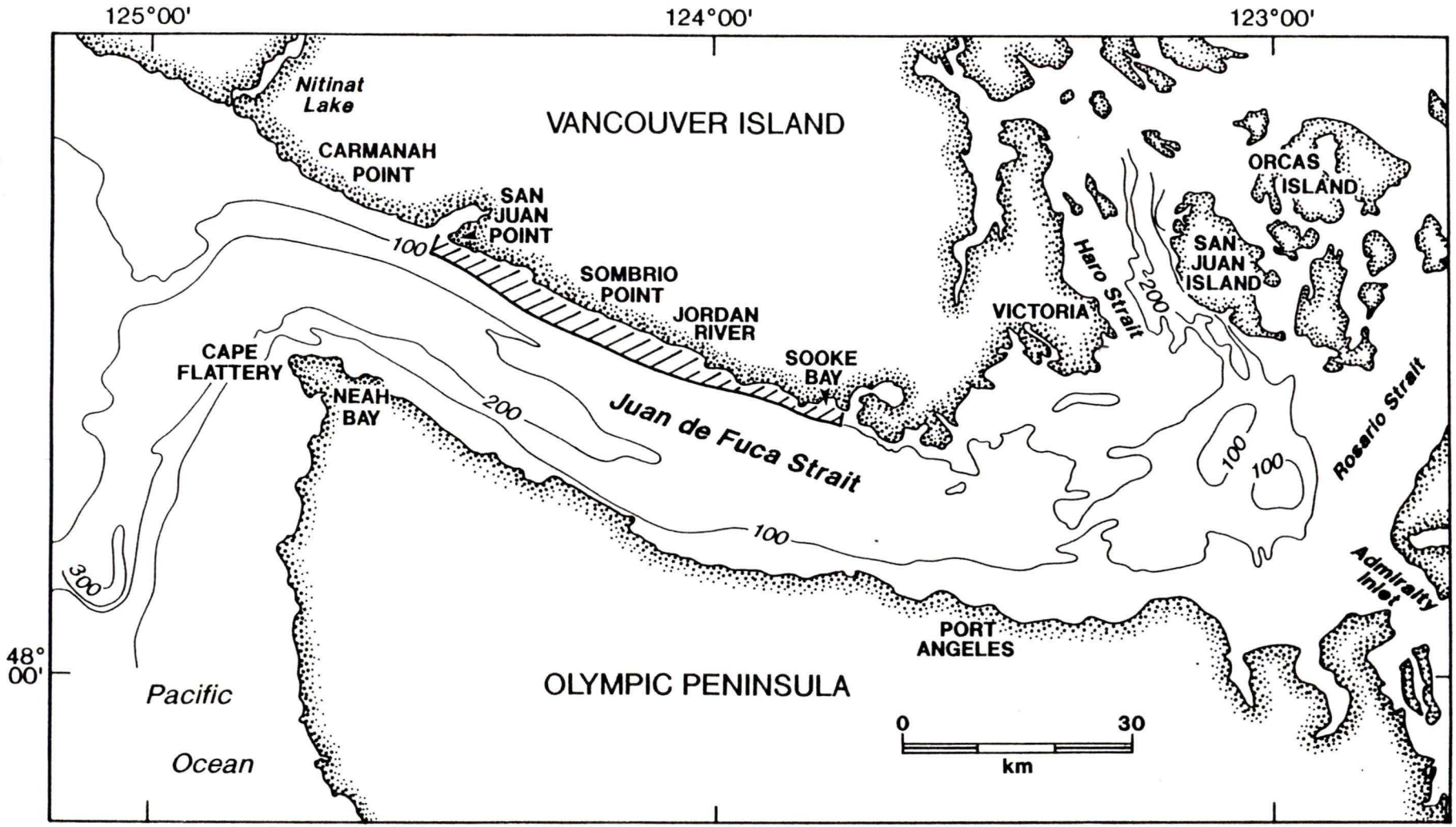

Figure 1. Map of Juan de Fuca Strait and approaches between Vancouver Island, British Columbia, and Olympic Penninsula, Washington. Study area is indicated from the northern shore out to the 100 m isobath, between San Juan Point and Sooke Bay.

echosounding.

The study was approached by identifying initially all archival beach and offshore samples, within the study area, which had been retained at the Pacific Geoscience Centre, Geological Survey of Canada, Sidney. In January 1988 a cruise along the northern strait obtained geophysical data (sidescan sonar, sub-bottom profiling and echosounding), and collected several dredge samples.

A cruise in March, 1989, added additional geophysical data. Further grab samples were obtained during July, 1989 at sites situated between other offshore samples. Between May and September additional samples were obtained along beaches not previously sampled. Four streams were identified within the study area as the most active contributors of sediment to the nearshore environment. Four shallow dives were performed, one at the mouth of each stream, to obtain samples to aid in studies of provenance and sediment dispersion along the adjacent shoreline. In addition, bulk sediment samples were taken from each of the four streams, above the highest tide mark, for provenance studies of the heavy minerals.

Textural analyses were carried out on all offshore samples, with some mud and silt fractions retained and submitted to commercial laboratories for geochemical analyses. Heavy mineral separations were performed on a large representative suite of samples, and mineral counts

performed on mounted sand grains, to obtain a general impression of heavy mineral distributions throughout the study area. The morphology of the seabed and its sediment cover were mapped using the geophysical coverage of the bottom combined with the grab-sample textural information. Results from the mapping and analytical work are used to describe the sediments covering the nearshore, their form, provenance, littoral dispersion and the heavy mineral content of the sands found along the northern strait.

2. Previous Work

Northwest of Port San Juan, near the entrance to Juan de Fuca Strait, the continental shelf of Vancouver Island has been the subject of several studies during the past two decades. The surficial sediments of Barkley Sound and the adjacent shelf area were first studied by Carter (1973). More recently, a large field program concentrating on the broader shelf area allowed analysis of the glacial and postglacial history of the continental shelf off southwestern Vancouver Island by Herzer and Bornhold (1982). Four seismostratigraphic units were distinguished and mapped along with their relation to sediments and sedimentary rocks present on the shelf. A history of glacial episodes and subsequent sea level fluctuations was outlined along with an explanation of the present shelf morphology and sediment regime. Other studies conducted off western or northwestern Vancouver Island include the surficial geology of the

continental shelf off northwestern Vancouver Island (Bornhold and Yorath, 1984), studies of oscillation ripples in deep water (Yorath et al., 1979), and the presence of glauconitic sediments along the shelf (Bornhold and Giresse, 1985).

Nearshore geology within the study area has not been extensively studied previously. Cockbain (1963) completed maps of the sediment distribution in the strait, including the nearshore area, although his work is based on limited samples. Nearshore sediments were generally found to consist of silty sand, while areas south of San Juan Point and Otter Point were finer grained, sandy silt.

East of the study area, Royal Roads Anchorage was the focus of a study by Linden and Schurer (1988). They described the sediments, which are largely glaciomarine at depth, and examined the postglacial sea level history, including a widespread unconformity evident in their cores. The cores included several collected in Sooke Bay, one of which was dated by radiocarbon and used for their calculations of postglacial sedimentation rates. This core, taken in 12 m of water, revealed an unconformity at 15 cm below the sediment surface, dated at 3320 +/- 190 years B.P., overlain by postglacial sediments which accumulated at an average rate of 0.45 cm per 100 years.

Shoreline sediment and geomorphic studies were undertaken by Harper (1980) and McLaren (1983) along the

northern Juan de Fuca coastline. McLaren's work entailed a study of the sediment transport regime from Jordan River eastward, to the western shore of Sooke Bay, and its implications in the event of oil spills. He concluded that within the beach environment there is a predominant offshore movement of sediment from berm to intertidal zone, with the maximum movement of sand-size material to water depths less than 30 m. Offshore sediment transport directions were dominantly to the east and northeast. McLaren also concluded that eroding Quaternary deposits are the largest source for the coastal sediments.

Harper (1980) studied seasonal morphologic changes along northern Juan de Fuca Strait from eight beach and nearshore profiles. Beaches generally showed erosion during the late fall with subsequent recovery throughout much of the remainder of the year.

3. Coastal Mining History

The northern Pacific coast of North America contains many sites where heavy minerals have been mechanically concentrated into placer deposits. Some of these deposits were considered economic and the sediments have been mined. Beach deposits are mined in the Gulf of Alaska, and gold has also been successfully mined offshore from the Stephens Passage area in southeastern Alaska (Clifton and Luepke, 1987). South of Coos Bay, along the southern Oregon coast, gold was discovered in the modern beaches in 1852 and mined

extensively for over ten years. These deposits are enriched in chromite, ilmenite, garnet, zircon, gold and platinum (Clifton and Luepke, 1987). Offshore mineral-related exploration in the State of Washington has centred on areas of titanium and iron-rich black sands (Lasmanis, 1988). However, gold and platinum were mined from beach placers earlier in this century on the northern Washington coast, south of Cape Flattery. These placer deposits are thought to have been derived from glacial sediment brought southward from British Columbia (Clifton and Luepke, 1987).

The potential for heavy mineral placers off the coast of British Columbia is uncertain. Holland and Nasmith (1958) compiled a summary of investigations of beach sand magnetite content for several locations on the British Columbia coast. Florencia Bay (formerly Wreck Bay), situated about 7 km northwest of Ucluelet, contains beach material which is derived from the erosion of till, sand and gravel. The gold-platinum-bearing black sands were mined between 1900 and 1935, producing over 1500 oz. gold (Holland, 1950). These placers have been worked sporadically since 1935. The study by Holland and Nasmith (1958) included a survey of the high magnetite content of these sands.

Nearshore heavy mineral assemblages and the potential for nearshore placer deposits on the shelf off southwestern Vancouver Island have not been previously examined. Recent

work by Barrie *et al.* (1988) studied the heavy mineral deposits of Hecate Strait and Queen Charlotte Sound. In the course of that study titaniferous placer deposits were identified on the inner continental shelf shallower than 20 m and between 120 and 140 m water depth. A study of the magnetic susceptibility of shelf sediments off central Vancouver Island revealed areas of anomalously high values (Currie and Bornhold, 1983) which could be of potential economic interest given the association between magnetite and heavy-mineral placers.

Placer gold occurs along the southwestern side of Vancouver Island. Adjacent to the study area, fluvial placers are associated with Loss Creek (formerly Lost River), Leech River, Sombrio River, Jordan River, San Juan River (Clapp, 1912), Muir Creek, Sooke River and other coastal streams (Holland, 1950). During the late nineteenth century, placer deposits in the Jordan River, Leech River and upper San Juan River were discovered and worked, the estimated yields being in excess of $200,000 (Clapp, 1912). With few exceptions, streams showing placer gold tend to have flowed for some distance over the Leech River Formation, the quartz veins of which are considered to be the source of gold (Clapp, 1912). Sombrio River Point was the site of an extensive hydraulic-placer-mining enterprise in 1910, with five hydraulic and four creek-mining leases and a twenty-man camp (Report of Min., 1910). Recovery was

probably from river-bed gravels derived from the former channel of Loss Creek (Reimchen Urlich, 1985), buried by a glacial delta formed at the coastal terminus of Loss Creek Valley. The amount of gold recovered from this site was not recorded. The site is presently being re-examined.

4. The Formation of Heavy Mineral Accumulations or Placers

High concentrations of heavy minerals form marine placer deposits which occur on both modern and ancient beaches and in shallow continental shelf areas. A placer is defined as "a surficial mineral deposit formed by mechanical concentration of [heavy] mineral particles from weathered debris" (Bates and Jackson, 1984).

The distribution of marine placer occurrences are influenced by five features of an area (Samson, 1984):

(1) bedrock geology
(2) drainage system onshore
(3) glacial history
(4) sea level history
(5) contemporary processes.

Contemporary processes would include the mechanical winnowing of wind, waves and currents. The creation of marine placers may depend on the history of a deposit, including the relationship of the deposit to its original environment, subsequent periods of exposure and level of consolidation (Samson, 1984). Ultimately, the number of times a deposit has been reworked and reconcentrated by fluvial or other agents will determine its likely potential to form placers.

Differential sorting processes which form marine placers are present on beaches and to depths in excess of 100 m. Isostatic and eustatic changes may result in submerged or raised beaches, and systematically move the zone of mineral sorting relative to sea level. Marine placers may, therefore, occur some distance inland from present shorelines, or some distance offshore from active beaches. For example, Barrie (1991) was able to identify both relict and modern placer formation located in deep water within Queen Charlotte Sound. Cores from bank sediments within the sound reveal relict heavy mineral laminates. These relict deposits formed during periods of lower sea level in a nearshore environment with high unidirectional current energy and a continuous sediment input with a significant concentration of heavy minerals. In contrast the overlying modern heavy mineral lag has formed under present shelf hydrodynamics. Rapid transgression following subaerial exposure preserved the underlying laminated sand facies which now forms the only heavy mineral source for the modern placer. Extreme storms have mechanically created a well-sorted fine sand which is sheltered from destructive shelf currents by the shielding configuration of the bank morphology.

Heavy minerals are defined as those minerals which have a specific gravity greater than 2.85, the specific gravity of bromoform liquid commonly used in the separation

process (Folk, 1974). More than 100 heavy minerals have been identified in sediments, but on average they only form 0.1 to 0.5% of the terrigenous fraction of sediments (Folk, 1974). Heavy minerals are accessory and varietal minerals of igneous and metamorphic rocks. Of the 100 or so minerals which may occur in these host rocks, many are reduced in quantity, or eliminated from the detrital record because they are chemically or physically unstable (Table 1). Chemical instability may result in the alteration of the original mineral to a more stable one. Physical instability may be in the form of structural weakness, making the mineral easily abraded by harder common minerals, particularly during transport. Heavy minerals which remain become important for purposes of correlation, analyses of provenance and transport studies.

Heavy minerals have been further classified into two sub-categories: heavy-heavy minerals and light-heavy minerals (Emery and Noakes, 1968). Gold (s.g. 15.0-19.3) and the platinum group minerals (s.g. 14-19), have significantly higher specific gravities than other stable heavy minerals which have specific gravities in the range of 3-6. The distinction is important because the high weight per volume of heavy-heavy minerals allows these minerals to have extreme vertical mobility within an environment. In a sedimentary environment they can migrate rapidly downward to an impervious layer, such as bedrock or clay.

TABLE 1. Heavy minerals of possible economic interest classified by stability. Specific gravity in parentheses (taken from Clifton and Luepke, 1987).

STABLE	MODERATELY STABLE
Anatase (3.9)	Andalusite (3.2)
Barite (4.5)	Ilmenite (4.5-5.0)
Brookite (3.9-4.1)	Marcasite (4.8-4.9)
Cassiterite (6.8-7.1)	Pyrolusite (4.7-4.8)
Chromite (4.3-4.6)	
Columbite (5.3-7.3)	
Corundum (4.0-4.1)	
Diamond (3.5)	
Fluorite (3.2)	UNSTABLE
Garnet (3.5-4.3)	
Gold (15.0-19.3)	Apatite (3.2)
Kyanite (3.5-3.7)	Pyrite (5.0-5.1)
Leucoxene (3.5-4.5)	Pyrrhotite (4.6-4.7)
Magnetite (5.2-6.5)	
Monazite (4.9-5.3)	
Platinum group (14-19)	
Scheelite (5.9-6.1)	
Rutile (4.2-4.3)	
Sillimanite (3.2)	
Spinel (3.5-4.0)	
Staurolite (3.6-3.7)	
Topaz (3.4-3.6)	
Tourmaline (3.0-3.3)	
Wolframite (7.0-7.5)	
Xenotime (4.5-4.6)	
Zircon (4.2-4.9)	

In water-borne sediments heavy minerals travel with the lighter, but harder, mineral quartz (s.g. 2.65 and hardness 7). Minerals which will be transported under a specific hydraulic regime generally have similar weights. This will result in smaller heavy minerals traveling with the less dense quartz grains, with a 0.5 to 1.0 phi larger size (phi = $-\log_2 d$; where d is the diameter in millimetres; Folk, 1974). This ratio is known as the hydraulic ratio (Rubey, 1933). For example a quartzitic sand with a median size of 2.5 phi would contain tourmaline with a median size of 2.9 phi and zircon of 3.5 phi (Folk, 1974). Grain size in a specific depositional location will be a function of a mineral's specific gravity, shape and original crystal size. As a result, in any given size fraction there will be a different ratio between the various minerals (Rubey, 1933).

Boyle (1979) notes that all placer-forming minerals have in common:

(1) great physical resistance to mechanical abrasion and comminution;
(2) great chemical resistance to solution in surficial waters; and
(3) a general equidimensional character in their form.

Finally, formation of a placer of any particular heavy mineral is dependent on the degree to which a mineral can exist in a subdivided form and still remain relatively chemically stable.

Research into the mechanics of placer formation has centred on four theories which describe various processes

which may contribute to differential sorting (Komar and Wang, 1984):

(1) settling velocity of various minerals,
(2) selective entrainment,
(3) selective transport,
(4) shear sorting.

(1) Settling velocity of various minerals

Settling velocity measures the "hydraulic equivalence" of various minerals. In such analyses settling rates may be measured directly for each mineral. Adjustments may be made to correct for variation due to angularity of grains. Beaches which have been reworked for extended periods of time may consist of sand grains which have similar hydraulic equivalence. Komar and Wang (1984) found this to be the case on the Oregon beach they studied. However, Slingerland (1984) was able to use the ratio of settling velocities of ilmenite to quartz to describe effectively the sorting process on the surface of a swashface on a beach in Virginia. On the upper third of the beach, following the maximum swash retreat, the ratio of settling velocities was at its greatest, and the percent of heavy minerals in surface samples had distinctly increased. Thus the role of settling velocities in placer formation may be dependent on the deposits being sorted.

(2) Selective entrainment

Small sand grains which are sheltered between larger and taller grains require higher water-flow velocities to

dislodge. Entrainment is referred to as the "flow bottom stress required to entrain" a grain of a specific diameter and density. Angles are derived to best describe the pivoting necessary to move a grain out of a bed (Komar and Wang, 1984). The angle must be adjusted to correspond to the ratio between the size and density of a heavy-mineral grain - to the surrounding larger and lighter, predominantly quartz, grains. Komar and Wang (1984) found that a systematic trend was revealed when threshold stress was plotted versus the concentration factor of each mineral, indicating that selective entrainment played a significant role in placer formation in their study.

(3) Selective transport

Following entrainment, differential transport rates of minerals can lead to their further separation. Komar and Wang (1984) calculated flow stresses for three levels of energy expected in the swash zone. These values were normalised to the transport rates of the quartz fraction, thereby indicating the degree of lag behind the fastest quartz grain. Where the flow stress would be capable of transporting only a few of the heavy mineral grains and all of the light-mineral grains, a placer could form. They concluded that selective transport is also a significant element in placer formation.

Selective transport can be an effective agent of placer formation in areas of diminished flow velocities, as

in areas of changing shoreline orientation. Peterson *et al.* (1986, 1987) discuss the accumulation of heavy minerals in surf and offshore zones where a decrease in fluid-shear stress occurs, resulting in the transport of only light minerals. This process creates a lag of ilmenite in the area of maximum shoreline curvature where fluid-shear stresses are too low to displace the ilmenite.

Slingerland (1984) analysed the role of differential transport in the formation of placers by employing the transport-evaluation approach of Einstein (1950). This approach includes a factor for the sheltering of smaller grains between larger particles - therefore including selective entrainment. In his study a medium-size quartz sand containing 10% fine-size magnetite displayed a pattern of differential transport. He concluded that the concentration of magnetite transported in a flow is due to variations in the reactive angles of grains and the extent to which they are hidden in the boundary layer.

Significant heavy mineral lags found at water depths of 100-140 m on the continental shelf of British Columbia (Barrie and Luternauer, 1986) have been explained by Barrie *et al.* (1988) in calculations of critical threshold velocities for selective transport with entrainment. These calculations, of quartz and hydraulically equivalent ilmenite, revealed water depths at which this mechanical sorting is occurring for specific sand fractions present

within the modern hydrodynamic regime. These marine placers are considered to be forming *in situ*.

(4) Shear sorting

As waves wash up a beach, granular material such as sand is sheared. The grains interact to produce a dispersive grain pressure at right angles to the shear direction (i.e. normal to the sediment). This pressure is believed to increase with grain size. The pressure would, theoretically, cause the larger grains to migrate to the surface of the sheared layer, producing an inversely graded bed (Komar and Wang, 1984). Equations for grain dispersive pressure, deduced by Bagnold (1954), produce values for shear sorting. Komar and Wang (1984) found that "dispersive equivalence" values did not provide as good an explanation as entrainment and transport for placer formation.

While all these factors describe possible processes of placer formation, other marine processes may be at work to destroy any placer which has formed. The change in wave shapes (wave orbitals) from summer to winter produces major changes to beaches exposed to oceanic wave and wind forces. Spring and summer mark periods of onshore transport of sand, burying and protecting winter placer concentrates from possible longshore currents active during fair weather conditions. Such seasonal sand exchange was recorded by Peterson *et al*. (1986) along an expanse of beach in Oregon.

While mechanical sorting of minerals may form heavy

mineral lags under some conditions, mechanical sorting under other conditions can effectively decrease heavy mineral concentrations. Barrie (1981) studied heavy mineral contents within the Bristol Channel and adjacent beaches, and the effect of wave superposition on the tidal regime (oscillatory *versus* unidirectional motion) which created variations in hydraulic equivalence and total placer concentrations. Hydraulic inequivalence in the channel was a result of mineral size from source and differential entrainment of the minerals. Sediments were subjected to increasing oscillatory motion over greater bed roughness, resulting in heavy minerals becoming increasingly finer in relation to the light minerals. Enrichment of heavy minerals occurred only at the extreme shoreward end of the dominant swell. Consequently, heavy mineral enrichment was found on the open (high energy) beaches and in the areas of local tidal current enhancement.

II. Geological Setting

1. Coastal Geomorphology

Southernmost Vancouver Island can be divided into two physiographic regions, the Insular Mountains and the Georgia Depression (Holland, 1976). The Insular Mountains on Vancouver Island consist of the Vancouver Island Mountains which are separated from the lowland areas of the Coastal Trough by a boundary drawn along the 600 m contour. The Nanaimo Lowland of the Georgia Depression lies below this boundary and wraps around a narrow strip of the southeastern tip of the island.

The highest peaks of the Vancouver Island Ranges are at an elevation of about 2200 m in the central part of the island, but are lower than 1525 m along the southeastern end of the island (Holland, 1976). South of the San Juan River the mountains form a broad plateau which slopes gently southward to Juan de Fuca Strait (Alley, 1974). Modification by continental ice-sheets has smoothed the southern mountain peaks and the valleys have been deepened through erosion by valley glaciers. The fault-controlled valleys of Loss Creek and San Juan River are conspicuous features which dissect the mountains in two near east-west lineaments (Holland, 1976) separating distinct geologic formations and ages.

Jordan River separates the Vancouver Island Ranges to the northwest from the low-lying terrain, below 600 m, to

the east. Glaciation along the Georgia Depression was intense, and as ice flowed south towards Juan de Fuca Strait and the open Pacific, the southeastern tip of the island was over-run, with weathered materials stripped, bedrock striated, and glacial deposits left as remnants (Holland, 1976).

The coastal region between Jordan River and Sombrio Point is underlain by glacial kame deposits. Between Sombrio River and Loss Creek, to the east, lies a large glaciofluvial delta at the mouth of Loss Creek Valley (Alley, 1974).

The coast between Port San Juan and Sombrio River is underlain by slightly friable, foliated Jura-Cretaceous metasediments which produce a largely low-relief, straight coastline of sharp, steeply-dipping rocks with only one area of pocket beaches towards the northwest. Southeast of Sombrio River the coast is underlain by Tertiary crystalline rocks which form tall resistant headlands forming bays and pocket beaches.

Poorly indurated Tertiary sediments fringe the entire coastline. Partly eroded above sea level along this part of the island's coast, the jointed sediments have been weathered to form a gently dipping intertidal platform. Narrow pebble-cobble and gravely sand beach material locally accumulates shoreward of the platform. North of Sombrio River the Tertiary sediments remain particularly wide at an

area just south of Point San Juan where they form coastal cliffs; several pocket beaches have formed behind the intertidal platform. South of Sombrio River the Tertiary sediments commonly form cliffs, up to 10 m high, as well as intertidal platforms. Headlands are generally of crystalline rocks and pocket beaches consist largely of rounded glacial gravel.

Sandy beaches have formed between headlands where the shoreline is largely exposed to the west, toward the mouth of the strait. China Beach and French Beach are the largest of these containing the finest textured beach material and the lowest profiles. The bays to the southeast, particularly Orveas and Sooke Bays have resulted from erosion of extensive underlying Tertiary sedimentary rocks.

2. Seabed Morphology

Juan de Fuca Strait is a long, narrow submarine valley carved by successive periods of continental glaciation (Figure 2). The strait is generally 22-28 km wide from the entrance eastward for 100 km, where it narrows at Race Rocks (north of Port Angeles) before widening again to the east (Thomson, 1981). Southwest of the City of Victoria the topography consists of a gently-sloping U-shaped valley with depths to 180 m. West of Jordan River the strait becomes more V-shaped with depths to 240 m (Figures 1 and 2). Farther west, beyond the mouth of the strait the valley turns sharply to the southwest where it becomes the deeply

incised Juan de Fuca Canyon. From Cape Flattery, Washington, east to Port Angeles, Washington, the valley has a gentle seaward slope of approximately 2 m/km (Anderson, 1968).

The study area stretches for roughly 60 km along the northern shore of Juan de Fuca Strait, from the centre of the mouth of Port San Juan ($48^{o}33'$, $124^{o}30'$), southeast to include the eastern shore of Sooke Bay ($48^{o}20'$, $123^{o}45'$). In the southeast, adjacent to Sooke Bay, the central part of the strait forms a smooth U-shape with depths to 170 m. As the strait extends to the northwest the deeper reaches become narrower, as shallow nearshore terraces extend away from shore; the depth in the central strait reaches 240 m off Port San Juan.

This relatively smooth submarine valley appears slightly steeper and narrower given the presence of three wide shallow terraces along the northern slope. The terraces extend from the shoreline, where they reach 5 to 10 m depth within a short distance, and into the strait as far as 3.5 km. The terraces are at depths of 10 to 20 m in the southeast and 10 to 30 m in the northwest. At the edge of the terraces the valley walls slope at 4.4^{o} - 5^{o} into the trough to depths of 100 m, after which the walls begin sloping more gently into the central trough.

Sooke Bay has a regular, gentle slope of 2.5^{o} directed southeast into the strait. The floor of the bay is shallow

(20 m) to a line even with the eastern headland (Figure 2).

The edges of the terraces, which extend from Orveas Bay to Sombrio Point, have a consistent strike of 106°, whereas the coastline has a general strike of 111° to 115°. The first terrace begins in eastern Orveas Bay and narrows close to Sheringham Point, followed by broadening westward until it extends about 3.5 km offshore adjacent to China Beach. This terrace then disappears as the scarp ends and slopes dip more gently to the west.

The second terrace begins just west of Jordan River and continues to southeast of Sombrio Point, again at a distance of 3.5 km offshore. This second terrace is cut by a large submarine channel along the northern slope (Figure 2). The head of the channel is located northwest of Magdalena Point, 2.25 km offshore and opens to the southeast with a bearing of 126°. The channel begins at 30 m depth and cuts the slope down to 80 m depth. Directly west of the channel mouth an isolated depression occurs in the slope to a depth of 130 m creating a slope of 14.5° off the adjacent terrace (Figure 2).

The third terrace is less pronounced nearshore. It begins off Magdalena Point and extends at a strike of 106° eastward to a point several kilometres northwest of Sombrio Point. This terrace also has an isolated depression south of the steepest edge of the terrace and ends by flattening quickly westward into a broad gentle slope. Northwestward,

off Providence Cove, only a very narrow terrace occurs at 30 m depth with a very gentle, regular slope of 2^{o}.

In Orveas Bay a channel of a few metres relief has been cut into the terrace off the mouth of Muir Creek. This shallow channel is only evident to 15 m depth where it appears to swing to the east. No similar channel is seen adjacent to the other rivers and streams along this coast, or at the entrance to Port San Juan, which has a simple, gentle, regular slope. Southeast of Sheringham Point a lone pinnacle rises from a depth of 140 m, 2.5 km offshore, to a depth of less than 80 m. The large offshore channel feature south of Magdalena Point is not connected by a channel to any present river or stream emptying into the strait. Loss Creek drains into the strait northwest of the channel head but no feature of the submarine surface connects the two.

3. Geology of the Shoreline Rocks

Southwest Vancouver Island and Juan de Fuca Strait are underlain by geologically distinct terranes, separated by major faults (Figure 3). The Jura-Cretaceous Leech River Complex is part of the Pacific Rim Terrane. The latter dips to the north where it underplates the Wrangellia Superterrane along the San Juan-Survey Mountain Fault. The Pacific Rim Terrane is in turn underplated by the rocks of the Crescent Terrane to the south, along the Leech River Fault. Rocks of the Crescent Terrane, consisting of the early Tertiary Metchosin Igneous Complex (Vancouver Island)

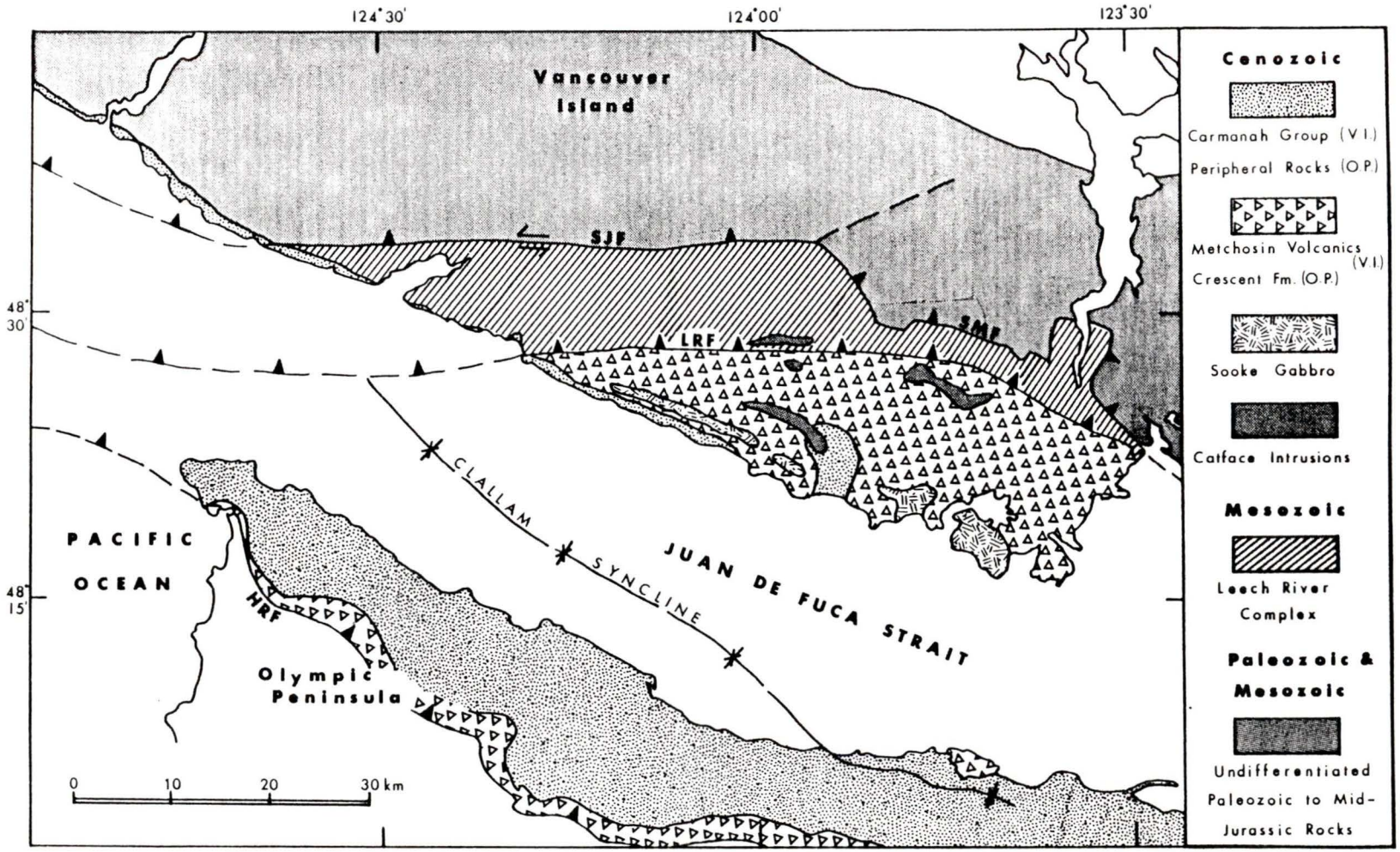

Figure 3. Geology of southwestern Vancouver Island (V.I.) and correlative rocks of the Olympic Penninsula (O.P.) after Muller (1983). Extension of geological structures into Juan de Fuca Strait after Hyndman *et al.* (1990); SJF=San Juan Fault, SMF=Survey Mountain Fault, LRF=Leech River Fault, HRF=Hurricane Ridge Fault.

and Crescent Formation (Olympic Peninsula) underlie the Strait (Figure 3) (Hyndman *et al.*, 1990).

Along the coast the older rocks are overlain by a narrow fringe of mid-Tertiary clastic strata of the Carmanah Group. A short distance inland from the study area igneous stocks of the Tertiary Catface Intrusions occur (Muller, 1983). Quaternary sand, gravel and till remain in patches exposed along river valley walls, and in coastal lowlands.

i) Leech River Complex

The Leech River Complex occurs in a narrow belt between the Leech River Fault in the south and the San Juan-Survey Mountain Fault to the north (Figure 3). The Leech River rocks are believed to be allochthonous (Fairchild and Cowan, 1982) neritic to bathyal metamorphosed clastic and volcanic rocks (Muller, 1982).

The Complex includes, in decreasing order of abundance, metamorphosed pelitic rocks, sandstone, and volcanic rocks. Small amounts of recrystallized chert and lithic conglomerate are also found (Fairchild and Cowan, 1982). Strong, pervasive foliation is present and commonly folded with structures generally oriented east-west (Fairchild and Cowan, 1982). The upper parts of the Leech River Formation exhibit southward increasing metamorphic grade from chlorite, biotite-chlorite, biotite-garnet-chlorite, to andalusite-staurolite-biotite zones (Fairchild and Cowan, 1982).

Rocks ascribed to the Pandora Peak Unit (Rusmore and Cowan, 1985) occur in a small splay along northern Port San Juan adjacent to the San Juan Fault. These rocks form part of the Leech River Complex, although they have different deformational styles and metamorphic minerals, including rare lawsonite veins (Rusmore and Cowan, 1985).

ii) Metchosin Igneous Complex

The Metchosin Igneous Complex consists of three components - gabbro stocks (Sooke Gabbro), a sheeted-dike complex, and a basaltic volcanic sequence (Metchosin Volcanics) (Massey, 1986). The units are probably contemporaneous and have been dated as early Eocene (Massey, 1986). The Complex dips about 30^{o} to the northeast (Massey, 1986).

Sooke Gabbro (Figure 3) occurs predominantly at the base of the complex (Massey, 1986) and is composed of coarse-grained gabbro with bytownite, diopside and about 5% olivine (Muller, 1983). Local amphibolization and mineralisation of the gabbro occurred later along shear zones at the time of emplacement of Catface Intrusions (Muller, 1983).

Muller (1983) divides the Metchosin Volcanics (Figure 3) into a lower unit of pillow basalt, tuff and breccia, and an upper unit of basaltic flows. These volcanics are of tholeiitic composition and exhibit low to medium grade metamorphism, up to epidote-amphibolite grade. Diabase

dikes and sills are common in this unit (Muller, 1983). Sheeted dikes, of dense, fine- to medium-grained diabase, have been identified in the eastern part of the complex (Massey, 1986).

iii) Catface Intrusions

Catface Intrusions are small stocks of hornblende quartz diorite that intrude the Metchosin and Leech River complexes (Figure 3). Muller (1983) describes the stocks as several west-northwest elongate bodies less than 2 km wide which have been dated as late Eocene. The stock which intrudes Leech River rocks is altered to muscovite-biotite orthogneiss containing pegmatitic zones with large tourmaline and muscovite crystals (Muller, 1983), and zircons (Muller, 1976).

iv) Carmanah Group

The Carmanah Group includes marine to intertidal clastic sediments of Tertiary age which form a narrow apron along the coast of western Vancouver Island (Figure 3), and lie in unconformable contact with underlying older rocks (Muller, 1982). The sediments are divided into the Hesquiat Formation, dated at Botanical Beach, and the younger overlying Sooke Formation which occurs along the coast southwest of Sombrio River (Bream, 1987). Sandstone outcrops northwest of Sombrio River have not been dated (Bream, 1987).

Within the study area, the Hesquiat Formation overlies

Leech River Rocks in discontinuous basins. The formation contains alternating siltstone-shale and sandstone-conglomerate units of neritic origin, dated as late Eocene to earliest Oligocene (Muller, 1982).

To the southeast, the Sooke Formation overlies basalts and gabbros of the Metchosin Igneous Complex. The deposits strike northeast-southwest with average dips of 8^{o} to the southeast. They are shoreface and lower foreshore lithic arenites with a modal grain size of fine sand (Bream, 1987). Bream (1987) divides the sediments into six facies, with the lowest three largely deposited by debris flows, displaying an interlayering of shoreface sands and conglomerates. The upper three facies show decreasing high-energy conditions with very-fine-grained to coarse-grained sandstone with minor siltstone and shale (Bream, 1987). Metchosin rocks are the probable source for significant volcanic clasts found in the Sooke Formation (Bream, 1987). Lenticular coquinas of bivalves and gastropods indicate a nearshore origin of late Oligocene age (Muller, 1982 and 1983).

v) Pleistocene Geology

The Fraser Glaciation is the most recent major glaciation of British Columbia. The advance phase began about 29 000 years B.P. with climatic deterioration at the end of the Olympia nonglacial interval (Howes and Nasmith, 1983). The major advance was during the Vashon Stade which had its maximum slightly after 15 000 years B.P. (Clague,

1981).

Evidence of pre-Fraser glacial deposits is absent along southwestern Vancouver Island, except for weathered erratics in high areas to the northwest and a few fragmentary exposures along the southernmost coast (Alley, 1974). Most deposits encountered in the area are related to the Fraser Glaciation, subsequent transgression and Holocene emergence.

Bedded glaciolacustrine clays, up to 25 m thick, containing striated ice-rafted pebbles, can be traced from approximately 90 m above sea level in lower Kirby Creek (west of Muir Creek) to almost 300 m elevation, near its headwaters. Similar pre-Fraser lacustrine sediments are found in adjacent Muir Creek, and farther west in the banks of lower Loss Creek. The pre-Fraser units along the Juan de Fuca coast are interpreted as a proglacial facies of the Vashon Stade (Alley and Chatwin, 1979).

Vashon till can be traced from eastern Vancouver Island to the western and southwestern coast. The till is variable in texture, pebble lithology and thickness. It is characterised by a compact, silty matrix and by abundant pebbles and boulders derived from Vancouver Island volcanic rocks and other local bedrock types (Alley and Chatwin, 1979). Vashon deposits are found behind French Beach, along the shoreline directly east of Sooke Bay, and in a large deposit stretching 3 km inland behind Orveas Bay (Muller,

1983).

Between Jordan River and Sombrio Point a prominent kame terrace, 60 m thick (Alley, 1974), was deposited along the coast. These deposits overlie and are intercalated with glaciolacustrine sediment which occurs in Loss Creek Valley. The latter is a continuous sequence with a measured thickness of 460 m. Pebble counts of the ice-contact kame materials show that 30-80% of the deposits consist of granitic, gneissic and schistose rocks, with a few percent of olivine gabbro rocks (Alley and Chatwin, 1979). The kame deposits overlie the Leech River and Metchosin rocks along the coast.

Capilano Sediments overlie Vashon till along Orveas Bay and around Sooke Bay and Sooke Harbour below 100 m above sea level (Muller, 1983). Capilano Sediments contain marine, fluvial and some glaciomarine deposits of silt, pebbly clay, sand and gravel, laid down during the retreat of the Fraser ice sheet (Muller, 1983) around 13 000 years B.P. (Howes and Nasmith, 1983).

4. Geology of Juan de Fuca Strait

Extension of Pacific Rim and Crescent Terrane rocks into the Strait of Juan de Fuca by Hyndman *et al.* (1990) (Figure 3) indicate that a minor wedge within the study area, northwest of Sombrio River to Port San Juan, is underlain by Leech River rocks. The remainder of the strait is underlain by Crescent Terrane rocks covered by younger

sediments.

Pillowed, layered basalt, probably representing ocean floor, of the Crescent Formation extends northward across the strait reappearing as the coeval and lithologically similar Metchosin Volcanics (Muller *et al.*, 1983). Late Tertiary littoral strata of the Carmanah Group overlie the basalts in a thick succession of clastic slope, shelf and shoreline strata. North of the Leech River Fault, along the northern coast, a more complete Tertiary sequence exists and is coeval with sediments across the strait on the Olympic Peninsula. South of the fault, along the northern coast, only the younger shoreline sediments of late Oligocene age occur (Muller *et al.*, 1983).

The volcanic flows and clastic strata form the broad Clallam Syncline which underlies the southwestern strait (Figure 3). Several minor faults offset the marine strata that overlie the volcanic units (Muller *et al.*, 1983).

MacLeod *et al.* (1977) described several geophysical anomalies within the study area. These include a linear magnetic anomaly near the coast between Sombrio Point and Jordan River, possibly caused by a gabbro body similar to the ones found onshore. A magnetic low west of Sooke, offshore from the Sooke Formation sediments found shoreward of Orveas Bay, suggests the extension of these sediments into the strait, with a thickness in excess of 500 m. The third area, one of complex high frequency magnetic

anomalies, is offshore southeast of Sooke. These coincide with broad gravity highs suggesting apparent seaward extensions of the Sooke Gabbro.

Mayers and Bennett (1973) were able to show the profile of glacial scouring in the strait and many features of subsequent periods of fluvial deposition. Their study revealed "delta-like" deposits from isopach maps and possible glacial "morainal" features. This regional study did not extend onto the nearshore platform area. Anderson (1968) extended his study of the Quaternary stratigraphy in the strait closer to the nearshore areas, completing textural and mineralogical work on cored sediments of the strait. Cockbain (1963) described the sediments of the northern strait as a silty sand, with the areas south of Port San Juan and Otter Point as finer-grained sandy silt. His work is based on a very limited number of samples. Both Anderson (1968) and Cockbain (1963) observed greatest sediment influx and thickness into the strait from Port San Juan and Otter Point.

5. Glacial History and Sea Level Change

The Strait of Juan de Fuca is believed to have been covered by continental ice sheets at least four times during the Pleistocene Epoch (Mayers and Bennett, 1973). However, the stratigraphic record of earlier glaciations, within the strait, has been poorly preserved except for that of the most recent, the Fraser glaciation (Alley and Chatwin,

1979).

The Olympia interstadial period (51 000 to 29 000 years B.P.) on southern Vancouver Island, is represented by a period of marine, estuarine and fluvial sedimentation (Howes and Nasmith, 1983). The Cowichan Head Formation (Armstrong and Clague, 1977), a diachronous unit comprised of non-glacial silt, sand and gravel, resulted from changing environments as sea areas became more restricted along the coast due to isostatic uplift and sediment influx (Howes and Nasmith, 1983). Remnant deposits of this formation can be found on Saanich Peninsula and elsewhere in southeastern Vancouver Island.

With the advance of the late Wisconsinan Fraser glaciation, the diachronous Quadra Sand unit was deposited in Georgia Strait with decreasing age from the north, 29 000 years B.P., to 15 000 years B.P., in the south near Seattle (Clague, 1977). As ice advanced south along the Strait of Georgia it split into the Puget lowland and the Juan de Fuca lobes. Pre-Fraser units occurring along the southwestern coast are interpreted by Alley and Chatwin (1979) as proglacial sediments formed as ice began to fill the strait, damming streams flowing down coastal valleys and forming small lakes. As the ice advanced along Juan de Fuca Strait to the west-northwest, towards the Pacific, and the Vashon Stade reached its maximum, ice on southern Vancouver Island flowed south-southwest across the southeastern lowlands and

across ridge tops joining valley glaciers to merge with the main lobe in the strait or flowed onto the Pacific shelf north of the strait as part of the Barkley Sound lobe (Alley and Chatwin, 1979; Herzer and Bornhold, 1982).

The Juan de Fuca ice lobe is estimated to have had a thickness of 1100-1200 m (Alley and Chatwin, 1979). The Juan de Fuca and Barkley Sound lobes probably coalesced near $48^{o}30'$, on the continental shelf, sometime after 17 000 years B.P. (Herzer and Bornhold, 1982). The proglacial sands and gravels were overridden by the ice and partially incorporated into the Vashon till. Isolated deposits of Vashon till extend along the coast, particularly in the low slopes around Sooke and in the Kirby Creek and Muir Creek valleys (Muller, 1983).

Deglaciation occurred through downwasting rather than the retreat of Vashon ice, which resulted in the emergence of the uplands first. Evidence of ice marginal channels and proglacial sediments suggest that the ice retreated and melted down into major lowlands, Juan de Fuca Strait and onto the continental shelf (Alley and Chatwin, 1979).

However, extensive deposits of ice-contact sediments along the coast and thick glaciolacustrine clays in Loss Creek Valley and the evidence of other glacial lakes, indicate a resurgence or major halt in deglaciation occurred (Alley and Chatwin, 1979). Glaciomarine silts in the Victoria area suggest that this resurgence of ice probably

occurred sometime before 12 000 years B.P. Sediments associated with this re-advance are known as the Capilano Sediments consisting of glaciomarine and glaciofluvial deposits (Howes and Nasmith, 1983). Deposits of Capilano Sediments overlie Vashon till along the low slopes and hills above Sooke Harbour and similarly overlie till along the coastal slopes above Orveas Bay (Muller, 1983).

Ice had disappeared and the sea penetrated beyond the eastern end of Juan de Fuca Strait by 13 000 years B.P. (Clague, 1981).

In Juan de Fuca Strait, the Tertiary and Mesozoic rocks beneath the strait were unconformably eroded during glaciation and subsequently covered by a layer of undeformed, interbedded glacial and marine Pleistocene and Holocene sediment 40 to 400 m thick attributed to the last several advances of the Juan de Fuca lobe down the strait. Possible glacial "morainal features" have been identified within the stratigraphy in deep water south of Otter Point (Mayers and Bennett, 1973).

During the last retreat, following the Vashon Stade, rapid melting of alpine glaciers is considered the cause for the formation of "delta-like" deposits, up to 100 m thick, above the glacial and marine sedimentary section (Mayers and Bennett, 1973).

Anderson (1968) identified three major stratigraphic units in his cores from central Juan de Fuca Strait. The

lowest was a clay unit, followed by a diamicton unit which was overlain by the central sand unit. The sand unit, dated at 11 300 years B.P. from a core in the central strait south of San Juan Point, reaches its greatest thickness on the northern side of the strait near Port San Juan and Otter Point. The diamicton unit was dated in the central strait at 17 100 years B.P. (and older) and could represent Vashon till (Anderson, 1968).

In six shallow water (45 to 78 m) vibro-cores from along the northern strait Conway (unpub. rep., 1989) identified medium to coarse sands, up to 2 m thick, which he interpreted as nearshore intertidal to shallow sublittoral with rapid deposition in a high energy environment, perhaps as a result of rapid transgression and terrestrial erosion following downwasting of ice. These were overlain by an olive grey sandy gravel, which may indicate a sea level change, and is correlated with an erosional horizon in Sooke Bay (K.W. Conway, unpub. rep., 1989). This unit may correspond to the green postglacial sediments at Royal Roads Anchorage (Linden and Schurer, 1988).

The sandy gravel was overlain by Holocene shelf sediments which in several additional vibro-cores from the terraces are up to 2.2 m in thickness (K.W. Conway, unpub. rep., 1989). The latter sediments are predominantly poorly sorted muddy-fine sand with minor gravel.

The relative position of sea level has varied

significantly in relation to Vancouver Island following the last glaciation. Various locations on Vancouver Island have experienced great fluctuations in sea level due to combinations of eustatic sea level changes, isostatic rebound and active tectonic events along the continental margin off western Vancouver Island. Periods of submergence and emergence in coastal areas over the past 12 000 years have resulted in the disequilibrium of coastal landforms with present dynamic processes (McLaren *et al.*, 1983).

As Vashon ice retreated and downwasted into Juan de Fuca Strait, the coastal lowlands were inundated resulting in the deposition of deltaic and marine sediments. Glacial marine silts were deposited up to 17 m above present sea level about 12 000 years B.P. (McLaren *et al.*, 1983). In Victoria, sea level history has been complex (Clague *et al.*, 1982; Linden and Schurer, 1988), but to the west, along Juan de Fuca Strait and on the outer coast, about 40 percent of the coastline is backed by relict marine scarps (Harper, 1981). The evidence of terrestrial and marine sediments and morphology suggests that most of the shoreline along the northern strait is presently stable or prograding (Harper, 1980) as proposed for the entire Holocene (Clague *et al.* 1982).

Linden and Schurer (1988) suggest a period of lowered sea levels to -55 m for the Royal Roads area followed by submergence based in part on airgun sub-bottom profiles from

areas as far west as Cullite Cove 3 km northwest of the study area.

Riddihough (1982) summarized available evidence to determine present vertical movement patterns for various locations along the North Pacific coast. Sea level changes deduced from long-term tidal records and leveling data showed a pattern of uplift along the west coast of Vancouver Island of 2 mm/year. Along northern Juan de Fuca Strait uplift appears to be near zero at Sooke, and increases westward, with about 1 mm/year uplift estimated near Jordan River and 2 mm/year near Port San Juan.

Clague (1989) provides some evidence to the contrary at Muir Creek, where he reports *in situ* fossil stumps in the intertidal zone. Geologic evidence from this site suggests a significant late Holocene sea level rise. However, Muir Creek is in the centre of the largest sedimentary trough of Sooke Formation sediments along the northern strait (McLeod *et al.*, 1977), and such a site may represent only local subsidence.

The sea level history of the northern coast of Juan de Fuca Strait has not been well-defined for the last 10 000 years. Although it is unclear whether glacial isostasy or tectonics is the major cause, it is likely that glacio-isostatic adjustments must be virtually complete (McLaren *et al.*, 1983).

6. Relevant Mineral Occurrences

Stable heavy mineral suites from the coastal crystalline and metasedimentary rocks will contribute significantly to those heavy minerals found offshore. In addition, eroding Quaternary deposits are also considered a significant source of shallow coastal sediments within the study area (McLaren, 1983). Other sediments, derived from the chemically weathering Carmanah Group (Harper, 1981), may supply only minor material to the littoral regime (McLaren *et al.*, 1983). Nevertheless, a significant source for both glacial material and sandstones of the Sooke Formation will have been the underlying bedrock.

Fairchild and Cowan (1982) describe the relative abundance of minerals in the metavolcanics and metapelites of the Leech River Complex. In the metavolcanic rocks epidote and hornblende are abundant, with lesser amounts of actinolite and minor amounts of magnetite, biotite and sphene. In the metapelites, biotite is the most abundant heavy mineral, followed by moderate amounts of garnet, andalusite and staurolite.

Fine gold, found throughout much of the Leech River Formation (Clapp, 1912) in association with quartz (Muller, 1983), is considered the source of the placer gold along streams of the southwest coast. Holland (1950) lists known production from various placer streams, noted in Chapter 1. Hydraulic placer mining near Sombrio Point, around 1912, is

believed to have been in river gravels of the former channel of Loss Creek, subsequently overlain by glacial debris (Clapp, 1912).

Heavy minerals in the Metchosin Igneous Complex include large amounts of augite in the primary basalt, with magnetite and secondary pyrite as accessory minerals. The augite may be altered to hornblende or serpentine. In diabase dikes, magnetite and pyrite are the chief accessories, forming up to 5-10% of the rock. Less frequently flows include secondary minerals of the epidote group. Elsewhere in shear zones, veins of epidote are common (Clapp, 1912).

Sooke Gabbro has significant augite and hornblende, with minor magnetite and ilmenite as the only important accessory minerals. Olivine is a prominent accessory and epidote is a common secondary mineral. Areas altered to amphibolites contain 95% hornblende and actinolite (Clapp, 1912). Layered lava flows contain significant diopsidic pyroxene and accessory magnetite and apatite (Muller, 1977).

Copper mineralisation has occurred where the Sooke Gabbro intruded the volcanics. Mineralization occurs in vertical fracture zones in the gabbro, up to 30 m wide, where it has been hornblendized or where hornblendized basalt is in contact with gabbro. The deposits are chalcopyrite with pyrite, pyrrhotite and some molybdenite. Although small veins predominate, economic deposits of this

type include the Jordan River Mine (discussed below) and the deposits of Sooke Peninsula that were mined 1915-1918 (Muller, 1977).

Assessment work performed on the Sombrio Point placer property includes mineralogic examination of heavy mineral concentrates separated from bulk samples taken from sand and gravel deposits (Urlich *et al.*, 1984). Heavy mineral content listed in decreasing order was pink garnet, followed by altered hornblende, green and brown epidote, rutile, zircon and magnetite. Smaller amounts of almandine, green garnet, tourmaline, hematite-ilmenite, specular hematite and chlorite, and minor gold were observed.

The bulk samples were taken from various locations on the property so that it is not stated specifically if these observations are for concentrates from glacio-fluvial or stream deposits.

Bream (1987) examined the heavy minerals from sands of the Sooke Formation and found significant amphibole, micas and less commonly pyroxenes. Muscovite and biotite occur, with biotite partially replaced by pyrite or altered to chlorite. Epidote constitutes a large proportion of the accessory minerals in the sandstones. Clinozoisite and zoisite are present in veins and lithic fragments. Pumpellyite and chlorite are also common accessory minerals, with minor prehnite and staurolite, and rare garnet and zircon. Pyrite is common as a pore-filling cement,

occurring in many crystal forms and frequently replaces grains.

i) Jordan River Mine

The Jordan River, or Sunro Mine, is the single major nearshore mining activity adjacent to the study area. A brief history of the mine's operation is presented below given its proximity to the coast and possible effect on littoral sediments along the northern strait.

The mine portal is located on the edge of the Jordan River, 1.6 km from tidewater. Mining production commenced in 1962 and continued with several interruptions until all operations closed down in 1978 (MINFILE, 1988). The mined deposits were chiefly chalcopyrite with pyrite, pyrrhotite and some molybdenum occurring in vertical fracture zones in hornblendized basalts in contact with gabbro (Muller, 1977). Economic production was chiefly of Cu with lesser amounts of Ag and Au, and minor concentrations of Mo (MINFILE, 1988).

Mine tailings were pumped 4000 m from the mill (located underground) to tidewater in a 15 cm plastic pipe (Billingsley, 1965). The location of the outfall is presumed to be Outfall Point (Figure 83) at the eastern edge of the town of Jordan River. Tailings consisted of fluidized crushed and ground rock with 79.4% of particles less than 0.074 mm; 11.2% > 0.074 mm and < 0.10 mm, and 8.5% > 0.10 mm and < 0.15 mm, all fine- to very-fine-grained sand (Billingsley, 1965).

In 1963 and again in 1964 the river broke through rock canyon walls into a stope, flooding the mine and washed downstream loading equipment, sheds, two locomotives, trestle and tracks, and substantial gravel and concentrate (Annual Report, 1964). Production ceased after 1968, and resumed in 1972.

On commencement of production in 1972 the mine tailings were discharged from a new sub-tidal pipe, and tailings were monitored for compliance to discharge constraints (Ellis and Popham, 1983). The new tailings pipe, a 20 cm polyethylene line, was designed to extend 800 m to 12 m depth over the sand platform in Outfall Bay (Figure 83) (Ellis, 1980).

Breaks in the line continually occurred and were eventually left unrepaired at about 600 m from shore. During the two years of the mine's operation a tailings cone grew over the terminus and a copper-bearing sediment spread with longshore drift to at least Desolation Point (Ellis, 1980). Effluent constraints provided for all outfall to pass through a 200 mesh (0.074 mm) sieve (Ellis and Goddard, 1975). However, Ellis and Popham (1983) reported that a well-sorted fine sand beach of tailings (median particle size 0.15-0.20 mm) was built along Outfall Bay (Figure 83). In 1974 milling ceased.

III. Oceanographic Setting

Juan de Fuca Strait is considered to stretch from the confined channel, 22-28 km wide, between southwestern Vancouver Island and the Olympic Peninsula, east to include the wider area south and southeast of Victoria, into which Haro and Rosario Straits and Admiralty Inlet drain (Figure 1). For the purpose of this study the oceanography of the narrower western part of the strait is emphasized. Wind, wave and current regimes are important given their effects on the distribution and character of shelf sediments.

1. Water Circulation Patterns

Juan de Fuca Strait has an estuarine circulation in which there is a net seaward flow of low-density fresh water in the upper 100 m of the strait, replenished with dense seawater by inflow at depth (Herlinveaux and Tully, 1961). The excess volume of fresh water, largely from the Fraser River, is apparent when tidal streams are subtracted from the current meter records. Near the surface this residual flow has average seaward speeds of 0.1-0.2 ms^{-1} (0.2 to 0.4 kn), with maximum values close to mid-channel at the western end of the strait. The residual eastward flow within the lower layer averages 0.1 ms^{-1} and is strongest away from mid-channel (Thomson, 1981). Values for the ratio of ebb speed to flood speed are lowest (0.7) along the southern strait, in deep waters, and greatest (1.5 or more) in the shallower northern waters within the study area. Therefore,

greatest outflow is along the northern coast, with greatest inflow along the southern coast. This tilt is due to the combined effects of the Coriolis force and channel curvature (Thomson, 1981).

2. Tidal Currents

Geostrophic currents enter Juan de Fuca Strait from their northward movement along the west coast of Washington (Herlinveaux and Tully, 1961), and are subsequently altered by fresh water run-off, winds, bathymetry, channel curvature and Coriolis force. Initially, the tidal stream heads toward the Vancouver Island shore, but farther eastward is directed down-channel by the confining geometry of the basin. At maximum flood the water moves parallel to the axis of the strait at all points, at speeds of 0.75-1.3 ms^{-1} (1.5-2.5 kn) on large spring tides. Floods are stronger on the U.S. side of the strait, in part due to the right-turning Coriolis effect (Thomson, 1981).

Maximum ebb currents flow in the opposite direction to maximum flood currents, are slightly stronger and of longer duration on the northern side of the strait, than along the southern shores (Thomson, 1981). Near the mouth of the strait, ebb currents along the northern coast maintain their westerly direction as far as Cape Beale (northwest of Nitinat Lake) before merging with southwesterly setting ebb currents off the B.C. coast (Herlinveaux and Tully, 1961).

The estuarine circulation pattern distorts the

strength and duration of the tidal streams resulting in ebb currents which are stronger and of longer duration than flood currents in the top 100 m (Figure 4). At greater depths however, flood currents are normally stronger and of longer duration than ebb currents (Thomson, 1981).

As a result of the confined nature of the strait, the currents tend to be rectilinear, such that the direction of the flood and ebb are diametrically opposite with very little rotary turning (Figure 4). The flow of observed currents is generally parallel to the channel at all stages of the tide. However, the motion of strong currents deflected by points of land may cause the flow to deviate slightly, or cause the formation of backeddies if there is an accompanying increase in the width of the channel and the deflecting point is symmetric in shape (Thomson, 1981). Thomson (1981) shows the formation of eddies in Sooke Bay and west of Otter Point during the ebb along the northern shore. Due to frictional effects, nearshore tidal streams will be weaker than those in mid-channel.

Mean tidal ranges within the study area are slightly higher than 2.15 m at Point San Juan, decreasing eastward to approximately 1.85 m in Sooke Bay (Barker, 1974).

3. Bottom Currents

No studies of bottom currents are known to have been performed in Juan de Fuca Strait (R. Thomson, personal communication, 1990). Anderson (1968) noted that a net

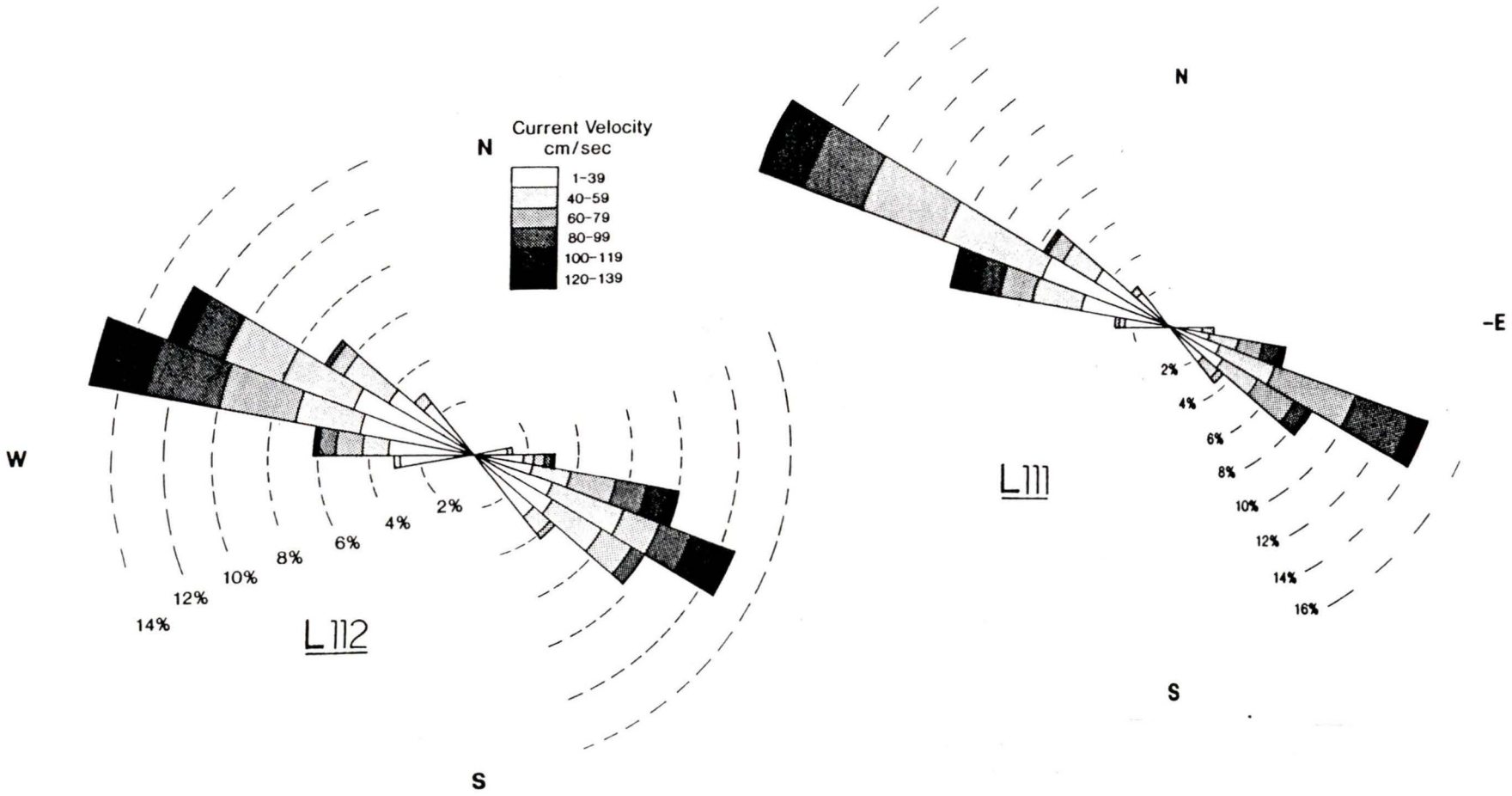

Figure 4. Current frequencies and rates for Stations L111 (at 15 m depth) and L112 (at 50 m depth) (Canadian Hydrographic Service, 1973). Data for both stations taken for a period of 60 days at 4 hour intervals. Location of Station L111 ($48^{o}23.3$ N, $124^{o}03.0$ W) and Station L112 ($48^{o}21.5$ N, $124^{o}02.5$ W) are indicated in Figure 21.

eastward drift at the bottom of the central portion of the strait was confirmed by sea bed drifter studies conducted by B.A. Morse, Department of Oceanography, University of Washington.

4. Wind Patterns

The prevailing oceanic winds approaching the British Columbia-Washington coast are from the southeast in winter and the northwest in summer. As winds enter Juan de Fuca Strait the flow of air is influenced by the adjoining mountainous terrain, resulting in wind directions that are easterly in winter and westerly in summer (Thomson, 1981). Easterly winds are associated with cyclonic oceanic winds of the Aleutian Low. As a result of funneling, wind speed generally increases seaward along the strait. Winds greater than 15 ms^{-1} (30 kn) occur 10-15 days per month in winter, and only 1-2 days per month in summer. Average winter winds over the western portion of the channel are 10 ms^{-1} (20 kn) (Thomson, 1981).

In summer, air flow is dominated by the North Pacific High off California, and winds from the northwest are redirected to westerlies within the strait. These are enhanced by a strong westerly sea-breeze component. Summer winds in the strait are from the west-southwest at about 4.5-9.0 ms^{-1} (8.7-17.5 kn). Winds from the southwest occur 75% of the time at Port Angeles during the summer months (Thomson, 1981).

5. Wave Conditions

As no direct measurements of waves have been made in Juan de Fuca Strait (Thomson, 1981), empirical wind-wave relationships were used to estimate heights at successive locations. Maximum attainable seas are limited by the total along-the-strait fetch of about 140 km, and the duration and strength of the wind. Seas generated by westerlies will likely encounter the shore before moving very far down the strait. Fully developed seas in Juan de Fuca Strait can attain significant wave heights of 1.5 m, or probable maximum heights of 2.7 m, for a 10 ms^{-1} (20 kn) wind blowing for ten hours over a fetch of 140 km. Only 10 percent of the waves in this example would be higher than 3 m. Generally, however, the fetch is significantly shorter, and fully developed seas would not exceed 2 m in height (Thomson, 1981).

From the mouth of the strait ocean swell propagates southeastward and alters the wave field by increasing the height of the seas and causing them to steepen. Maximum probable wave heights near the entrance to the strait, based on records off Tofino along the west coast of the island, may exceed 6 m at least 10% of the time in summer with periods of 6-20 s, averaging 9-10 s (Marine Environmental Data Service, 1976). Dispersion, refraction and dissipation will reduce the height of the swell as it moves inland (Thomson, 1981).

IV. Field & Analytical Methods

1. Field Techniques

Samples of surficial sediment and geophysical information for this study were derived from a variety of sources. Whole or part of three cruises in 1988 and 1989 conducted geophysical surveys and collected samples within the study area. Samples from previous studies, archived at Pacific Geoscience Centre (G.S.C.), were used, as well as beach and river samples collected in 1989 along the coast.

i) Offshore Samples

One hundred and fifty offshore samples were used in this study of which 83 were obtained from the archives at Pacific Geoscience Centre (G.S.C.). The latter were derived from two separate studies conducted at the Centre in 1979 and 1981.

a) Archival Samples

Samples from the earliest study consist of six transects between Sooke Bay and French Beach which were sampled by Harper (1980) in 1979 at a sample spacing of 100 m (Figure 5). Samples were taken during a one year survey program conducted to monitor seasonal morphologic changes of British Columbia beaches (Harper, 1980). The transects are normal to the strike of the beach or shoreline at each site. From east to west the six transects consist of 62 bottom sediment samples: 15 from eastern Sooke Bay; 3 from eastern Otter Point; 3 from western Otter Point; 15 off French

Beach; 11 off Sandcut Beach; and 15 off China Beach. Samples were obtained by Shipek grab sampler dropped from the *Seatech Jet* in water depths from less than 5 m to 23 m. Sample coordinates were obtained by an onboard microwave system; a Motorola Mini Ranger.

Textural data were determined for each sample, and sand subsamples were available in the archive for further analyses. The mud fractions were not retained.

In 1981, a study of sediment transport directions for beachface and shallow water sediments by McLaren (1983) resulted in the sampling of beach and nearshore sediments from Jordan River along the coast as far southeast as Sooke Bay. Twenty-one offshore samples have been used in the present study (Figure 5). These grab samples were obtained from depths between 2 m and 65 m, with 11 collected by Shipek sampler from the CSS *Richardson* and 10 collected by diver. Sample locations were determined by radar. Grain size analyses completed previously are used here. The archived sand subsamples have been further analysed in this study.

b) New Samples

Subsequently, additional samples were collected during two cruises and several dives from small boats, in order to represent more fully the entire study area. From these recent sampling programs 67 samples have been analysed.

A preliminary cruise by J.V. Barrie along northern

Juan de Fuca Strait in February 1988 collected 11 bottom sediment samples. The samples are mainly from sites in the northern half of the study area (Figure 5). Five grab samples were taken by Shipek sampler and 6 pipe dredge hauls were taken from the CSS *Tully*. Sample depths ranged from 15 to 87 m. Sample coordinates were obtained by Loran C and Global Positioning System.

In July 1989, 66 additional shipek samples were taken from the CSS *Parizeau*, at depths ranging from 12 to 101 m, of which 52 were analysed for this study (Figure 5). Navigation was by a combination of G.P.S. and Loran C.

During late August and early September, 1989, four dive sites, located adjacent to the four principal streams, were sampled. Samples were taken off the mouth of Jordan River, Muir Creek, Loss Creek and Sombrio River (Figure 5). Dives were taken from a sport fishing boat and large herring skiff in depths of 6-11 m. Samples were taken by plunging wide-rim glass jars into the surficial material and quickly capping, or scraping sediment from between cobbles. Several compass bearings placed on air photos were transferred to NTS 1:50,000 map sheets to establish the sample locations.

ii) Onshore Samples

Samples along the shoreline of the study area were used to obtain information concerning the heavy mineral content of the sediments in the intertidal zone. Samples collected for this study are not representative of overall

beach aggregate, but rather are samples of the finest sand or fines (excluding gravel) which could be obtained from the boulder strewn beaches. No grain-size data were determined for the samples.

a) Archival Samples

Fifty-three beach samples were used in this study, of which 38 were derived from an earlier study. The latter represent the beach component of samples collected for sediment transport studies in 1981 by McLaren (1983). The 38 samples were obtained from beach profiles at 17 sites (Figure 5). The number of samples taken along each profile varies from one to six depending on the size of aggregate and the width of the beach. The first profile is along the northwest shore of Sooke Bay, with the profile sites following the shoreline to the northwest as far as Sandcut Beach, about 2 km east of Jordan River. Pacing from each profile site to a known location provided a single pair of coordinates for the samples from each profile. Full grain size analyses were completed for these samples; subsamples were archived at Pacific Geoscience Centre and have been further analysed for this study.

b) New Samples

As noted above, additional samples of fine sand were collected along the shore of the study area. During June to August, 1989, 15 samples were collected at various beach sites accessible by foot or small boat (Figure 5). Samples

taken were located between archive profiles and where additional beach material could be found. The northern half of the study area had not been previously sampled.

Beach samples were taken using a hand trowel to scoop sand into plastic sample bags. Material greater than approximately 2 cm in diameter was discarded at this time. Sample material was often scraped from sediment around boulders to obtain any fines. An attempt was made to obtain the darkest fine sediment possible, or to locate fines in areas of constricted movement within the intertidal zone where concentration of heavier minerals may be favored. Sample sites were located on air photographs and transferred to 1:50 000 NTS map sheets.

In order to address questions of heavy mineral sources to the offshore sediments, four major streams which drain south into northern Juan de Fuca Strait were sampled above the highest tide mark. Two samples were taken from each of Muir Creek, Jordan River, Loss Creek and Sombrio River during the summer months of 1989 (Figure 5). Jordan River represents the most significant drainage area and is dammed more than 10 km inland.

At Sombrio River, Jordan River and Muir Creek the first river bars, which occur directly below the last significant change in stream gradient as the streams approached sea level, were sampled. These sites were generally 1 to 2 km from the stream mouth and adjacent to

narrow steepened gorges cut in bedrock, at elevations between approximately 3 m (Muir Creek) to 10 m above mean sea level. Large boulders and well-imbricated cobbles and gravel, generally representative of local bedrock, covered much of the bar surfaces.

The Jordan River site was similarly located but only poorly formed gravel banks exist below a large bedrock gorge.

Loss Creek descends through a bedrock gorge over 100 m to the strait in the last 1 km of its length. It was necessary, due to difficulty of access, to sample this stream 2.5 km upstream from its mouth. In this case, the last gravel bar on the stream immediately before its gradient steepened through a bedrock gorge, was chosen as the sample site. The bar is located at approximately 125 m elevation above mean sea level.

Two samples were taken from the bar on each stream; the first sample was collected from the upstream curve of the bar and a second sample was obtained from midway downstream on the bar, adjacent to the present water course. Sediment excavated from a sample hole and scraped from between adjacent cobbles was placed into a plastic 18 mesh sieve fitted over a five gallon (Imperial) plastic bucket. River water was poured over the mesh, washing through the material less than 1 mm in diameter. Larger material was dumped, the sieve was cleaned in the river, and the process

repeated. The routine continued until 2-3 kg of fines had been collected. Sample sites were fixed by air photo and transferred to NTS 1:50,000 scale topographic maps.

iii) Offshore Geophysical Data

During the two survey cruises conducted for this study, 382 km of geophysical survey track were collected.

In February 1988, 144 km in four survey lines were obtained from the CSS *Tully* (PGC88002). Each survey track ran parallel to the coastline (Figure 6) and included 3.5 kHz sub-bottom profiling, detailed high-resolution EG & G SMS 260 side-scan sonar and echosounding.

In March 1989, during CSS *Tully* cruise (PGC89003) additional geophysical data were collected for 238 km along 3 lines run in a zig-zag fashion oblique to the coastline, traversing the nearshore submarine terraces and their slopes (Figure 6). For each line four types of record were collected: 3.5 kHz sub-bottom profiles, Huntec DeepTow Seismic, EG & G SMS 260 side-scan sonar and echosounding.

Navigation during both cruises was provided by a combination of G.P.S. and Loran-C. Corrections were later made to coordinates of track sections run using Loran C.

iv) Sources of Error in the Field

a) Location Accuracy

Several types of error are introduced into a study during the course of geophysical data and sample collection. Navigation survey coordinates, and depths from which samples

are taken, involve errors in location measurements.

1) **X,Y Offshore**

Positioning accuracy during geophysical surveying and sample collection is dependent on the navigational system. As noted above, G.P.S. was the system employed, and system to which sections of Loran-C were corrected, during collection of the geophysical data during both cruises. Under normal conditions an accuracy of 50 m can be expected (R. Currie, pers. comm., 1990).

Sampling conducted during cruises in 1988 and 1989 was positioned using G.P.S. However, sites of earlier sampling programs were determined using several other systems or techniques. The Motorola Mini Ranger, used for sampling in 1979 has a measurement accuracy of 3 m within a range of 80 km (Thomson et. al., 1981). System capabilities compiled from original equipment manufacturers' published specifications (O.S.P.S., 1985) state that the instrumental accuracy for the Mini Ranger is a probable 2 m up to a range of 74 km.

Radar navigation was employed to position the 21 samples collected offshore in 1981. In this case, the sample coordinates can be expected to have an accuracy of 200 m (R. Currie, pers. comm., 1990).

Three or more compass bearings were used to locate the four dive sites conducted in 1989. Bearings were taken to recognizable points on airphotos. The bearings were

transferred to 1:50,000 scale NTS sheets, and through triangulation the point was determined. Assuming that a deviation of +/- 3^{o} could exist for a single bearing, a maximum error of 30 m along the shore at Jordan River, the dive point farthest from land, would be expected. If all three bearings had maximum deviations, then 90 m would be an expected error. In addition, the affect of a metal boat hull on the compass may be significant. Samples were taken at the anchor site which could have been up to 5 m distant from the surface point depending on the winds and currents.

2) **X,Y Onshore**

Sample sites for those samples collected in 1989 were marked on airphotos and transferred to NTS 1:50 000 scale map sheets. Air photos at a scale of 1:10 000 were used, so despite distortion along the edges of the photo, the greatest error, about 25 m, will be in positioning the point on the map sheets.

Archived beach samples collected in 1981 were positioned using pacing. The exact method used at the time is not available, but is likely to produce a similar minimum error as the previous method.

3) **Z, Depth**

Depths are recorded for all offshore samples, and are determined by echosounding. The accuracy of soundings are largely dependent on the properties of seawater which affect the velocity of propagation of acoustic waves in water.

Calculations are made using a general averaged figure for sound velocity through water for the area of study, generally assumed to be 1500 ms^{-1}. Other environmental sources of error may include the effects of waves, ship movements and meteorological changes in sea level. However, in general, depth determinations by echosounding are considered to be within 1 % of true depth (Thomson et al., 1981).

Depths of samples taken during dives were derived from scuba depth gauges. Accuracy of these instruments in the shallow waters sampled are less than 1 m.

Depths for samples were not corrected to any of the coastal reference surfaces, or datums, for tidal level at time of sampling. Within the strait, mean tidal ranges are low, from 2.0 m at Point No Point, to 2.3 m at Port Renfrew (Canadian Hydrographic Service, 1989). This general tidal range should be added to the 1 % error of the original depth measurement, resulting in minimum depth accuracies between 2.4 m (10 m depth) and 3.3 m (100 m depth).

b) Sampling Techniques

1) **Offshore**

Shipek grab sampler and pipe dredge were the sampling methods used in the offshore. Dredge samples represent a sample collected as the device is dragged for a short distance along the seafloor. For this reason the sampled material will not represent a point, but rather a length of

seabed.

All surficial sediment sampling underwater, including that performed by diver, is subject to some minor winnowing of fines during the sampling procedure or during ascent. However, the greatest error introduced by these techniques is in poorly defining the gravel content of an area. Cobble and boulder size material is not sampled, and can only be noted by a diver or observed on a sonogram. Capture of isolated coarse gravel clasts may also skew the sediment weight percentages resulting in an overestimate of gravel material.

Subsampling of Shipek grab samples is performed on the ship between sample sites for samples without gravel. Occasionally, subsampling of muds and sands may occur when minor gravel is present but undetected due to other debris such as shells or sponges. Samples with gravel cannot be accurately subsampled.

2) **Onshore**

Sampling techniques applied along the shoreline have been discussed previously, and it has been noted that samples taken in 1989 did not attempt to be representative of typical beach material or of the intertidal zone.

The sampling method used on the four stream bars was specifically designed to capture enough fine sand for geochemical analysis, as well as to compare the fine sand heavy mineral fraction with the fine sand heavy mineral

assemblages in the offshore. The sampling techniques are not likely to capture significant fine heavy-heavy minerals such as gold. Large boulders were not moved and significant depths within the sand bars were not reached. A notable amount of mud was unavoidably lost over the rim of the buckets during the washing process. Thus, although three or more kilograms of fine material were obtained at each site, less than 20 grams of mud were regularly obtained from each sample.

2. Laboratory Analytical Methods

All laboratory analyses were performed in the Sedimentology Laboratory, Pacific Geoscience Centre (G.S.C.), unless noted otherwise.

i) Laboratory Techniques

a) Sample Fractionation

Samples were brought into the laboratory and emptied into pyrex or enameled containers and dried in 80^{o}C ovens. Exceptions to this were the eight river samples and six dredge samples from 1988, which were left wet in the five gallon buckets.

Subsampling of dried samples occurred when no gravel was present and when the sample was greater than approximately 300 gms. The whole sample was weighed in large stainless steel bowls, then stirred and halved repeatedly until a desired weight of material remained. Generally, mud content prohibited the use of coning and

quartering. Samples with gravel were not split.

The six dredge samples were subsampled by digging through the mud and sand in the buckets. Five of the samples had gravel sized material, but had to be subsampled in order to perform analyses. The resulting subsamples were about 1 kg in weight.

The weighed dry samples (subsamples) were then soaked overnight in a 10% solution of sodium hexametaphosphate, following the procedures described by Ingram (1971). This dispersal procedure largely removes clay particles adhering to sand grains.

Samples were then separated into gravel, sand and mud components by wet sieving (Figure 7) through W.S. Tyler brass sieves with stainless steel meshes of 2 mm and 0.063 mm (U.S. Standard sieve mesh Nos. 10 and 230). Mud passing through the 0.063 mm sieve was retained via a wide-mouth funnel in large beakers. A sample was washed until the water was clear. Muds were retained for all samples collected for this study except the fifteen beach samples.

Large shells were separated from gravel retained on the 2 mm sieve where feasible. Gravel found in beach samples was not retained. Gravel, shell and sand fractions were placed in 80^{o}C ovens to dry.

The eight river samples were subsampled during the washing process. Eight buckets each contained several kilograms of fine material smaller than 1 mm in size. In

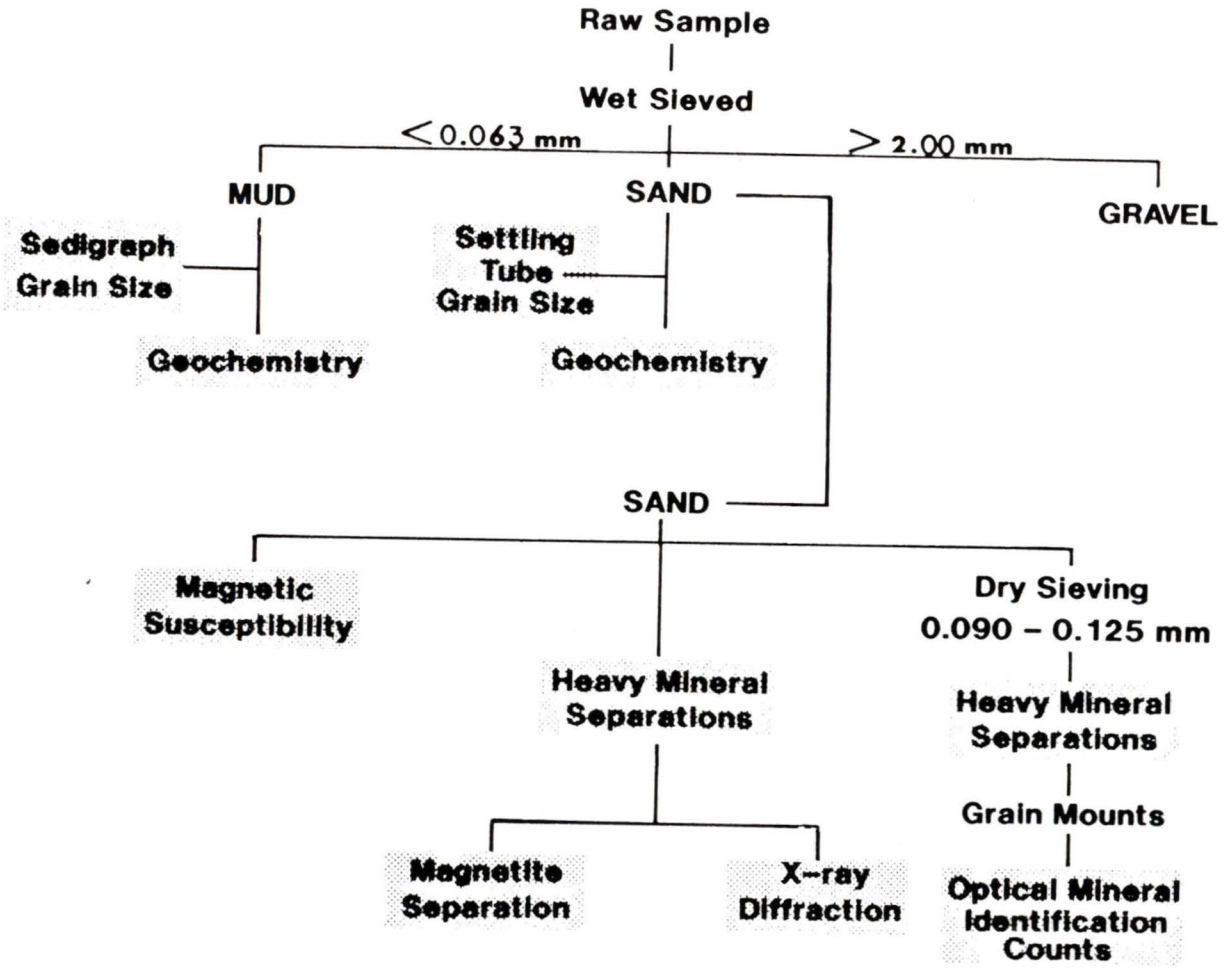

Figure 7. Flow chart for laboratory processing of samples from northern Juan de Fuca Strait. Sands from adjacent beaches and rivers were not analysed for grain size.

order to reserve a significant amount of the mud content of the entire sample, water was repeatedly poured into the bucket which was then decanted through a 0.063 mm sieve. Eventually, the sand was subsampled through the bucket and placed on the sieves, an additional "raw" sample was retained, and the bottom 2-3 cm of sand and fines were poured over the sieves as the buckets were cleaned. The sandy material not retained or washed was discarded.

Offshore samples were found to have high silt contents, necessitating the use of a second 0.063 mm sieve once the first became clogged. Such samples were often large (400 to 900 gm), due to the presence of gravel, and required several days to wash.

Following wet sieving, the muds from each sample, suspended in beakers of wash water, were concentrated by centrifuging. Samples were spun for 90 minutes at 2000 rpm in an I.E.C. Model K Industrial Centrifuge. Following each spin the clear water was decanted and new muddy water added over the mud coating the bottom of the containers. Eventually all mud from a sample was collected in one plastic bag, spun, and covering water decanted. Muds were then frozen and freeze-dried. The latter technique extracted the water from the sediment through sublimation, and provided a sample that was easily disaggregated.

The dried sand and gravel components of each sample were weighed and percent data calculated for each fraction.

Weight of mud was determined by difference.

All archive samples used in this study had been previously washed, and no muds had been retained.

b) Textural Analysis

1) **Sand**

Sands were analysed for grain size using a 2-m settling tube, with an internal diameter of 20 cm, filled with distilled water at room temperature. Following Stokes' law, with corrections for sand size fractions, the actual physical size or diameter of a grain is not determined, but instead the "sedimentation diameter" is ascertained, a function of particle size, shape and density (Galehouse, 1971*a*).

A sample is adhered to the bottom of an inverted plate, using Kodak Photo-flo 200, which is lowered to the water surface at the top of the tube. At the moment of contact the sand grains are released and fall through the water. They are collected on a suspended plate 2 m below water surface, which is connected to an electronic balance which records the cumulative weight over time. Software developed at P.G.C. allowed the information to be fed directly to an IBM-PC microcomputer. A real-time curve is displayed on the screen and subsequent grain-size fractionation results are derived based on the experimental work of Gibbs, Mathews and Link (1971).

Each sample was split, using a micro-splitter, for two

2.0 gm (+/- 0.1 gm) subsamples. Water temperature was recorded, and each of the two subsample splits were run for 10.5 minutes. Heights of the cumulative curves from the two runs are averaged in the subsequent computer calculations.

Analysis of sand fractions of all offshore samples were completed. As noted previously, grain size analyses were not performed on the beach or river samples. Archive samples from 1981, both beach and offshore, had previously been analysed for grain size. However, grain size analyses of the 62 offshore samples taken in 1979 had not been previously done, but were determined in this study.

2) **Mud**

Grain size analysis of the clays and silts in the mud portion of the sample were analysed by Sedigraph (Micromeritics, 5000D, Particle Size Analyser). This instrument records decreasing attenuation of an X-ray beam by particles, over time, establishing particle size through settling, as determined by Stokes' law.

Mud samples were stirred and approximately 2-2.5 gm of dried sample were placed in a 50-ml beaker and mixed with 40 ml of 0.5% sodium hexametaphosphate solution. An ultrasonic probe was immersed into the liquid, and the sample sonicated for one minute to ensure complete dispersion of the clay particles. The beaker contents were placed within the operating cell to equilibrate with the compartment temperature. At the time a sample is run, temperature is

recorded and the related "rate" is set. The latter is a number which programs the Sedigraph to solve Stokes' law for a particular fluid viscosity (Sarracino and Forbes, 1981). Samples were stirred by magnet and circulated through the glass cell until the computer is prepared to record the analysis. Once the computer is activated, and the sedigraph is initiated, the circulation ceases, and recording of the beam attenuation begins. A sample is run until the reverse cumulative curve reaches the equivalent spherical diameter of 0.0004 mm, which occurs after about 40 minutes. Software completes sample statistics by extrapolating the slope to 0.0002 mm.

The mud fractions of 14 offshore samples, chosen to best represent the general nature of the mud content in the area of study, were analysed by Sedigraph. Four archive samples from the offshore had previously been analysed for their mud fractions. Information collected from Sedigraph analyses were merged with data from settling tube analyses and tabulations of complete grain size were produced.

3) **Gravel**

The gravel component of all samples was not analysed for specific size fractions in this study.

c) Separation of Heavy Minerals

The separation of light and heavy minerals of the sand fraction of the sediment was performed on 156 samples. In addition, the 3.0 to 3.5 phi fraction of 26 of these samples

were separated and subsequently mounted for optical examination (discussed below). The non-toxic, high density medium, sodium polytungstate ($3Na_2WO_4.9WO_3.H_2O$), manufactured in West Germany by Sometu, was used as the separating agent. During the analyses its specific gravity was recorded before each set of separations. The heavy liquid was kept at specific gravities between 2.97 and 3.06. The technique employed was adapted from Smith (1988) for the Sediment Lab at P.G.C., based on concepts discussed by Carver (1971) and Callahan (1987). The use of sodium polytungstate and the centrifuge method was shown to have favorable results in the study of analytical techniques by Hein (1989).

Sand samples were split and 5 gm subsamples retained for separation. Sets of 4 to 10 samples were separated at one time. Each sample was weighed to 0.0001 gm and emptied into a numbered, 10 cm x 2 cm centrifuge tube. The specific gravity of the sodium polytungstate was measured, recorded, and then approximately 45 ml of the heavy liquid was added to each tube, bringing the surface to just below 1 cm from the top of the tube.

Each sample was mixed with the heavy liquid in the tube using a vortex mixer until the sample was floating in the liquid, and only individual mineral grains remained on the bottom of the tubes. The procedure took about one minute. The plastic tubes were then centrifuged for 15

minutes at 2000 rpm.

Once retrieved from the centrifuge, most samples displayed varying amounts of dark heavy minerals at the bottom of the tubes and a thick cap of lighter minerals, up to 5 mm thick, at the top of the liquid. Some samples had a very limited amount of the fine fraction dispersed in the heavy medium which had not separated, and were interpreted to be close to the specific gravity of the liquid.

Each tube was held in liquid nitrogen to freeze the bottom half of the liquid, up to 1 cm below the light mineral plug, until solid (about 40 to 60 seconds). The floats were poured off into large coffee filters and the tube rinsed with warm deionized water. Samples were rinsed of all sand grains down to within 1 to 2 cm of the heavy mineral plug at the bottom of the tube. The heavy mineral plug was rinsed into a labeled Whatman #4 filter. A water soluble, thin white precipitate occasionally occurred with the heavy minerals in the bottom of the tube. This was rinsed into the filter with the heavy minerals, during which time it dissolved. Samples were repeatedly washed with deionized water, and then moved to a sink and rinsed with distilled water. Filters holding each sample were placed in beakers and dried in a low temperature oven (about 40 to 50^{o}C) overnight.

Dried sample filters were opened over clean white paper and brushed until all sand grains were removed from

the filter. The heavy mineral grains were then weighed, from which the heavy mineral percent was calculated.

Generally, the light mineral fraction was not retained. However, light minerals were kept for grain mounts and to occasionally calculate error percentages in analyses. When light minerals were kept, a similar procedure was used as above, except Whatman filters were used for both halves of each sample. Rinsing was similar to that noted above, except if the sample was very large it was rinsed more often.

The sodium polytungstate was reclaimed from the samples by capturing the undiluted heavy liquid from the coffee filters, and reconcentrating the diluted liquid from the rinsed filters. Evaporation of excess deionized water from the liquid eventually brought the specific gravity back to the range of 3.00. Prior to re-using, the sodium polytungstate was filtered for impurities and centrifuged. The clear liquid was decanted into plastic bottles and any precipitate was discarded.

d) Magnetic Susceptibility

Ferromagnetic minerals produce an induced magnetization M when placed in a weak magnetic field H. The ratio $x = M/H$ is the *magnetic susceptibility*, a dimensionless quantity in relation to a unit volume of material. *Magnetic susceptibility* divided by the density is equal to the specific susceptibility (Currie and Bornhold,

1983).

The magnetic properties of rocks are generally related to magnetite content, although other minerals, such as ilmenite, are of minor significance. For this reason the term *percent magnetite equivalent* is used when testing for *magnetic susceptibility*.

A magnetic susceptibility meter, the Bison 3110-6 meter, was used to determine the percent magnetite equivalent (range: 1.26×10^{-3} to 1.26 SI units). In this instrument a primary coil is set opposite two secondary coils in voltage opposition. When an AC current is induced by the primary coil a null voltage output occurs. When a sample (with magnetic material) is placed between the primary and two secondary coils, a second current is generated and the rectified output is relative to the magnetism of the sample; recorded as *percent magnetite equivalent*. The meter is pre-calibrated in the factory using known quantities of magnetite (Sheehan, 1989).

Magnetic susceptibility readings were taken on sand splits (Figure 7) placed in plastic containers which conformed closely to the dimensions of the sample holder of the meter. The containers were 3.8 cm in diameter and 5.1 cm in height. When adequate quantities of sample were not available, small glass vials were used instead, and placed in the center of the sample holder, and a correction factor for diameter and height was applied (Sheehan 1989). True

density as opposed to apparent density was also computed for the sediment samples: *true magnetic susceptibility* (x 10^{-6}) = (m x 10)X_cY_cD where m = magnetic susceptibility meter reading; X_c = corrected sample diameter; Y_c = corrected sample height; D = corrected sample density.

The instrument was recalibrated approximately every ten samples. Samples periodically retested to assess measurement variability, were found to have values (cgs units) which deviated by an average of 2% (Sheehan, 1989).

e) Separation of Magnetite

Magnetite was removed by hand to determine its quantity, and thereby significance, in the heavy mineral separates (Figure 7). Only a few minerals are ferromagnetic (strongly attracted by a simple hand magnet), the two most common being magnetite, Fe_3O_4, and pyrrhotite, $Fe_{1-n}S$ (Berry and Mason, 1959). Pyrrhotite is an unstable mineral (Table 1) and would not likely be found in the marine environment.

Magnetite was removed from the heavy mineral separates of the whole sand fraction for 64 samples. Magnetite removal was achieved by using a bar magnet wrapped tightly in onion skin paper. Pre-weighed heavy mineral samples were distributed on paper to minimize grain overlap. The magnet was then used to extract magnetite and deposit it on an adjacent sheet of paper. The magnetite was then weighed and a heavy mineral fraction percentage was calculated based on raw sample weight (Sheehan, 1989).

f) Grain Mounts

To facilitate optical identification of minerals comprising the heavy mineral fraction of the sand, grain mounts were made (Figure 7). Of the 156 samples with heavy mineral fractions separated, 26 were chosen for optical examination to best represent the study area. The sand fraction was dry-sieved for the selected phi range and heavy mineral separations were performed on the limited sand fraction. The heavy mineral separates were then permanently mounted on glass slides.

Choice of sample fraction for optical examination was determined specifically for this study in the absence of an established standard size fraction (Carver, 1971). Carver (1971) discusses the range of practices in this area, such as studies of reproducibility by Van Andel and Poole (1960) in which mineralogy was found to be independent of grain size in the 0.063-0.500 mm fraction and van Andel (1964) which found percentages of some minerals correlated with the median size of the sample for grains larger than 0.063 mm. Clifton and Luepke (1987) illustrated (in their Tables 2 to 5) the variety of size ranges used by various researchers studying heavy-mineral placer deposits along the Pacific coast of North America. Barrie (1978) noted that individuals involved in provenance studies using heavy mineral suites commonly use only a limited size range for separation and mineral identification. Carver (1971)

suggested that it is desirable to restrict heavy-mineral studies to a single size class narrow enough to produce uniform optical effects and thus reduce or eliminate variation in heavy-mineral proportions caused by differences in grain size of the samples.

However, the variety of mean grain sizes within the study area, from coarse beach material to fine sands and silts at 100 m depth, suggests it will not be possible to characterise the full heavy mineral suite using any one limited size fraction. Beach and river samples, examined for provenance source or path, often consist of coarse rock fragments which eliminate the usefulness of the sample. As a compromise, J.V. Barrie (pers. comm., 1989) suggested the 3.0 to 3.5 phi range (0.090 to 0.125 mm) as an approach to minimize rock fragments, maximize the volume of heavy minerals available in low concentrations in offshore samples, and still retain an adequate sample size for mineral identification with minimal errors.

Samples were dry sieved in a pair of clean screens of 0.090 mm and 0.125 mm size (U.S. Standard sieves No. 170 and 120). Samples were poured over sieves, placed in a Ro-Tap mechanical shaker, and operated for 15 minutes (Ingram, 1971). Sieves were subsequently cleaned, fractions weighed, and the 3.0 to 3.5 phi fraction placed in a labeled vial. Heavy mineral separations were then conducted on this fraction as described earlier. Grain mounts were created in

a manner similar to that of Swift (1971) with minor modifications.

g) Mineral Counts

Quantitative mineralogy of sand grains was determined by optical identification of minerals (Figure 7) which was then expressed as percentages. This was performed by the ribbon method summarised by Galehouse (1971*b*). In this technique the grain mount is placed on a stage attached to the polarised microscope, and minerals are identified along traverses within a certain band, or ribbon width. In this case the width of the band was equal to the viewing field of the microscope. All grains, or minerals, which entered the field of view were identified. Traverses were randomly arranged over the slide, and traverses maintained by stage gauges. The result of this method may be considered a number percent (Galehouse, 1971*b*).

For each slide at least 300 grains were counted, including at least 200 non-opaque minerals. The level of accuracy which is desired will determine the number of grains which must be counted. Hubert (1971) illustrated the 95% confidence limits for including the real population means in a series of sample sizes. This indicated that an increase in precision occurs from 50 to 250 grains, but does not decrease the confidence interval enough to justify the additional time spent making the analysis. Finally, a minimum count of 200 non-opaque grains is commonly seen in

the literature by the majority of heavy mineralogists (Barrie, 1978).

h) Geochemical Analyses

Two suites of samples were submitted to commercial laboratories for geochemical analyses, one in 1989 and another in 1990.

In February 1989, trace element analyses of marine sediments were performed for 51 samples of sand or mud (Figure 7) selected from archive suites and the 1988 *Tully* cruise samples with reference to magnetic susceptibility values (27 offshore and 24 beach samples). Analyses were performed by Bondar-Clegg & Company Ltd., North Vancouver, B.C. Fire assays for gold, platinum and palladium were performed on 14 of the samples and inductively coupled plasma-atomic emission spectroscopy (ICP-AES) was completed on all 51 samples for the following 17 elements;

Ag	Fe	Pb	Ti
Bi	Hg	Sb	V
Cd	Mn	Se	Zn
Cr	Mo	Sn	Zr
Cu.			

Samples were treated with a multi-acid digestion for extraction prior to ICP-AES analysis for 16 of the elements. Analysis for Hg was completed by use of hot-extraction technique using HNO_3-HCL and employing Cold Vapour Atomic Absorption Spectrophotometry. Discussion of these techniques is found in Fletcher (1981).

In June 1990, a second suite of samples was submitted

to Chemex Labs Ltd., North Vancouver, B.C. The 59 samples were composed of sand or mud (Figure 7) fractions from beach and offshore samples collected during the summer of 1989 in addition to other archive samples of interest (41 offshore and 18 beach samples). Insufficient material from the earlier sample set remained so that the 1990 samples represent a totally different sample set, although samples in both years may occasionally alternate along beach profiles or offshore transects (as at Sandcut Beach).

Eighteen samples, including sand and mud fractions, underwent fire assay for gold, platinum and palladium. They were subsequently analysed for 19 other elements; the 17 listed above with the addition of Co and Ni. Sand or mud fractions of 56 additional samples were analysed for these 19 elements. Duplicate subsamples were submitted for two samples in order to indicate precision of the analytical values.

Analytical procedures differed from the 1989 geochemistry not only in the lab which performed the work, but in the methods used to detect some elements, and the required digestion to extract more completely a specific element from the sample. A nitric acid-aqua regia digestion and ICP-AES was used for Co, Cu, Fe, Mn, Mo, Ni, Pb, V, and Zn. Digestion by nitric acid-aqua regia and analysis by Atomic Absorption Spectrophotometry (AAS), with background correction, was performed for Ag and Cd. Digestion by HCl-

$KClO_3$ and analysis by AAS was employed for Sb and Bi, again with background correction. X-ray Fluorescence was used to measure Ti and Zr. For Hg, HNO_3-HCl was used for digestion, and Flameless AAS was employed. Finally, digestion and extraction for Se were performed by NH_4I sublimation and analysis by AAS. These techniques were suggested by the laboratory chemists for this project. Description of these digestion and geochemical analytical methods are given by Fletcher (1981).

i) X-ray Diffraction Analysis

In the spring of 1989, the heavy-mineral separates from the whole sand fractions (Figure 7) of six offshore samples were submitted to the Analytical Sciences Laboratory, British Colombia Geological Survey, Victoria, B.C., for X-ray diffraction analysis. This technique was employed to assist in the initial stage of optical identification of minerals. The samples represented the range of water depths and heavy mineral concentrations within the samples. A description of the theory and methods employed in this form of analysis is given by Nicol (1975).

ii) Sources of Error & Variability in Analytical Techniques

Raw samples brought into the laboratory undergo successive processes each of which has inherent possible sources of loss, contamination, or introduction of other inaccuracies. Some of these sources of error and variability between samples, which appear relevant to this

project, are discussed below.

a) Subsampling

Subsampling of raw samples introduces an initial possible major error in the grain size ratios and contents of the subsample. Attempts were made to minimize this by stirring samples, and equipment was cleaned between samples to minimize contamination. During sieving (both wet and dry), stretching or bending of the 0.063 mm screen mesh was possible (Ingram, 1971), particularly for samples with a high silt and sand content. Screens were cleaned between samples to minimize contamination.

Subsampling for geochemistry, grain size analyses, and all subsequent work (Figure 7), again introduced possible error. Mud fraction (powder) was stirred in its plastic bag, and then sampled for the requisite amount; sand was split using a microsplitter. Although the instrument gave relatively even splits, by weight, the more often a sample was split, a steady increase in the loss of fines could be observed around the microsplitter. Since samples were large, numerous splits were often required to halve the sample. To avoid loss of fines, samples were split a minimum number of times to reach the required sample weight.

b) Textural Analyses

Settling tube analyses require a constant viscosity throughout the length of the tube. The continued introduction of Photo-flow to the water column may have a

minor effect on viscosity as it builds up before the tube is drained and cleaned. Temperature changes are also significant if the water does not warm or cool evenly over the length of the tube. Temperature changes as large as $3^{o}C$ over eight hours were noted. However, the averaging effect of two runs per sample should correct for most instrument errors.

Sedigraph samples are particularly prone to temperature changes between the room and much warmer X-ray compartment. In addition, the sample is initially stirred a few minutes within the compartment by means of a magnetic stirrer. After completion of an analysis it can be seen that the magnets may be heavily covered in scavenged magnetite (and possibly ilmenite). If the latter mineral is largely represented in one size range, it will introduce a significant error in that size fraction.

Both the Sedigraph and settling tube depend on applications of Stokes' Law and subsequent theoretical extensions, such as outlined by Gibbs et al. (1971). Errors in determination of physical dimensions and density of sand grains will occur due to the use of settling velocity as the sizing technique. However, this study is concerned with the recent sedimentological history of an area, and as Galehouse (1971a) suggested, sedimentation analysis, using settling velocity, will give useful relative physical sizes which are a function of grain shape and density laid down at a

particular time and a particular place, and will therefore tend to be more valid than techniques describing physical parameters alone.

d) Geochemistry

Concentrations of elements obtained as a result of different acid digestions and different analytical methods, with different detection limits preclude their values being combined. In addition, identical analytical tools and digestions may still yield varying results between labs, due to operator variation and distinct sample preparation methods. The techniques used for the second sample set were chosen to ensure full extraction of the element from the minerals present, and total analysis of their abundance. Detection limits listed in Appendix C, along with the geochemical results from both years, give an indication of magnitude of error for each element and detection technique.

e) Heavy Mineral Separation

Heavy mineral separation techniques necessarily evolved during the course of laboratory work. Initial separations weighed raw sample and resulting heavy residue by difference, within the filter. Filters, however, will retain some heavy residue, and so cannot be used in this manner. This error was corrected in later analyses, and weights were taken before and after separation and drying, without the filter. Early results of whole sand fraction separations were corrected by using weights recorded for

heavy minerals before magnetite extraction. Those values will represent, at worse, minimum heavy mineral values, as there will likely have been some minor loss in transfers in and out of the plastic vials. Lights were retained for four samples (whole sand fraction) to calculate error in recombined weights. Sample totals ranged from 99.79% to 100.20%, average errors of 0.21%, based on samples weighing on average 5.4 gm. Errors for separations performed on the 0.125-0.090 mm fraction were similarly calculated from 5 samples of recombined weights. Sample totals ranged from 98.25% to 100.02%, with average errors of 0.41%. These latter results are based on samples with a smaller average weight of 3.4 gm.

Two samples had separations performed on nearly equal weighted splits to compare heavy residue weights. Comparisons of results by percent weight yielded differences of 0.08% and 0.15%.

Several errors occur in the separation technique. The sodium polytungstate varied in specific gravity between 2.97 and 3.06, with most samples performed with the liquid at greater than 3.00. Two samples were separated with the liquid at 2.93. This variation in specific gravity between samples will produce some variation between results if minerals within that range, such as chlorite or biotite, are abundant in the samples.

Washing floats from the tubes, after freezing the

heavy mineral sinks, involved a decision as to when the few grains dispersed in the heavy liquid (which did not settle or float during centrifuging) were heavy or light minerals. In general grains were washed out with the floats to within one centimeter of the sinks.

e) Magnetite Separation

Hand separation of magnetite presented several sources of error. The inclusion of associated magnetic minerals, such as titanomagnetite or pyrrhotite, might occur; magnetite grains may be missed if sheltered by larger grains; and the transfer of magnetite to another sheet, all present possible sources of error. Rock fragments which contain significant magnetite may be separated and introduce error into the weight percent calculations for magnetite.

V. Surficial Geology

1. Surficial Sediments

Delineation of the surficial sediment distribution was based on the acoustic geophysical records and the results of grain size analyses performed on offshore samples. Textural changes of the surficial sediments, interpreted from side-scan sonograms, were used to delineate specific units which were then defined by sample descriptions and data. Surficial sediments are classified using a modified scheme after Folk (1974).

The distribution of surficial sediments along the northern strait shows an overall fining with water depth away from the terraces adjacent to much of the coast, and from west to east (Figure 8). In these shallow, nearshore areas, where the terraces slope from intertidal zone to 30 m depth, coarser sediments predominate. Gravelly sand (gS) is dominant along the nearshore zone from Point San Juan to Sombrio Point, east of which mud becomes significant. Southeast of Loss Creek, sandy gravel (sG) covers the nearshore to China Beach where it narrows and becomes restricted to an area farther offshore, although shallower than 20 m, and continues southeast past Point No Point.

Sand (S) (>0.063 mm and < 2.0 mm) is distributed in a broad shallow area along the shore from China Beach to the western side of Sheringham Point. It is also found in the nearshore zone at Loss Creek and to the southeast from the

creek's mouth.

Isolated patches of gravel (G) (>2.0 mm) occur, generally close to shore, but an area of significant gravel accumulation is present along the edge of the shallow terrace several kilometres off Magdalena Point. Below this terrace there are a series of gullies, or short channels, which appear to funnel debris downslope.

Distribution of sediments which contain significant amounts of mud (<0.063 mm) are found below 30 m. In terms of the seafloor morphology these depths are associated with slopes and areas of topographic low, particularly facing northwest, away from prevailing current direction. Towards the northwest, muddy-sandy gravel (msG) is found along slopes south of Sombrio Point to depths of 100 m. Similar sediments are found along the slopes below Jordan River to Point No Point, and in the nearshore area of Sooke Bay.

Gravelly-muddy sand (gmS) occurs nearshore in the broad shallow northwest sloping area south of Sombrio River, and in a similarly sloping area south of China Beach, at greater depths. This unit also extends over much of Orveas Bay from shallow depths to 100 m.

Muddy sand (mS) was the most distinctive and consistent textural unit identifiable on sonar images given its high absorption (light images). The unit is well evidenced at many sample sites. Generally the unit begins abruptly at the base of the terrace slopes, usually near 80

m depth, and extends farther offshore forming a sediment wedge which extends southward into the strait. In Sooke Bay muddy sand predominates into the nearshore, and similarly occurs as the surficial sediments at the mouth of Port San Juan. Muddy sand also occurs in areas of low gradient in Orveas Bay and in patches a few hundred metres from shore along extensive beach areas (China Beach and Sandcut Beach).

i) Analysis of Grain Size Distribution

Moment statistics of sediments finer than 2 mm were used to characterise the samples. Values were plotted and contoured to analyse their geographic distribution. A tendency to extend contour values parallel to the trend of the shoreline did not appear justified by sample values. To test for any anisotropy in the sample value distribution, variograms were constructed.

Mean, mode and standard deviation (sorting) of a sample may be termed regionalised variables because there is assumed to be a relationship between the value of these properties and their relative positions. In constructing the variograms it was assumed that the difference in value between two positions in the sediment distribution depends only on the distance between them and their relative orientation (Clark, 1979). Models were fit to variograms (Appendix A) whose resulting ranges of influence strongly support extensive shore-parallel relationships for all three properties, and relatively restricted ranges of influence

for samples in the direction perpendicular to the coastline (Table 2).

TABLE 2. Variogram results for grain-size statistics.

	Range of Relationship	Angle of Pairs	Pairs used	Model Type
MEAN	6000 m	120°	6057	spherical
	400 m	200°	224	spherical
MODE	9000 m	120°	6057	linear
	600 m	200°	224	linear
STANDARD DEVIATION	15000 m	120°	6057	linear
	300 m	200°	224	linear

The distribution of mean grain size (Figure 9) for the entire study area suggests only a general decrease in grain size occurs with depth (range 0.76 to 4.54 phi, coarse sand to coarse silt). Terraced areas contain coarser material, medium to fine sand, with slopes and deeper water containing fine sand to silt. The main exception to this general pattern occurs off Sombrio Point where mean values of very fine sand occur near the river mouth and occupy much of the broad shelf which slopes to the southeast and southwest. A similar pattern was suggested by the surficial geology units discussed earlier.

Moving northwest to southeast along the nearshore, more detailed patterns are evident. At the mouth of Port San Juan very fine sand extends into the strait, whereas to the east coarser sediments occur along the northwest shore adjacent to Loss Creek and Providence Cove (0.76 and 0.98 phi, coarse sand).

The finest mean grain sizes (4.54 phi, coarse silt) are found below one of the steepest terrace scarps southwest of Mystic Beach. The complex pattern described by the sample transect off China Beach suggests the development of a coarser lag of sand to the southeast of the headland, west of the beach. Shoreward of this sand an area of fines has developed, with sample means of coarse silt.

Adjacent to Jordan River a tongue of medium to fine sand extends from the river mouth onto the terrace infilling a depressed area of 10 to 15 m depth. The sampled transect off Sandcut Beach shows the inverse trend of increasing mean grain size away from shore. East of Point No Point all sediments are finer than 2.0 phi (fine sand).

A similar, but less distinct, pattern to that found near Sandcut Beach is present at French Beach. The significance of this inverse trend can be related to relative abundance of heavy minerals, which will be discussed later.

A histogram of the sample means suggests a normal population (Figure 10), although a cumulative probability plot (Figure 11) shows several inflections which would invite a polymodal interpretation. Sinclair (1981) describes such patterns as representing polymodal data which can be explained as the combination of several intersecting or non-intersecting populations. It is possible that one population dominates the others by an order of magnitude or

more.

An understanding of the mean grain size distribution was enhanced by dividing the samples into western and eastern subsets along a line at 416 000 E, west of Mystic Beach. Western samples had a mean depth of 42 m, compared to 17 m in the east. An F-test of the two sample set variances supports the hypothesis that the two variances are not the same. Whereas the whole sample set revealed a significant correlation (at the 0.005 level; one-tailed test) between depth and mean grain size ($r=0.48$), the western samples show a much improved correlation ($r=0.63$), with mean grain size decreasing with depth. A lower significant correlation ($r=0.34$) is observed in the eastern subset.

A division of the whole sample population by average terrace scarp depth, 30 m (Figure 12), attempts to represent grain size distributions covering the shallow platforms, as opposed to those which characterise the sediments in deeper water (Figure 13). Mean grain size shallower than 30 m is 2.7 phi, and below 30 m the mean is reduced to 3.4 phi. This suggests that the size of the sample set above 30 m (65 %) will dominate the analysis of trends in the mean.

The distribution of sample modes (Figure 14) displays a number of trends which did not exist with the sample means. Between China Beach and Sheringham Point no relation is evident between the modal grain size, depth or distance

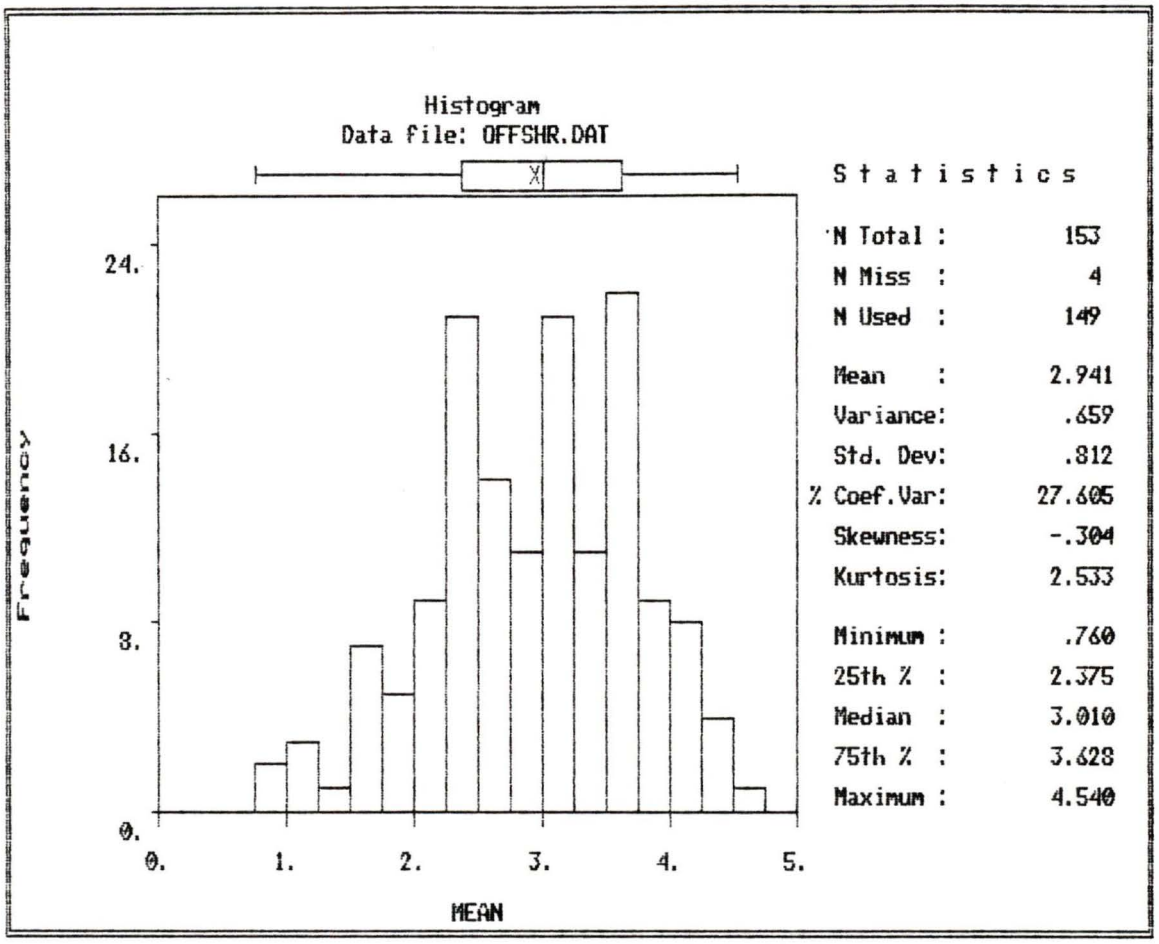

Figure 10. Histogram of mean grain size, in phi units, of sand fractions of 149 offshore samples from the study area. Four additional sample sites returned no sample or insufficient sample for analysis.

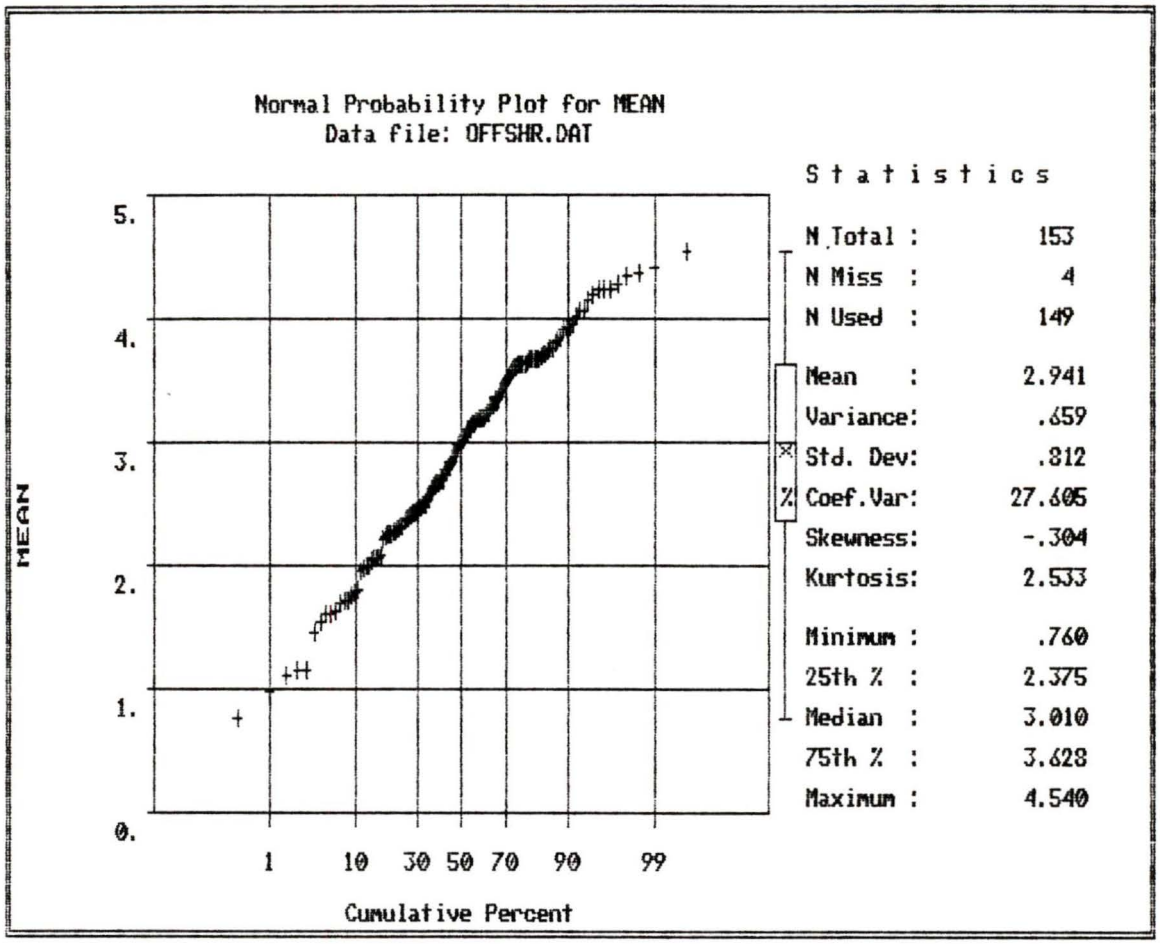

Figure 11. Probability plot of mean grain size, in phi units, of sand fractions of 149 offshore samples from the study area.

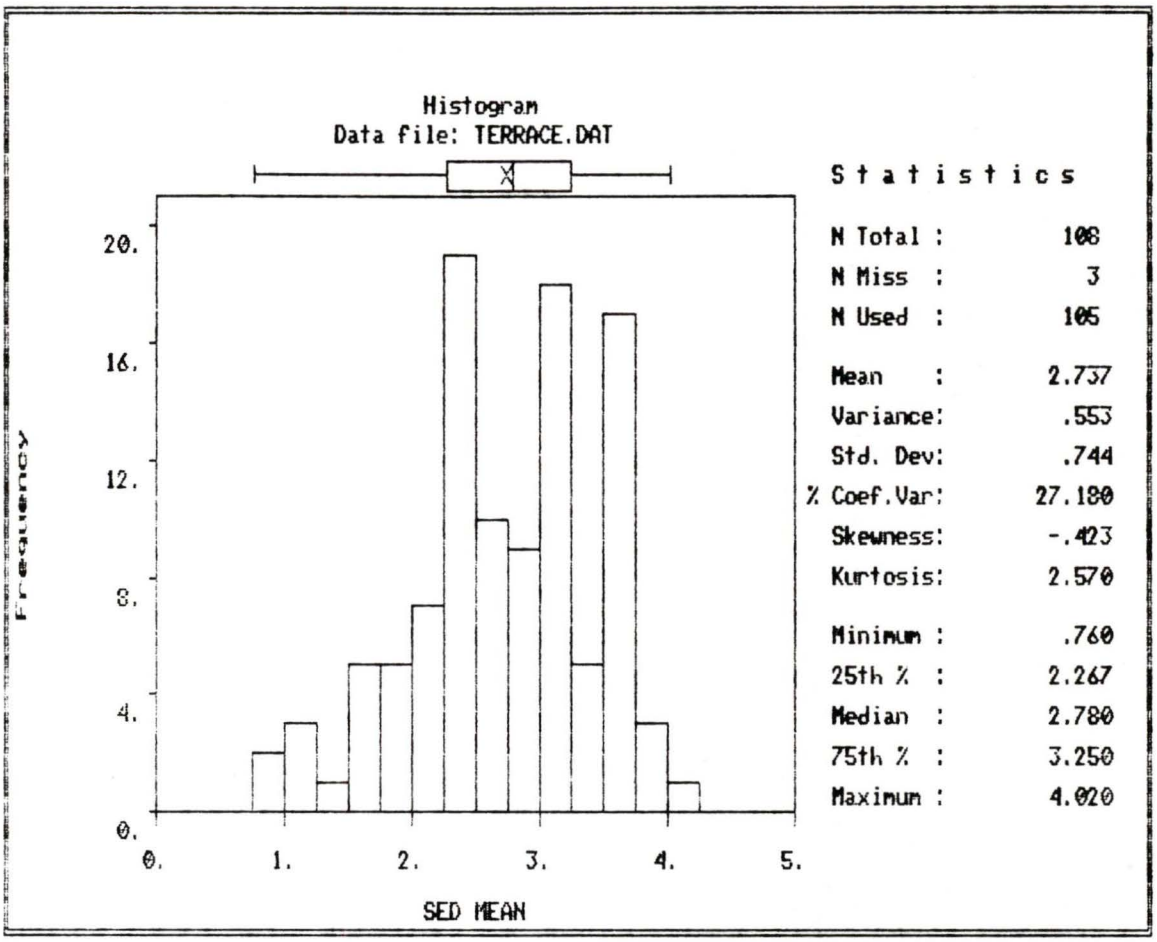

Figure 12. Histogram of mean grain size, in phi units, for sand fractions of 105 samples taken from a depth of 30 m or less, within the study area.

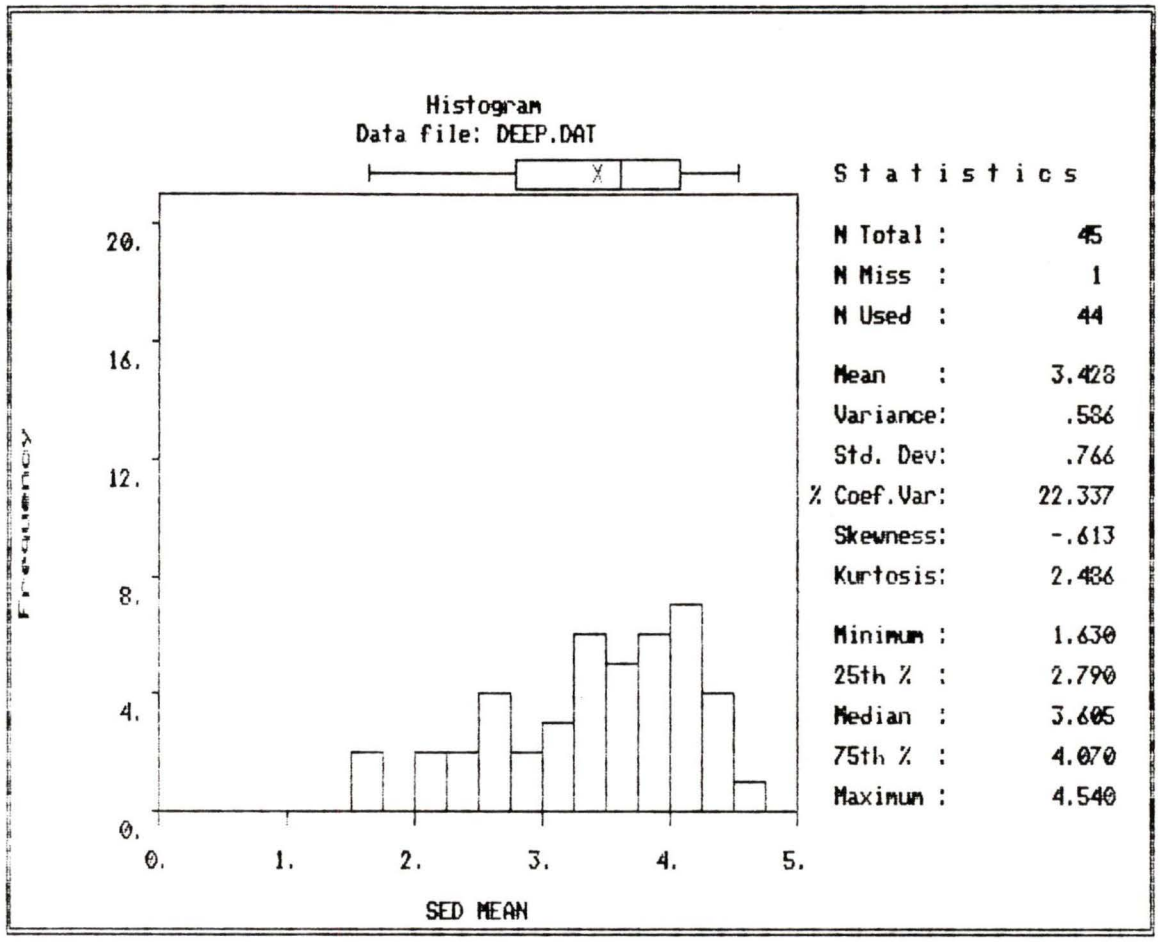

Figure 13. Histogram of mean grain size, in phi units, for sand fractions of 44 samples taken from depths of greater than 30 m within the study area.

from shore, or direction east or west. The distribution of sample modes also shows a distinctly finer modal grain size from China Beach eastward. The only exceptions to this are a few coarser nearshore samples. Northwest of Mystic Beach and east of Sheringham Point sample modes do show a general decrease in size with depth.

A comparison between modal and mean sample sizes shows a general trend for sample modes to be coarser than sample means. This relation suggests individual sample grain-size distributions tend to be positively skewed towards the finer grain sizes. Distribution of modes for the whole sample set (Figure 15) shows a slight negative skewness.

Three extensive nearshore areas sampled by offshore transects at China, Sandcut and French Beaches, all show a pattern of fining grain size for several hundred metres offshore, followed by coarsening of samples starting at about 800 m from shore. This trend is also apparent with the sample mean. Sediment from Jordan River may have a slight coarsening effect on the adjacent terrace.

A significant change occurs in the shallow platform area near Sombrio River and Loss Creek where samples with means of fine and very fine sand have sample modes of coarse and medium sand. The area is mapped as gravelly-muddy sand and will be shown to be very poorly sorted. This material may be derived from the erosion of shallow exposures of Sooke Formation.

East and west modal distributions (Figures 16 and 17) reveal significant coast-parallel changes. The modal size in the east is 2.25 to 2.75 phi, fine sand. To the west this size fraction is nearly absent. Sample mode distributions in the west are separated into a very fine grained component (2.75 to 3.5 phi) and a coarser component of medium-grained sand (1.25 to 2.0 phi). As noted previously, the western very-fine sand may be attributed to a much greater mean sample depth than in the east. The fine sand which predominates in the east may reflect the finer, less stable volcanic source rocks which extend as far as Sombrio Point from the southeast. Samples taken near the mouths of Jordan River and Muir Creek are 2.0 phi or finer.

In the west, medium sand (1.25 to 2.0 phi) forms the second modal group. This size range is poorly represented in the east, suggesting its source may be the metasediments and metavolcanics of the Leech River Complex which extends along the shoreline west of Sombrio Point. The western population of modes is negatively skewed showing a group of coarse grained sands. The coarse sands may reflect the coarser, although softer, metamorphic minerals found in shallow waters. Samples obtained near the mouths of both Loss Creek and Sombrio Rivers, which drain the metamorphic rocks, are composed of coarse sand.

A third modal group appears in both east and west, between 2.75 and 3.5 phi, fine to very fine sand. This

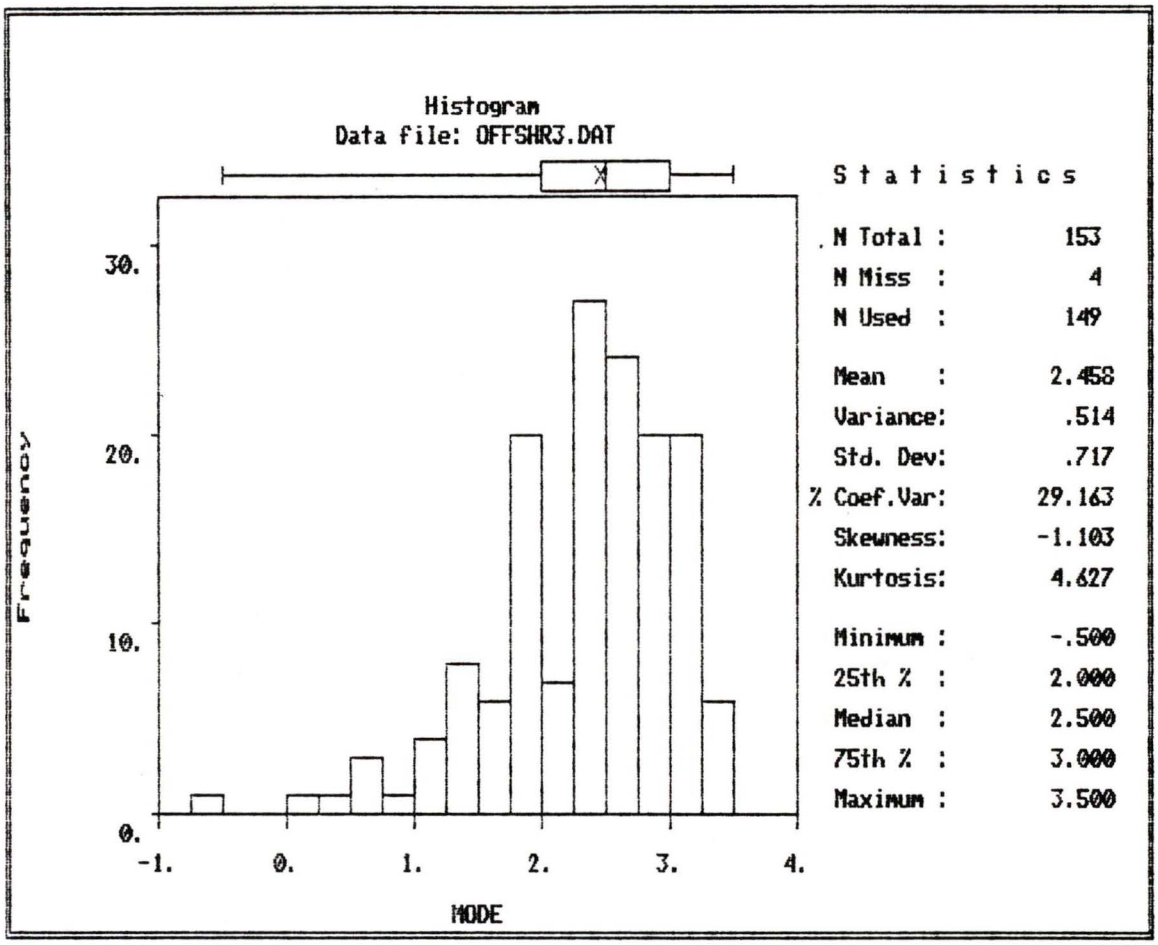

Figure 15. Histogram of grain size modes, in phi units, for sand fractions from 149 offshore samples within the study area.

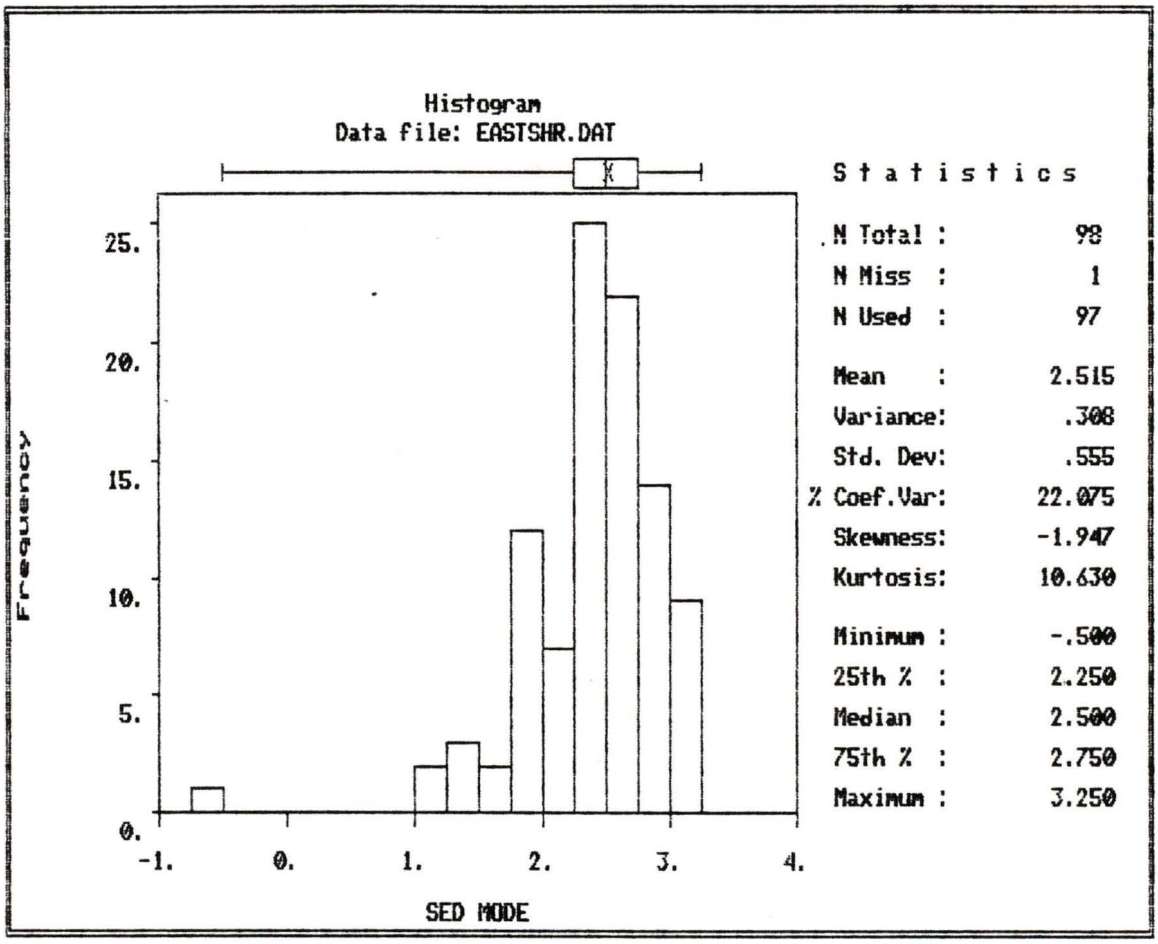

Figure 16. Histogram of grain size modes, in phi units, of sand fractions from 97 offshore samples located within the study area but east of 416 000 E (UTM) (west of Mystic Beach).

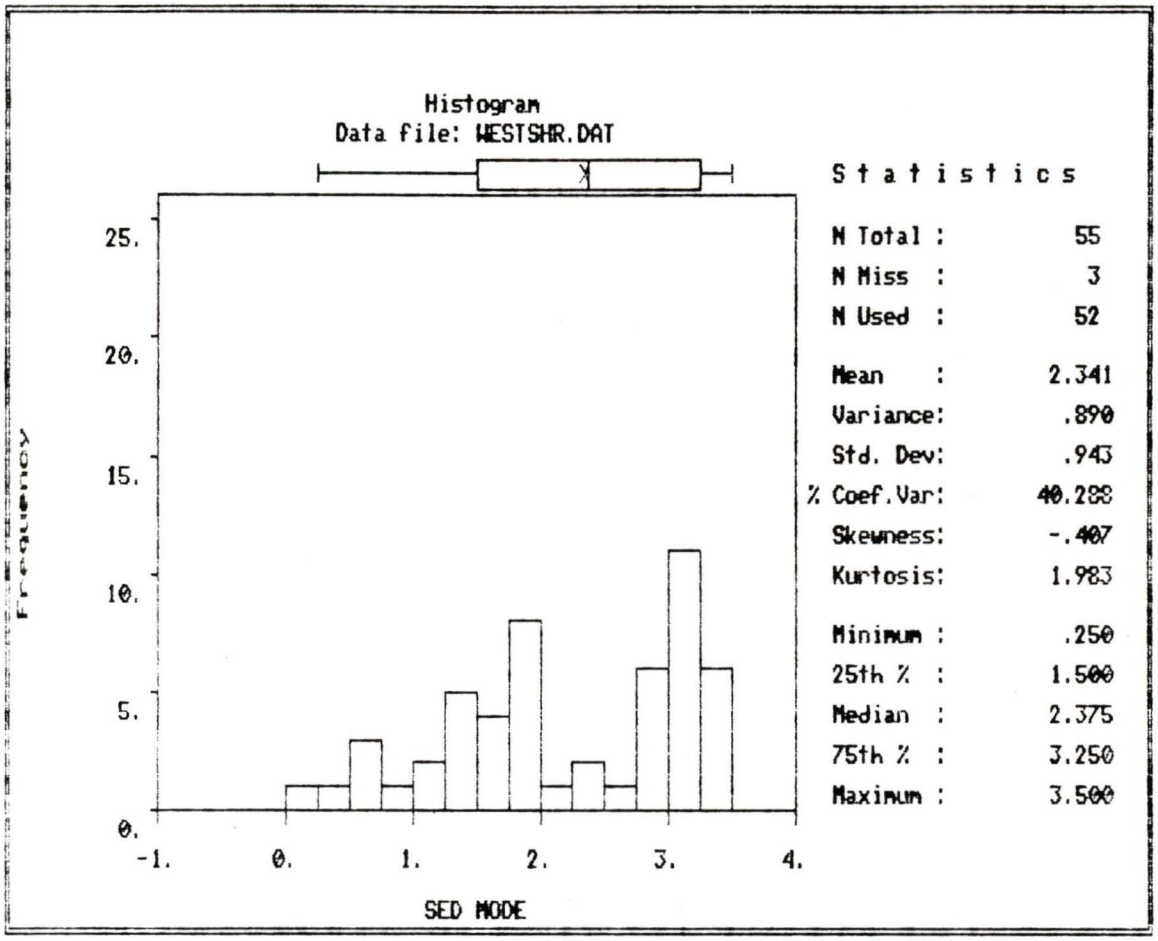

Figure 17. Histogram of grain size modes, in phi units, of sand fractions from 52 offshore samples within the study area but west of 416 000 E (UTM) (west of Mystic Beach).

modal group may be the contribution of eroding fine sands of the Sooke Formation along coastal bluffs and nearshore platforms.

Standard deviation (sorting) shows no regional shore-parallel change along the northern strait (Figure 18). Samples are moderately (0.5 to 1.0) to poorly sorted (1.0 to 2.0) with a few samples very poorly sorted (Figure 19). Eastern and western sample subsets show very similar distributions, with the majority of very poorly sorted samples originating in the west, as would be expected with the greater mean depth.

Sample sorting is highest (well sorted) in shallow water adjacent to three eastern beaches, Sandcut and French Beaches, and along eastern Orveas Bay. Moderate sorting is found along most of the nearshore particularly off Loss Creek and east of Jordan River, in waters less than 20 m in depth. However, anomalous patches of moderately sorted samples are found in deeper waters, notably southwest of Mystic Beach, occurring to depths of 90 m.

With increasing distance from shore, samples are poorly sorted, and the deepest samples are commonly very poorly sorted. Samples off Muir Creek show relatively poor sorting, particularly in the channel area. However, the poorest sorting occurs off Sombrio River and off Magdalena Point (Figure 20). Of the very poorly sorted samples, the two off Sombrio River have been shown to be medium to coarse

sand with grain size distributions strongly skewed to silt. Very poor sorting on what is otherwise a high energy platform area would suggest samples were from material (Sooke Fm) weathering *in situ*.

Sorting generally decreases with depth and decreasing grain size, as illustrated by the well-sorted very shallow nearshore samples and the more poorly-sorted, muddy sand at the base of terraces. However, this is not borne out by statistical correlations. It is probable that sorting decreases with distance from shore, with less relation to actual water depth. This contention is supported by the variogram results (Table 2) which show a large shore-parallel range of influence for sorting, 15 km, and a very short range, 300 m, for sorting normal to the coast.

2. Seabed Features

i) Terraces

Slope breaks, or scarps, for the shallow terraces described in the bathymetry (Chapter 2), are depicted on the high-resolution geophysical records (Figure 21) (Plates 1 and 2). The successive terrace breaks have a consistent strike of 106^{o} and extend from the shallow terrace tops, at 10 to 30 m, to depths of 70 m where they grade into gentler slopes. Terrace slopes range from 4.4^{o} to 5^{o}, with the steepest slope of 14.5^{o} occurring below the terrace promontory southwest of Magdalena Point.

The presence of indurated rock outcropping below

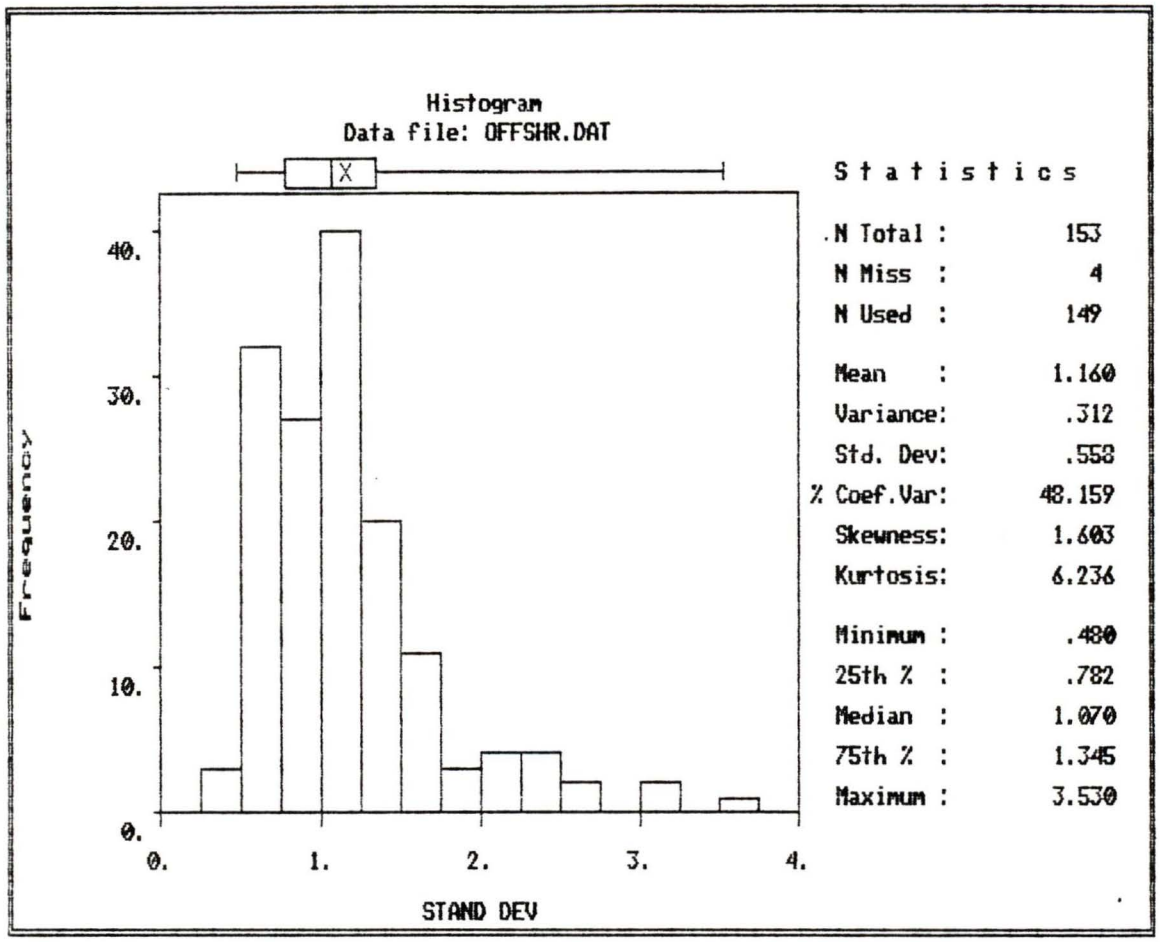

Figure 19. Histogram of sorting values (standard deviation), in phi units, for sand fractions from 149 offshore samples obtained within the study area.

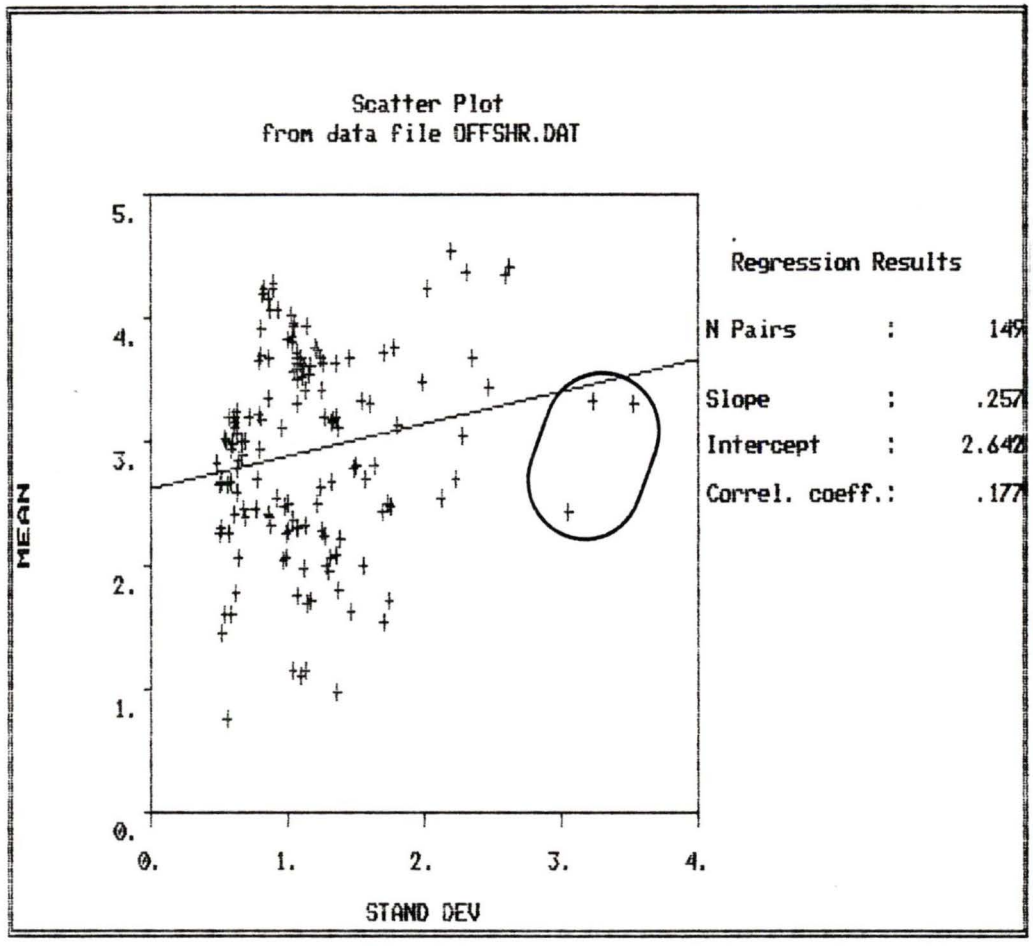

Figure 20. Crossplot of sample sorting (standard deviation) and sample means, both in phi units, for sand fractions from 149 offshore samples taken within the study area. The three very poorly sorted samples encircled may originate from the *in situ* weathering of underlying substrate.

terrace scarps was observed in a few locations. Geophysical records are ambiguous about the substrate which underlies the terraces. Larger outcrops of bedrock were observed in Sooke Bay and in deeper water south of Orveas Bay. The latter outcrop rises more than 30 m above the seafloor. Layered sediments adjacent to the outcrop on the north and northeast sides are considerably thicker than sediments on the south and southwest sides by up to 20 m.

ii) Channels, Gullies and Debris Flows

Southwest of Magdalena Point the terrace scarp, at 30 m depth, is dissected by a large channel feature (Figures 2 and 21), described in Chapter 2. Geophysical records indicate that little or no sediment accumulation occurs within the feature. A sample taken within the channel consisted of fine sand. In deeper water, at the base of the channel, some coarser textured material and gravel is present. The channel may act as a conduit for sediment transport to deeper water.

A second channel, 200 m in width, is found nearshore, with its head at the mouth of Muir Creek, extending to the southwest where it ends at the terrace scarp. The channel is relatively flat-floored and presently contains cobbles overlain by a thickening veneer of fine sand (sample dive site). Kelp leaves which were strewn over the bottom had a thin layer of fine sediment accumulating over them suggesting sediment load from the adjacent stream is

significant. This channel appears to be a relict feature, presently being buried by sediment.

Directly south of Magdalena Point the terrace scarp is broken by a succession of gullies stretching for at least 3.5 km parallel to the scarp. These features are well defined on geophysical records, the gullied scarps appear as areas of strong reflection (dark image) outlined by the strongly absorbing muddy sand (light image) in deeper water at their base (Plates 3 and 4). Samples taken along the scarp consist of gravel, with muddy-sandy gravel from the gullied area, and muddy sand or sandy mud at the base.

Gravel can be observed directly at the foot of these gullies and within the eroded features, although only one distinct debris fan is observed, in a separate gully 600 m farther east. In this instance, the fan extends to the southeast and has a width of 250 m.

Along the seafloor south of the rocky shoreline at San Juan Point, survey lines twice cross over what are likely two sections of one channel. The scoured conduit is 250 m wide and 5 m deep as observed in the geophysical record at just above 40 m depth. A deeper section occurs at 70 to 90 m depth (Plate 5). The channel appears to have been eroded into the substrate material. Below this conduit, towards the southwest, a fan of coarse debris can be observed. The debris fan has a width of over 200 m, extending south below 110 m depth (Plates 5 to 7). Two areas of similar submarine

slide or small debris flow deposits occur directly to the west.

Offshore from Loss Creek in 8 m of water, parallel channels, greater than one metre in depth and width, are eroded into the sandstone substrate with orientations roughly normal to the shore. Scarce fines were observed during the dive and ultimately resulted in the sampling of a single ripple found in one channel. Similar channels have been observed between San Juan Point and Providence Cove 200 m from shore at 20 m depth (D. Swanston, pers. comm., 1990).

iii) Boulder Fields

Extensive fields of boulders can be observed on the shallow terraces in two main areas, off Jordan River and the Sombrio River - Loss Creek area (Figure 21). Situated in waters generally less than 30 m deep, the boulders are largely confined to areas of slight depression or gentle slope. Sidescan images suggest some boulders may be as large as 3 m in diameter (Plate 8).

Boulders 1 m or greater in diameter were encountered while diving for samples in 10 m of water off the mouth of Sombrio River. Rounded boulders were stacked to heights of 3 m, and sat on exposed indurated sandstone bedrock (Sooke Fm). Only occasional openings resulted in exposed bedrock at these sites and the only fines observed were small sandy oscillation ripples.

Since geophysical surveys were not extended to shallow

waters (less than about 15 m), it is likely that the areas of boulder fields extend closer to shore.

iv) Sedimentary Bedforms

Ripples of varying dimension and orientation occur on the seafloor along the northern strait (Figure 21). Most ripples had amplitudes less than 0.5 m, making some occurrences difficult to classify as to their genesis, since knowledge of ripple profile was lacking. The term dunes (Ashley, 1990) has been introduced for flow-transverse ripples where spacing is 0.6 m or greater. Ashley (1990) classified dunes by spacing and height as follows:

	small	medium	large	very large
Spacing	0.6-5 m	5-10 m	10-100 m	> 100 m
Height	0.075-0.4 m	0.4-0.75 m	0.75-5 m	> 5 m

Small, medium and large dunes are identified within the study area. Wave-induced oscillation ripples are the second bedform type identified within the study area.

Dunes (Ashley, 1990) were found in water depths ranging from 10 to 135 m, with greatest frequency in two depth ranges, 10 to 20 m on the shallow terraces and between 70 and 90 m, often at the base of terrace slopes. The latter represents 40% of the 48 dune occurrences recorded by sidescan sonar. Crests of dunes are primarily oriented north-northeast to south-southwest (Figure 22), normal to the strong ebbing tidal current (Chapter 3) at 280^{o} to 310^{o} (Figure 4). Dune migration appears to be to the northwest towards the mouth of the strait. Amplitudes are generally

less than 0.5 m, the resolution of the Huntec Deeptow Seismic System in use. However, amplitudes as great as 2.4 m are observed at the base of terrace slopes, with highest amplitudes occurring at the steepest point of dune advance (Plates 1 and 2).

Dune wavelengths range from 1.5 to 30 m. Small dunes (0.6-5 m) represent one fifth of the observed dunes, and were restricted to water depths of less than 70 m. Medium dunes (5-10 m) represent the modal size group, although a large number of dunes are found with wavelengths between 15 and 20 m. Mean wavelength of the observed occurrences is 11 m, significantly smaller than the mean wavelength of 25 m observed for dunes throughout Hecate Strait (Barrie and Bornhold, 1989).

Both 3-dimensional and 2-dimensional dunes are present, as well as occasional compound dunes (Ashley, 1990). Bifurcation of the crest in the 2-dimensional dunes is common. Samples obtained adjacent to dune fields reveal proximate sediments of muddy-sandy gravel and gravelly-muddy sand. Although no bottom current data are available, the current velocities recorded at a moored current meter above one of the terrace slopes (Station L111, Canadian Hydrographic Service, 1973) (Figure 4) at a depth of 15 m below sea level (approximately 30 m above the slope) suggest the bed current velocities necessary for dune formation (2-dimensional), 40-60 cms^{-1} (Amos and King, 1984), are

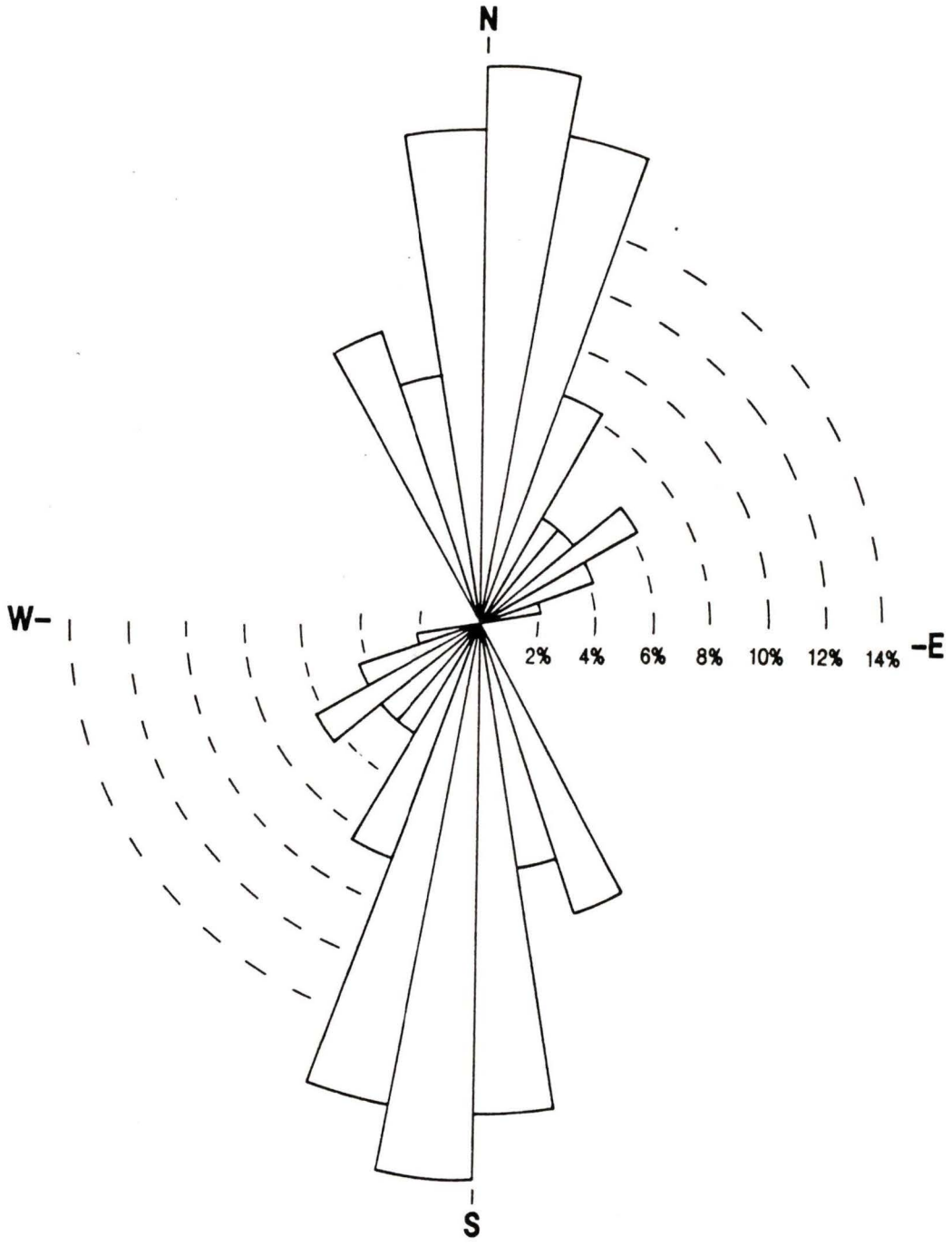

Figure 22.

Orientation frequency of dune crests (crest-parallel), northern Juan de Fuca Strait. Location of dune fields shown in Figure 21.

present.

The presence of a thin veneer of muddy-sand in dune troughs (Plates 1 and 2) between coarser material (sand) is difficult to interpret without bottom current data. It is possible that the majority of these bedforms are storm-generated and may be considered only intermittently active.

Wave or oscillation ripple fields occur in greatest numbers west of Mystic Beach, where nearshore waters experience the greatest exposure to the dominant direction of ocean swell. These ripples tend to have long parallel crests, and are frequently recognised only by sediment lineation where crest amplitudes are too low to be resolved by the sub-bottom profiles (i.e. less than 0.5 m). They are observed to depths of 90 to 110 m, with crests striking generally east-southeast to west-northwest. Ripples group into two general depth ranges, 10 to 30 m and a deeper set, generally greater than 90 m (Plate 7).

Ripples in shallow water have spacings of less than 5 m and occur on the terraces. During a dive in 9 m of water, near the mouth of Loss Creek, symmetrical oscillation ripples of coarse sand were found oriented sub-parallel to the coast (155^{o}) with a height of about 15 cm and spacings of 20 cm. These ripples occurred on exposed sandstone bedrock which has been eroded into small channels (just over a metre deep and wide, and several metres long) oriented normal to the shore.

Also in shallow water (less than 20 m) are patches of "confused bedforms" found in shallow depressions (Figure 21) which may be areas of combined tidal current and wave oscillatory movement. A few ripple occurrences classified as oscillation ripples, generated on low slopes, had a general crest orientation parallel to the axis of the strait, but were too poorly imaged or irregular in plan to classify or describe further.

Sedimentary structures, tentatively identified as ripple crest lineations, observed in water depths greater than 90 m are generally aligned parallel to the axis of the strait. These bedforms have been categorized as oscillation ripples given their orientation and parallel trend. Amplitudes were not observed, and only one spacing measurement was attempted, giving 1-5 m.

Formation of oscillation ripples may be modified by superimposed predominantly unidirectional bottom currents, although the nature of these is unknown in the area. Oscillation ripples have been described in similar depths on the continental shelf of northwestern Vancouver Island, although in coarser material by Yorath *et al.* (1979) and Bornhold and Yorath (1984). Symmetrical oscillatory ripple marks were observed in sand as well as coarser material at various depths as great as 204 m on the Oregon continental shelf by Komar *et al.* (1972).

Conditions necessary for generation of oscillation

ripples (Komar and Miller, 1974) are met by the surface wave heights and periods estimated by Thomson (1981) (Chapter 3). Maximum waves in the strait are greater than 3 m, 10 % of the time, thus meeting the threshold of sediment motion for fine sand at 90 m depth (with wave periods of 15 seconds). However, near the mouth of the strait ocean swell will heighten the waves such that they will be greater than 6 m, 10 % of the time, with periods commonly from 9 to 10 seconds, but reaching 20 seconds or more (Thomson, 1981). These waves meet the requirements of height and period necessary to move fine sand at depths greater than 110 m, based on wave periods of 15 seconds (Komar and Miller, 1974). Clearly the incidence of waves with heights and periods long enough to allow sediment motion at depths of 100 m or more is limited, and restricted to the northwestern end of the strait.

v) Moraine, Lineations and Observations on Sediment Thickness

The surface expression of a hummocky moraine persists under a veneer of modern sediments several metres thick near 100 m water depth, directly south of Sombrio Point (Figure 21, Plate 9). Elsewhere moraine was observed at greater depth in the sub-bottom, with no surface expression.

Complete discussion of sediment thickness and sub-bottom morphology are beyond the range of this study. However, a few observations from the shallower seismic

reflection profiling are relevant to the present surficial sediment discussion.

The shallow terrace morphology which occupies much of the nearshore strait appears to consist of bedrock or morainal material with only a thin veneer of sediment. This sediment surface is generally not observable in profiles, being therefore less than approximately 0.5 m thick. In areas of shallow depressions sediments up to several metres in thickness can be observed, although these areas tend to be discontinuous, occurring in patches with diameters of 50 m or less. Morainal, structureless material with point reflectors, was observed in the sub-bottom records near Otter Point, Sooke Bay and adjacent to the mouth of Port San Juan. A thick wedge of (bedded) glaciofluvial sediments extends from the mouth of Port San Juan effectively burying a terrace similar to those to the southeast.

Diving observations and coastal outcrops suggest that the sandstones of the Sooke Formation extend out to a kilometre from shore underlying part of the nearshore terrace in some locations.

Lineations created by narrow negative and positive structural features observed on the terrace tops and slopes (Figure 21) do not reveal any one general orientation. These lineations varied in length and may be due to diverse causes or sources, including glacial souring, weathered fault planes or joints in bedrock.

Bases of terrace slopes are onlapped by a thick sediment wedge stretching towards the centre of the strait. Two areas of thickest sediment accumulation are south of Muir Creek, Orveas Bay, and Port San Juan. The last is effectively burying a shallow terrace which is plainly revealed in sub-bottom profiles.

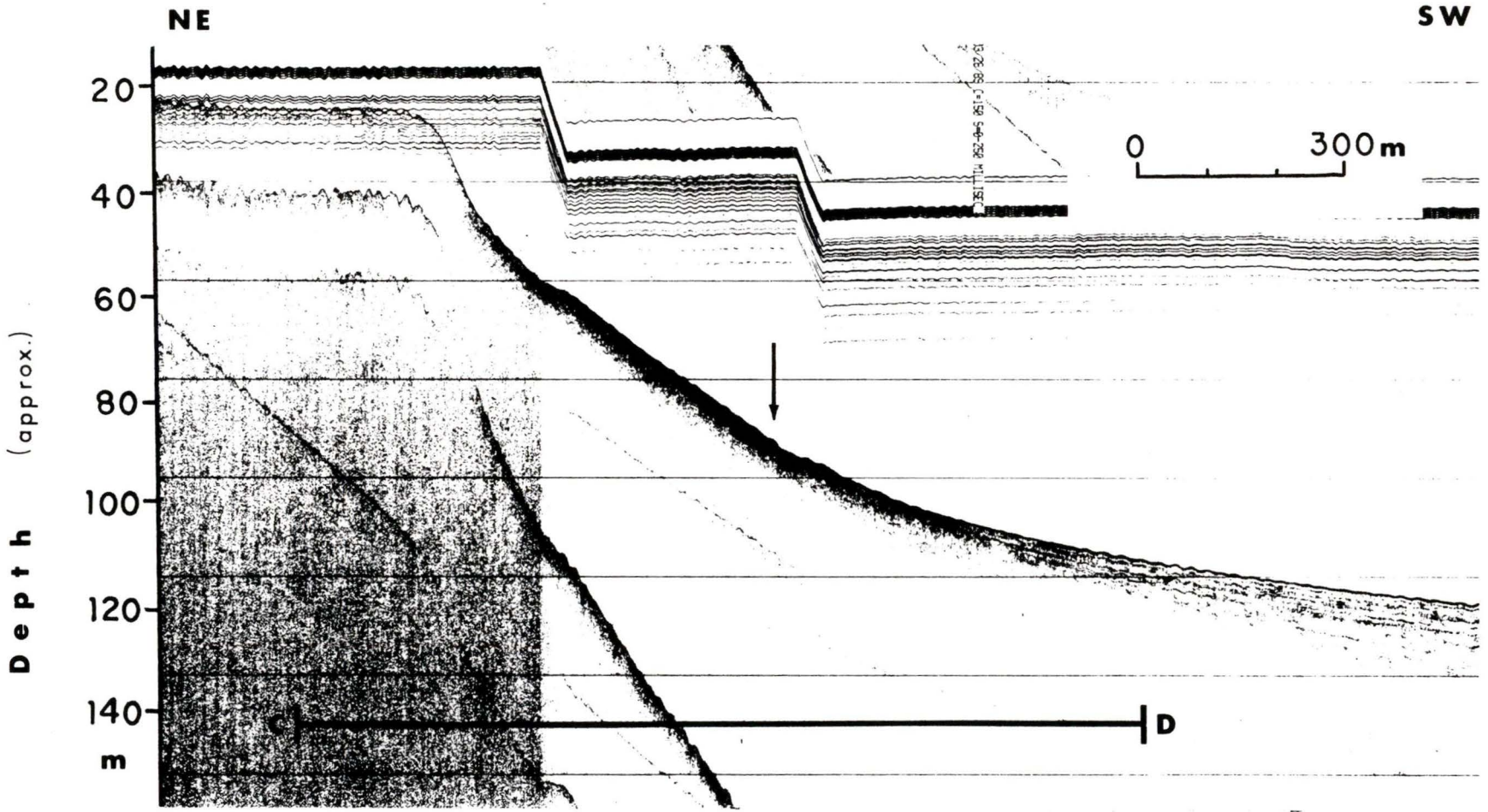

Plate 1. Huntec sub-bottom profile of shallow terrace scarp and slope southwest of Point No Point. Arrow indicates location of large dunes on slope. Line C-D corresponds to location of sidescan image in Plate 2 (vertical exaggeration is x 7.5).

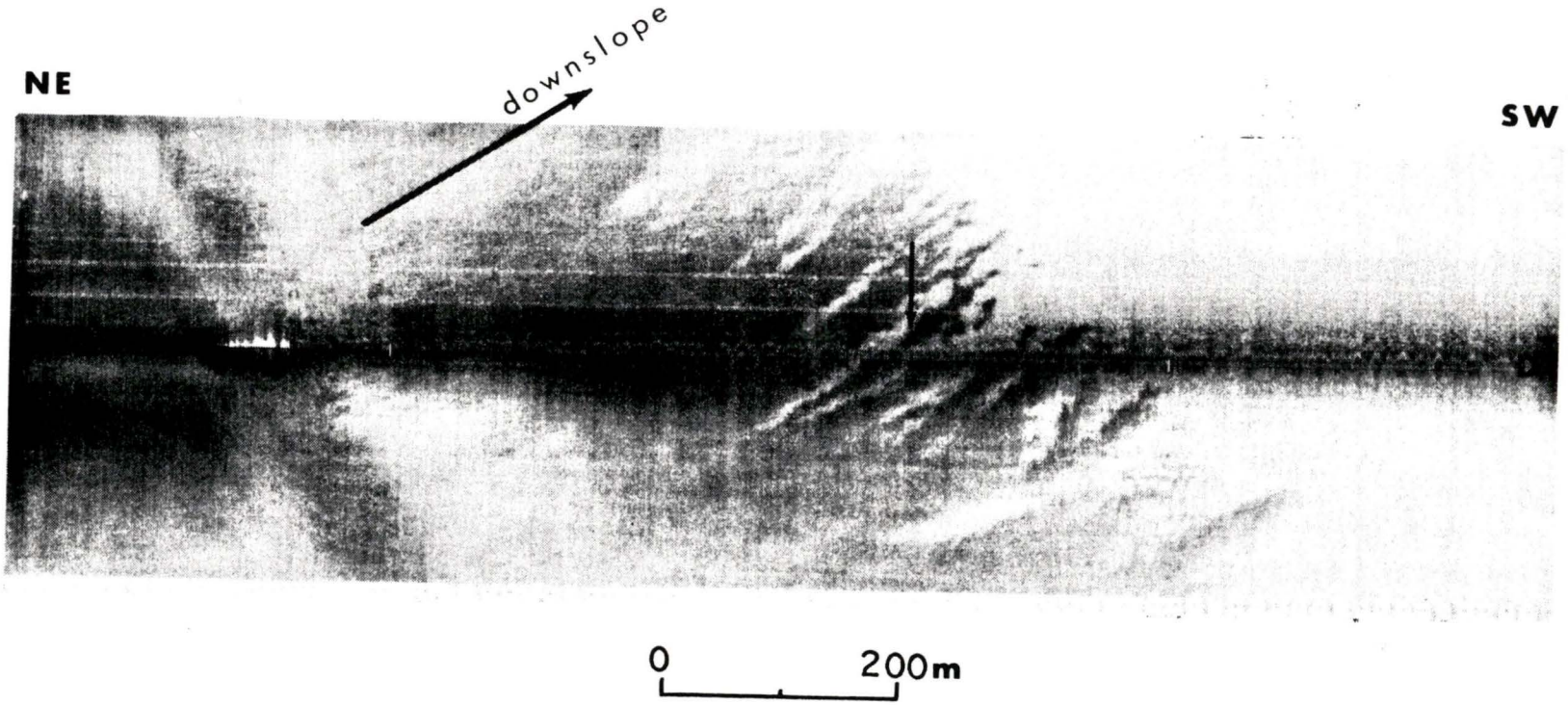

Plate 2. Sidescan image of terrace scarp in northeast, slope with large dunes (arrow) and muddy sand of sediment wedge in southwest. Dunes are oriented close to north-south, normal to terrace scarp which runs diagonally from upper left corner. Line C-D indicated in sub-bottom profile (Plate 1).

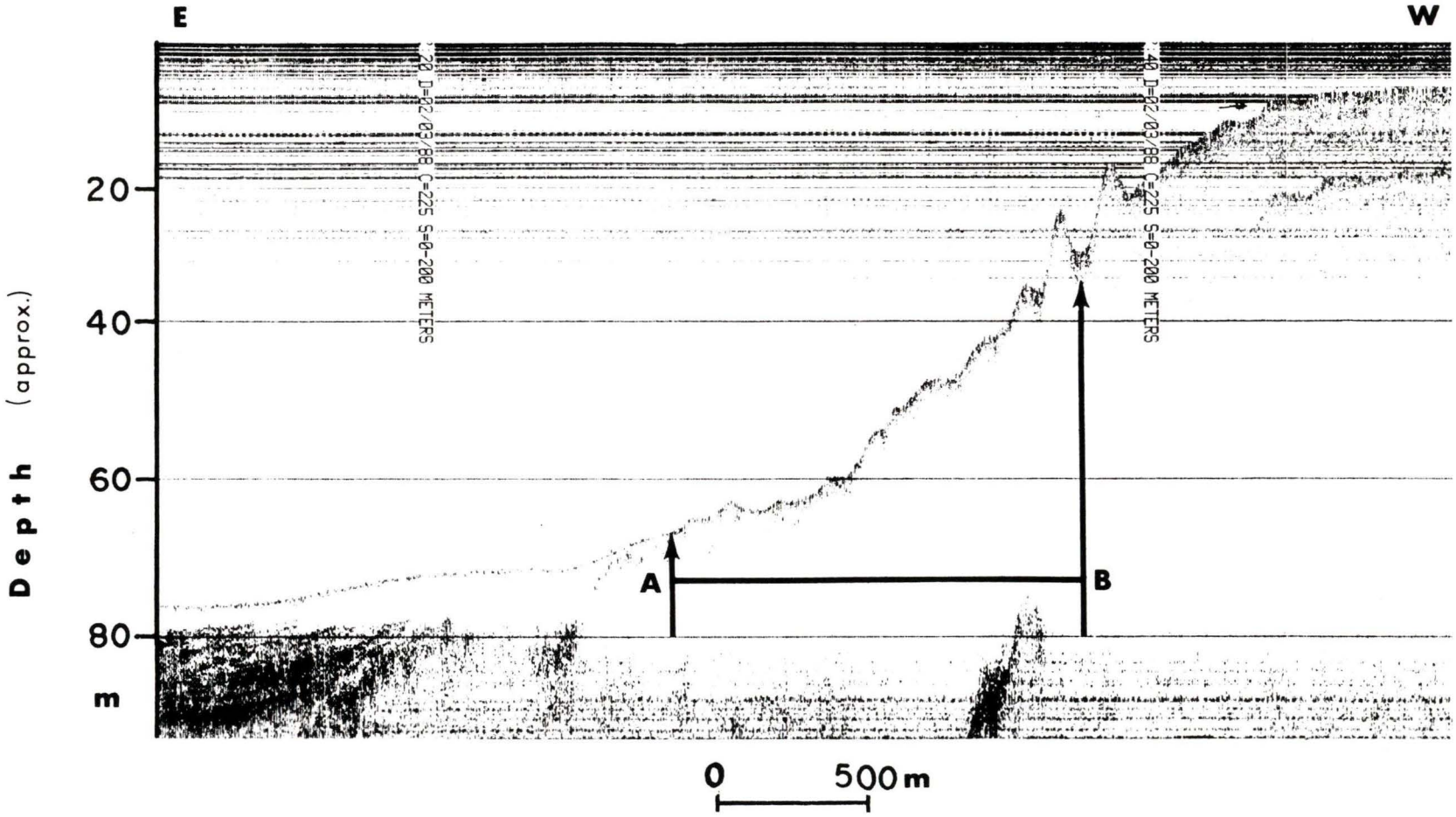

Plate 3. A succession of gullies line the terrace scarp directly south of Magdalena Point. Track of the 3.5 kHz sub-bottom profile climbs the scarp at an oblique angle (vertical exaggeration is approximately x 26.5). Sidescan image of line A-B is shown in Plate 4.

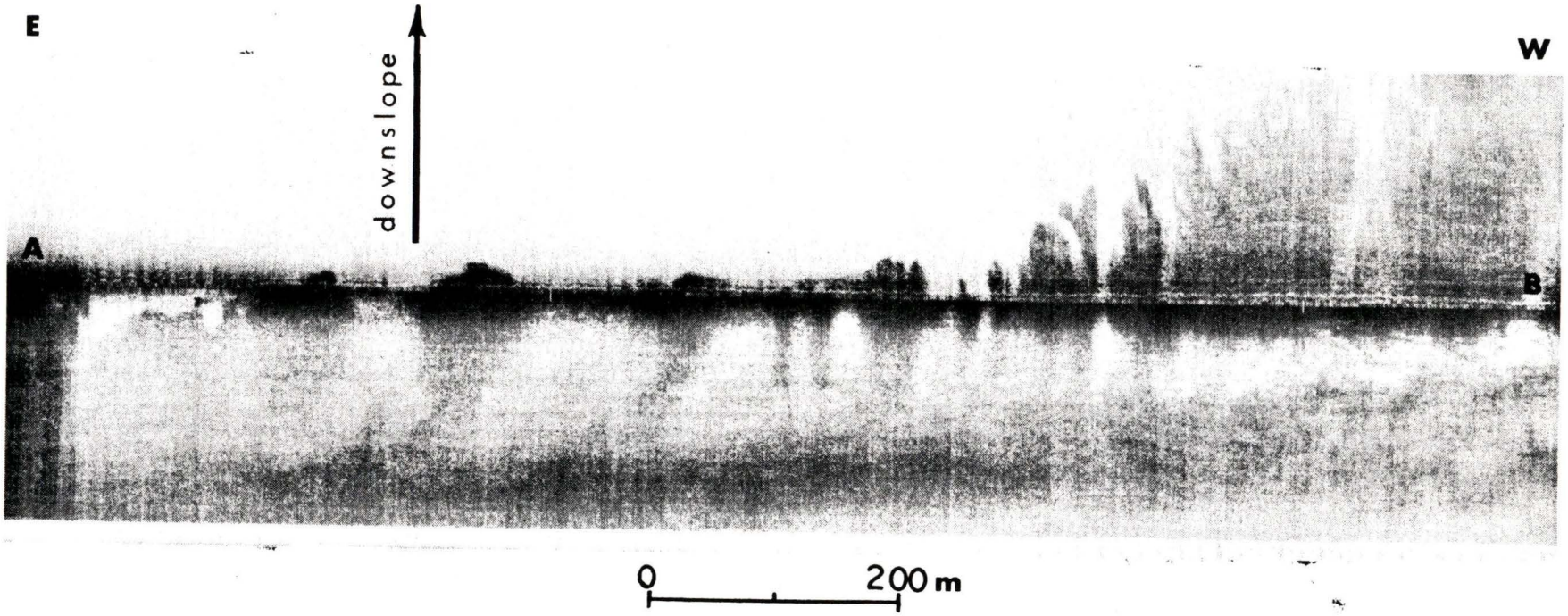

Plate 4. Sidescan image of gullied scarp along line A-B (Plate 3). Survey line climbs scarp at an oblique angle towards west.

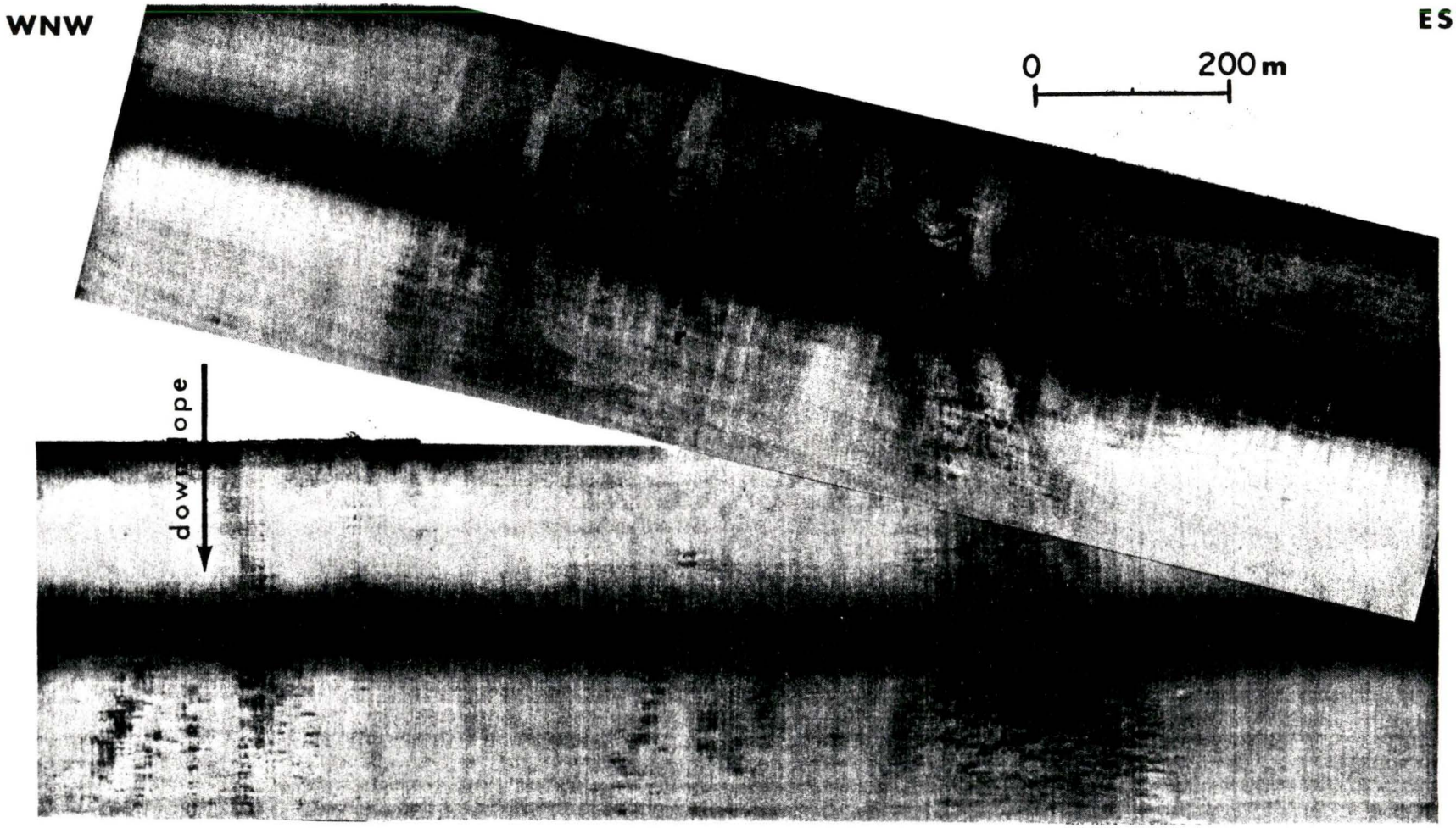

Plate 5. Sidescan mosaic of several channels (centre, top), eroded into substrate (90 m depth), funnelling debris southward into fans below them on the slope, south of San Juan Point (Figure 21). Profile along line E-F crosses debris fans in Plate 6. Oscillation ripples, r, are observed in debris fans (Plate 7).

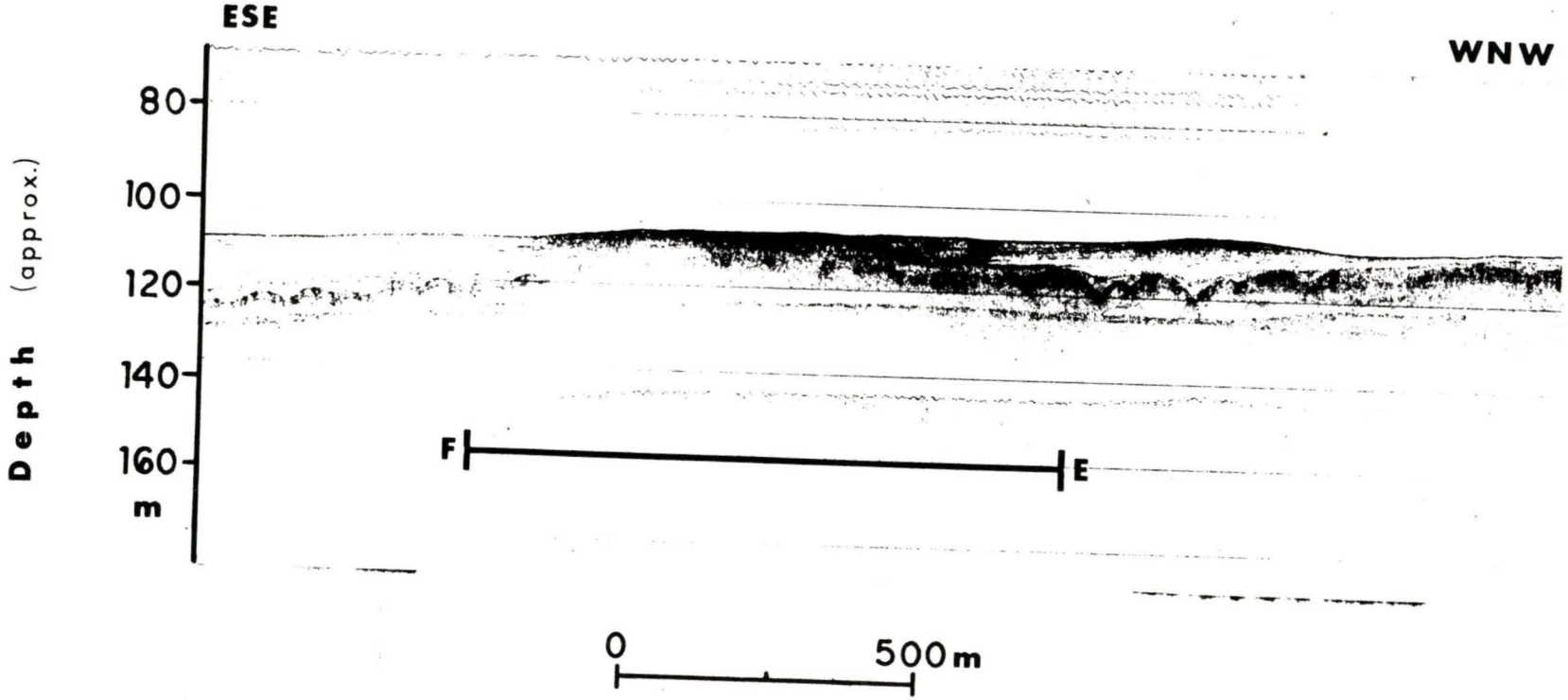

Plate 6. Huntec sub-bottom profile across debris fan below scoured channels. Sidescan image along line E-F shown in Plate 5 (vertical exaggeration is approximately x 7.5).

Plate 7. Sidescan image enlarged from Plate 5, showing oscillation ripples, r, in debris fans. Ripple crests are oriented parallel to sidescan line and strike of strait. Depth of ripples is approximately 90 m.

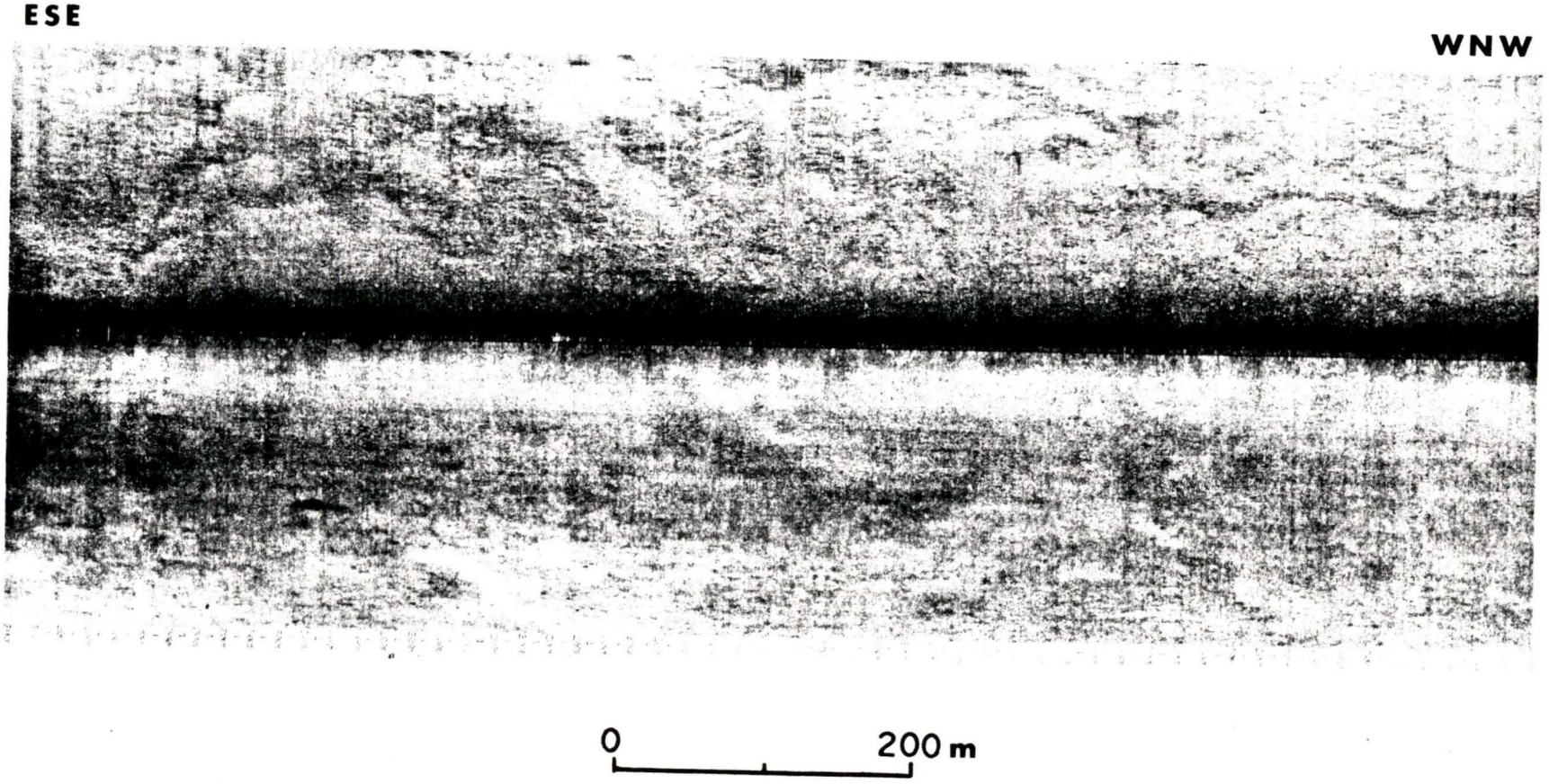

Plate 8. Sidescan image of boulder field on nearshore terrace at a depth of 30 to 40 m.

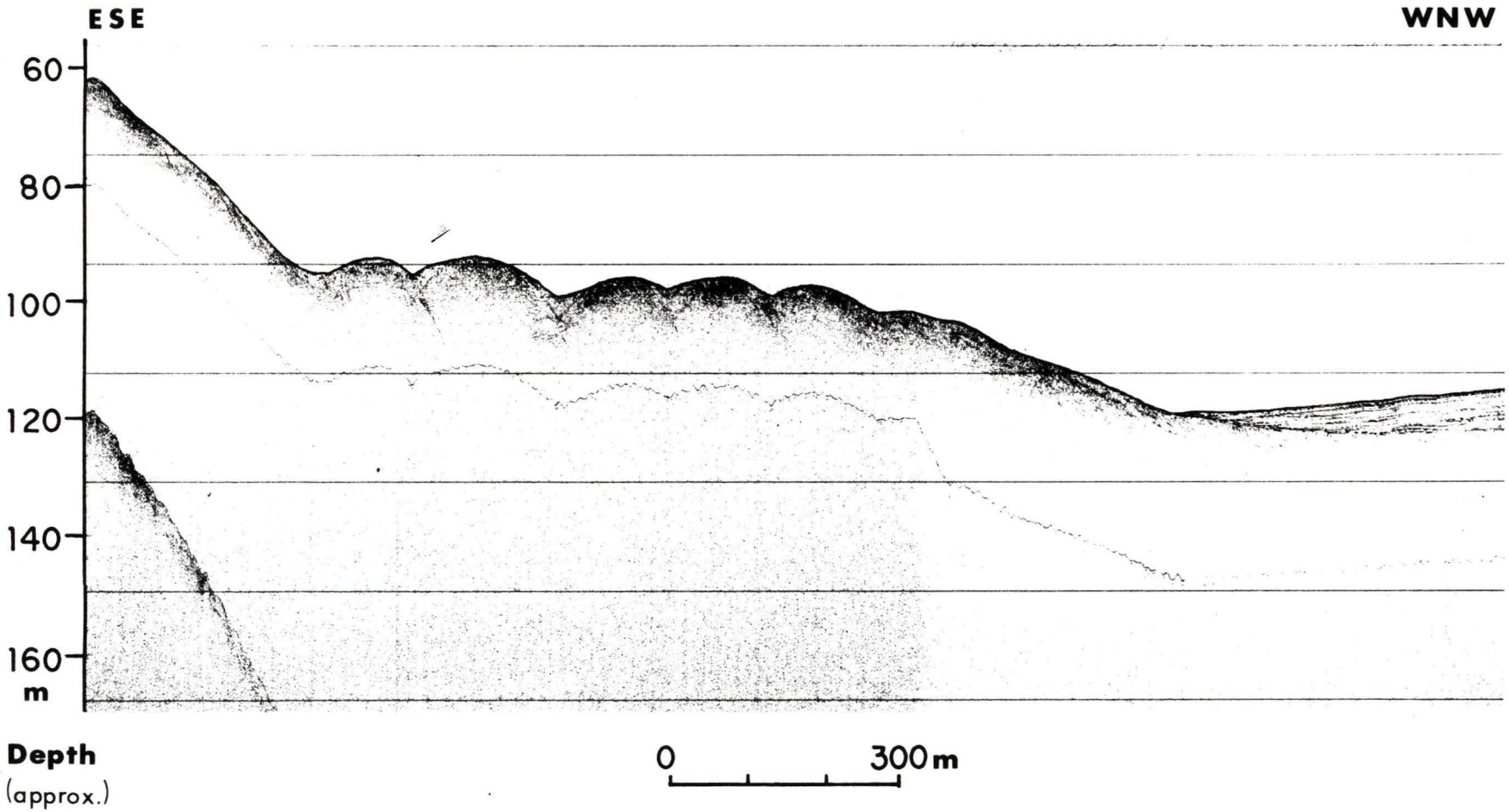

Plate 9. Huntec sub-bottom profile of hummocky moraine located directly south of Sombrio Point (Figure 21). Modern sediments blanket the feature (vertical exaggeration is approximately x 7.5).

VI. Heavy Minerals & Geochemistry

1. Quantitative Heavy Mineral Distribution

Weight percent heavy mineral contents for the sand fraction were obtained for 107 samples in the offshore and for 41 beach and eight river samples adjacent to the study area (Figure 23).

i) Offshore samples

Samples from depths of less than 100 m indicate that a significant part of the offshore area contains 5% or less heavy minerals (Figure 23). Distribution of heavy mineral contents for offshore samples with values greater than 5% are largely found in the nearshore between French Beach and China Beach, to depths of usually less than 15 m. This area encompasses the broad terrace off Jordan River and its depressions. Heavy mineral values from Sandcut Beach and the adjacent nearshore reveals an area of anomalous heavy mineral content (20-45%) parallel to shore, concentrated in waters of less than 10 m depth.

Elsewhere, from Sooke Bay to Sombrio Beach, values greater than 5% can be found in shallow nearshore areas. Farther offshore an area south of Loss Creek contains several samples with greater than 5% heavy mineral content, located along a terrace scarp, with one sample in a large channel feature at 70 m depth. Similar values are found in slightly depressed areas of the seafloor at depths between 15 and 20 m off Magdalena Point and at a site in Muir Creek

channel.

The offshore samples have a mean heavy mineral content of 7.02% +/-6.64% (standard deviation), with a range of 0.77% to 42.35%. A histogram of logged heavy mineral percentage values (Figure 24) shows a polymodal distribution. One population is indicated by the change in slope above Ln 2 in the probability plot (Figure 25). This plot is enhanced when the four anomalous samples (from Sandcut Beach transect) are removed from the sample set (Figure 26). The remaining 103 samples have a mean of 5.99% +/-3.99 heavy mineral content, a range of 0.77% to 19.36%, representing a decrease of more than half in sample range. The population above Ln 2 (7.39%) may represent those samples whose heavy mineral content has been enhanced by the addition of a localised heavy mineral source and/or differential sorting.

The population at the lower end of heavy mineral percentages in this set do not appear to fit the sample population due to high variation (Figure 26). Some samples were so coarse that heavy mineral separations resulted in very low values mainly due to the scarcity of individual heavy minerals disaggregated from lithic fragments. Truncation in this coarse (low percentage) end range of the distribution may also occur due to sieving of the samples at 2 mm.

No linear correlation is apparent between sample mean

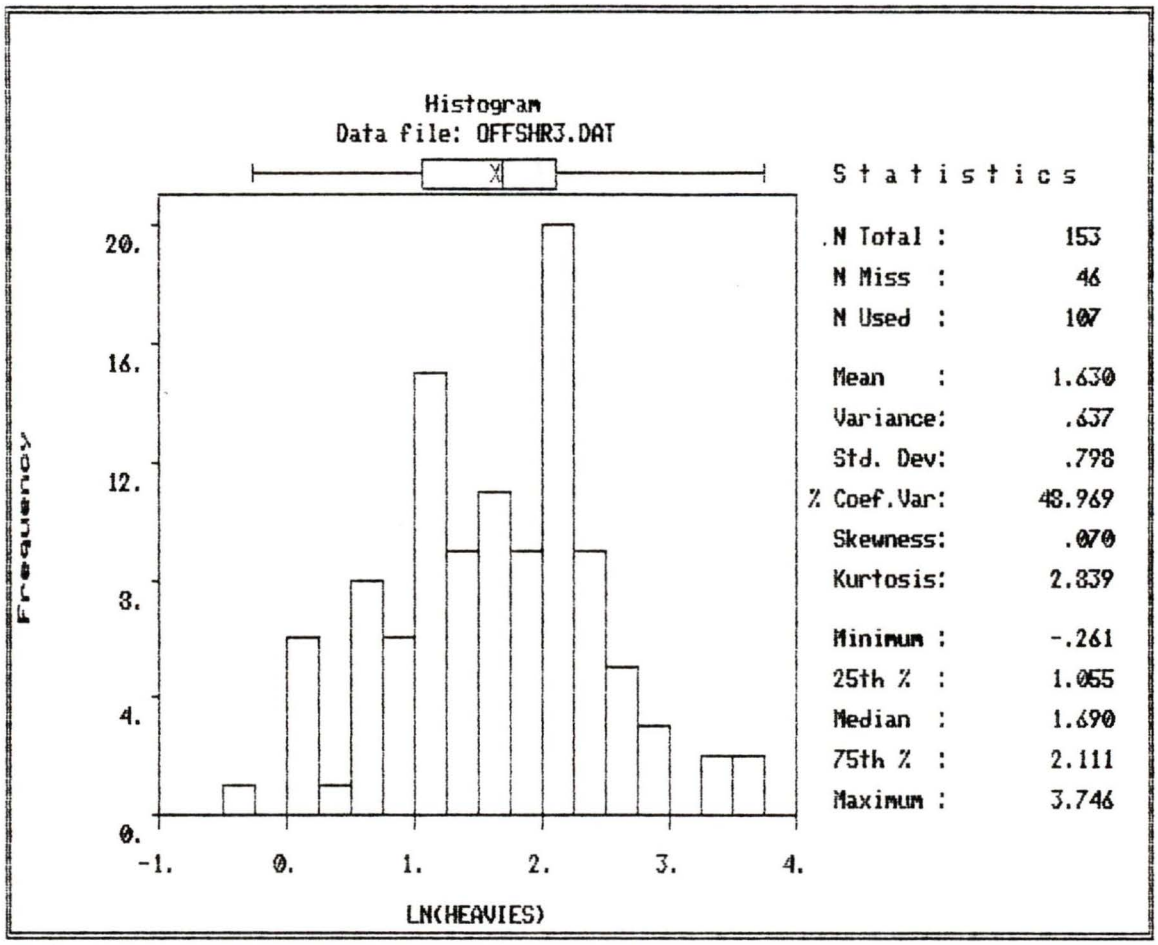

Figure 24. Histogram of 107 heavy mineral weight percent concentrations (logged) from the offshore study area.

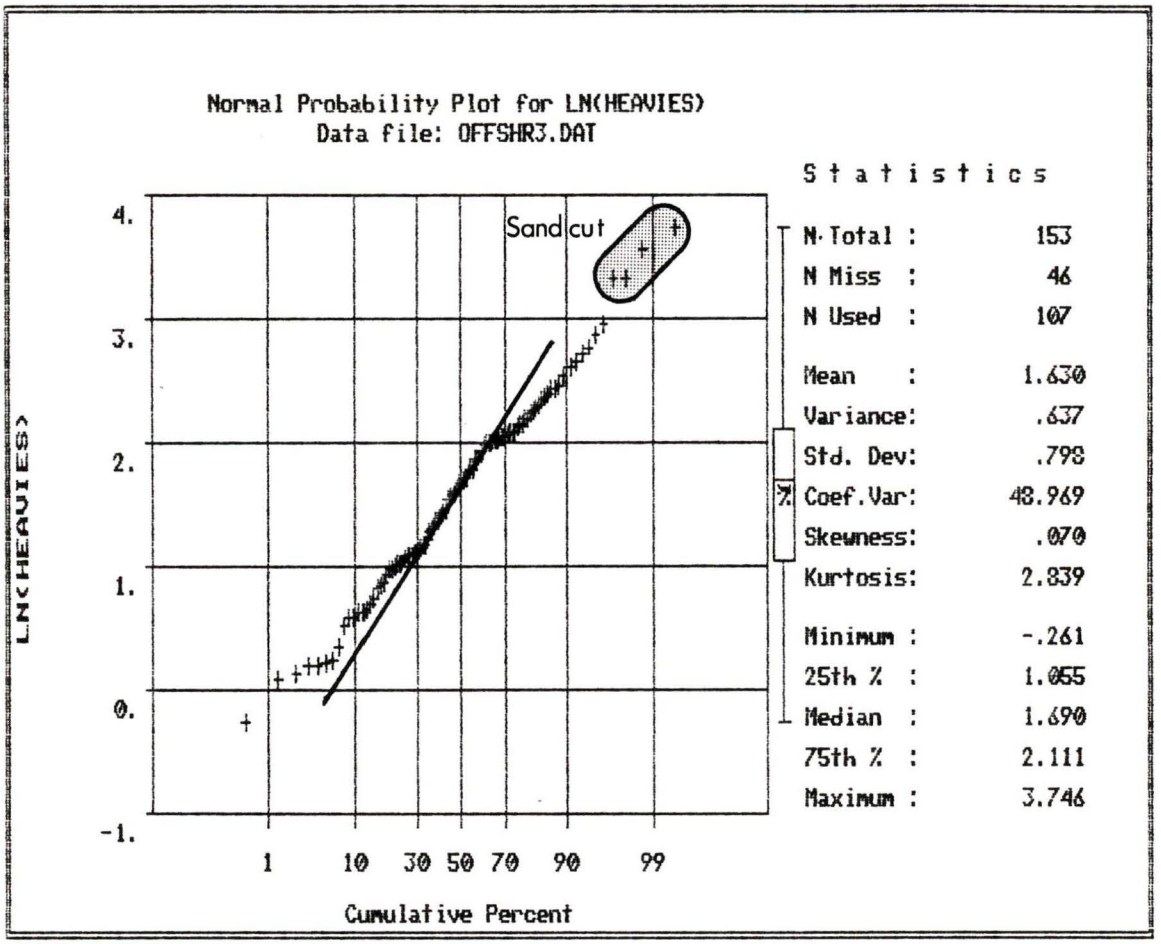

Figure 25. Probability plot of 107 heavy mineral weight percent values (logged) from the offshore study area. Four highest values occur off Sandcut Beach.

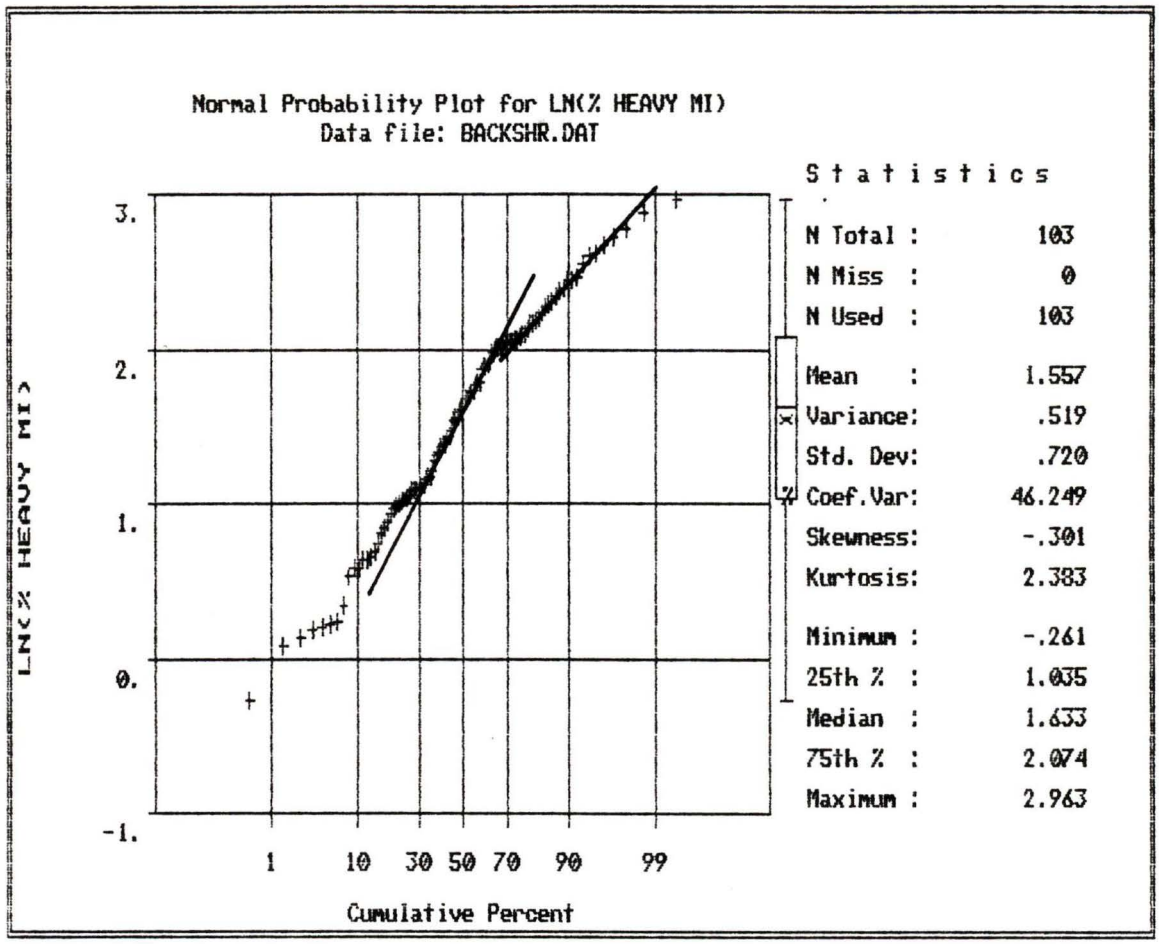

Figure 26. Probability plot of 103 heavy mineral weight percent values (logged) from the offshore study area. Four highest values shown in Figure 25 are omitted.

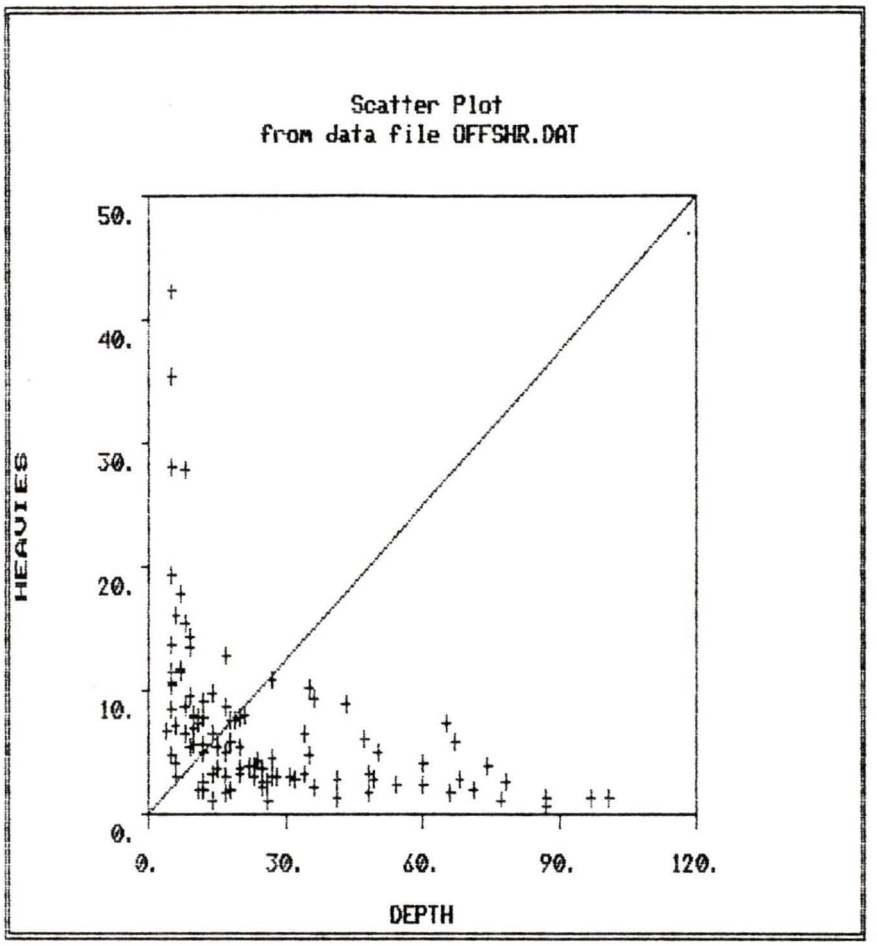

Figure 27. Crossplot of offshore sample depth with sample weight percent of heavy minerals.

grain size and percent heavy mineral content, but a few general trends occur. Heavy mineral contents of 10% or higher are found in sands which have mean grain sizes between 2 and 3 phi (fine sand). Exceptions to this generalisation are three of the four anomalous samples which have phi values of 3 and 3.25 (very fine sand). Samples with between 5% and 10% heavy minerals commonly have mean grain sizes between 1 and 3 phi (fine to medium sand) while samples with values below 5% are largely finer than 3 phi (very fine sand).

No distinct relationship between percent heavy mineral content and sorting or sample modes for the whole sample set is observed. However, locally off Sandcut Beach the transect of eleven samples (including the four anomalous heavy mineral values; Figure 25) generally increases in heavy mineral content towards shore, only decreasing in heavy mineral percentage at 100 m from shore. The mean grain sizes for these samples, as noted earlier, tend to decrease shoreward with a local coarsening just 100 m from shore. Sorting (grain size standard deviation) improves shoreward, although all except the deepest sample are moderately sorted.

The relationship between depth and heavy mineral content is inconclusive; results suggest a general tendency for the latter to decrease with depth (Figure 27). All samples with heavy mineral content greater than 15% are

found in depths shallower than 15 m (8 samples), and all samples obtained from water depths greater than 70 m have less than 5% heavy mineral content (8 samples).

ii) Beach and River Samples

Heavy mineral percentages obtained for the 41 beach samples have a mean of 19.51% +/-11.62, with a range of 0.88% to 45.87%. Distribution of the heavy mineral concentrations reveal a strongly bimodal sample set on both histogram and probability plots (Figures 28 and 29).

The sample set splits at Ln 3 (20% heavy mineral content) into a second slope (Figure 29), distinguishing the two different populations. The population of high values, above 20%, contains 17 samples with a mean of 31.56% +/- 6.31, and a range of 24.37% to 45.87%. Fifteen of the seventeen samples are from the shore between Sandcut Beach and Point No Point (Jordan River area) (Figure 30). Only two samples taken along the latter shoreline have values which fall below this sample range. Outside of the Jordan River area the last two anomalous samples are from sands at Sombrio Beach and near Magdalena Point (Figure 30).

The remaining 24 samples have a mean of 10.97% +/- 4.88, with a range of 0.88% to 18.49%. These samples represent a different population, or populations, from that discussed above.

Variation in east to west heavy mineral concentration is difficult to assess due to a scarcity of samples in the

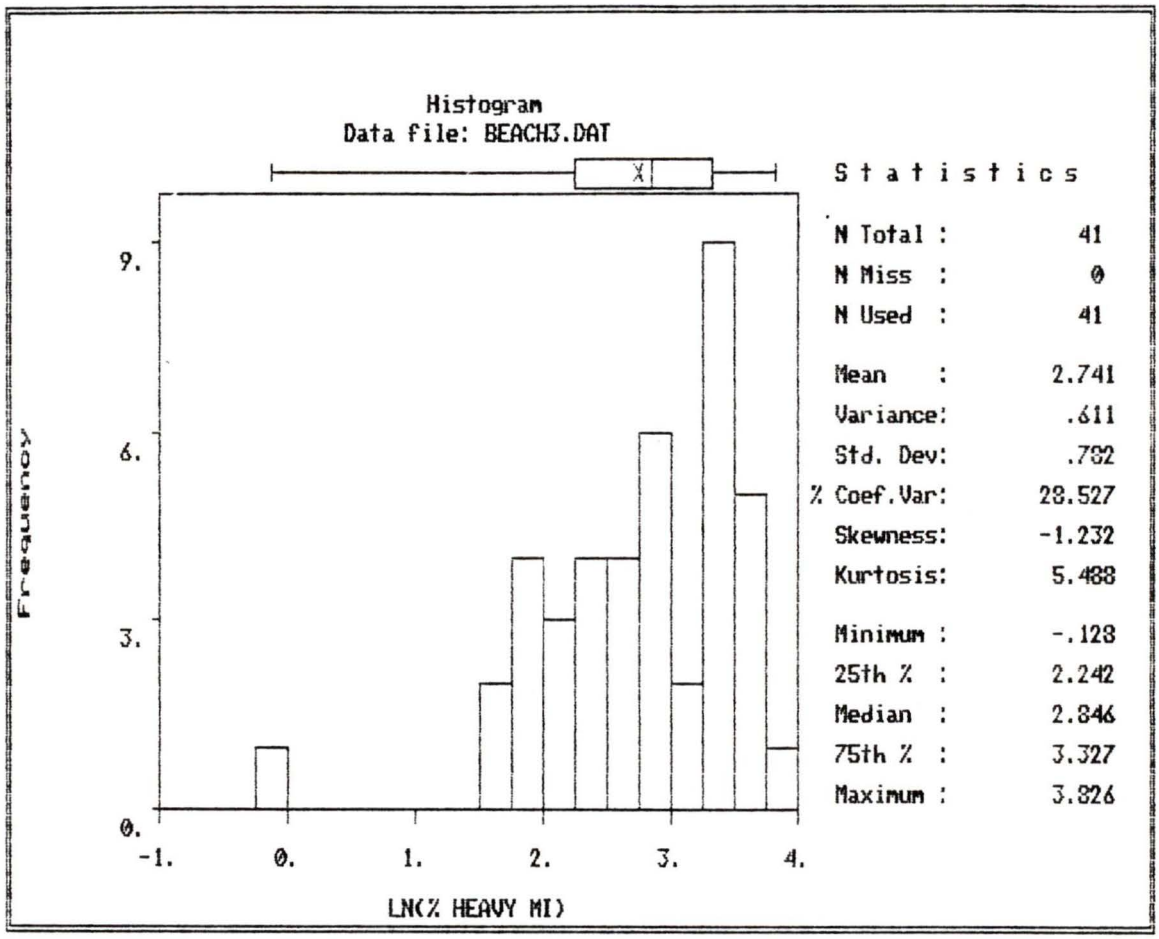

Figure 28. Histogram of 41 heavy mineral weight percent values (logged) from beaches within the study area.

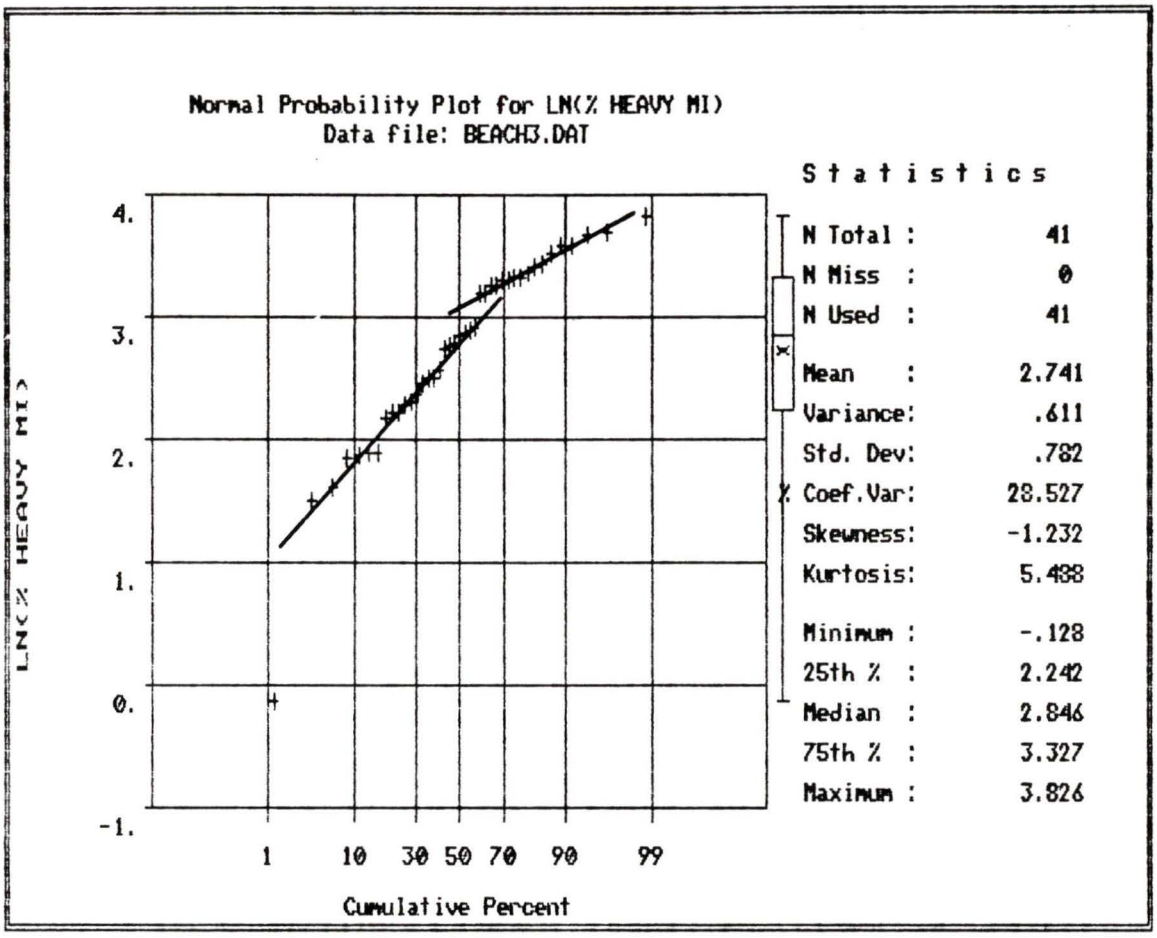

Figure 29. Probability plot of 41 heavy mineral weight percent values (logged) from beaches within the study area. Locations of the 17 samples forming the higher population are noted in Figure 30.

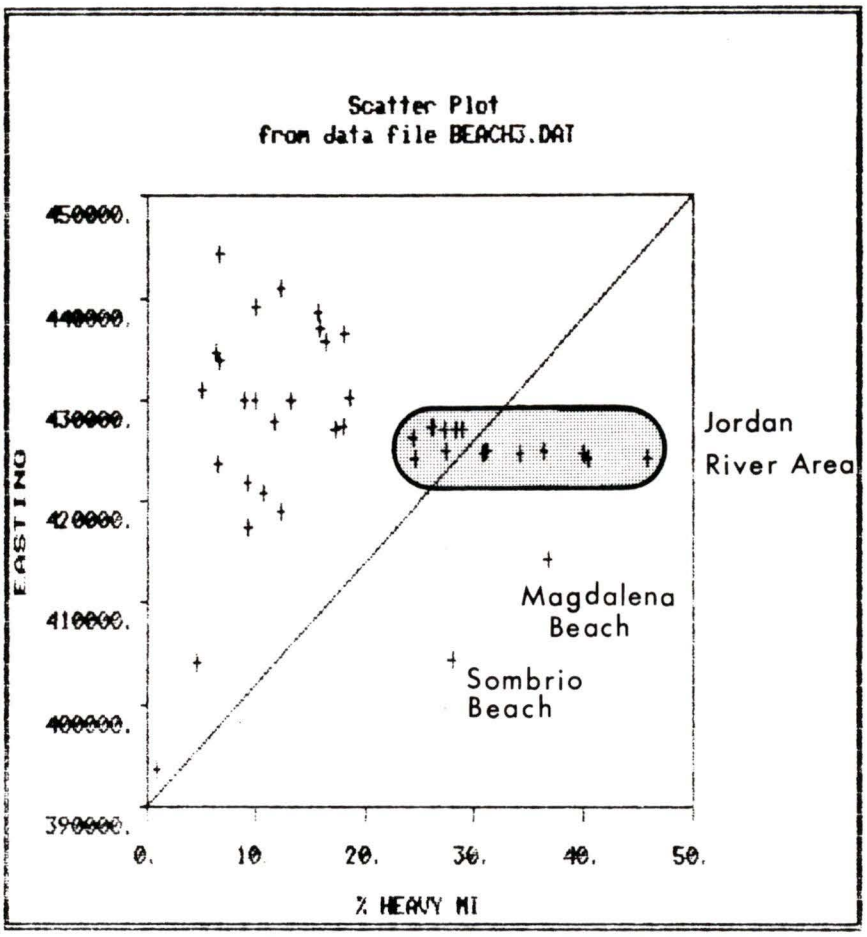

Figure 30. Crossplot of beach sample heavy mineral weight percent values with sample eastings (UTM). Location of highest sample values shown.

west (Figure 30), resulting from a lack of sand size material on western beaches.

River samples collected at four streams, above the high tide level, had heavy mineral contents with a mean of 16.90% +/-5.46. These values are not directly comparable to beach and offshore values as sieving excluded the very coarse sand fraction from samples. Upstream bar-head samples had higher heavy mineral contents, by weight, for 3 of the 4 streams compared with samples taken along the lateral edge of bars. The four bar-head samples alone had a mean of 19.16% +/-6.54, whereas the sample sites along the side of the bars had a mean of 14.64% +/-3.65.

The two Sombrio River samples had significantly lower values for heavy mineral content, 9.83% and 10.06%, than the three other streams (which ranged from 14.42% to 25.04%). Sombrio River was the single stream with a bar-head sample heavy mineral value lower than the sample taken from the side of the bar.

2. X-ray Diffractometry of Heavy Mineral Fraction

Heavy mineral fractions from separations of six offshore samples were submitted for X-ray diffraction analysis (Figure 31). The samples were taken from a variety of depths and represent the range of weight percents for the heavy mineral fraction. Lab analysis of diffractograms indicate that amphibole was the most significant mineral in all but one sample (Table 3). Epidote, augite, magnetite

and garnet (almandine) were present in all samples in varying proportions. Minor amounts of various heavy minerals such as chlorite, clinozoisite, ilmenite, hypersthene-enstatite, staurolite and rutile were found in one or two samples. Quartz appeared in two samples.

3. Magnetite

Magnetite normally represents all the observed opaque minerals separated by hand magnet. However, the occurrence of ilmenite in these sands is implied by the elevated levels of titanium observed in the geochemistry, and suggests that ilmenite, often intergrown with magnetite, may represent some portion of the magnetite weight recovered.

i) Offshore samples

Magnetic separations were performed on 49 samples located from Point No Point in the east to Providence Cove in the northwest. Sample depths range from less than 5 m to 87 m, with the majority of samples centred on the broad Jordan River submarine terrace area.

Magnetite as a weight percent of the whole sand fraction had a mean of 0.64% +/-0.33%, with a range of 0.10% to 1.42%. No areal distribution pattern was observed in the distribution of values in the offshore.

The values for percent magnetite indicate a polymodal distribution (Figures 32 and 33). However, the level of error which accompanies the separation technique implies that limited confidence in sample groupings is warranted.

TABLE 3. X-Ray Diffraction results for six heavy mineral sand fractions. Minerals are listed in order of descending abundance.

Sample 1.
(JF38-200) depth 5m
42.35 % Heavy Minerals

Amphibole
minor: Epidote
Augite
Magnetite
Almandine

Sample 2.
(JF38-1100) depth 20m
7.60 % Heavy Minerals

Epidote
Amphibole
Magnetite
Almandine
Augite
trace: Quartz
Chlorite

Sample 3.
(JR44-1000) depth 10m
6.91 % Heavy Minerals

Amphibole
Augite
Epidote
Clinozoisite
Chlorite
Quartz
Plagioclase?
Magnetite
Almandine

Sample 4.
(JR81-85) depth 12m
7.77 % Heavy Minerals

Amphibole
Epidote
Augite
Clinozoisite
Almandine-Manganoan
Magnetite
Enstatite-Hypersthene
Ilmenite
Forsterite
Staurolite

Sample 5.
(TUL88A-01) depth 87m
1.23 % Heavy Minerals

Amphibole
Augite
Enstatite
Epidote
Rutile
Ilmenite
Magnetite
Almandine
Chlorite?

Sample 6.
(TUL88A-10) depth 17m
2.96 % Heavy Minerals

Amphibole
Epidote
Magnetite
Augite
Staurolite
Almandine-Manganoan
Kyanite &/or
Andalusite?

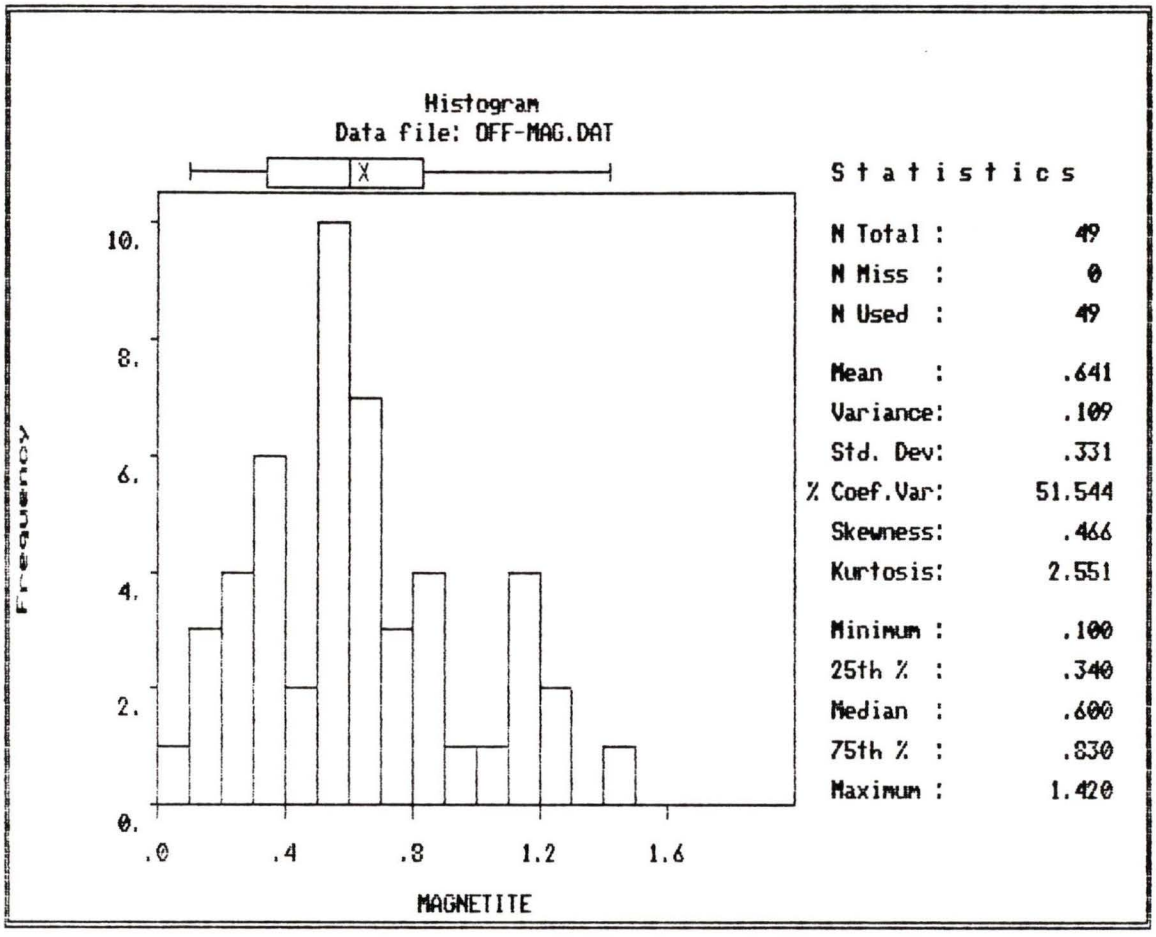

Figure 32. Histogram of weight percent magnetite content for 49 offshore samples within the study area.

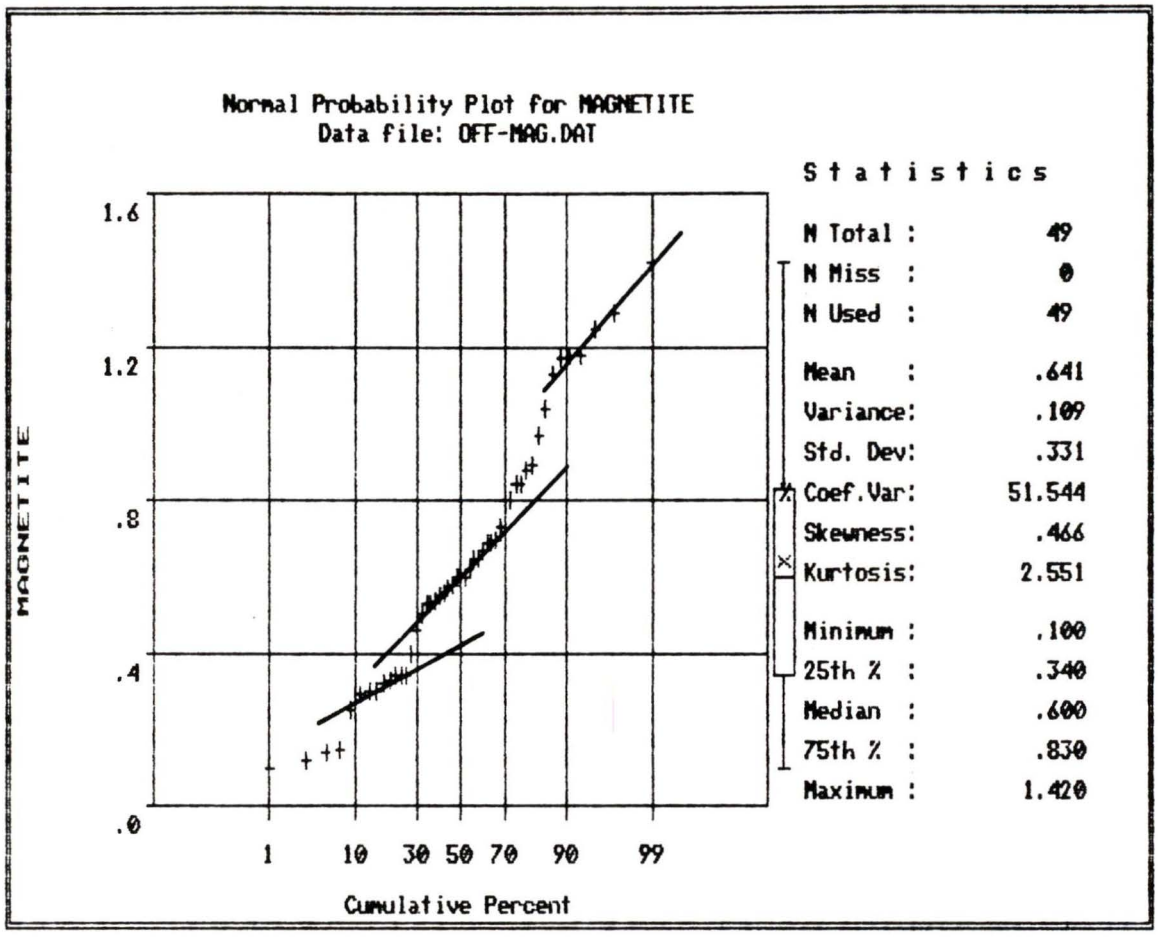

Figure 33. Probability plot of weight percent magnetite content for 49 offshore samples within the study area.

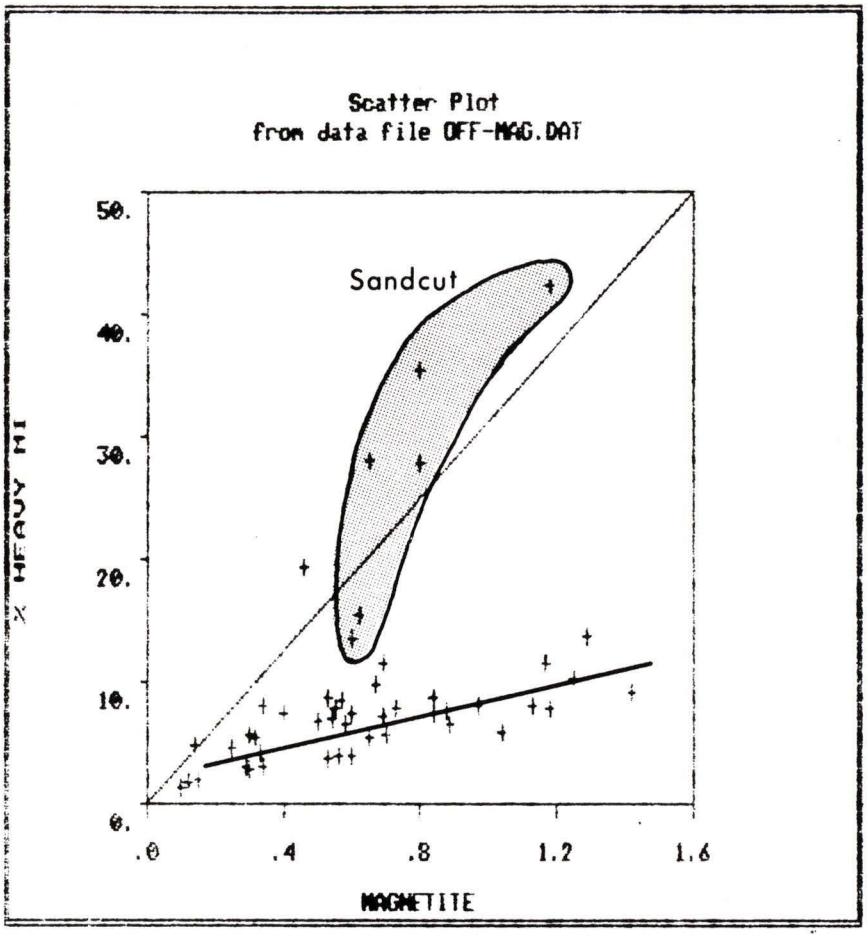

Figure 34. Crossplot of offshore sample weight percent magnetite with sample weight percent heavy minerals. Six samples in shaded zone were obtained adjacent to Sandcut Beach.

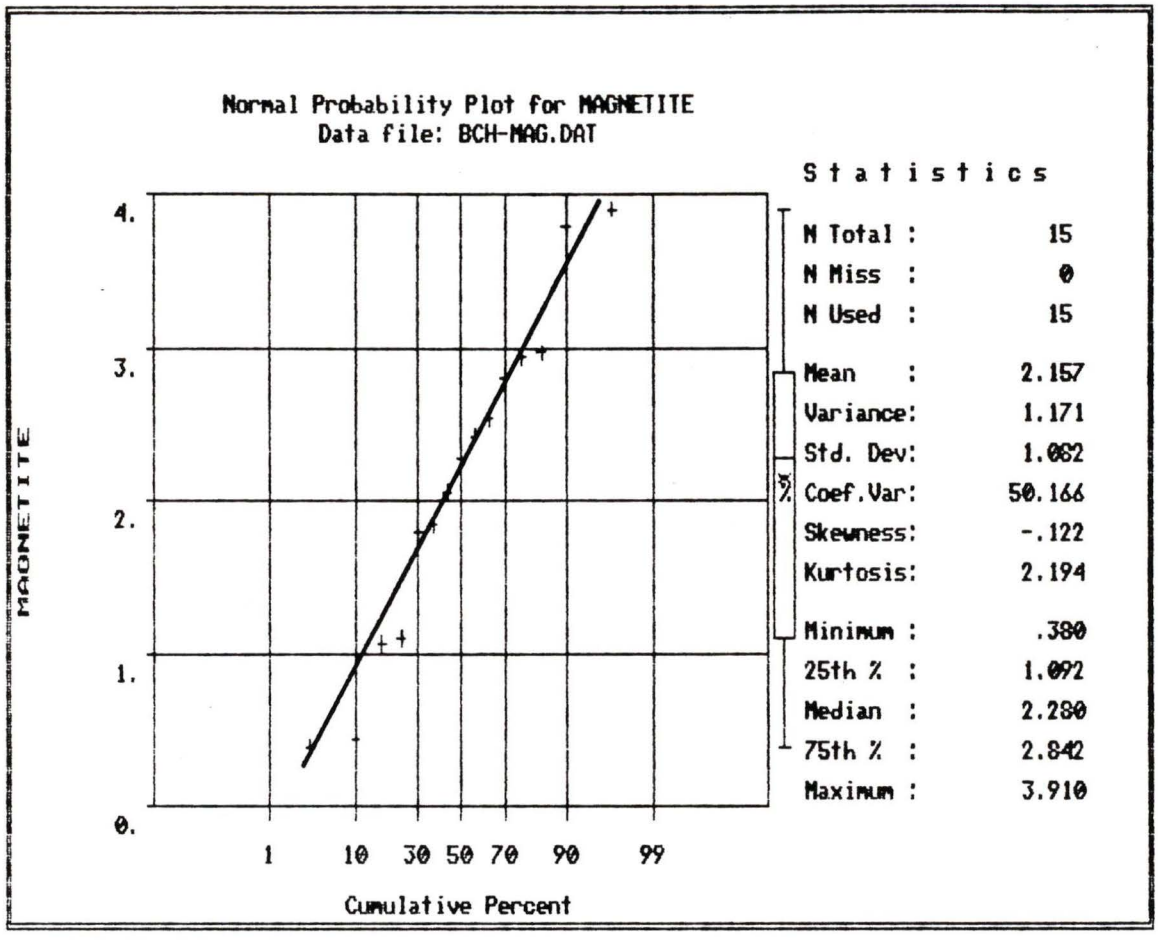

Figure 35. Probability plot of weight percent magnetite content obtained from 15 beach samples taken from Sandcut Beach and Point No Point.

Seven of the highest magnetite concentrations are located in various disparate areas between Jordan River and China Beach, forming no pattern with adjacent samples.

The magnetite content of the 49 samples analysed averaged 8.7% of the heavy mineral fraction of the sand, ranging from 2.2% to 17.5%.

No relationship was observed between magnetite percentages of the sand fraction and grain size parameters, sorting or water depth.

However, magnetite values appear to increase gradually with an increase in percent heavy mineral content (Figure 34). Of the samples showing high heavy mineral percentages, six are from the transect off Sandcut Beach. These samples show little or no increase in magnetite with a dramatic increase in heavy mineral content. These six samples are included in a set of nine samples showing lowest magnetite as a percent of the heavy mineral fraction, with the six samples having heavy mineral fractions of only 2.24% to 4.46% magnetite. These values indicate a reduced concentration of magnetite, relative to other heavy minerals. Alternatively, intergrowth between magnetite and ilmenite where the latter dominates and dilutes the magnetic character of the grain could explain the low relative magnetite values. The former explanation is preferred as values for magnetite percent of the sand fraction remain in the centre of the range for the whole sample set.

It follows that the high concentrations of heavy minerals at Sandcut beach represent enrichment by minerals other than magnetite. Concentrated heavy minerals in the Sandcut area must represent the addition of a different population than that found elsewhere in the study area.

ii) Beach samples

Magnetic separations were performed on heavy mineral sand fractions for 15 beach samples. The samples are representative of five profiles, three along Sandcut Beach and two from pocket beaches at Point No Point.

Sample magnetite content has a mean of 2.16% +/-1.08%, and a range of 0.38% to 3.91%. Magnetite averages 7.06% of the heavy mineral fraction of samples (ranging from 2.11% to 13.82%), only slightly lower than is found in the offshore samples. Beach magnetite contents are, on average, more than three times greater than magnetite contents in the adjacent offshore samples. Beach magnetite samples appear to have been sampled from one normal population (Figure 35).

No correlation was observed between magnetite content of beaches and direction east or west, or with heavy mineral content.

4. Magnetic Susceptibility

Values were calculated for true magnetic susceptibility for 89 offshore archive samples and 56 beach archive samples. Extensive use of this technique was terminated early in the study when it was determined that

magnetite occurs only as a minor component of the heavy mineral fraction of the samples. Only a few general comments will be made on the findings of this work.

Results obtained for the whole sand fraction of offshore samples range from 1960 x 10^{-6} in a few meters of water in Sooke Bay, to 85,800 x 10^{-6} at 35 m water depth south of Jordan River. Offshore samples have a mean susceptibility of 26,200 x 10^{-6}. No areal distribution pattern could be discerned from the susceptibility values.

Magnetic susceptibility values obtained for beach samples ranged from 8520 x 10^{-6} at Point No Point to 86 400 x 10^{-6} east of the mouth of Muir Creek. Mean of beach values is 37 100 x 10^{-6}, showing an increase of 30% over offshore mean susceptibility.

Sheehan (1989) attained a correlation coefficient of r=0.73 between magnetic susceptibility and percent magnetite separated by hand for the samples used in this study and a few additional samples adjacent to the study area.

5. Detrital Heavy Mineralogy

Mineral counts were performed on 20 samples broadly distributed over the study area, which consist of 11 offshore bottom samples, 5 beach samples and 4 river samples (Figure 31). Counts were performed on heavy mineral residues in the 0.125 mm to 0.090 mm size fraction. Counts were performed on the light mineral residues, for the same size fraction, from three sites (Figure 31).

Epidote, hornblende and lithic fragments are the major transparent minerals or detrital grains (Table 4). Pyroxene, clinozoisite-zoisite, staurolite and garnet also occur in relatively low, varying amounts. Undifferentiated magnetite-ilmenite constitutes the majority of the opaques. Pyrite is infrequent, although it is common locally, comprising 59.9% of the heavy mineral counts near the mouth of Sombrio River. Descriptions of the minerals and their groupings are found in Appendix B. Complete counts of minerals (Table 4) were recalculated without the lithic fragment category (Table 5) for comparative analysis of transparent detrital minerals and magnetite-ilmenite.

The eleven offshore samples examined for mineralogy appear to be representative of the 107 offshore samples in terms of heavy mineral concentrations, as discussed earlier. A decrease in percent heavy mineral with depth is observed in the narrow size fraction examined for mineral counts, with $r=-0.76$ (logged depth values). For all 20 samples the

TABLE 4. DETRITAL HEAVY MINERAL PERCENTAGES

	hornblende bl-gn	hornblende br-gn	pyro-xene	epid-ote	clin/ zois.	staur-olite	garnet	mag/ ilm.	others	lith. frags
Offshore										
PAR89A-19	5.6	21.7	6.6	29.0	2.1	0.7	0.0	3.9	14.3	16.1
PAR89A-35	4.7	13.0	4.7	23.0	5.7	0.3	5.3	17.0	8.7	17.6
TUL88A-04	11.1	0.8	0.5	19.5	2.1	3.2	7.1	44.6	6.3	4.8
SR89-D1	5.4	2.0	1.0	7.6	2.7	1.3	1.6	4.8	3.7	69.9*
PAR89A-51	14.0	0.6	1.1	16.0	6.1	0.6	5.9	38.6	8.4	8.7
JR89-D1	16.9	11.8	4.0	20.9	2.0	6.8	4.4	10.5	9.5	13.2
JF38-100	69.3	4.8	0.7	8.2	0.0	0.3	2.1	1.0	3.4	10.2
JR81-102	24.2	3.7	4.7	14.1	2.3	1.3	3.4	22.5	7.4	16.4
PAR89A-81	26.5	2.1	1.8	30.5	3.6	2.9	3.6	2.1	11.5	15.4
MC89-D1	13.0	7.2	2.4	21.6	8.2	4.8	2.8	7.5	13.0	19.5
PAR89A-83	3.8	6.2	10.9	25.6	3.4	2.0	4.4	8.2	14.7	20.8
Beach										
MB89-02	25.4	3.7	1.7	21.7	3.7	8.4	3.7	7.7	8.0	16.0
JF-B18-3	79.0	1.3	1.7	6.0	0.0	0.0	2.0	0.7	3.3	6.0
JF-B12-2	9.2	1.1	3.7	19.8	3.3	11.4	19.5	9.2	8.5	14.3
SG89-01	23.0	5.4	2.4	23.3	5.1	5.7	3.0	11.5	10.5	10.1
SO89-03	17.8	3.8	0.7	32.4	4.5	0.0	0.0	2.4	9.8	28.6
River bar										
RSR89-01	16.8	6.4	0.7	8.1	2.4	15.1	5.0	25.3	15.8	4.4
RLC89-01	21.7	6.4	1.7	18.3	10.5	6.4	4.4	11.9	6.1	12.6
RJR89-01	45.8	4.1	3.0	21.2	1.7	0.3	0.3	9.1	3.7	10.8
RMC89-01	15.4	7.0	2.6	31.8	8.0	0.7	0.7	9.7	7.7	16.4

* This sample contains 59.9% pyrite which is included under lithic fragments.

TABLE 5. TRANSPARENT HEAVY MINERAL PERCENTAGES
(plus magnetite-ilmenite)

	hornblende bl-gn	hornblende br-gn	pyro-xene	epid-ote	clin/ zois.	staur-olite	garnet	mag/ ilm.	others	%* no.
Offshore										
PAR89A-19	6.7	25.8	7.9	34.6	2.5	0.8	0.0	4.6	17.1	240
PAR89A-35	5.7	15.8	5.7	27.9	6.9	0.4	6.5	20.6	10.5	247
TUL88A-04	11.6	0.8	0.6	20.5	2.2	3.3	7.5	46.8	6.7	361
SR89-D1	17.9	6.6	3.3	25.5	9.0	4.2	5.2	16.0	12.3	212
PAR89A-51	15.3	0.6	1.2	17.5	6.8	0.6	6.5	42.3	9.2	326
JR89-D1	19.4	13.6	4.7	24.1	2.3	7.8	5.1	12.1	10.9	257
JF38-100	77.2	5.3	0.8	9.1	0.0	0.4	2.3	1.1	3.8	263
JR81-102	28.9	4.4	5.6	16.9	2.8	1.6	4.0	26.9	8.9	249
PAR89A-81	31.4	2.6	2.1	36.0	4.2	3.4	4.2	2.5	13.6	236
MC89-D1	16.2	8.9	3.0	26.8	10.2	5.9	3.4	9.4	16.2	235
PAR89A-83	4.7	7.8	13.8	32.3	4.3	2.6	5.6	10.4	18.5	232
Beach										
MB89-02	30.3	4.4	2.0	25.9	4.4	9.9	4.4	9.2	9.5	251
JF-B18-3	84.0	1.4	1.8	6.4	0.0	0.0	2.1	0.7	3.6	282
JF-B12-2	10.7	1.3	4.3	23.2	3.9	13.3	22.7	10.7	9.9	233
SG89-01	25.6	6.0	2.6	25.9	5.6	6.4	3.4	12.8	11.7	266
SO89-03	24.9	5.4	1.0	45.4	6.3	0.0	0.0	3.4	13.6	205
River bar										
RSR89-01	17.6	6.7	0.7	8.5	2.5	15.8	5.3	26.4	16.5	284
RLC89-01	24.8	7.4	1.9	20.9	12.0	7.4	5.0	13.6	7.0	258
RJR89-01	51.3	4.5	3.4	23.8	1.9	0.4	0.4	10.2	4.1	265
RMC89-01	18.4	8.4	3.2	38.0	9.6	0.8	0.8	11.6	9.2	250

* After dropping those grains or opaque minerals included under Lithic Fragments, this column indicates the number of mineral counts on which these percentages are based.

percent heavy mineral residues of the whole sand fraction and 0.125-0.090 mm size (both logged) were correlated at r=0.70.

Comparative mineralogy at the 20 sample sites was achieved by various methods. Mineral percents are illustrated in three regional figures and correlations are examined between minerals and between mineral/sediment parameters. Ratios are used to discuss hydraulic fractionation, and principal component analysis was applied to the matrix of mineral percentages. Results of counts (frequencies) are expressed as percentages, introducing the statistical problem of *closure* (Kelley, 1971). Variables of this type are subject to a linear constraint as they are not independent because the variables always have a constant sum. For example the confined values may induce negative correlations (Davis, 1973). For this reason many statistical techniques have not been used, or have been used with caution.

i) Transparent Minerals

Minerals which predominate in this study fall into Folk's (1974) metastable group of heavy transparent minerals. Only minor amounts of ultra-stable rutile, zircon and tourmaline were counted, and are included in the "other minerals" category.

Blue-green and brown-green hornblende are the two principal amphiboles which, along with epidote, dominate the

samples. In the west and eastern-most offshore samples, brown-green hornblende is most common, but elsewhere the blue-green variety dominates the hornblendes (Figures 36, 37 and 38). It should be noted that contact between the metamorphic minerals of the Leech River Formation in the west and the Metchosin Volcanic Complex (including Sooke Gabbros) in the east occurs in a wide zone on shore at Sombrio Beach and upstream along Loss Creek. This contact occurs in proximity to the increase in blue-green hornblende both offshore and most strongly in the four river samples (Figure 38).

Blue-green hornblende exhibits a singular peak at Sandcut Beach both offshore and on the beach, and upstream on Jordan River. A crossplot of blue-green hornblende to mean grain size, in phi units, for 11 offshore samples (Figure 39) shows a very general increase in mean grain size (sand) with an increase of blue-green hornblende. The fine sand sample with highest blue-green hornblende off Sandcut Beach (Figure 39), also has the highest heavy mineral content from the offshore samples.

A correlation coefficient of r=-0.78 between blue-green hornblende and sediment sorting (in phi units, both logged) (Figure 40), suggests that well-sorted sands have higher contents of blue-green hornblende. The single sample site off Sandcut Beach contained 77.2% blue-green hornblende, and occurs as a well-sorted sand. However, the

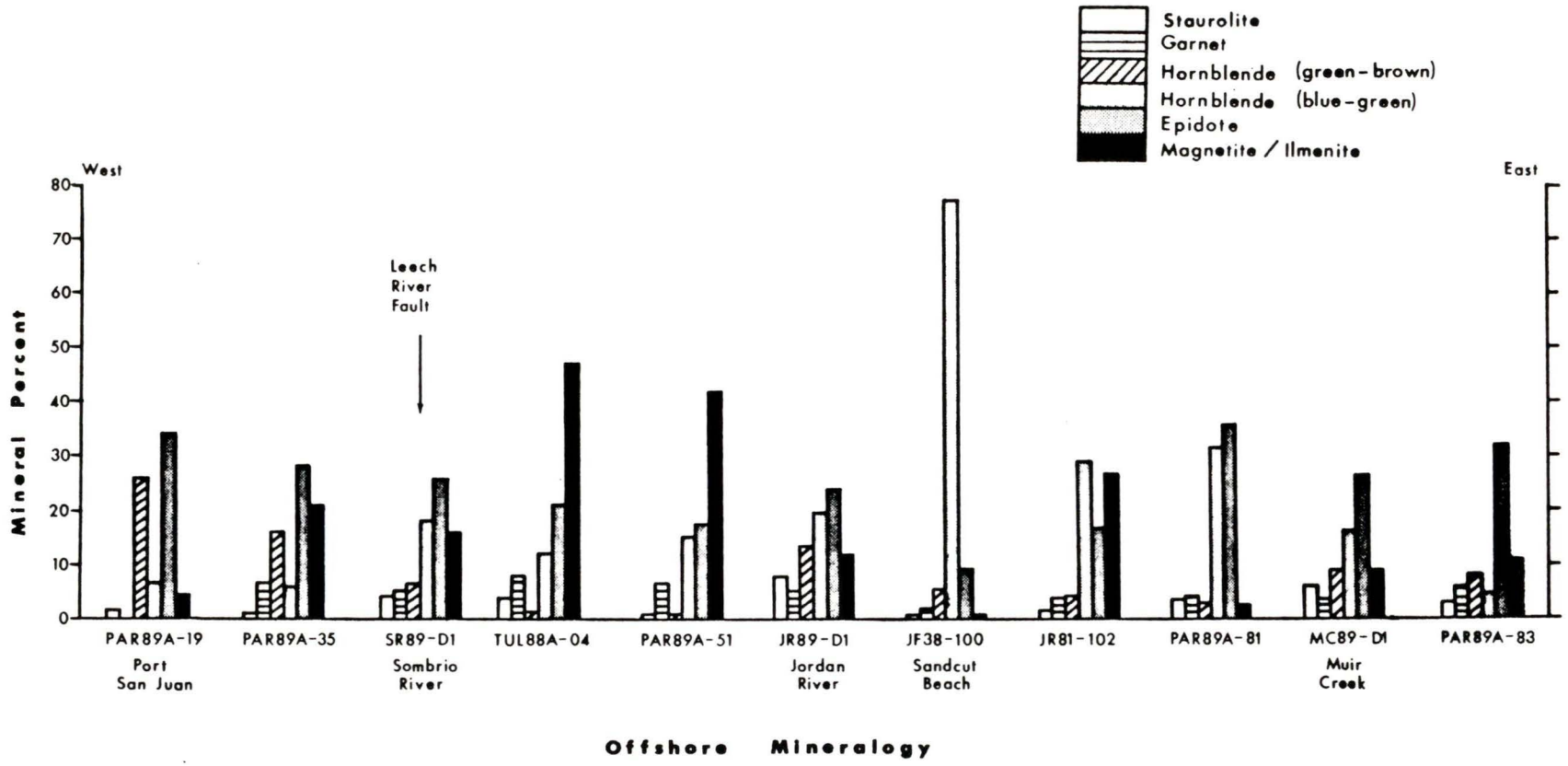

Figure 36. Offshore mineral percentages from optical mineral counts (Table 18), northern Juan de Fuca Strait. Samples are displayed by location, west to east (Figure 31). The Leech River Fault extends westward into the strait indicating a change in coastal lithologies.

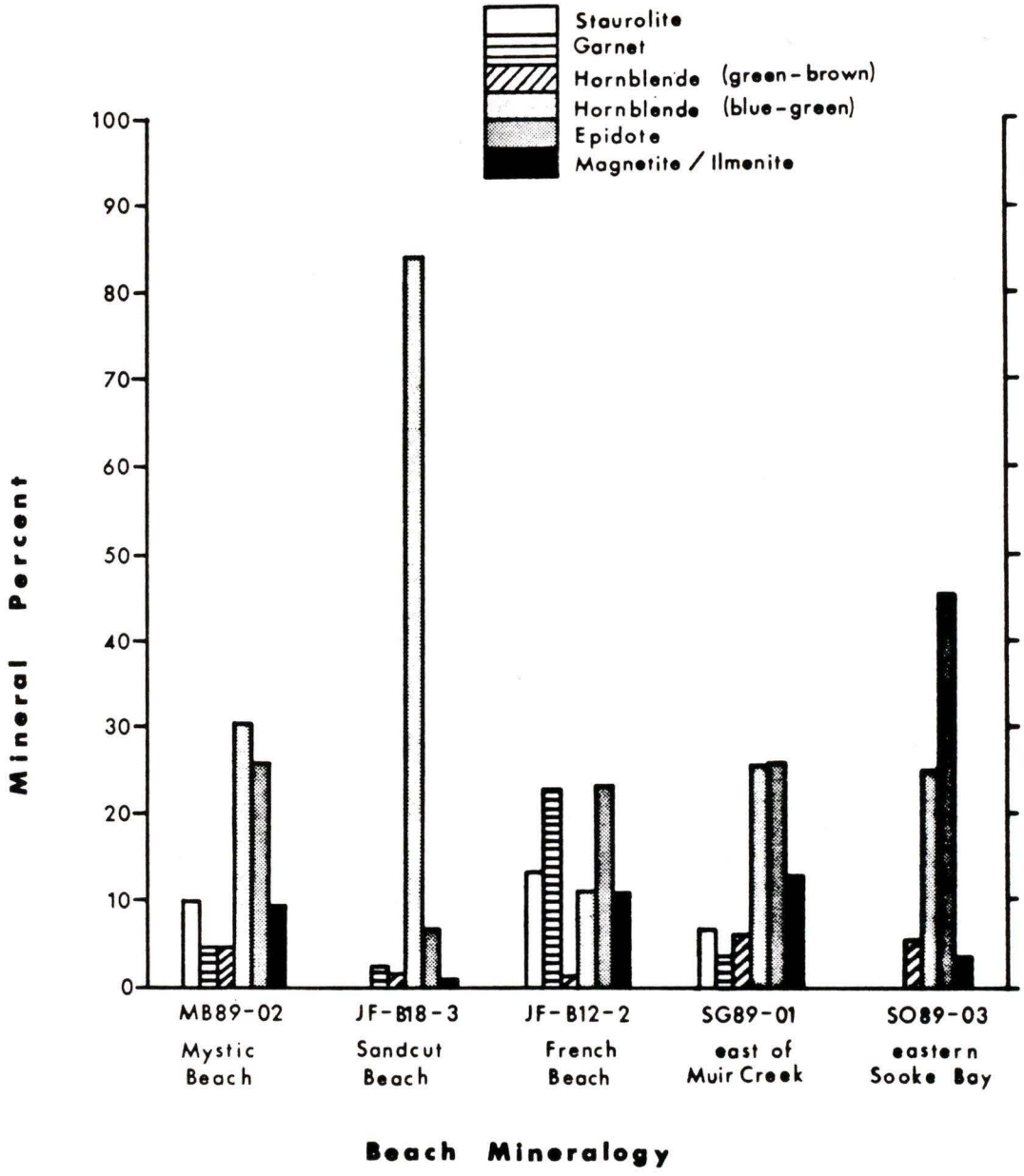

Figure 37. Beach mineral percentages from optical mineral counts (Table 18), coastal southwestern Vancouver Island. Samples are displayed by location, west to east, with all five beach sites adjacent to the Metchosin Igneous Complex, south of the Leech River Fault.

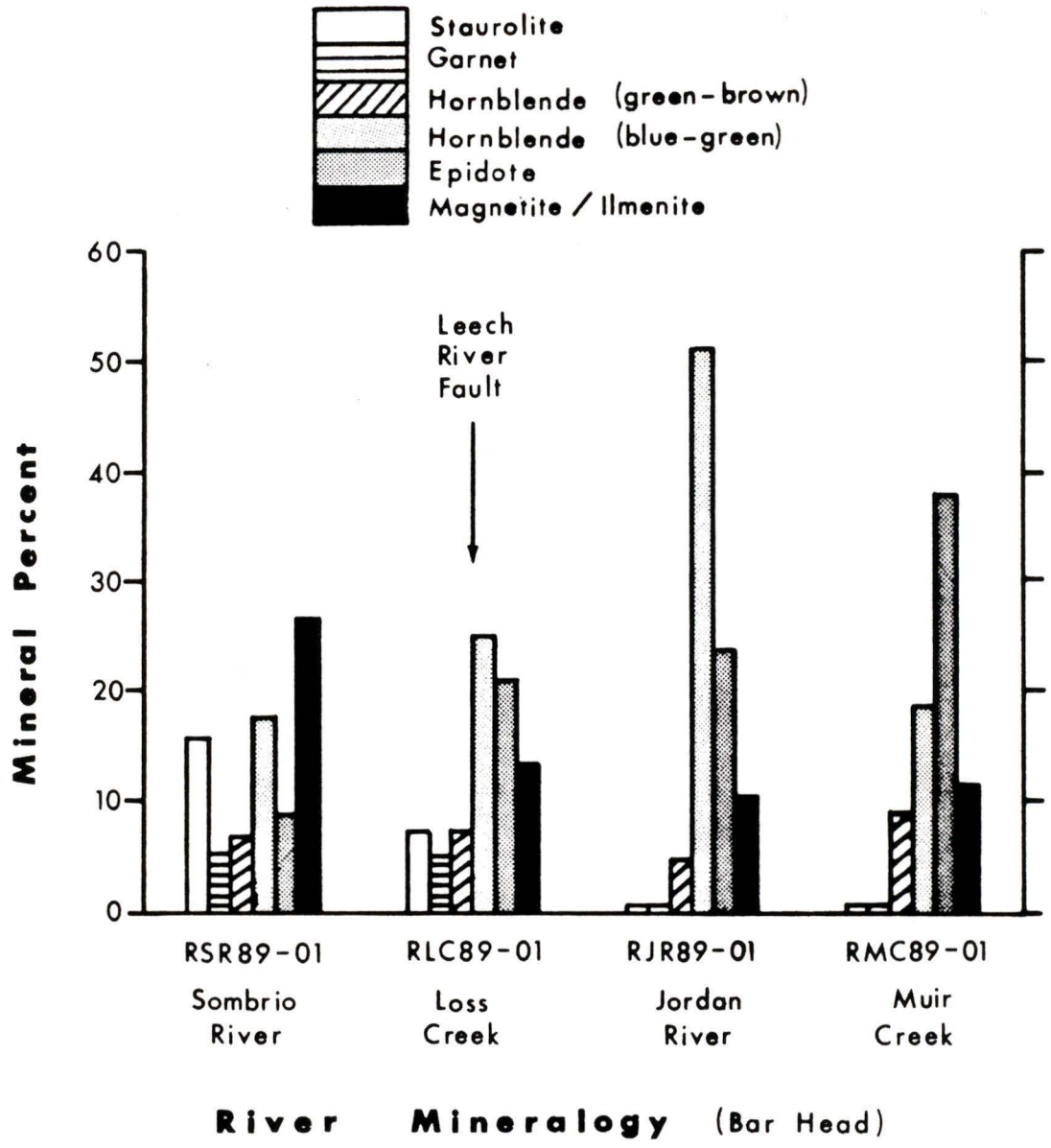

Figure 38. River mineral percentages from optical mineral counts (Table 18), southwestern Vancouver Island. Results from bar-head samples are shown by location, west to east, for each river. Leech River Fault follows the valley of Loss Creek, with the Leech River Complex to the west, and the Metchosin Igneous Complex to the east.

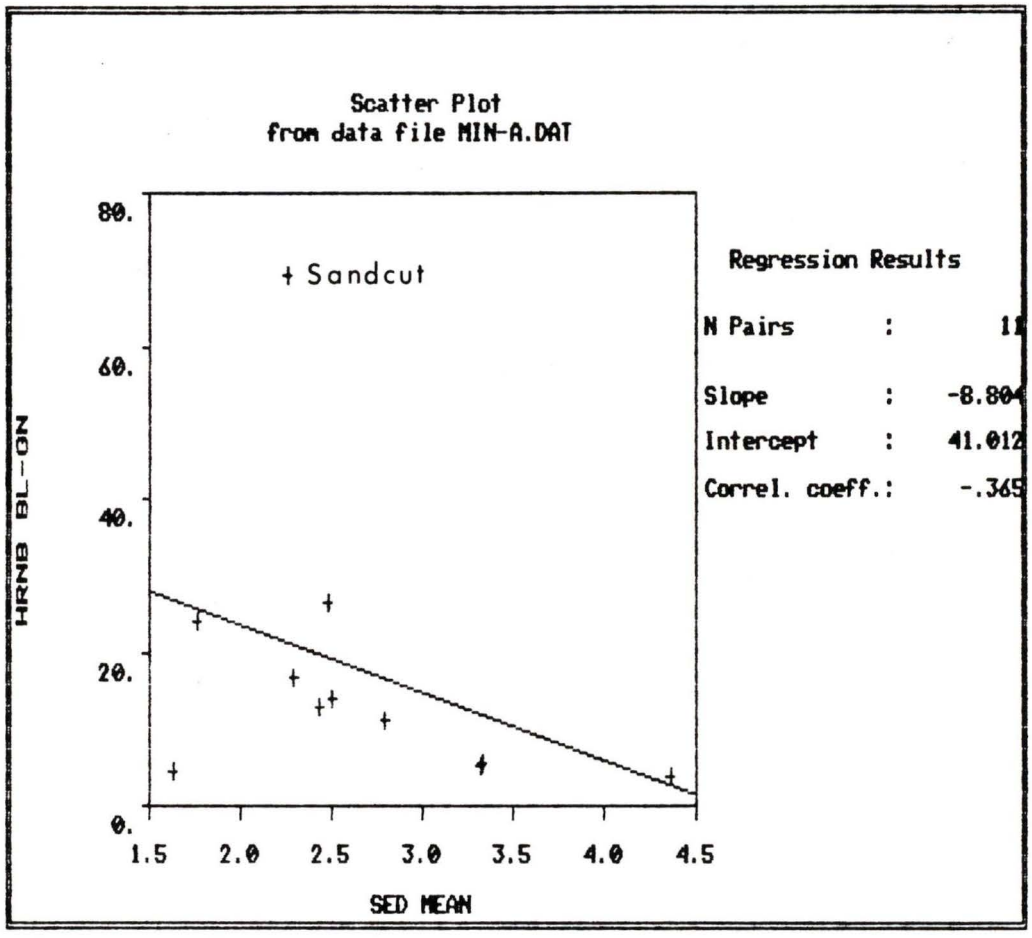

Figure 39. Crossplot of mean grain size (phi units) for the sand fraction (-1.0 to 4.0 phi) of 11 offshore samples with their number percent of blue-green hornblende (representing the narrow 3.0 to 3.5 phi fraction). Highest blue-green hornblende content is found offshore from Sandcut Beach.

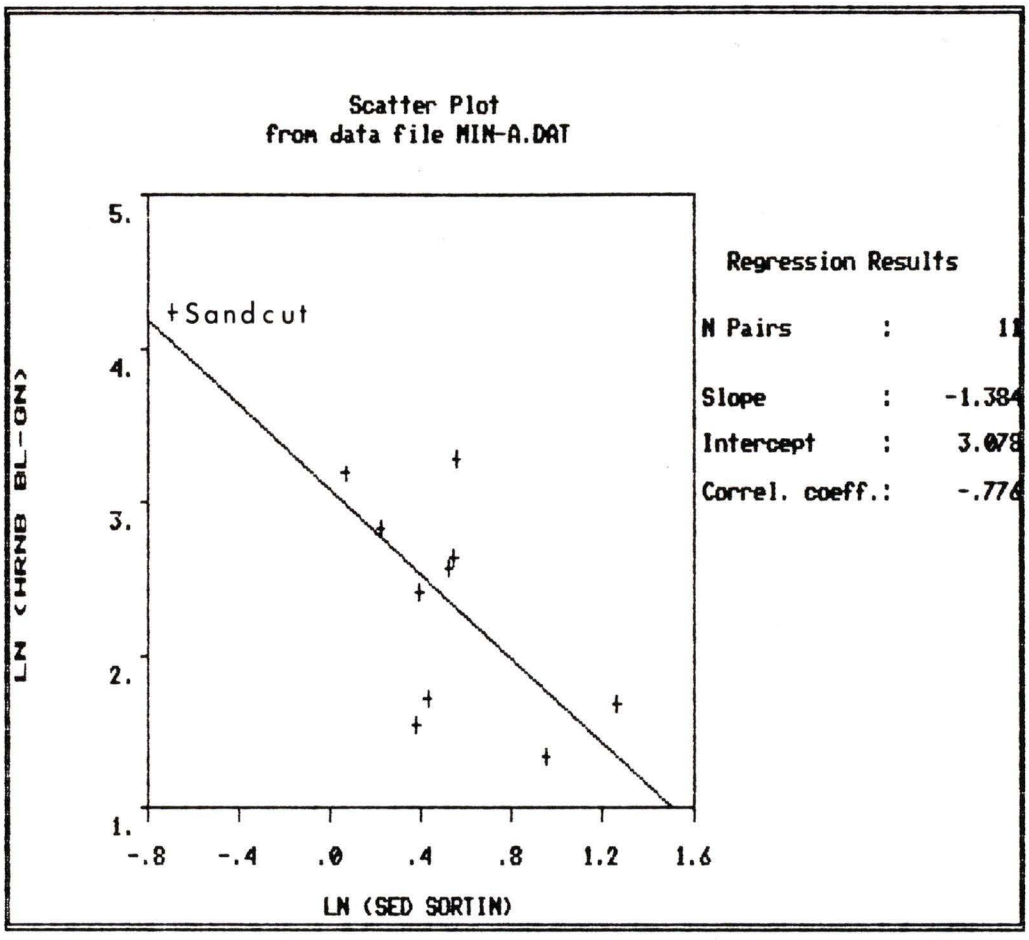

Figure 40. Offshore samples, from Figure 39, in crossplot of sorting values (logged phi units) with their number percent of blue-green hornblende (logged).

mineral percent was counted for a narrow size fraction range, and as the sorting value is for the whole sand fraction, this relationship may not be true for other size fractions.

The 20 samples have a correlation of r=0.84 between heavy mineral percentage (whole sand fraction) and blue-green hornblende. This value is strongly influenced by the Sandcut and Jordan River samples. However, no significant correlation occurs between blue-green hornblende and heavy mineral percentage of the fine fraction (0.125-0.090 mm) being examined. This may result from the variety of environments being observed, particularly the beach samples where large portions of their heavy mineral contents are concentrated in the finer sand fraction, due to more intense hydraulic sorting.

Metamorphic minerals - staurolite and garnet - decrease eastward from Loss Creek (Figure 38). Both Leech River and Metchosin rocks can be seen to supply minerals to Loss Creek. This pattern is not distinct offshore (Figure 36) or along the eastern beaches (Figure 37). No significant correlation could be obtained between the two minerals.

French Beach (JF-B12-2) is notable for the highest garnet and second highest staurolite counts in the sample set. Source rocks for these metamorphic minerals may be the Leech River rocks to the west, or they may be derived from

reworked glacial material. Beach mineralogy may be strongly affected by local streams or sediment influx, particularly where sediment transport is obstructed by prominent headlands. The latter is the case at French Beach, and, because no significant stream drains this area, beach sands may be derived from local bluffs and nearshore sediment transport. In this sample the fine sand fraction examined contained 97.4% heavy minerals, whereas the whole sand fraction contained 18.5% heavy minerals, suggesting significant sorting of the sand.

The category of "others" includes all minor transparent minerals. These are rutile, zircon, tourmaline, andalusite, apatite, sphene, chlorite, other amphiboles and unknowns. Individual "other" minerals occurred less than 3% in any one sample, and generally as 1% or less.

ii) Opaque Minerals

Counts of undifferentiated magnetite-ilmenite decrease east of Sombrio River (Figure 38). Offshore these opaques appear to increase in the samples some distance from shore (TUL88A-04 and PAR89A-51), then decrease eastward, particularly at Sandcut Beach (JF38-100) (Figure 31 and 36).

Whole sand fraction heavy mineral percentages were correlated with Ti ppm for these twenty samples (Table 4) at r=0.83. No significant correlation was found between Ti ppm and magnetite-ilmenite in the fine sand fraction.

Magnetite-ilmenite also showed little correlation with

the heavy mineral percentage in the fine fraction, exemplified by its near absence at Sandcut Beach, suggesting that the high Ti values stem from ilmenite in a larger or smaller size fraction than the one examined here.

To explore the relationship between magnetite-ilmenite and blue-green hornblende, in the limited fine size fraction, their ratios were examined (magnetite-ilmenite:blue-green hornblende). Values ranged from 0.01 to 4.0, with a mean of 1.1. The three lowest ratios 0.01, 0.01 and 0.2 were found at Sandcut Beach, offshore at Sandcut, and from upstream on Jordan River, respectively. These also represent the locations of the highest Ti values, again indicating that the preferred grain-size of the Ti (ilmenite correlating with blue-green hornblende) must be outside the sand size sampled.

Highest ratio values (magnetite-ilmenite:blue-green hornblende) are found in three offshore sites in the northwest (PAR89A-35, TUL88A-04 and PAR89A-51). These sites have relatively low heavy mineral percentages (less than 10%) and occur adjacent to the metamorphic rocks of the Leech River Formation. Highest river magnetite-ilmenite values occur in Sombrio River. These results suggest that the magnetite-ilmenite supplied from Leech River Formation may be the source of the adjacent values, supplying minerals in the size range being examined here. Magnetite-ilmenite to the southeast may occur in association with the blue-

green hornblende, but may dominate another size range, particularly in zones of higher heavy mineral content, and be derived from the adjacent volcanic terrain.

iii) Rock Fragments

Rock fragments and altered minerals were combined with minor opaques (hematite, leucoxene and pyrite) and unknown opaques. They represent between 4.8% to 28.6% of the heavy mineral counts (Table 4), except at SR89-D1 with a value of 69.9% due to local enrichment of pyrite (discussed below).

Lithic fragments were generally rounded and transitional from translucent to opaque. Comparable numbers of rock fragments occur in all environments examined although the distant offshore samples in the northwest had lowest values (TUL88A-04 and PAR89A-51) (Figure 31). Sombrio River had the lowest value for lithic fragments, and Sandcut Beach had a similar low value (Table 4).

No correlation was observed between lithic fragments and sediment mean grain size. However, a correlation of r=0.82 was found between lithic fragments and sediment sorting (in phi units), indicating an increase in lithic fragments with a decrease in sorting.

The dive sample obtained off Sombrio River mouth (SR89-D1) is unique due to its high percentage of pyrite (59.9%). The pyrite most frequently occurred as framboids. This sample was obtained from loose sediment on the exposed bedrock surface around the base of large submerged boulders

in 11 m of water.

iv) Hydraulic Fractionation

In order to observe the possible influence of hydraulic fractionation in the observed heavy-mineral environments, ratios were utilized. The shape-fractionation index is expressed by ratios of bladed-elongate minerals to equant minerals (Flores and Shideler, 1978). In this study the ratio is between (pyroxene + hornblende)/(garnet + epidote). The ratio is confined to the narrow grain size examined, limiting most deductions and comparisons to that range.

The shape-fractionation index has a range of 0.4 to 10.2 for all 20 samples. Means of 1.0, 0.9 and 1.3 for offshore, beach and river samples, respectively, are derived for the 17 samples excluding the three anomalous samples from Sandcut Beach, offshore Sandcut and Jordan River. Index values are uniform in all three environments, although beaches tend to have slightly lower values and rivers slightly higher (shorter period of mechanical abrasion and sorting).

Offshore from Sandcut Beach, however, the index is 7.3, seven times the mean of the other ten offshore samples. On Sandcut Beach the index is 10.2, and upstream on Jordan River is 2.5. These three samples illustrate that the very fine sand at Sandcut beach has undergone very little shape-fractionation compared to all other sites and environments.

These samples have likely travelled a very limited distance and have had little hydraulic sorting. It is interesting to note that if Jordan River is the source of the mineral assemblage occurring at Sandcut Beach, the river heavy minerals have a lower shape-fractionation index than found at the beach site. The index would be assumed to decrease as river material underwent continued abrasion downstream and into the marine environment, as observed in the mean values for the three environments.

Lowest offshore shape-fractionation index values are found farthest from shore at 0.5, 0.7 and 0.7 at TUL88A-04, PAR89A-51 and PAR89A-83, respectively (Figure 31). The mineralogy suggests that these samples, within this fraction of the sand, have experienced the greatest sorting by shape, although these sites are from sediments that are poorly to very poorly sorted by size.

The lowest beach ratio, 0.4, is found at French Beach (JF-B12-2). This is not surprising, as evidence of extremely high heavy mineral concentration in this fine fraction was discussed earlier. The index suggests that very fine sand at French Beach experiences the greatest mechanical sorting (and abrasion) by shape of all samples examined.

Hydraulic fractionation by density can be observed by the ratio of opaques to non-opaques (Flores and Shideler, 1978), in comparable sample grain sizes. Opaque minerals

have a higher average specific gravity (4.7) than non-opaques (3.7), such that an increase in opaques to non-opaques may likely represent an increase in hydraulic sorting (Flores and Shideler, 1978).

This index for hydraulic sorting by density was used by Flores and Shideler (1978) on bottom sediments from the continental shelf. The index assumes that with an increase in hydraulic sorting by density the number of opaques will increase relative to other minerals. The index, strictly speaking, is probably not suitable for beach grab samples, or shallow trenches. The possibility exists that heavier opaques have moved downward into underlying sediment layers due to active hydraulic sorting in the beach environment. If samples are obtained during a season when lighter sediments cover the beach surface a low number of opaques will be obtained indicating low sorting when high sorting by density is actually taking place. If this is the case on any of these five beaches, then greater concentrations of opaques may be found on such a beach in a finer fraction than examined in this study.

In this study the value for magnetite-ilmenite percent (Table 4) is used for the 3.0-3.5 phi range examined. Values for the three environments are:

offshore	X = 17.1	range = 1.0 to 80.5
beach	X = 6.8	range = 0.7 to 13.0
river	X = 16.3	range = 10.0 to 33.9.

For very fine sand, fractionation by density appears to be

only slightly higher offshore than in river samples. Beach values show relatively low hydraulic sorting by density. Lowest two values from 20 sites are found at Sandcut Beach, with 1.0 and 0.7, for offshore and beach, respectively. Lowest river value is found at Jordan River at 9.1. This suggests that hydraulic sorting by density at Sandcut Beach is poorer than the samples entering the coast from the river. If poor sorting by density is present in this fine size fraction it may support the view that more opaques will be found in larger size fractions, as suggested earlier.

Two samples with the highest O/NO ratio are again from the very fine sand fractions of the samples farthest offshore (TUL88A-04 and PAR89A-51), noted as having high sorting, or abrasion, from the shape-fractionation index. To the southeast PAR89A-83 was identified earlier as having high sorting by shape-fractionation, but appears to have relatively low sorting by density. This may be due to a grain size effect from a different provenance and size range for magnetite-ilmenite in the north than in the south, possibly supported by the low magnetite values in this fine size fraction in the eastern river samples.

Evaluation of this index for hydraulic sorting by density must be used with caution. Although relatively few minor opaques are found in the lithic fragment category, the lithic fragments themselves may have significant densities, particularly with inclusions of opaques. In addition,

mineral percentages used in the index represent only a narrow window into the grain-size distribution of each sand sample.

v) Principal Component Analysis

It was desirable to employ a multivariate analysis technique to obtain what information could be derived from the variance and covariances among the heavy minerals. Q-mode factor analysis is commonly used for such work in detrital mineral analysis (Hubert, 1971). In this technique a similarity matrix is calculated across variables, so that the data are allowed to have a linear restraint (closure). Ultimately, the goal is to group samples, by showing similarity between samples, as in cluster analysis (Davis, 1973). In the present study, however, the 20 samples represent specific locations and environments, and their similarities can be predicted from the mineral percentages.

It is of greater interest to compare the total mineral assemblage at each site, the minerals present and their amount, forming vectors of each sample, and then comparing vectors and variances. However, this is R-mode factor analysis, a technique which theoretically prohibits the use of data with a linear restraint (Hubert, 1971).

In the place of these techniques principal component analysis was employed. Principal component scores may be interpreted in much the same manner as factors, and are the starting points for factor-analytic schemes (Davis, 1973).

Although closure remains a problem, the technique did show some applicable results. Davis (1973) describes principal component analysis as not, strictly speaking, a statistical technique, but rather a mathematical manipulation, and its utility can be judged by performance.

Mineral percentages for eight transparent mineral groups plus magnetite-ilmenite (Table 5) were used with the U.S.G.S. Statpac programs for Principal Component Analysis and Varimax Solutions (Grundy, 1988).

Principal component scores were extracted for the first three components. Together they represent 71% of variance in the data set.

Principal component scores for component 1 and component 2 are used to create a crossplot (Figure 41). Component 1 will, by definition, describe the elements of greatest variation in the data set. Along the axis for component 1, the three samples with anomalously high concentrations of blue-green hornblende at Sandcut Beach and Jordan River are separated out. This group is followed by TUL88A-04 and PAR89A-51 which have been shown earlier to have the greatest relative enrichment in magnetite-ilmenite. At the negative end of the component are PAR89A-83 and PAR89A-19. Both samples represent offshore sites at the two geographic extremes of the study area (Figure 31), and exhibit the greatest mineralogic differences from the anomalous samples. At the mouth of Port San Juan the

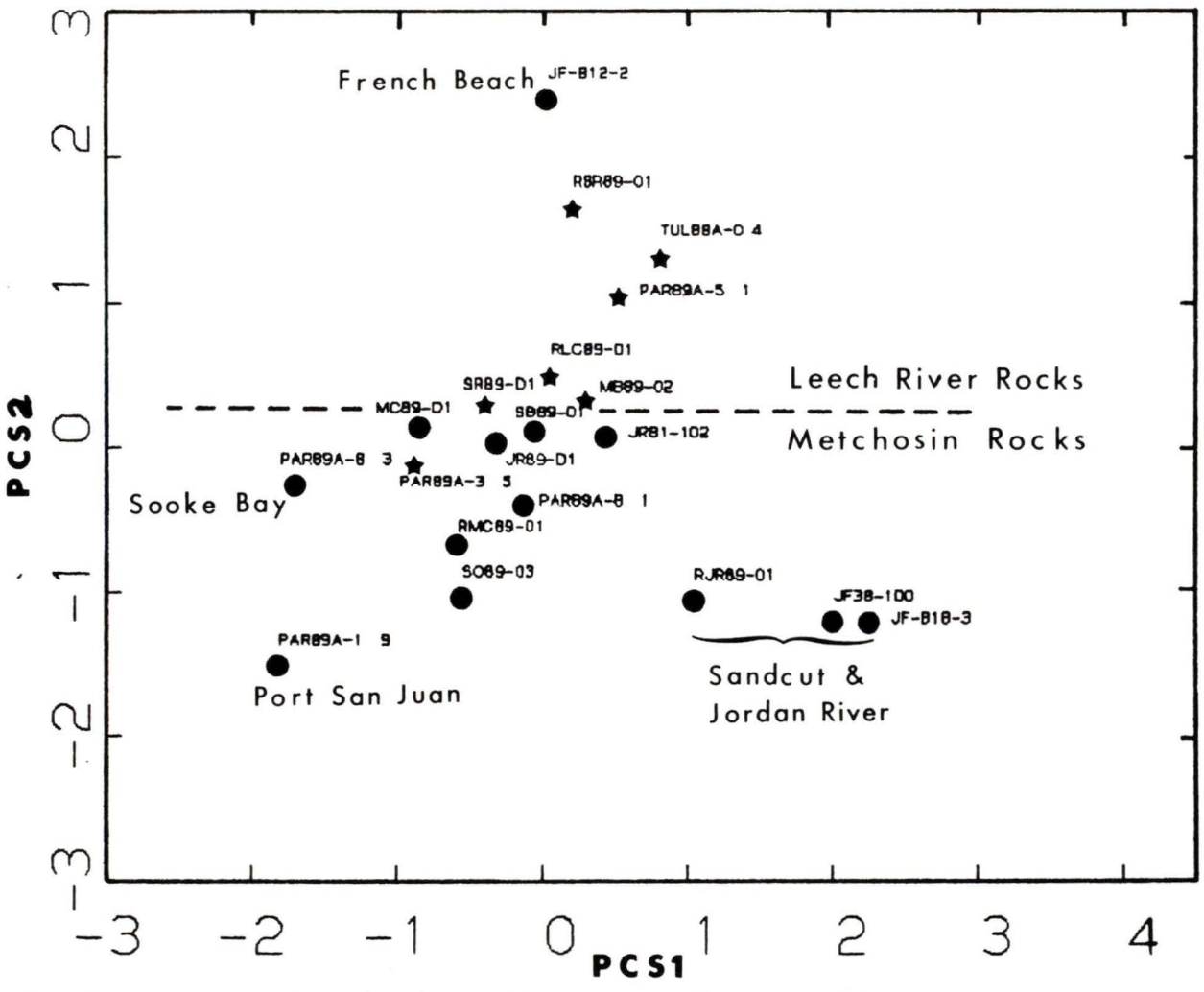

Figure 41. Crossplot of Principle Component Scores (PCS) one and two. PCS1 indicates greatest variation between sample mineralogy (and anomalous samples), while PCS2 indicates the probable provenance of mineral assemblages at each site.

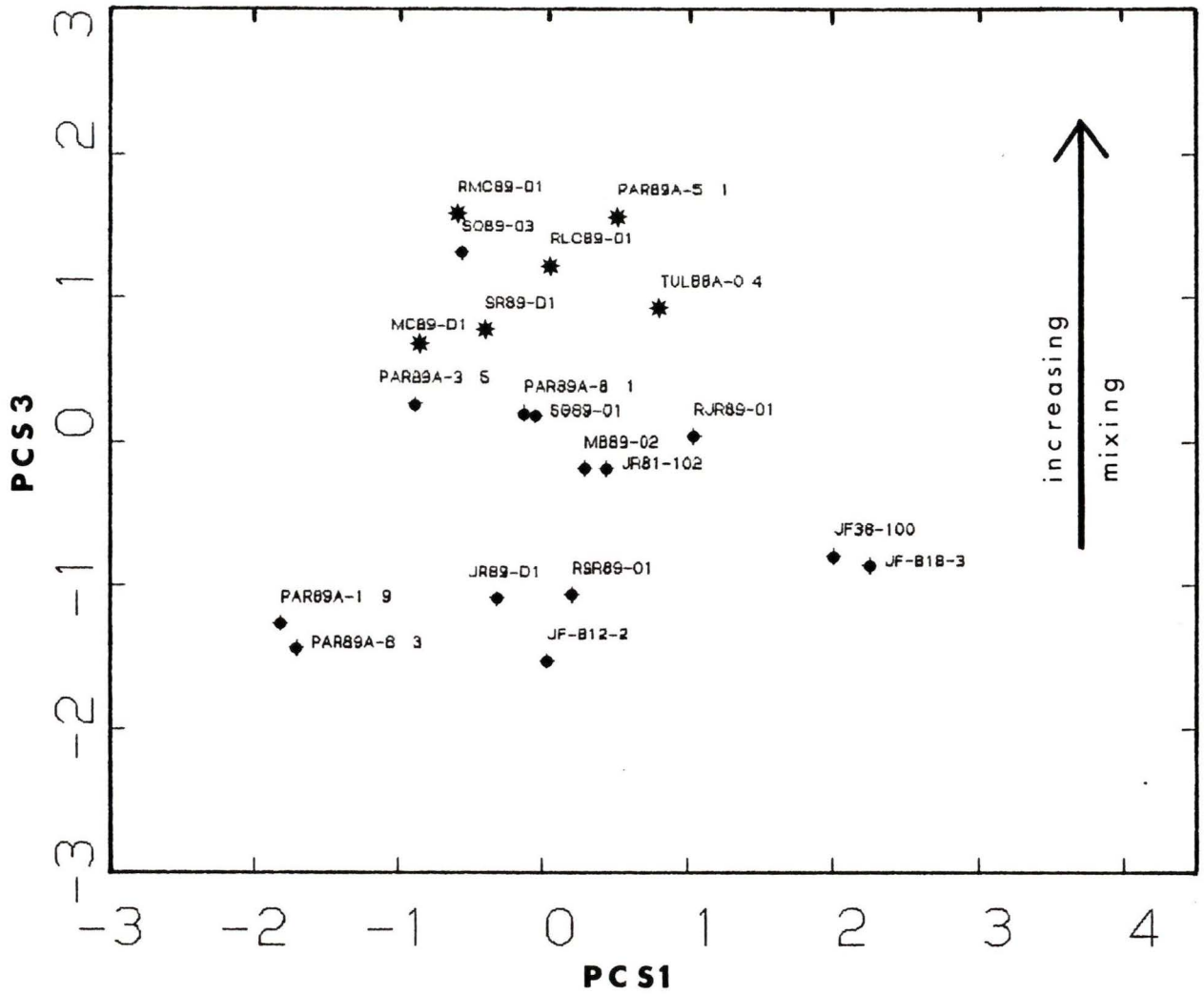

Figure 42. Crossplot of Principle Component Scores (PCS) one and three. PCS3 may indicate degree of mixing of two or more mineral assemblage populations.

mineralogy represents a foreign provenance (with low blue-green hornblende), and in Sooke Bay little blue-green hornblende is present at 67 m depth (the deepest sample site in the set). At least 69% of the variation in blue-green hornblende and 54% of the epidote variance is explained by component 1.

Component 2 may be regarded as indicating the probable provenance of mineral assemblages at each site. Samples which are derived adjacent to the Leech River Formation tend to group above zero. Samples representing mixing, such as along Loss Creek itself, and samples from offshore and southeast of the fault contact plot together near zero, including MB89-02 from Mystic Beach, the first beach included southeast of the fault. Generally the samples sited adjacent to the Metchosin Volcanic Complex group together at, or below, zero. Samples with the greatest variation from the Leech River Formation mineral assemblage appear to be the Sandcut Beach samples and the sample from the mouth of Port San Juan. French Beach (JF-B12-2) is distinguished by its high concentration of garnet and staurolite, as discussed earlier. Component 2 explains 65% of the variation in garnet and 55% of the variation in staurolite.

Component 1 is plotted against component 3 in a second crossplot (Figure 42). The cause for variation explained by component 3 is less clear than for the first two components.

Nevertheless, this variation may be due to mixing of two or more mineral assemblage populations. The combination of minerals from various sources may be due to glacial transport and deposition, or erosion of the bluff-forming and underlying sandstone of the Sooke Formation.

Percentage of variation in clinozoisite-zoisite and pyroxene are explained 47% and 23%, respectively, by component 3. These two mineral groups will have been largely derived from the Metchosin volcanics, but were found in relatively uniform (although low) amounts in most samples. Mixing is indicated not just by longshore transport, but the occurrence of garnet and staurolite upstream in the volcanic rocks illustrates that introduction of minerals by other means has occurred. Mineralogy may be complicated by the introduction of minerals due to erosion of Quaternary deposits, or the erosion of the poorly-indurated Sooke sandstones.

In this crossplot (Figure 42) the samples with large positive scores for component 3, showing more than local mineralogy, include two river samples draining the two largest basin areas, Loss Creek (RLC89-01) (draining both provenances) and Muir Creek (RMC89-01), which cuts extensively through the Sooke Formation. In addition, two offshore samples near Leech River Fault (PAR89A-51 and TUL88A-04), but farthest from shore, and the samples from the mouth of Muir Creek (MC89-D1) and Sombrio River (SR89-

D1) show high mixing. The latter two sites occur adjacent to extensive exposed sandstone bluffs of the Sooke Formation, and its intertidal platform. The sample from near the mouth of Sombrio River may be derived from eroded sands of the Sooke Formation rocks at the sample site. Many samples less than -1 in component 3 have been indicated earlier as containing strictly local (as at Sandcut Beach), or mainly foreign (PAR89A-19) mineral concentrations.

These three components illustrate the relationship between samples in terms of high variance, particularly anomalous zones of interest, mineral provenance, and the existence of mixing due to glacial transport and deposition or erosion of the underlying sandstones.

vi) Light Mineralogy

The light mineral residue from three widely distributed samples (Figure 31) were mounted and counts of mineral percentages performed to derive a general picture of the light minerals predominating in the offshore (Table 6).

TABLE 6. LIGHT DETRITAL MINERAL PERCENTAGES

West	PAR89A-51	JR89-D1	MC89-D1	East
depth	*36m*	*9m*	*6m*	
Quartz	34.7	49.0	62.0	
Feldspars	7.7	6.3	3.7	
Micas (chlorite)	1.3	5.7	3.0	
Lithic fragments	36.3	26.7	25.3	
Volcanic glass	13.0	6.7	0.0	
Others	7.0	5.6	6.0	

A few general observations can be made. Quartz and

lithic fragments largely dominate the offshore light fraction. Quartz appears to increase eastward and shoreward. This dramatic change is probably related to the presence of volcanic source rocks to the east. In contrast, feldspar appears to decrease eastward and with a decrease in depth. Micas, mainly chlorite, increase shoreward, particularly near Jordan River.

Caution is necessary in making observations about lithic fragments as they have been seen to be transitional into the heavy mineral fraction. Very angular volcanic glass appears to be preserved in deeper water, and decreases or is lacking in more turbulent nearshore waters.

The category of "others" includes biotite, hematite-coated minerals, unknown minerals and infrequent microcrystalline calcite, usually infilling a microfossil test.

6. Geochemistry

Two sets of samples were sent for geochemical analyses, one each in 1989 and 1990. Analytical techniques in 1990 were more specialised and digestion of material attempted to be more complete. No attempt is made to combine these sets; rather, statistical analyses were performed on each set separately.

The two sets of geochemical values represent the same geographic provenance, with some variation (Figure 43). Overall depths of the two sets are comparable, with 64% and 61% of sample depths being less than or equal to 20 metres for 1989 and 1990, respectively. For ease of understanding, samples analysed in 1989 will be referred to as Group A, and those analysed in 1990 referred to as Group B.

i) Offshore Sand Geochemistry

a) Univariate Statistics

Offshore sand fractions for 22 samples were analysed in Group A, and 28 samples in Group B. Univariate statistics were calculated for each element (Tables 7 and 8). Detection limits varied between groups (Appendix C). For group A, analysis for Co and Ni was not performed.

Limited assays were performed for Au, Pd and Pt. Values of these elements for these marine sediment samples were generally near or below the detection limits. However, the dive sample at the mouth of Jordan River revealed 100 ppb Au (B).

TABLE 7. OFFSHORE SAND FRACTION GEOCHEMISTRY - 1989
(*Group A*, 22 Samples)

	Samples > det.	$\bar{X}$	s	skew-ness	kurt-osis	Min.	Median	Max.
Au ppb	1*	5.0	-	-	-	-	-	-
Pd ppb	9*	3.0	4.5	1.8	4.5	2.0	2.0	8.0
Pt ppb	6*	23.3	5.2	0.7	1.5	20.0	20.0	30.0
Co ppm	NR	-	-	-	-	-	-	-
Cu ppm	22	29.3	17.9	3.6	15.9	18.0	26.0	105.0
Fe %	22	1.4	0.3	0.4	2.9	1.0	1.4	2.0
Mn ppm	22	294.5	90.6	0.5	2.2	155.0	268.5	471.0
Mo ppm	22	2.8	0.6	-2.4	7.2	1.0	3.0	3.0
Ni ppm	NR	-	-	-	-	-	-	-
Pb ppm	22	48.0	3.5	0.5	2.5	43.0	47.5	56.0
V ppm	22	110.1	23.2	0.4	3.1	74.0	108.0	169.0
Zn ppm	22	31.5	6.0	0.7	3.2	23.0	30.5	47.0
Ag ppm	22	0.7	0.1	-0.1	2.0	0.5	0.7	0.9
Cd ppm	0	-	-	-	-	-	-	-
Se ppm	1	12	-	-	-	-	-	-
Sn ppm	6	10.2	0.4	1.8	4.2	10.0	10.0	11.0
Hg ppb	22	23.0	8.0	1.1	2.9	15.0	20.0	40.0
Sb ppm	17	11.7	3.6	-0.3	2.3	6.0	12.0	18.0
Bi ppm	0	-	-	-	-	-	-	-
Ti ppm	22	3345.5	708.3	0.1	2.0	2200.0	3400.0	4500.0
Zr ppm	22	83.2	14.2	1.0	3.3	65.0	80.5	118.0
Cr ppm	22	120.5	41.6	0.2	1.8	57.0	119.0	199.0

* Only 9 sand samples assayed for Au, Pd and Pt.
NR = samples not run for that element in 1989.

TABLE 8. OFFSHORE SAND FRACTION GEOCHEMISTRY - 1990
(*Group B*, 28 Samples)

	Samples > det.	$\bar{X}$	s	skew-ness	kurt-osis	Min.	Median	Max.
Au ppb	2*	53.0	66.5	0.0	1.0	6.0	53.0	100.0
Pd ppb	0*	-	-	-	-	-	-	-
Pt ppb	0*	-	-	-	-	-	-	-
Co ppm	28	10.5	6.0	1.9	5.7	6.0	8.0	30.0
Cu ppm	28	90.5	118.3	2.1	6.2	10.0	43.0	470.0
Fe %	28	2.7	0.8	1.2	3.3	1.8	2.4	4.5
Mn ppm	28	325.7	98.8	0.5	2.0	205.0	300.0	510.0
Mo ppm	6	1.0	0.0	0.0	0.0	1.0	1.0	1.0
Ni ppm	28	20.5	6.2	0.9	3.4	11.0	19.0	37.0
Pb ppm	28	15.9	17.2	2.0	6.8	2.0	8.0	76.0
V ppm	28	67.4	24.6	0.9	2.5	35.0	59.5	120.0
Zn ppm	28	41.9	8.0	0.3	2.0	30.0	39.0	58.0
Ag ppm	0	-	-	-	-	-	-	-
Cd ppm	0	-	-	-	-	-	-	-
Se ppm	6	0.4	0.3	0.8	2.0	0.2	0.2	0.8
Sn ppm	13	5.0	3.3	0.6	2.0	2.0	4.0	11.0
Hg ppb	28	29.6	10.4	1.1	3.9	20.0	30.0	60.0
Sb ppm	23	0.2	0.1	2.9	9.6	0.2	0.2	0.4
Bi ppm	2	0.1	0.0	0.0	0.0	0.1	0.1	0.1
Ti ppm	28	7455.4	2347.8	0.9	3.0	4250.0	6600.0	13300.0
Zr ppm	28	109.7	15.2	0.1	3.3	78.0	110.0	145.0
Cr ppm	28	192.0	42.4	1.1	3.9	128.0	182.0	300.0

* Only 5 sand samples assayed for Au, Pd and Pt.

For the elements Mo, Ag, Cd, Se, Sn and Bi, sample values in both groups, and Sb in Group B, are not above or are not sufficiently above the detection limit (considering at least the margin of error in analytical techniques) to imply that no further analysis is warranted.

Mercury values in the offshore were very low and because concentrations were reported as grouped data further analysis was prevented.

In both groups enrichment of six elements, Cu, Fe, Mn, V, Ti and Cr, was found in the nearshore from China Beach as far east as Sheringham Point headland. Nine samples obtained from the shallow submarine terrace in the Jordan River area (China Beach to Sandcut Beach) frequently represented the highest concentrations for these elements in Group A, often indicating the introduction of another population which enriched the first. Highest values for this enrichment are found in the transect of samples extending into the strait from Sandcut Beach. This transect is represented by six samples in Group B which display the highest values for the six elements above, plus Co, Ni and Zn. The four samples nearest the beach have the highest offshore heavy mineral contents.

Logged Cu values indicate a polymodal population with enrichment in the Jordan River area (A) (Figure 44) and along Sandcut transect (B) (Figure 45). The single anomalous Cu value (A) is from a sample in deeper water in

the northwestern part of the study area.

Fe values approximate a single normal population with highest values located in the Jordan River area (A) (Figure 46). In Group B, logged Fe values show a polymodal population with distinct enrichment along the Sandcut transect (Figure 47). Two additional samples showing enrichment in Fe are the dive samples at the mouths of Loss Creek and Muir Creek.

Mn shows bimodal populations in both groups which include enrichment (Figures 48 and 49) in the Jordan River area and Sandcut. Mn is one of several elements which derives one of its highest concentrations from the samples taken from the three southeastern river mouths.

The probability plots for V suggest polymodal populations for the background values in both groups (Figures 50 and 51), with highest values forming separate populations. In Group A the latter represents Jordan River area and in Group B the five anomalous V values include the dive sample off Loss Creek as well as the four transect samples from Sandcut Beach.

Ti concentrations break into two distinct normal populations in both groups (Figures 52 and 53). The enriched population from Group A is again from the Jordan River area while Group B includes the six Sandcut Beach samples, three river mouth dive sites, and two proximal Jordan River area samples.

Cr values present two normal populations in Group A, as above, with the highest population drawn from samples in the Jordan River area (Figure 54). However, in Group B only three high values form an anomalous population (Figure 55). The highest 11 values represent sites around the Jordan River terrace area.

Logged Co values (B) typify the offshore normal background pattern and the enriched transect samples (Figure 56). The grouping of samples at the low end of the probability plot are an artifact of the artificial line drawn at the detection limit of the analytical technique.

Ni concentrations (logged) (B) show a single normal population where the highest values are from the dive site off the mouth of Loss Creek, followed by five samples from the transect off Sandcut Beach (Figure 57).

Zn has a normal population (logged) of low background values in Group A (Figure 58). In Group B the highest Zn values (logged) are also found in the six Sandcut Beach transect samples (Figure 59). Although two approximately normal populations appear (B), this may be an artifact of the evident grouping of sample results. Both sample groupings describe parallel lines, suggesting minor, if any enrichment.

Sb concentrations in Group A approximate a single normal population with highest values located in the Jordan River offshore area (Figure 60).

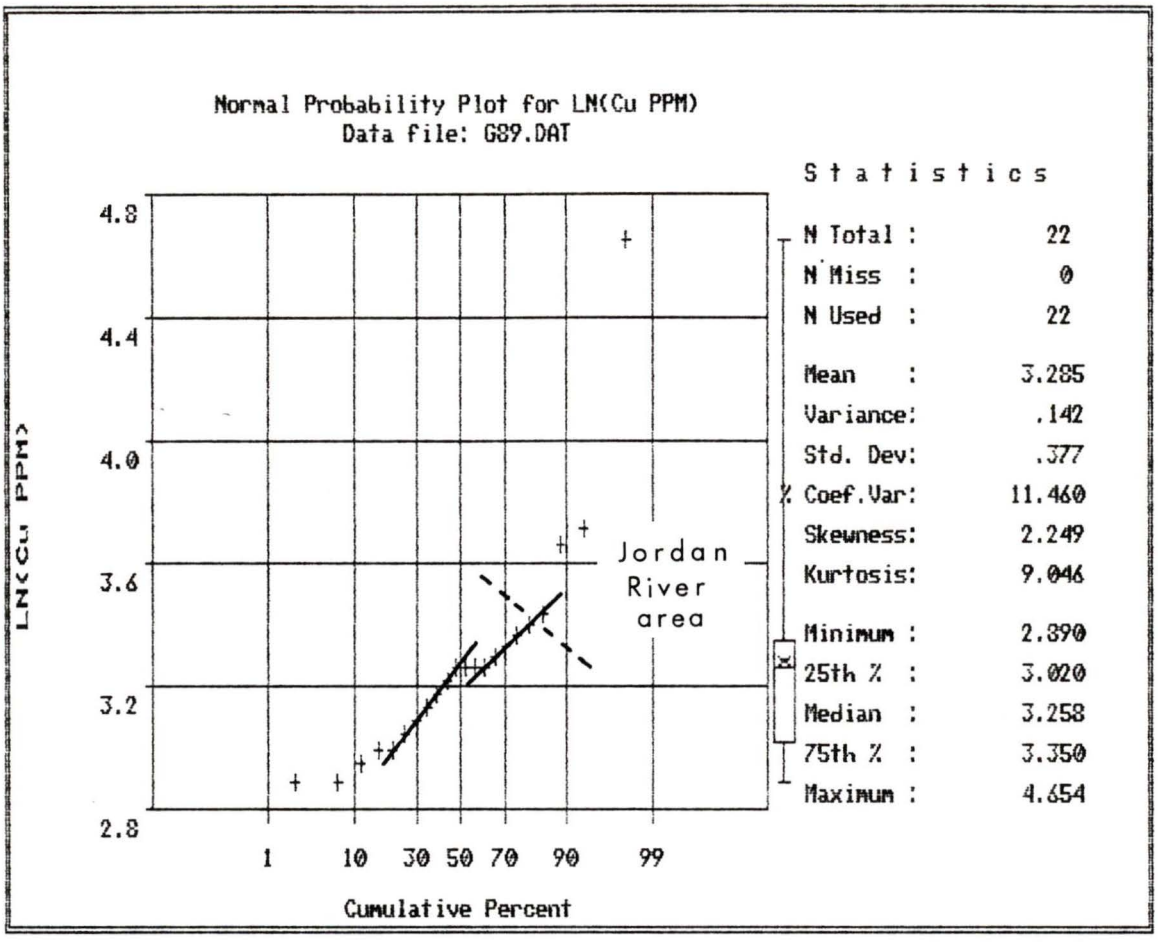

Figure 44. Probability plot of offshore Cu concentrations (logged), 1989 (Group A). Highest grouped values derive from the Jordan River area; anomalous sample from deep water.

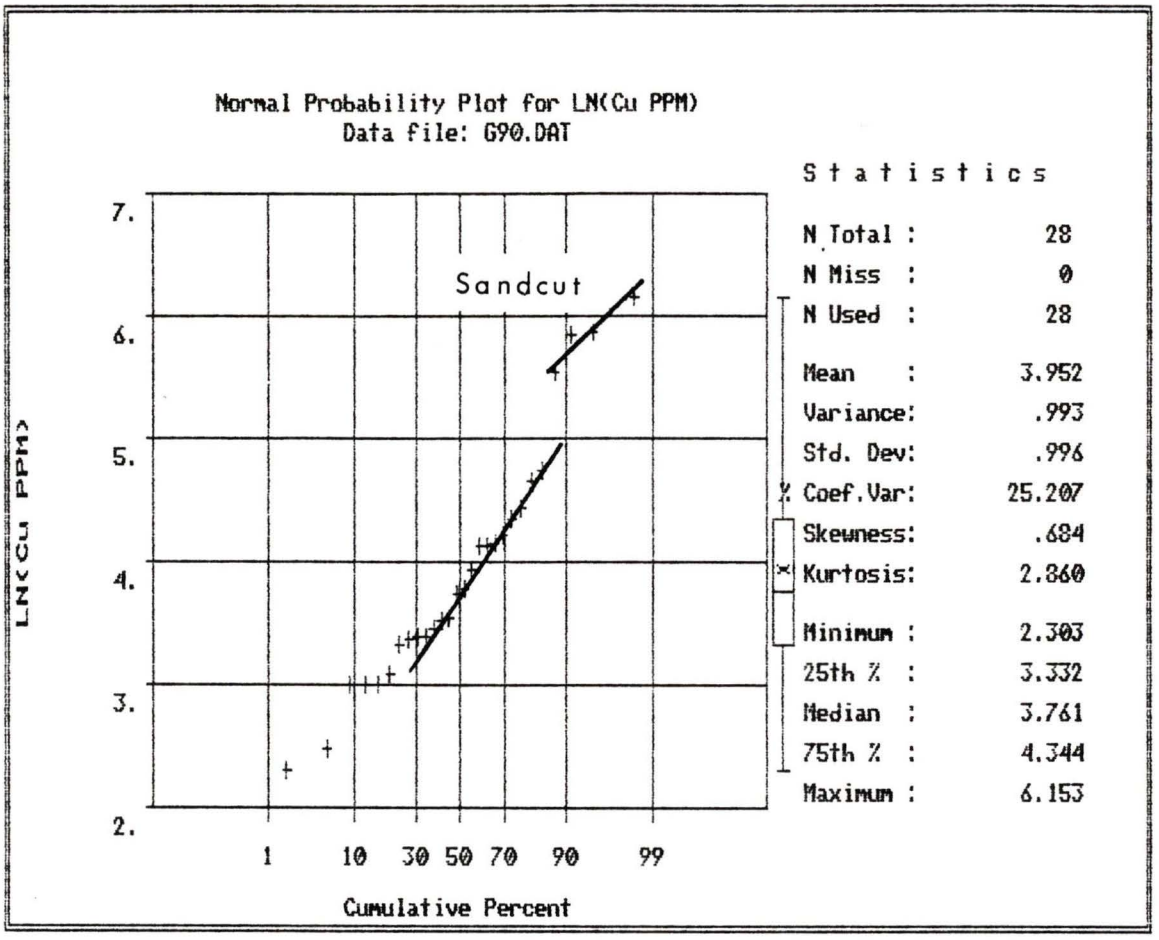

Figure 45. Probability plot of offshore Cu concentrations (logged), 1990 (Group B). Highest values found in samples from the Sandcut transect.

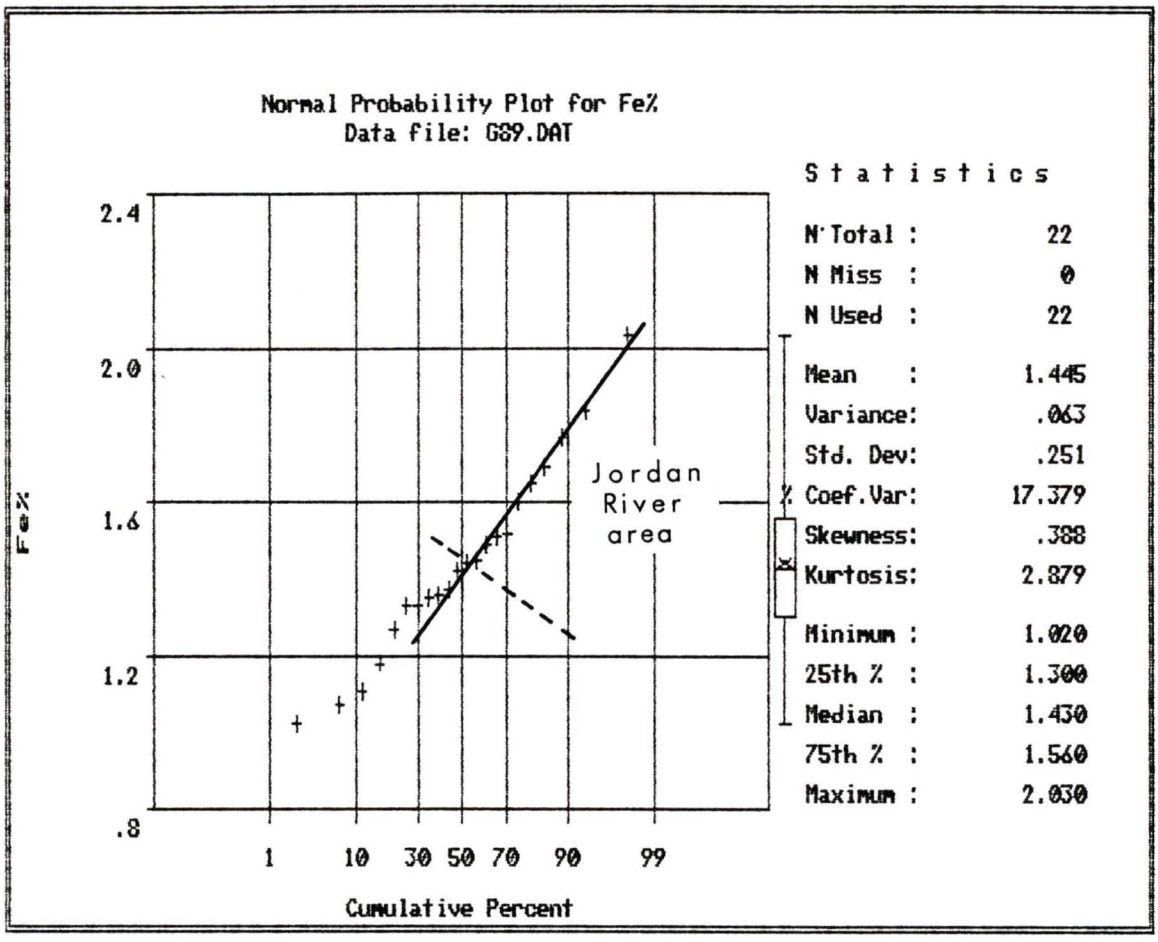

Figure 46. Probability plot of offshore Fe concentrations, 1989 (Group A). Highest values derive from the Jordan River area.

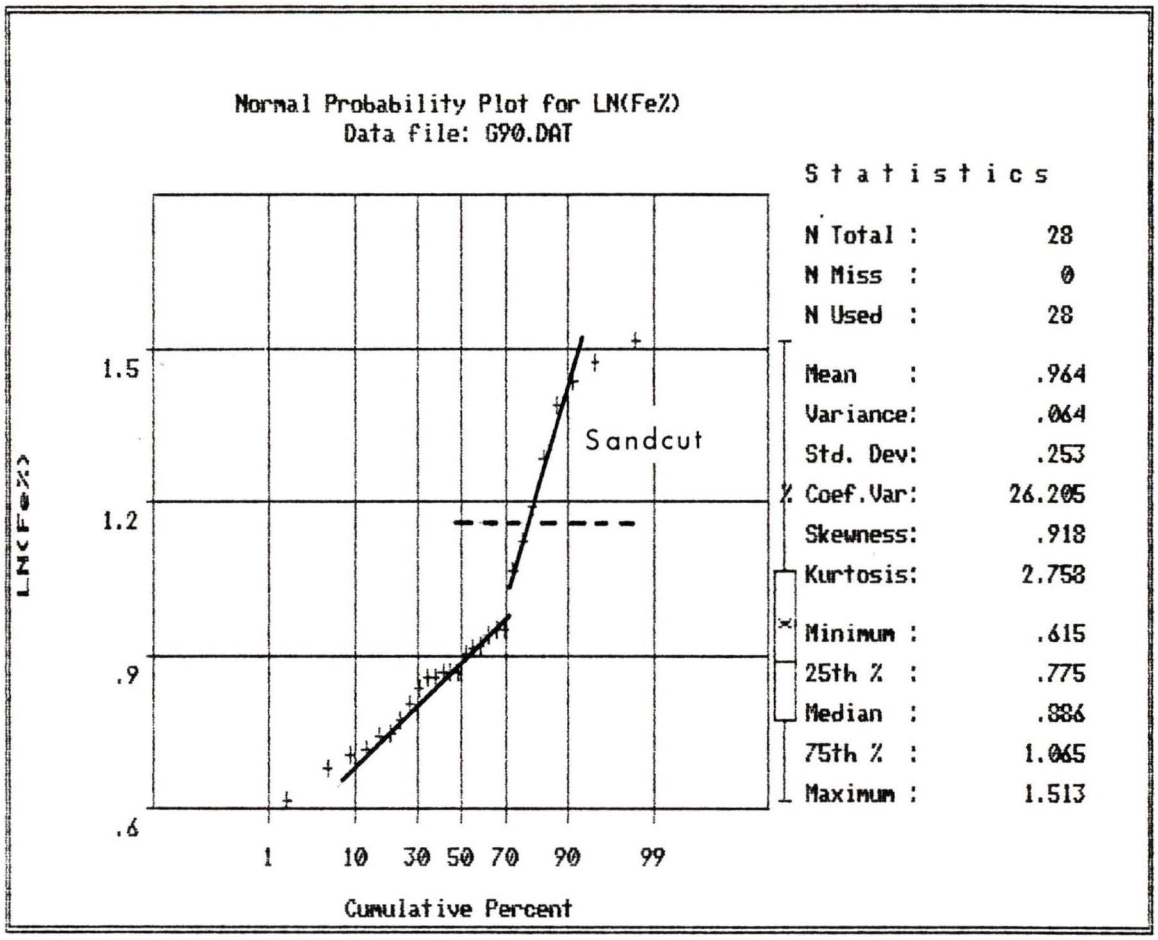

Figure 47. Probability plot of offshore Fe concentrations, 1990 (Group B). Highest values found in samples from the Sandcut transect.

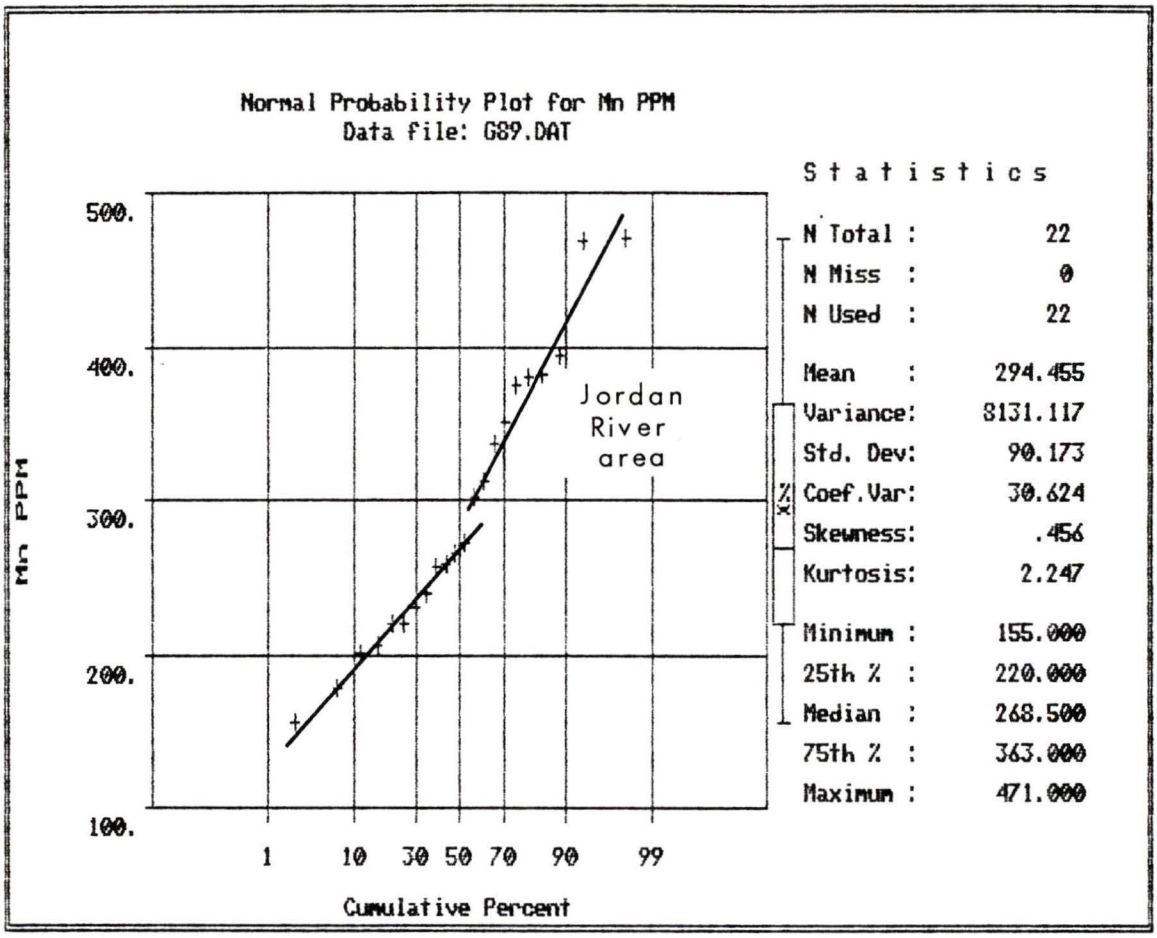

Figure 48. Probability plot of offshore Mn concentrations, 1989 (Group A). Highest values derive from the Jordan River area.

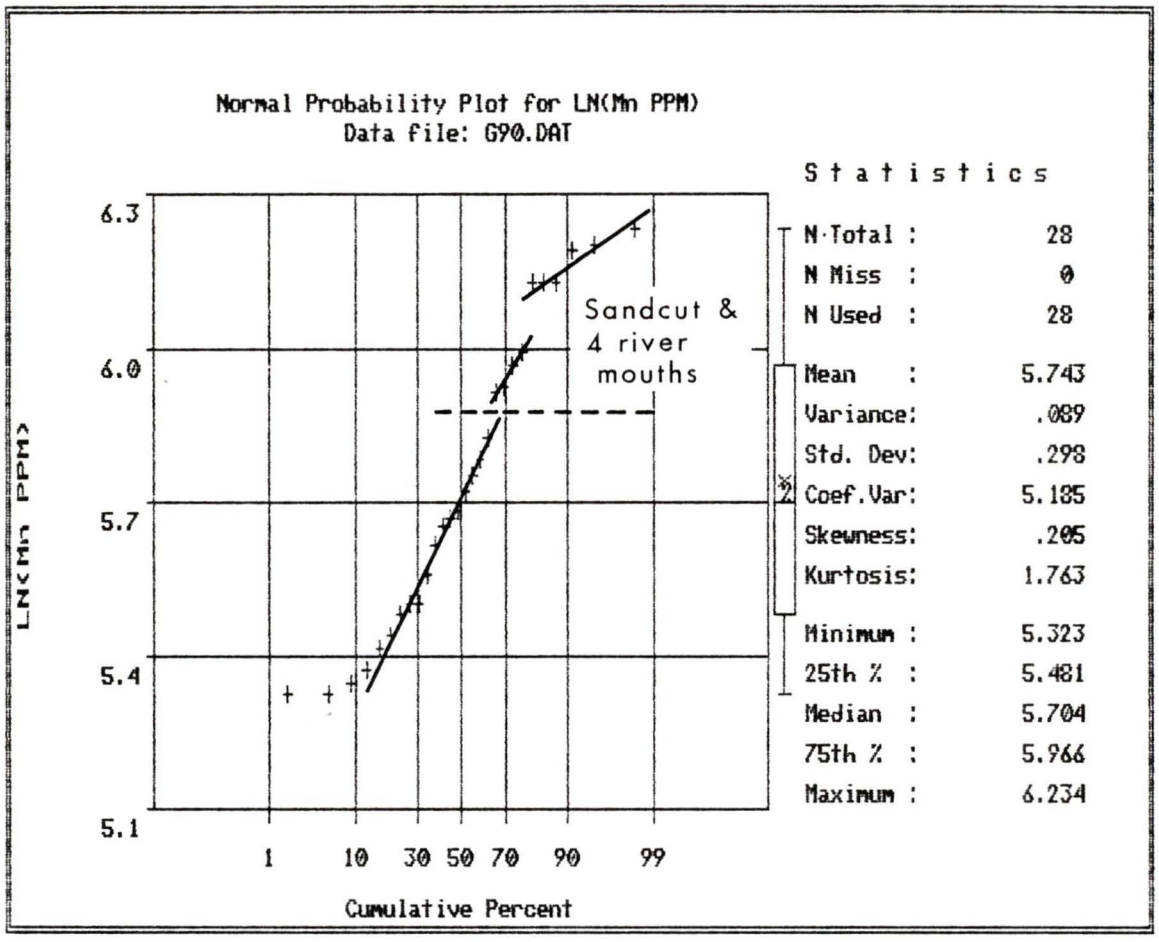

Figure 49. Probability plot of offshore Mn concentrations (logged), 1990 (Group B). Highest values found in samples from Sandcut transect and include samples obtained near the mouths of four rivers.

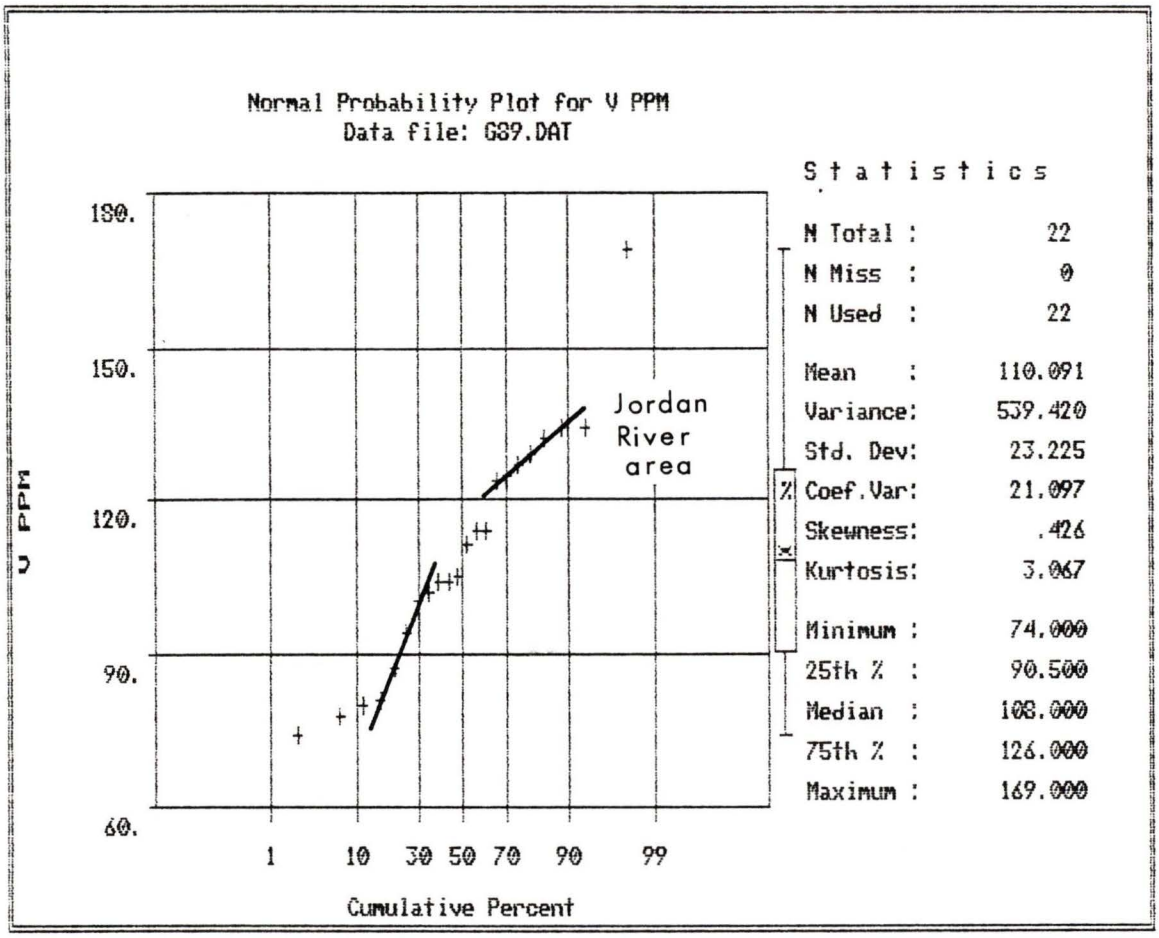

Figure 50. Probability plot of offshore V concentrations, 1989 (Group A). Highest values derive from the Jordan River area.

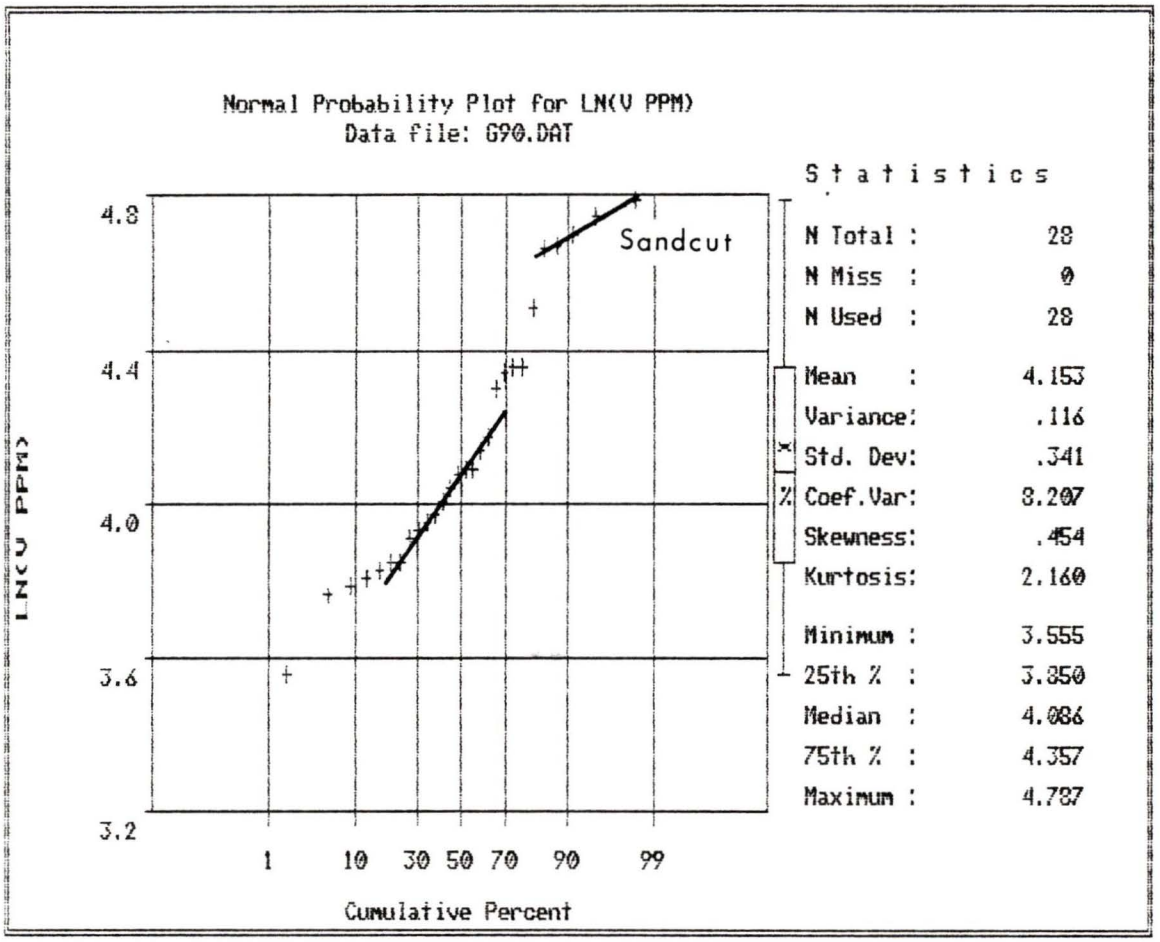

Figure 51. Probability plot of offshore V concentrations, 1990 (Group B). Highest values found in samples from Sandcut transect, and include a sample from the mouth of Loss Creek.

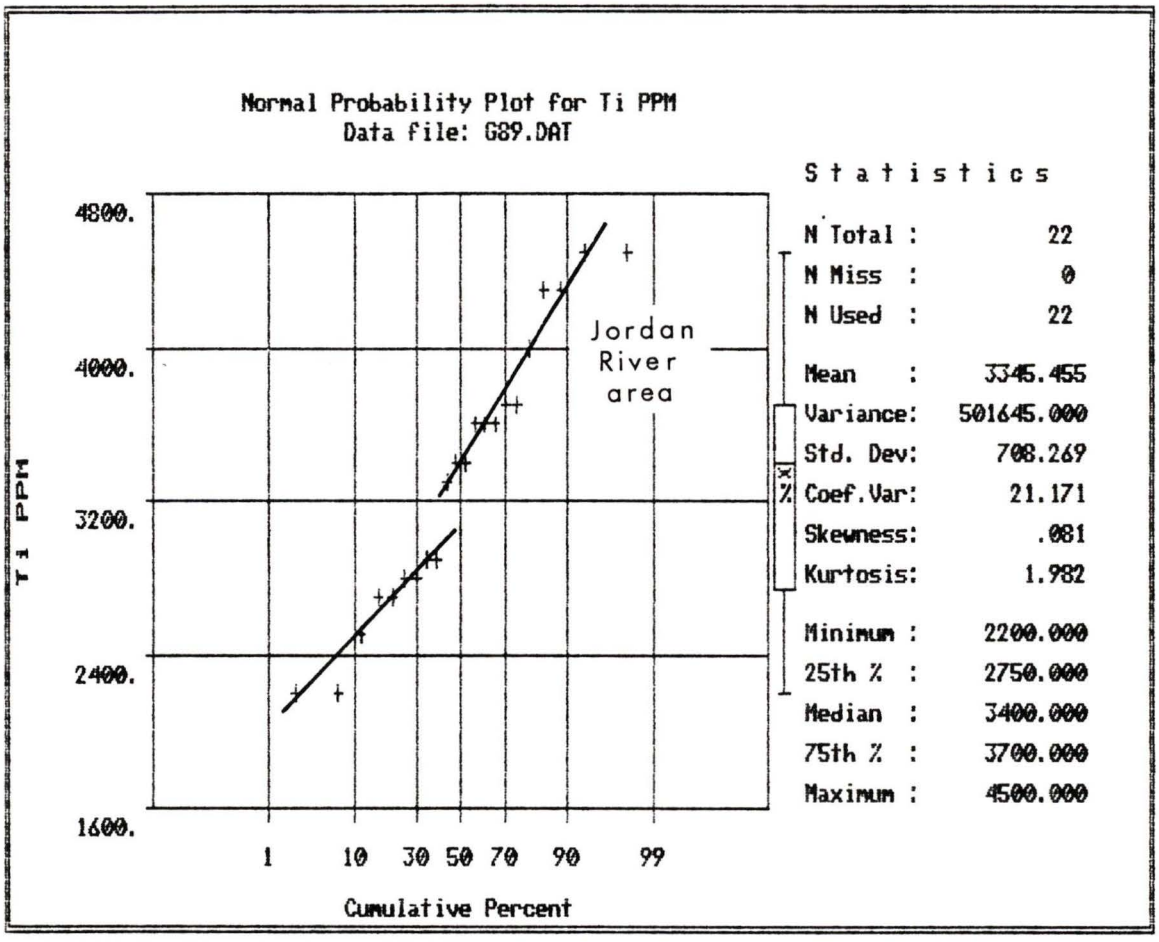

Figure 52. Probability plot of offshore Ti concentrations, 1989 (Group A). Highest values derive from the Jordan River area.

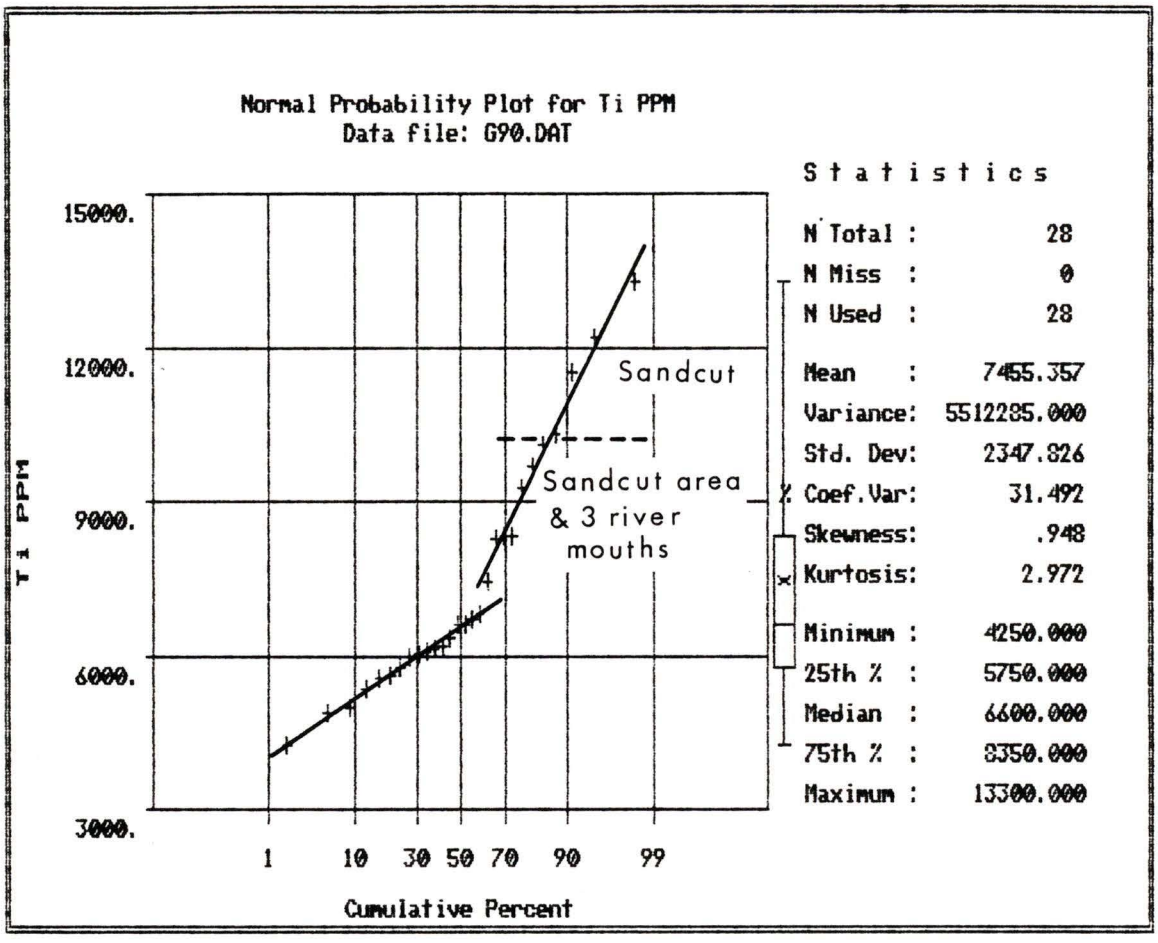

Figure 53. Probability plot of offshore Ti concentrations, 1990 (Group B). Highest values found in samples from Sandcut transect, two adjacent sites, and three river mouth samples.

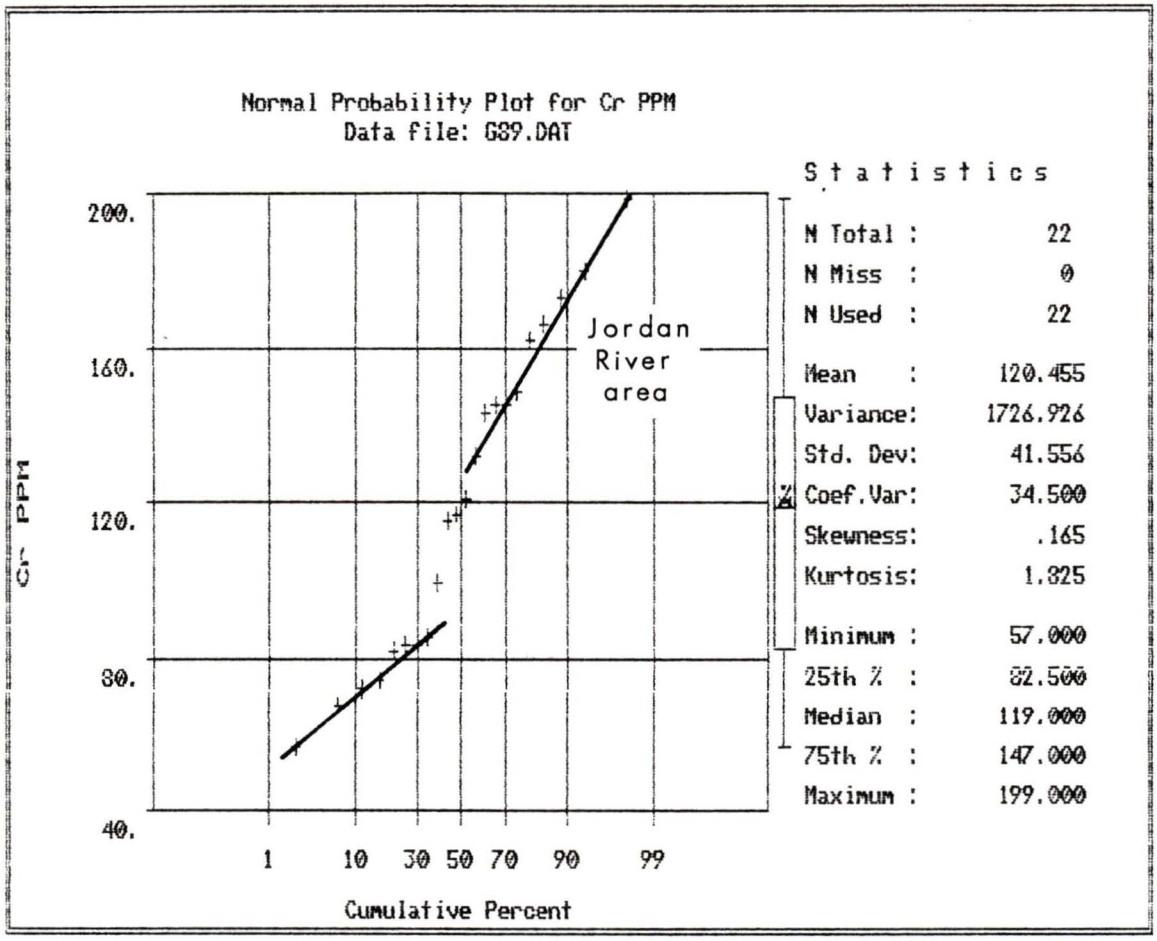

Figure 54. Probability plot of offshore Cr concentrations, 1989 (Group A). Highest values derive from the Jordan River area.

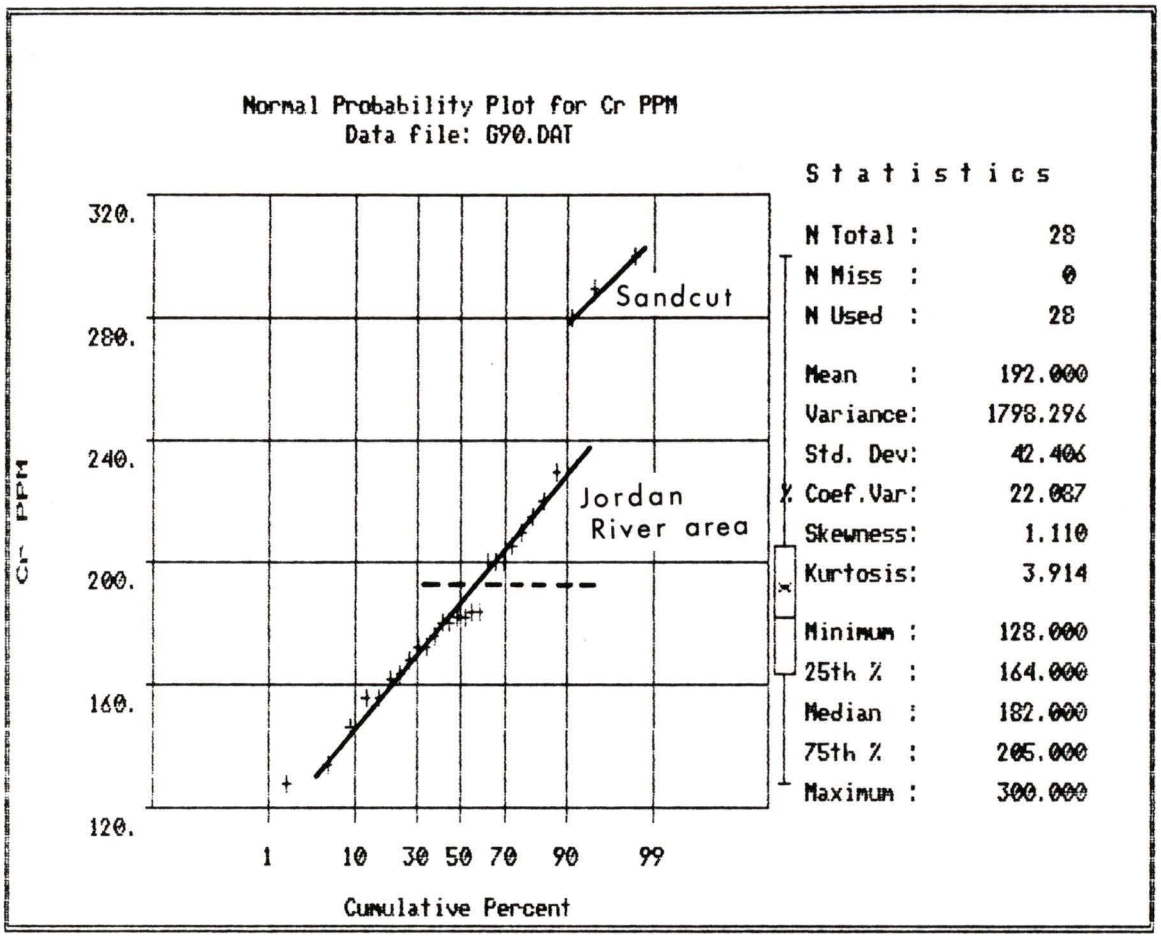

Figure 55. Probability plot of offshore Cr concentrations, 1990 (Group B). Highest values are found in the Sandcut transect, followed by samples from the Jordan River area.

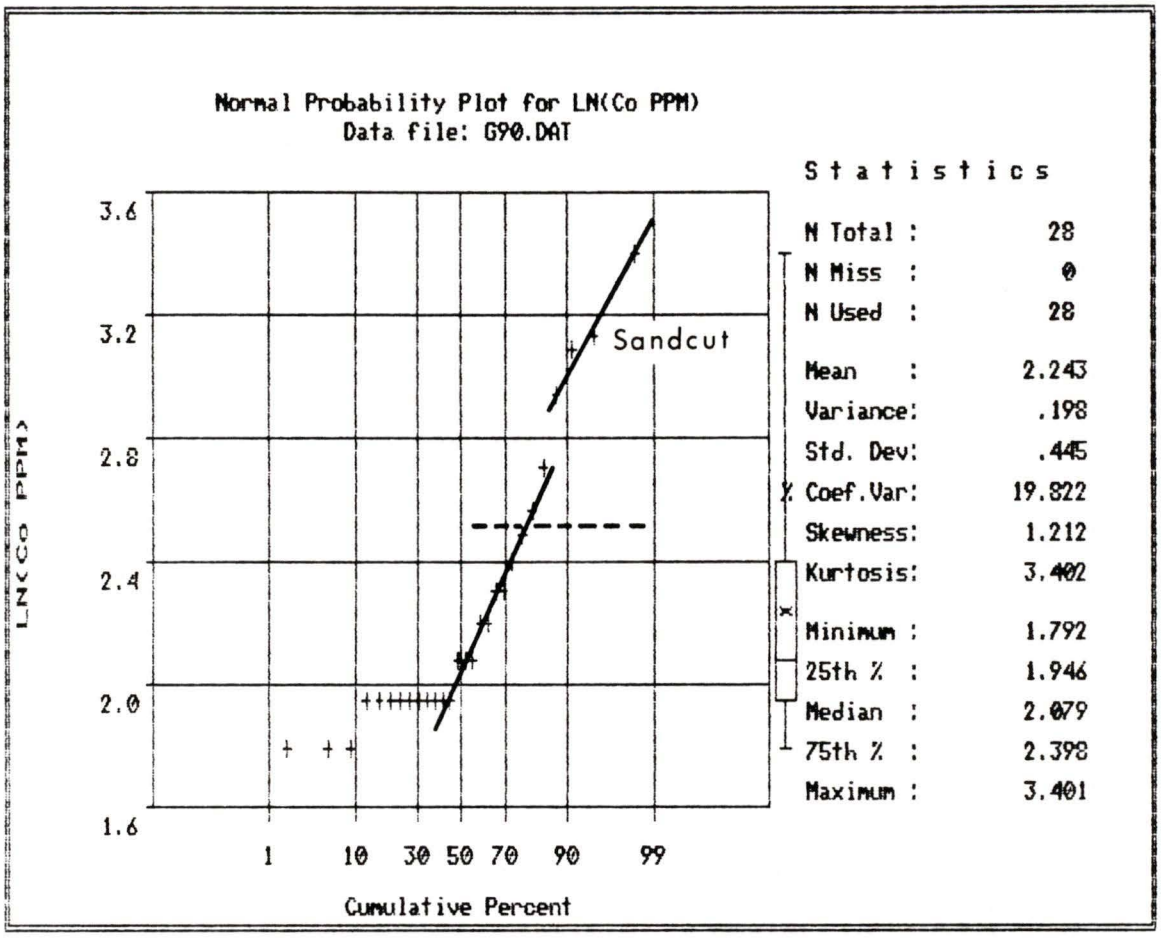

Figure 56. Probability plot of offshore Co concentrations (logged), 1990 (Group B). Highest values derive from the Sandcut transect.

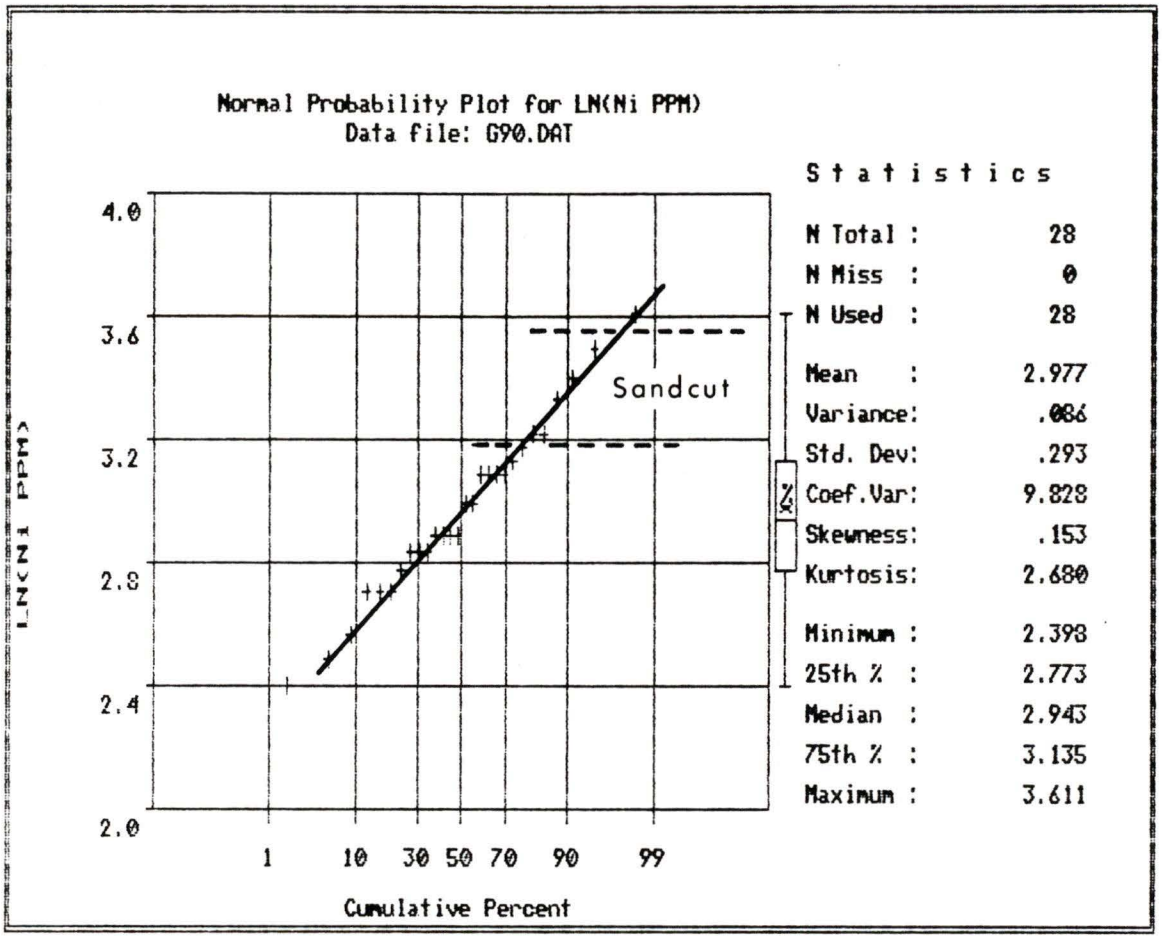

Figure 57. Probability plot of offshore Ni concentrations (logged), 1990 (Group B). Highest value is from the mouth of Loss Creek, followed by five samples from the Sandcut transect.

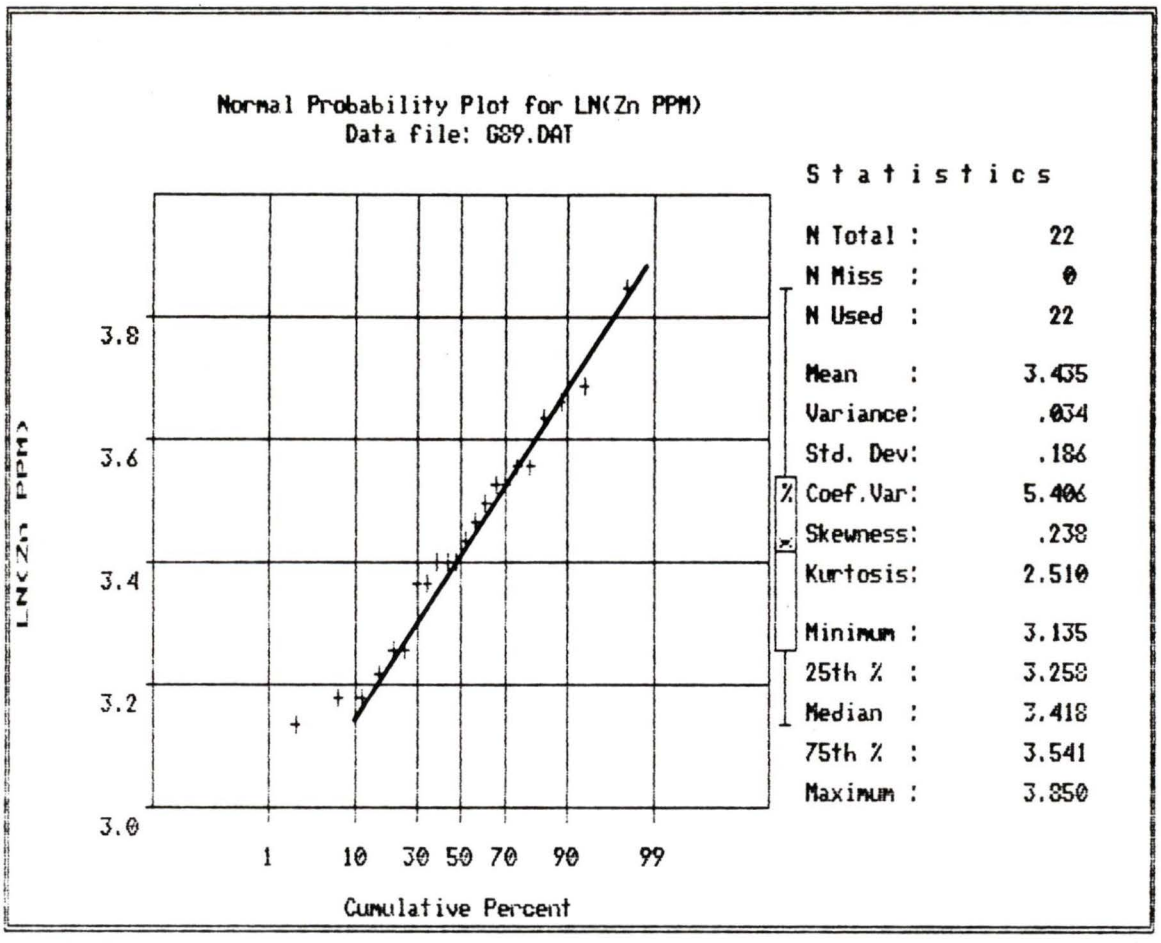

Figure 58. Probability plot of offshore Zn concentrations (logged), 1989 (Group A).

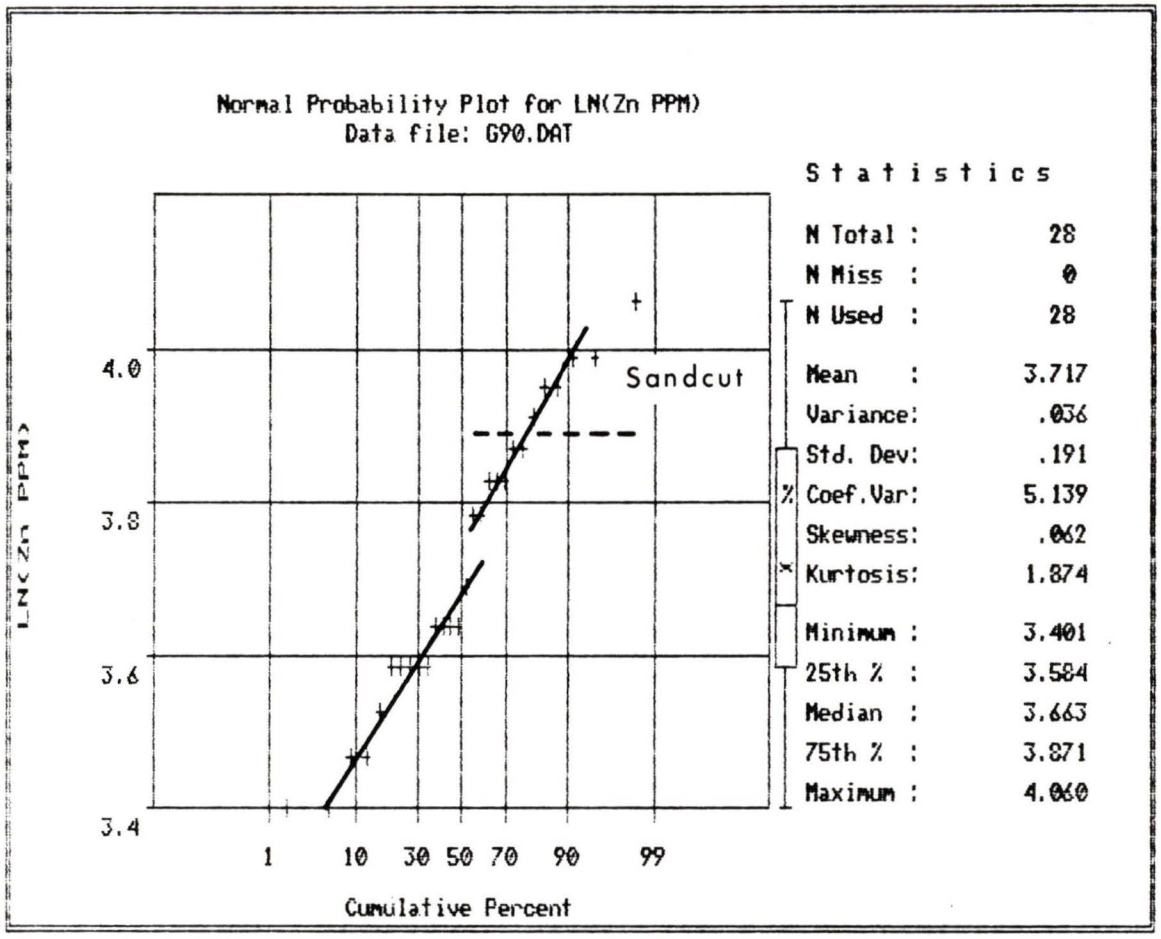

Figure 59. Probability plot of offshore Zn concentrations (logged), 1990 (Group B). Highest values derive from the Sandcut transect.

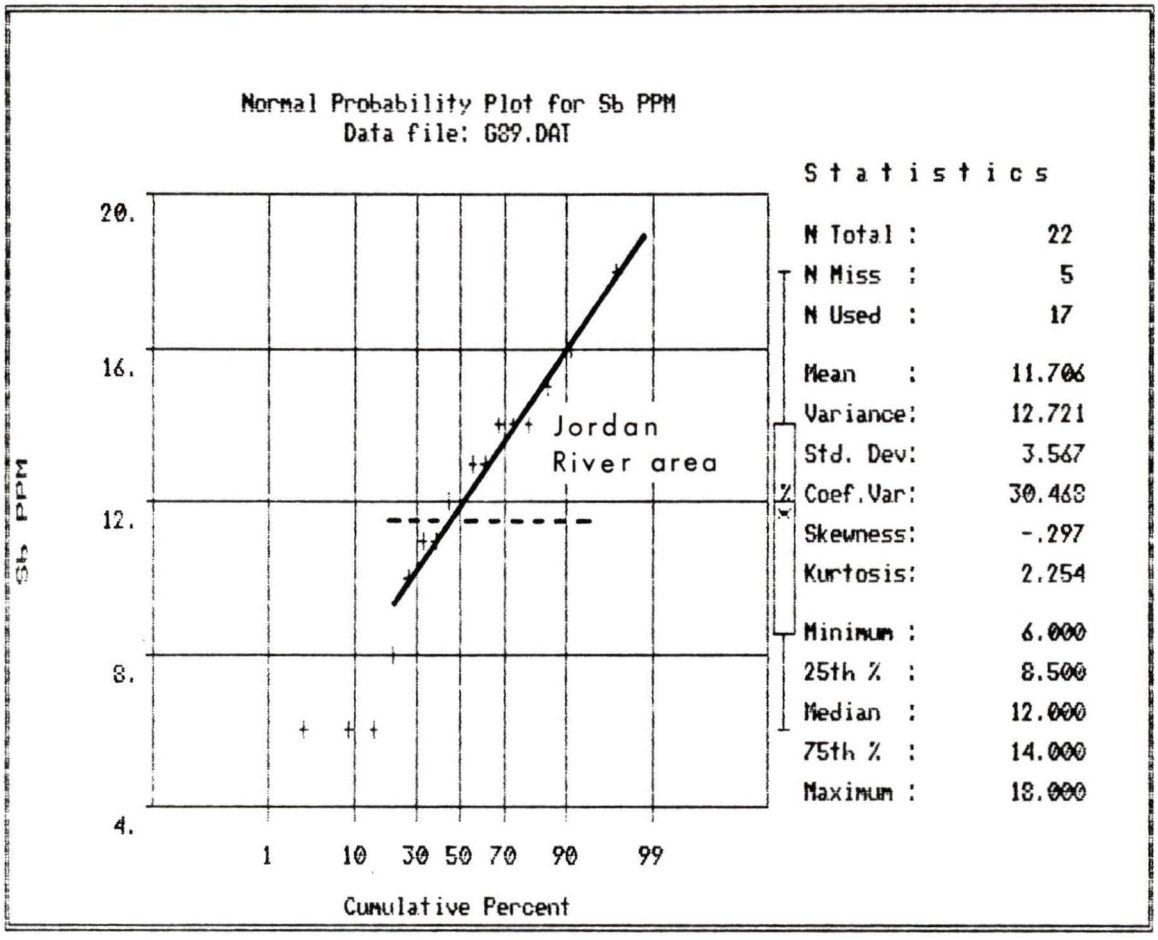

Figure 60. Probability plot of offshore Sb concentrations, 1989 (Group A). Highest values derived from the Jordan River area.

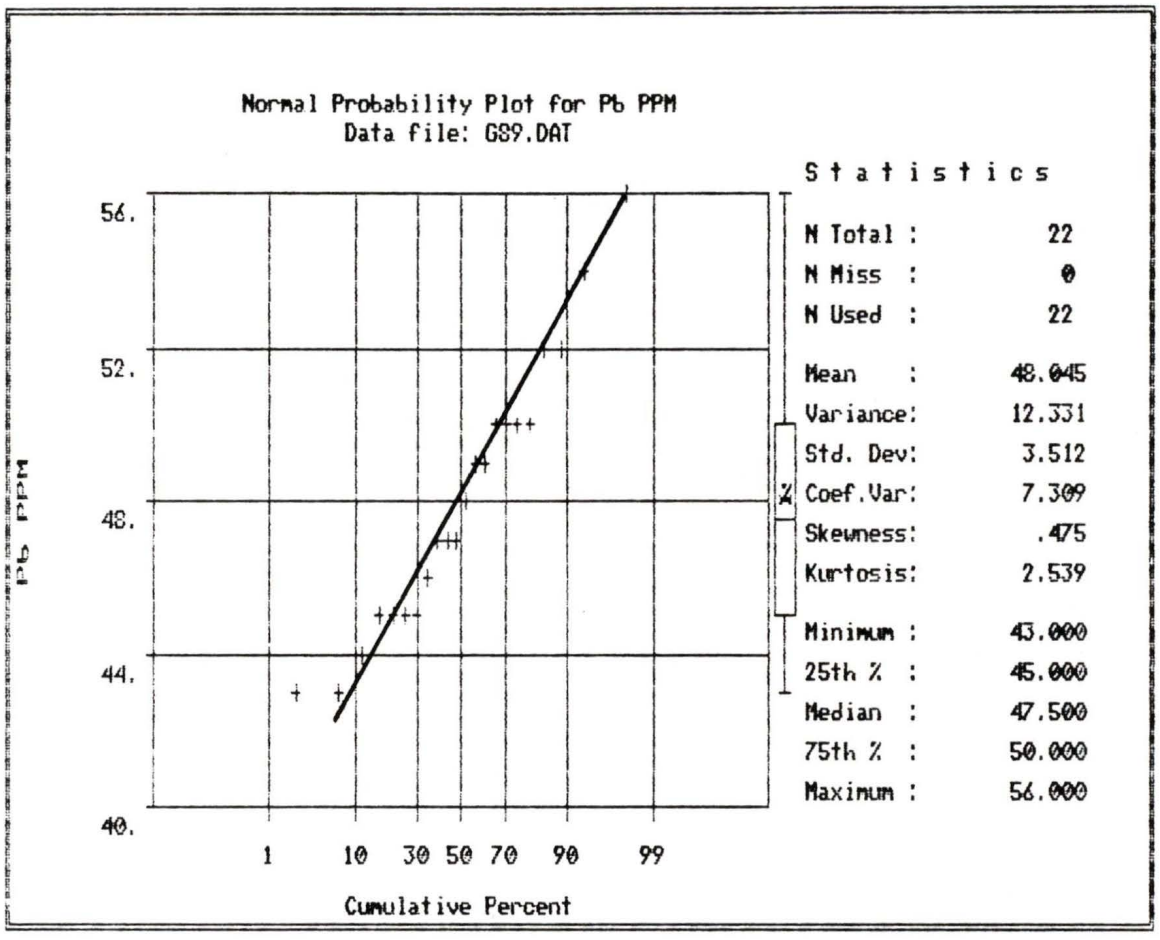

Figure 61. Probability plot of offshore Pb concentrations in sand, 1989 (Group A).

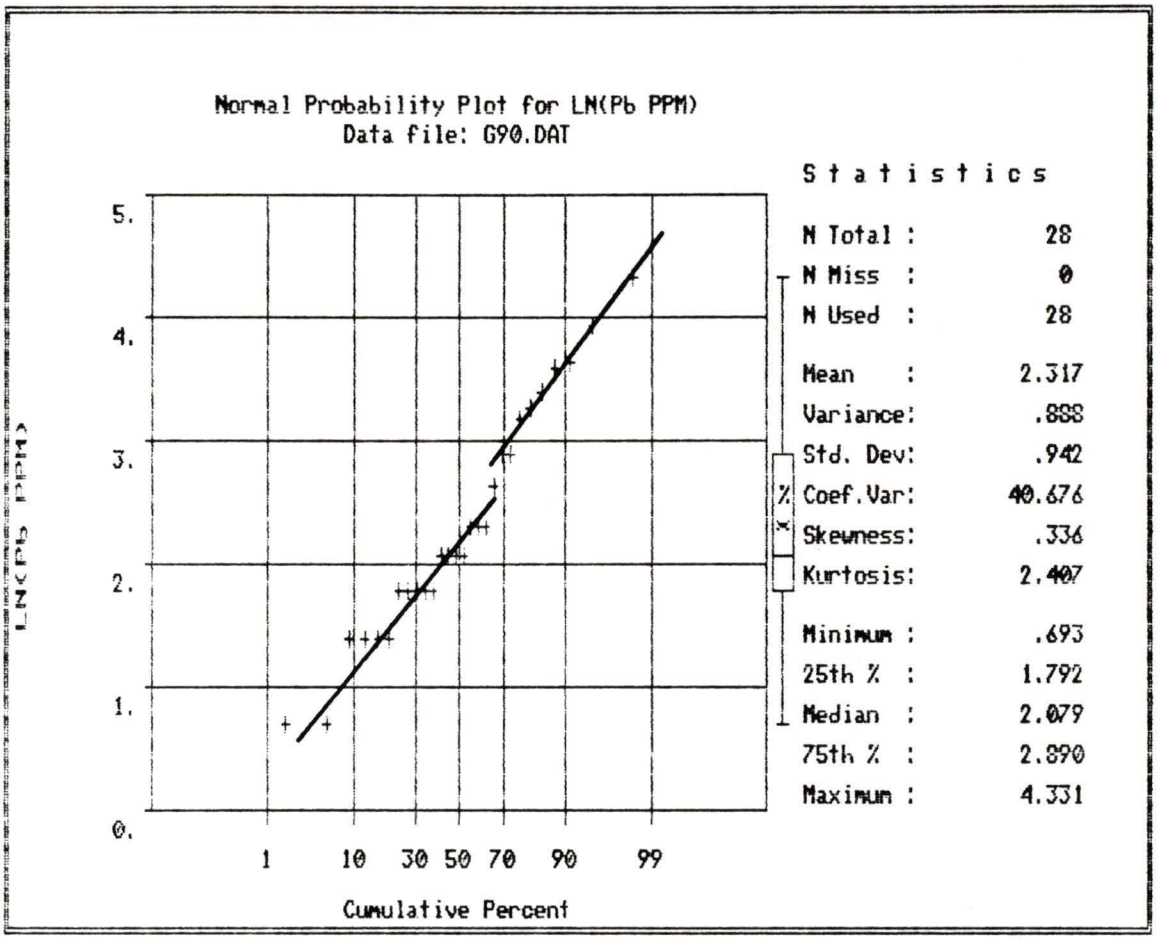

Figure 62. Probability plot of offshore Pb concentrations (logged) in sand, 1990 (Group B).

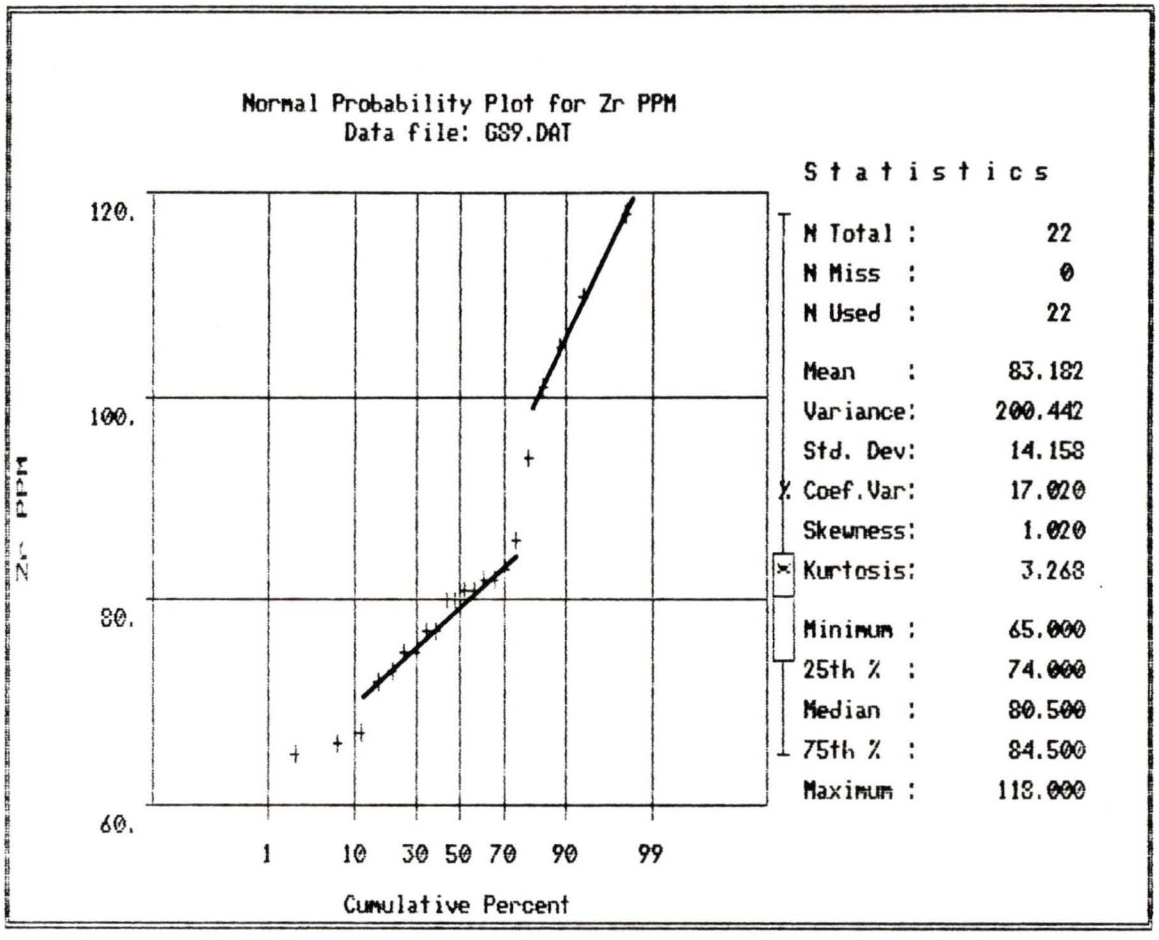

Figure 63. Probability plot of offshore Zr concentrations in sand, 1989 (Group A).

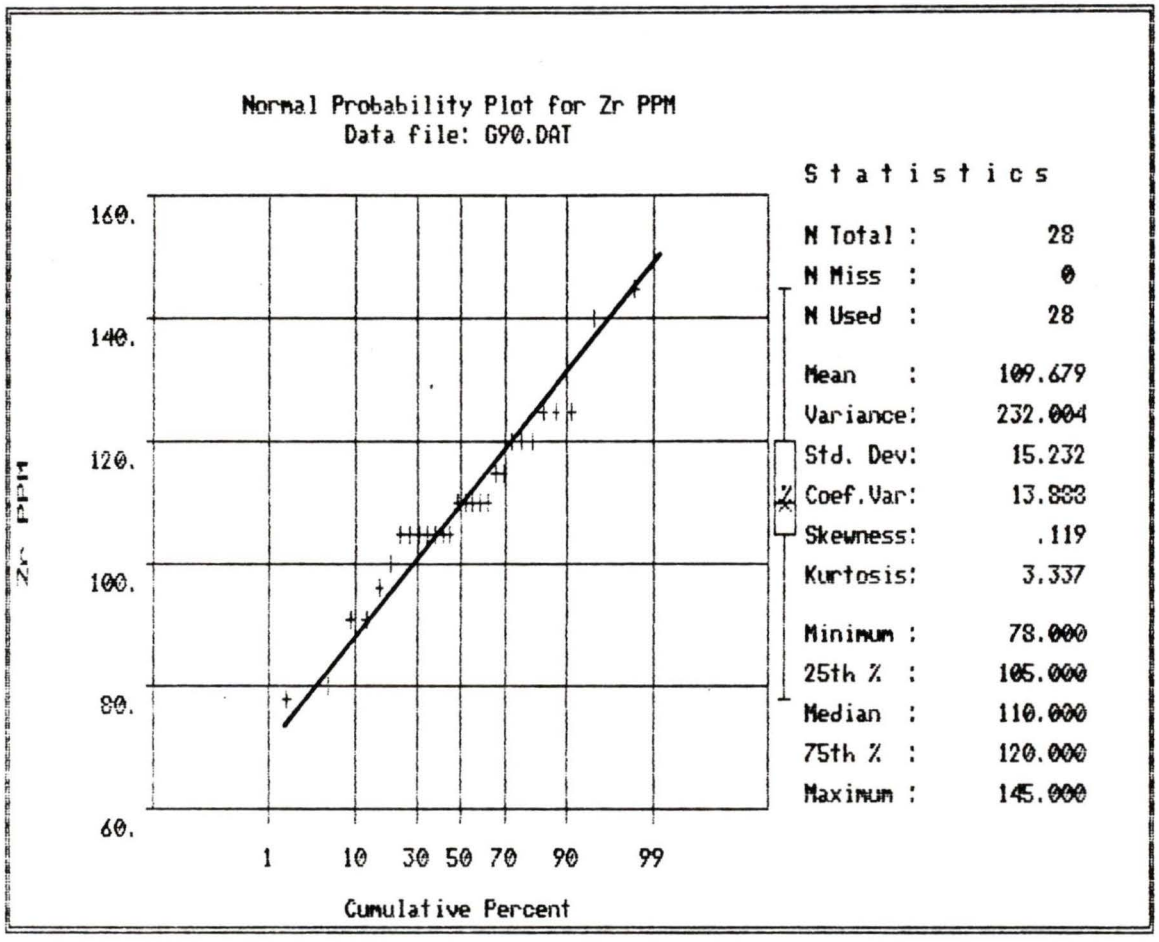

Figure 64. Probability plot of offshore Zr concentrations in sand, 1990 (Group B).

Pb consists of low background values which appear to approximate a single normal population both years (Figures 61 and 62). Grouping of lower values in Group B may account for the correction in slope in the centre of the probability plot.

Zr describes a bimodal population in Group A (Figure 63) in which the five higher values represent disparate areas from Sooke Bay to the northwestern end of the study area. The relation between these samples may be their mean grain size, discussed below under correlations. Zr in Group B consists of a single population although values appear to be slightly grouped (Figure 64).

b) Elemental Correlations

A correlation matrix was created for each of (A) and (B) (Tables 9 and 10), for 10 and 11 elements respectively. Statistical significance of each correlation was obtained by testing against a hypothesis $H_O(p=0)$ using a one-tailed Student's *t*-test at the 0.005 level, and assuming bivariate normal distributions (Till, 1974). Integrity of all correlations were verified by examination of crossplots.

In Group A strong correlations occur between Fe, Ti and V (Table 9, Figures 65 to 67) followed by slightly lower correlation with Mn. Sb shows significant correlation to Fe and Ti.

In Group B strongest correlations are observed between Fe, Ti and V (Table 10, Figures 68 to 70), as in Group A,

TABLE 9. CORRELATION MATRIX, OFFSHORE SAND - 1989
(*Group A*)

	Cu	Fe	Mn	Pb	V	Zn	Sb	Ti	Zr	Cr
Cu	0	-0.03	-0.01	-0.04	-0.03	0.72	0.47	-0.02	-0.19	-0.18
Fe		0	0.79	0.44	0.92	0.32	0.69	0.92	0.28	0.42
Mn			0	0	0.81	0.04	0.32	0.85	-0.25	0.68
Pb				0	0.24	0.51	0.72	0.41	0.66	-0.35
V					0	0.15	0.53	0.87	0.07	0.50
Zn						0	0.64	0.22	0.38	-0.40
Sb							0	0.64	0.40	0.16
Ti								0	0.10	0.50
Zr									0	-0.56
Cr										0

Values of correlation coefficient "r" derived from 22 samples for each element except Sb, with 17 samples. The critical values of "r", for the 0.005 level of significance, are r=0.54 (for 22 samples) and r=0.61 (for 17 samples).

TABLE 10. CORRELATION MATRIX, OFFSHORE SAND - 1990
(*Group B*)

	Cu	Fe	Mn	Ni	Pb	V	Zn	Ti	Zr	Cr
Co	0.95	0.95	0.73	0.79	-0.25	0.90	0.64	0.90	-0.09	-0.21
Cu	0	0.87	0.61	0.64	-0.25	0.78	0.58	0.79	-0.15	-0.18
Fe		0	0.79	0.82	-0.20	0.92	0.73	0.93	0.02	-0.18
Mn			0	0.68	-0.08	0.91	0.45	0.72	-0.05	-0.12
Ni				0	-0.34	0.83	0.67	0.79	-0.03	0.06
Pb					0	-0.18	-0.12	-0.14	-0.05	-0.27
V						0	0.54	0.92	0.03	-0.14
Zn							0	0.58	0.18	0.04
Ti								0	0.18	-0.18
Zr									0	0.15
Cr										0

Values for correlation coefficient "r" derived from 28 samples, with critical value r=0.48 for the 0.005 level of significance.

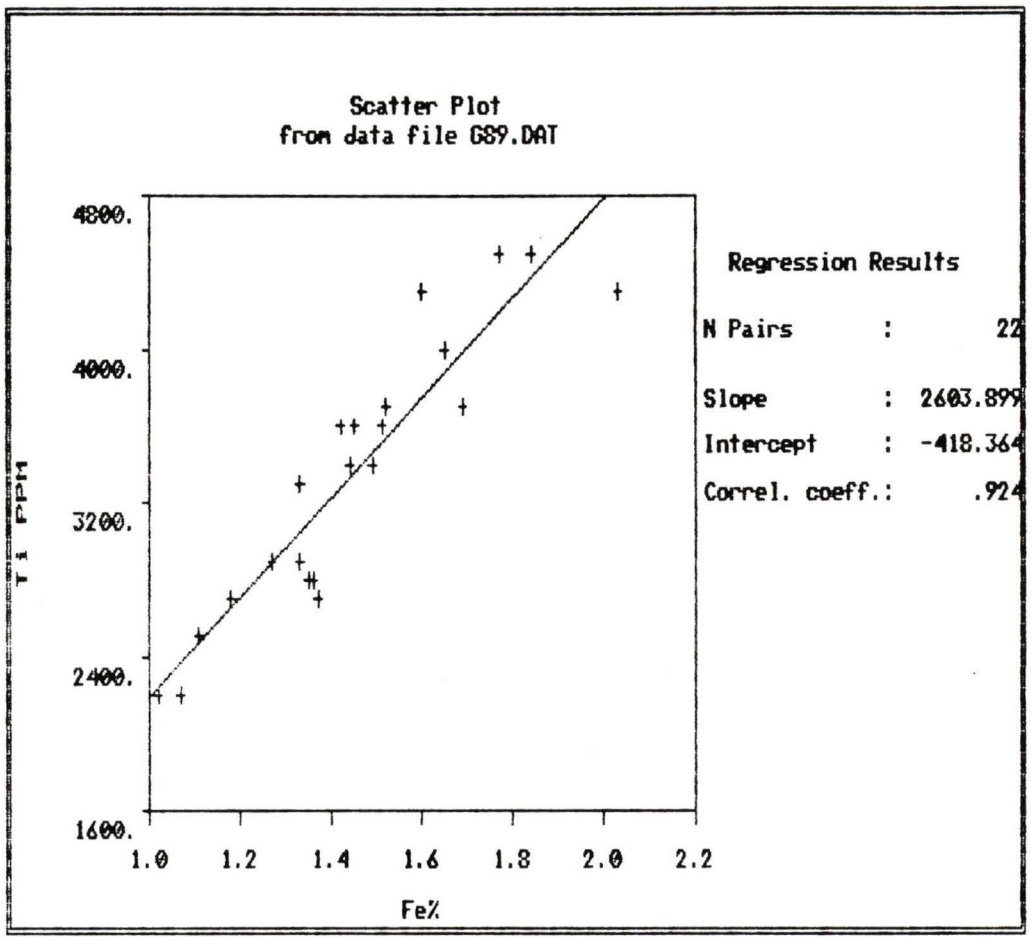

Figure 65. Crossplot of offshore Fe and Ti concentrations from sands, 1989 (Group A).

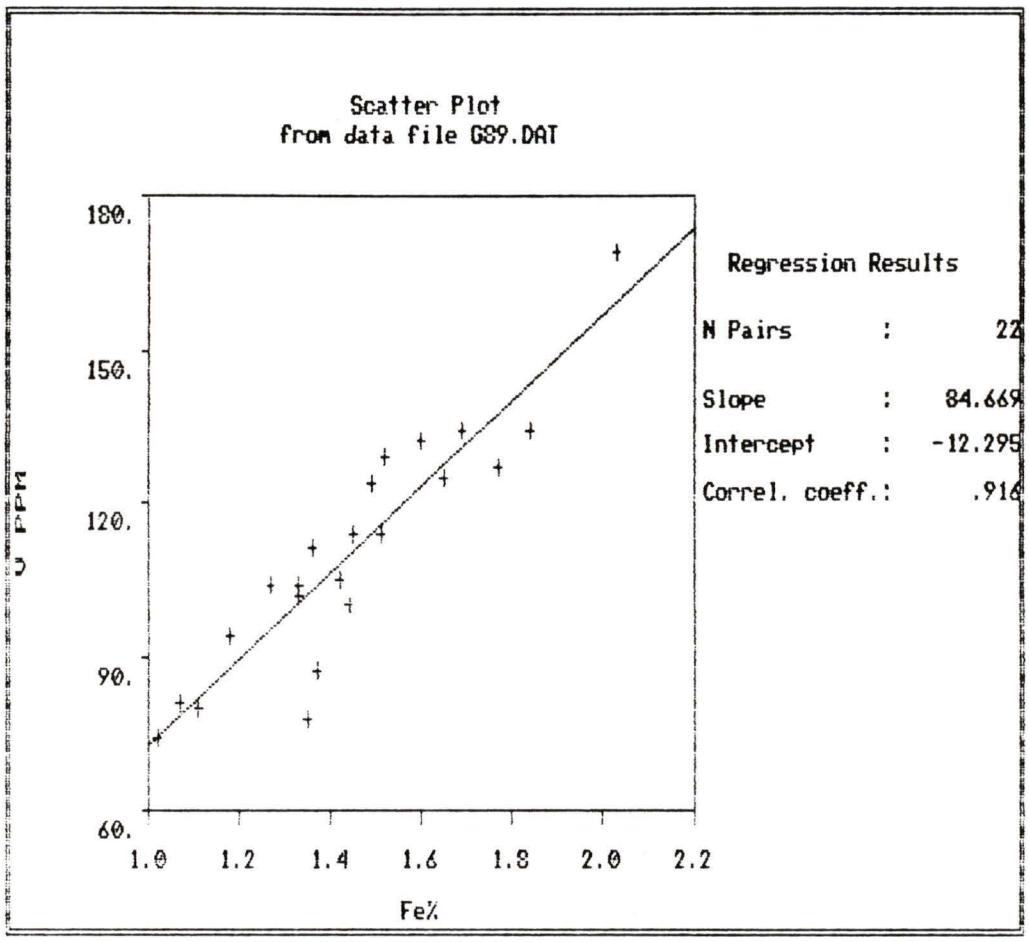

Figure 66. Crossplot of offshore Fe and V concentrations from sands, 1989 (Group A).

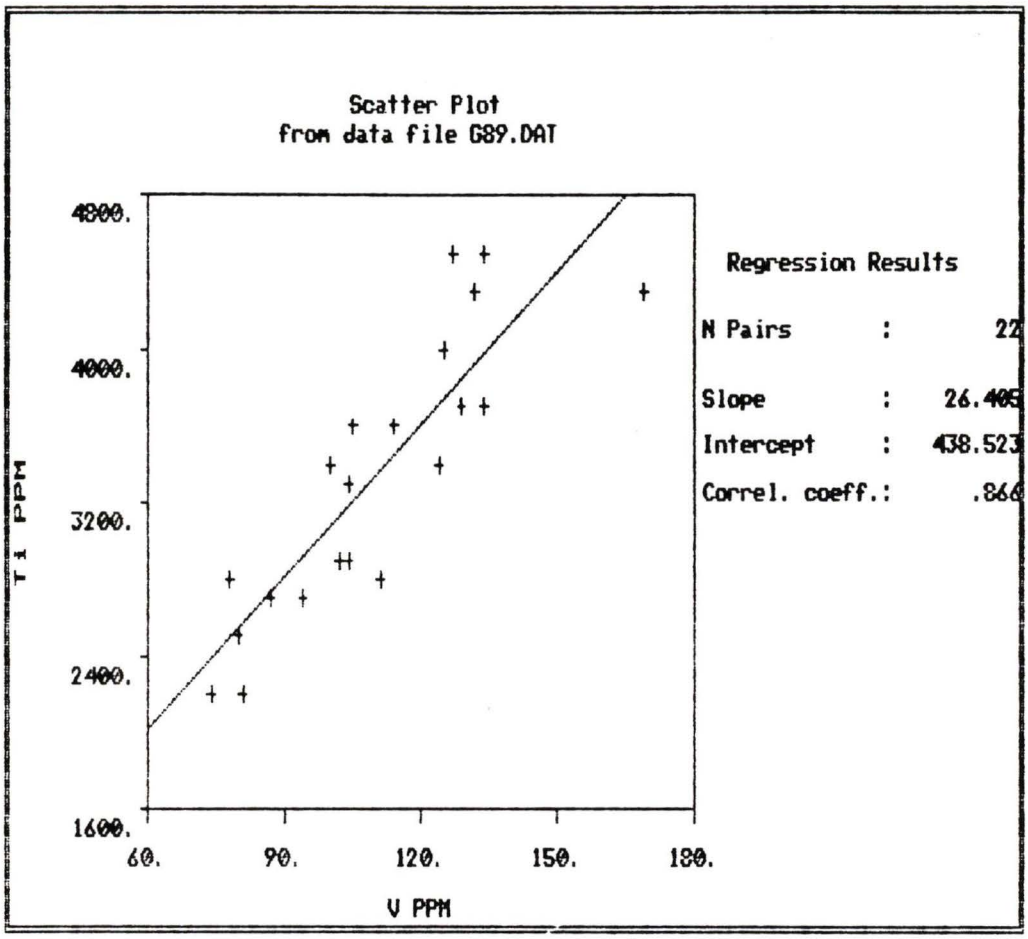

Figure 67. Crossplot of offshore V and Ti concentrations from sands, 1989 (Group A).

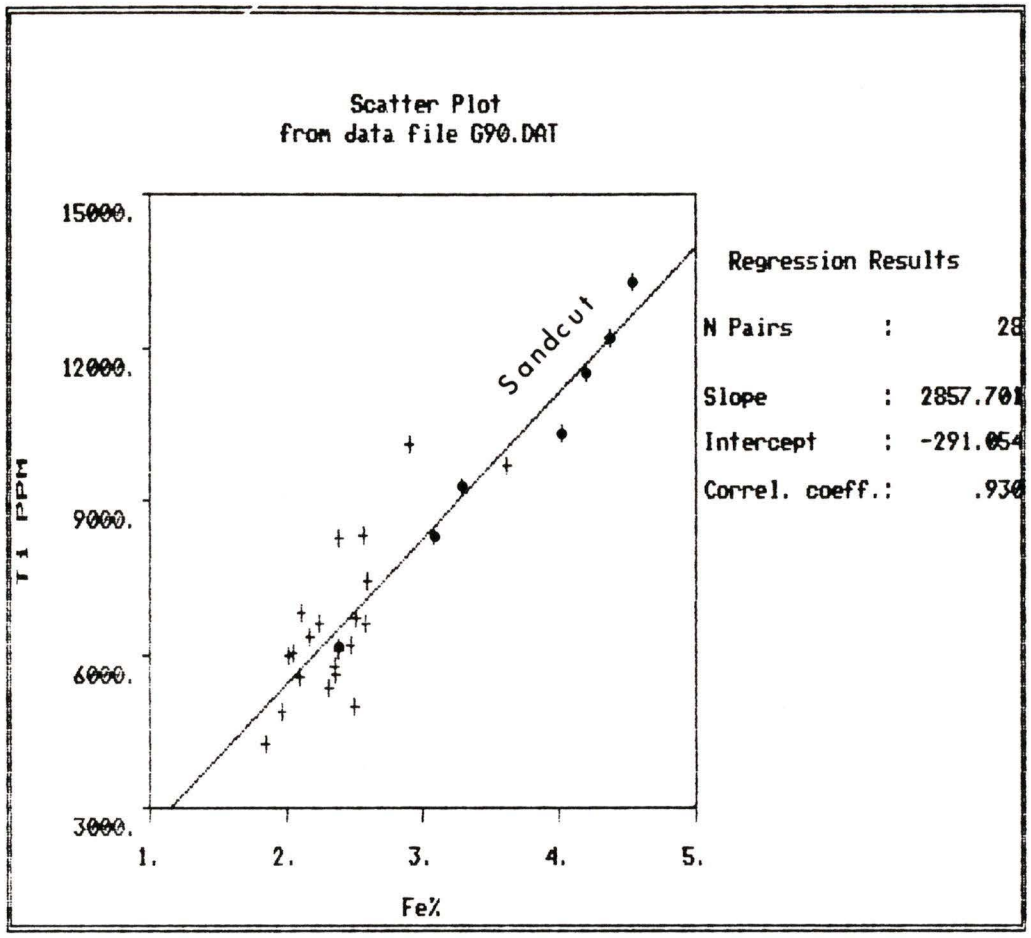

Figure 68. Crossplot of offshore Fe and Ti concentrations from sands, 1990 (Group B). These elements have a near-linear correlation in samples from the Sandcut transect.

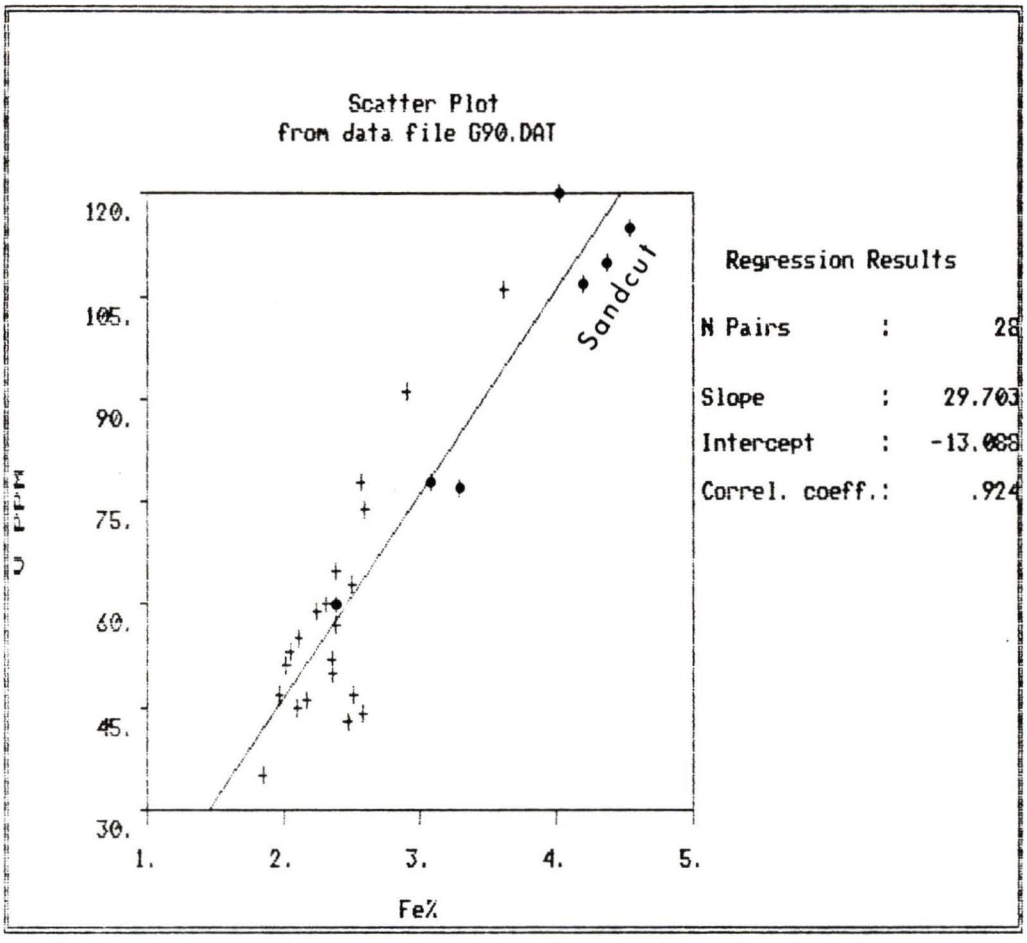

Figure 69. Crossplot of offshore Fe and V concentrations from sand, 1990 (Group B). These elements have a near-linear correlation in samples from the Sandcut transect.

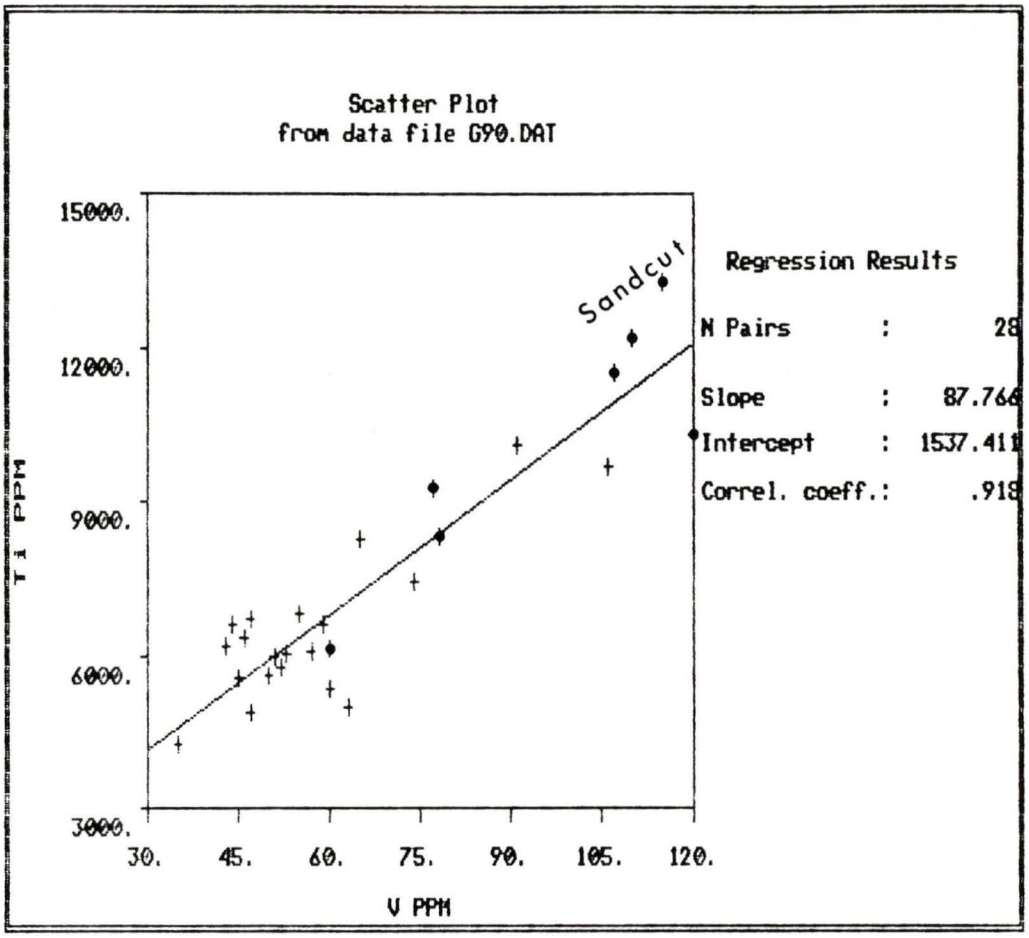

Figure 70. Crossplot of offshore V and Ti concentrations from sand, 1990 (Group B). These elements have a near-linear correlation in samples from the Sandcut transect.

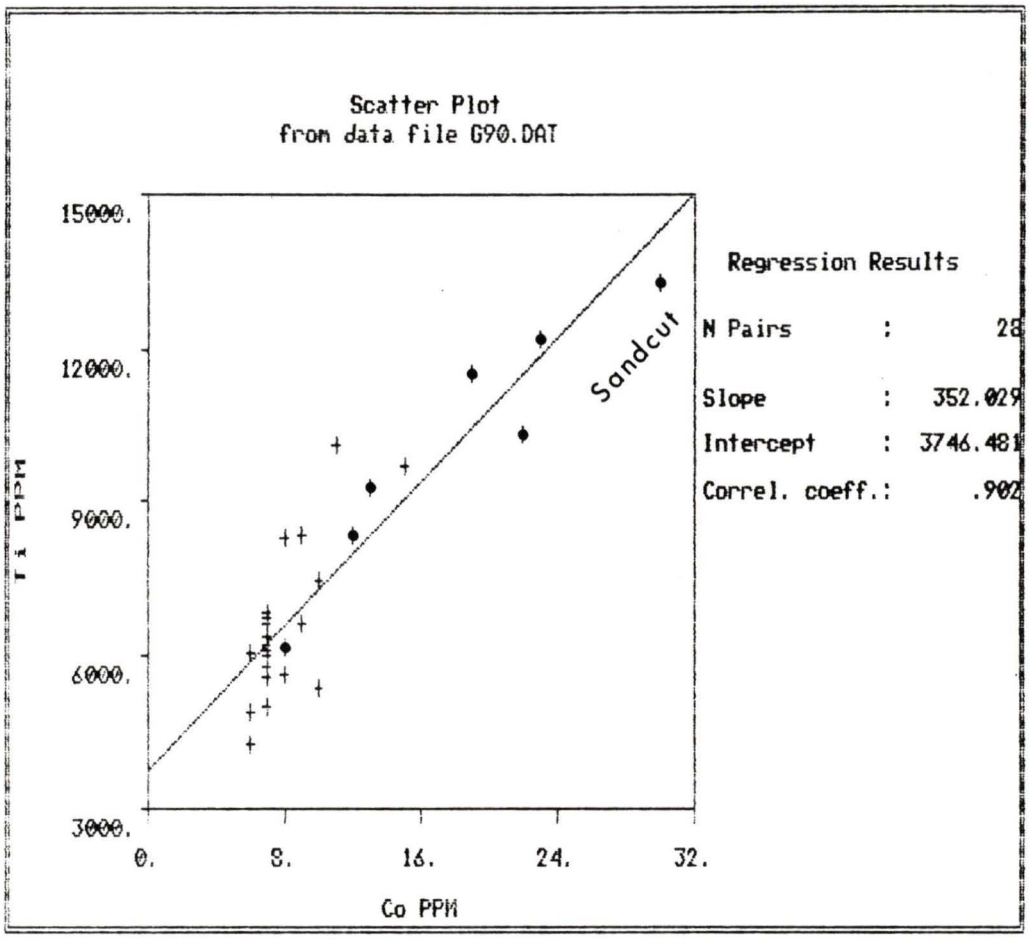

Figure 71. Crossplot of offshore Co and Ti concentrations from sand, 1990 (Group B). These elements have a near-linear correlation in samples from the Sandcut transect.

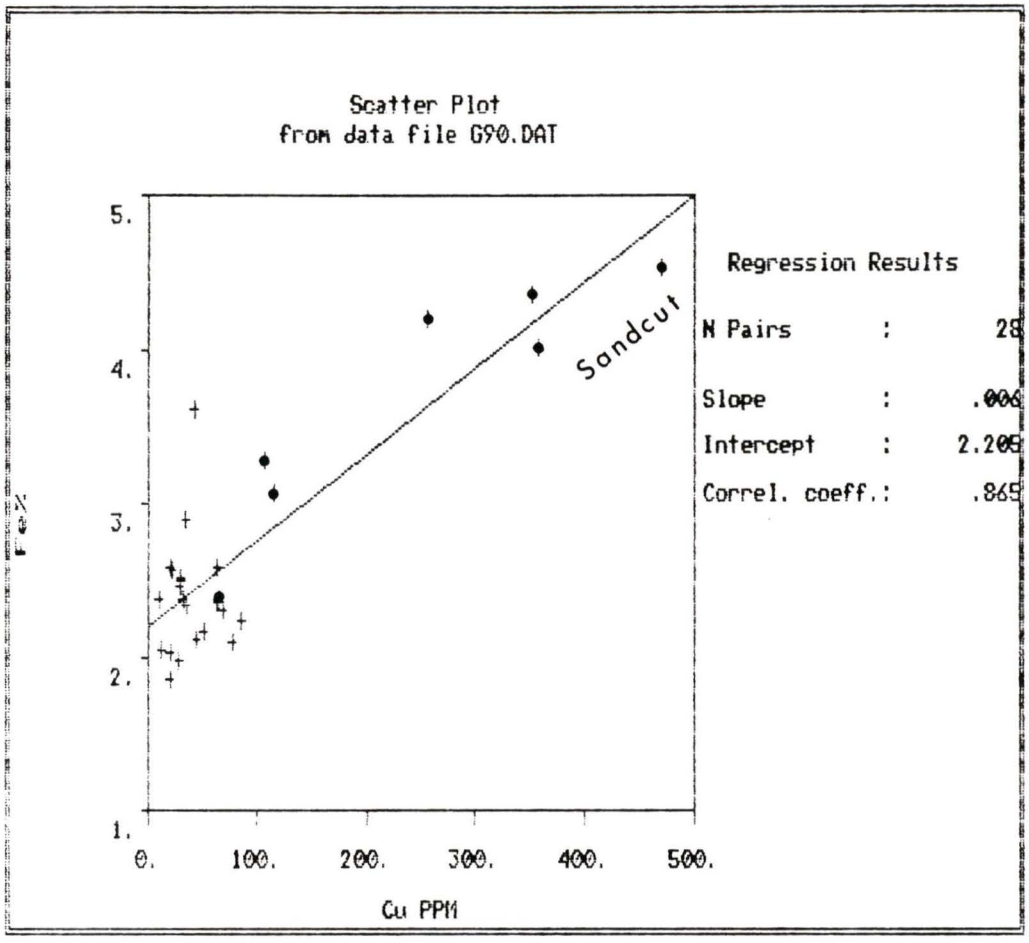

Figure 72. Crossplot of offshore Cu and Fe concentrations from sand, 1990 (Group B). Samples from the Sandcut transect show strong correlations and anomalous concentrations of these elements.

augmented by Cu. These are correlated with slightly less strength to Mn (as in Group A) and Ni. Co shows some very strong correlations with this group of 6 elements, but is based on the low value range of 6.0 to 30.0 ppm.

The anomalous samples from the transect at Sandcut Beach have a significant impact on the correlations calculated for results in Group B (Table 10). These samples have high, near-linear correlations in the elements noted above, and by nature of their having the highest values for these elements, they heighten the correlation coefficients (Till, 1974). Their effect can be seen in the crossplots for Fe, Ti and V (Figures 68 to 70), and is especially noticeable in correlations with Co, such as with Ti (Figure 71). The crossplot of Cu:Fe (Figure 72) illustrates the anomalous values found in four of the transect samples, and also demonstrates the low background concentrations of Cu, appearing clustered due to scale.

Comparing correlations in Groups A and B, similar patterns are evident (Tables 9 and 10). Anomalous Sandcut transect values in (B) heightened correlation coefficients, but high correlations were found in both analytical sets between Fe, Ti, V and Mn. Examination of each element revealed background values which are enriched by second populations in Fe, Ti, V and Mn both years, followed by Cu and Zn. In (B) Cr and Sb showed no correlation with the other elements as seen in (A), but Co and Ni (run only for

Group B) showed strong correlations to the enriched elements.

The geographic distribution of these enriched elements is best illustrated by Ti values, contoured by group (year), within the study area (Figure 73). Despite the irregular and overlapping distribution of samples in the two groups, both sets of contours confirm the enrichment of values along the nearshore, particularly near Sandcut Beach. Values farther offshore suggest higher background values in the southeast. A crossplot of Ti values and Eastings (B) confirm this observation. The crossplot shows a gradual, but distinct increase in minimum Ti values from west to east.

c) Other Correlations

Geochemical results for Group A showed significant correlations (0.005 level) between weight percent heavy mineral content and Mn (r=0.81), Ti (r=0.72), V (r=0.68) and Fe (r=0.64). As noted earlier, Zr correlates with mean grain size (r=0.66), suggesting an increase in Zr with an increase in phi number, or decrease in grain size.

Samples analysed from (B) also show significant correlations between weight percent heavy mineral and Co (r=0.97), Cu (r=0.93), Fe (r=0.92), Ti (r=0.91) and V (r=0.90).

Five elements in (B) show a correlation between increased sediment sorting (logged) and an increase in

element concentrations (logged); Co (r=-0.71), Ni (r=-0.68), Ti (r=-0.64), Fe (r=-0.63) and V (r=-0.61).

Magnetite, expressed as a weight percent of the whole sand fraction in 18 samples from (A) had significant correlations with Mn (r=0.77), V (r=0.69), Cr (r=0.62) and Ti (r=0.61). Values were somewhat dispersed around the regression line in all crossplots (e.g. Ti, Figure 74).

Seven elements in Group B which are enriched off Sandcut Beach correlate well with values derived for weight percent magnetite from 12 samples (e.g. Ti, Figure 75); Ni (r=0.92), Co (r=0.88), Fe (r=0.84), Ti (r=0.84), Cu (r=0.82), V (r=0.80) and Mn (r=0.76).

ii) Offshore Mud Geochemistry

Mud fractions of offshore samples represent subsamples consisting of sediment finer than 0.063 mm. Five mud samples from Group A were analysed for their geochemistry followed by another 13 samples from Group B. These samples are broadly distributed from northwest to southeast, at various offshore depths (Figure 43). Three dive site samples (omitting Loss Creek, which had no fines) are the only samples to represent the shallow nearshore.

a) Univariate Statistics

Univariate statistics were calculated for each element in both Groups A and B (Tables 11 and 12). Group A consists of five samples which, for some elements, contained insufficient data above the detection limit to allow a

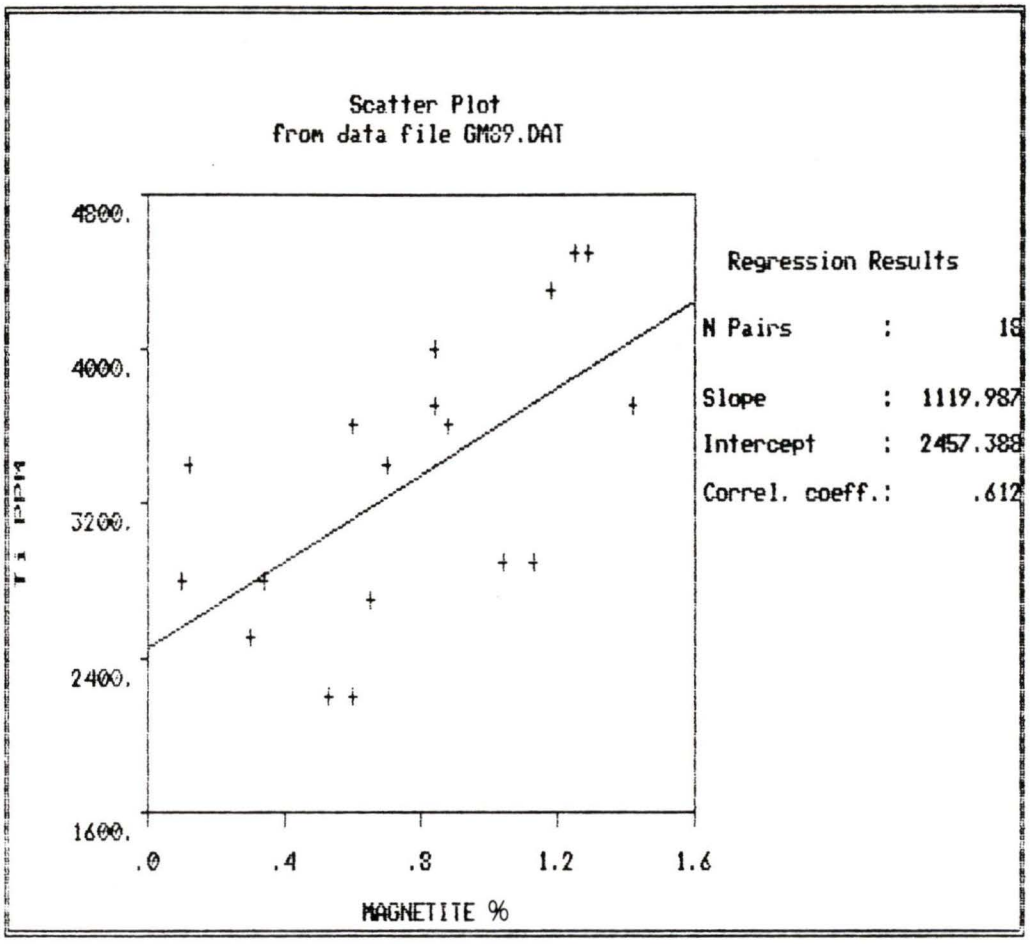

Figure 74. Crossplot of offshore magnetite weight percent and Ti concentrations in sand from 18 samples, 1989 (Group A).

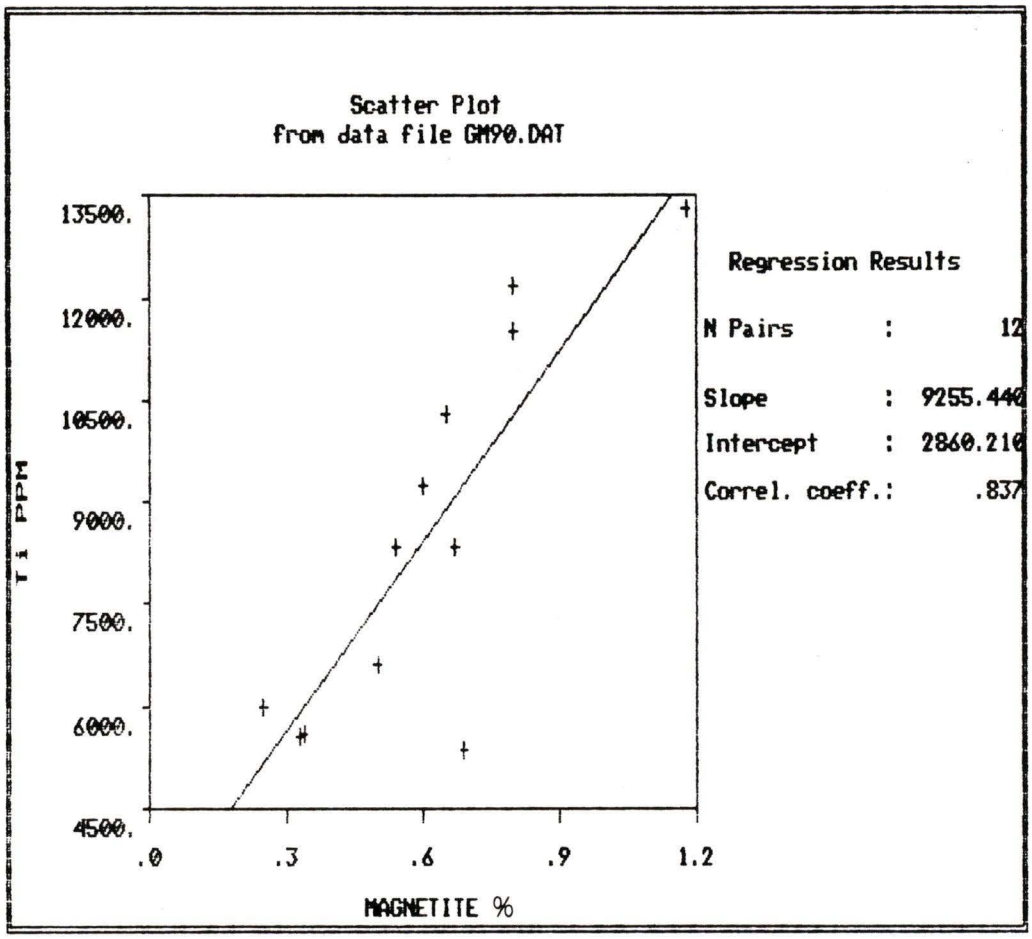

Figure 75. Crossplot of offshore magnetite weight percent and Ti concentrations in sand from 12 samples, 1990 (Group B).

TABLE 11. OFFSHORE MUD FRACTION GEOCHEMISTRY - 1989
(*Group A*, 5 samples)

	Samples > det.	$\bar{X}$	s	skew-ness	kurt-osis	Min.	Median	Max.
Au ppb	0	-	-	-	-	-	-	-
Pd ppb	4	2.8	1.5	1.2	2.3	2.0	2.0	5.0
Pt ppb	5	19.0	2.2	-1.5	3.2	15.0	20.0	20.0
Co ppm	NR	-	-	-	-	-	-	-
Cu ppm	5	54.0	7.2	-0.3	1.8	44.0	55.0	62.0
Fe %	5	1.8	0.2	1.2	2.9	1.7	1.8	2.2
Mn ppm	5	252.8	85.1	1.4	3.1	193.0	218.0	402.0
Mo ppm	5	3.8	0.4	-1.5	3.2	3.0	4.0	4.0
Ni ppm	NR	-	-	-	-	-	-	-
Pb ppm	5	69.2	3.3	-0.7	2.6	64.0	70.0	73.0
V ppm	5	128.2	9.9	0.5	1.6	119.0	124.0	142.0
Zn ppm	5	57.8	10.1	1.2	2.8	50.0	54.0	75.0
Ag ppm	5	0.8	0.1	-1.5	3.2	0.6	0.9	0.9
Cd ppm	0	-	-	-	-	-	-	-
Se ppm	0	-	-	-	-	-	-	-
Sn ppm	5	11.2	0.4	1.5	3.2	11.0	11.0	12.0
Hg ppb	5	46.0	24.8	0.7	2.3	20.0	45.0	85.0
Sb ppm	5	19.4	1.7	-0.3	1.8	17.0	19.0	21.0
Bi ppm	0	-	-	-	-	-	-	-
Ti ppm	5	4740.0	364.7	0.7	2.0	4400.0	4600.0	5300.0
Zr ppm	5	127.8	11.2	0.9	2.5	117.0	124.0	146.0
Cr ppm	5	53.0	9.9	0.2	2.0	41.0	53.0	67.0

NR = samples not run for that element in 1989.

TABLE 12. OFFSHORE MUD FRACTION GEOCHEMISTRY - 1990
(*Group B*, 13 samples)

	Samples > det.	$\bar{X}$	s	skew-ness	kurt-osis	Min.	Median	Max.
Au ppb	1*	4.0	-	-	-	-	-	-
Pd ppb	0*	-	-	-	-	-	-	-
Pt ppb	0*	-	-	-	-	-	-	-
Co ppm	13	8.6	1.5	1.2	3.2	7.0	8.0	12.0
Cu ppm	13	108.4	53.2	0.6	2.4	47.0	116.0	219.0
Fe %	13	3.1	0.3	0.6	2.0	2.8	3.1	3.7
Mn ppm	13	259.6	37.9	1.1	3.7	215.0	250.0	350.0
Mo ppm	5	1.0	0.0	0.0	0.0	1.0	1.0	1.0
Ni ppm	13	21.0	2.7	0.9	3.0	18.0	21.0	27.0
Pb ppm	13	46.0	21.3	0.7	2.2	22.0	40.0	86.0
V ppm	13	66.8	11.5	1.2	2.8	56.0	63.0	91.0
Zn ppm	13	81.5	9.9	0.0	2.0	66.0	80.0	98.0
Ag ppm	0	-	-	-	-	-	-	-
Cd ppm	2	0.3	0.0	0.0	0.0	0.3	0.3	0.3
Se ppm	3	0.3	0.1	0.7	1.5	0.2	0.2	0.4
Sn ppm	12	8.3	4.5	0.8	2.8	3.0	7.0	18.0
Hg ppb	13	65.4	12.7	0.4	2.2	50.0	60.0	90.0
Sb ppm	13	0.5	0.2	0.6	2.6	0.2	0.4	1.0
Bi ppm	1	0.1	-	-	-	-	-	-
Ti ppm	13	11473.1	1586.2	0.9	3.1	9150.0	11000.0	14900.0
Zr ppm	13	248.8	60.9	0.4	2.6	145.0	245.0	370.0
Cr ppm	12	112.0	55.8	1.0	3.0	40.0	91.0	232.0

* Only 2 mud samples assayed for Au, Pd and Pt in 1990.

meaningful statistical analysis.

In both groups concentrations of Mo, Ag, Cd, Se and Bi were low (with limited range) or below the detection limits of the analytical technique (Appendix C). Similarly, Au (A) and Pd, Pt (B) returned no values and Sn from Group A had too low a concentration for further work.

The single Au value from Group B above the detection limit was from a dive sample off Muir Creek (Table 12).

The remaining elements, in the mud fraction, consist of one or more populations defined by linear distributions on probability plots with at least one sample showing significant deviation from this linearity.

Bimodal populations are found in both Groups A and B for Fe, Mn, Pb, V, Ti and Zr. The second population, of the higher values, may consist of one (as in Group A) or more samples (as in Group B). Probability plots for V and Ti illustrate these bimodal distributions (Figures 76 and 77). More than one population is also indicated for Zn (A), Ni and Cr (B).

A consistent pattern found in these results is that the highest values for several elements, Co, Fe, Mn, Ni, V, Ti and Zr, are from the three river-mouth samples. In addition, the sample closest to the mouth of Port San Juan was included in the set of highest values for Cu, Fe, Pb, Zn, V, Ti, Sn, and Hg.

Comparing sand and mud results from both groups, a few

comments can be made. In both Groups A and B mud values tend to have substantially higher means, where the means are separated by more than two standard deviations (of the higher mean) for Zn, Ti and Zr. In Group A, Pb and V, and in Group B only Hg have similarly higher means than found in the sand fraction. This is most notable for Ti and Zr (B) which have values substantially above the sand fraction. Cr has a higher mean concentration in the sand fraction than mud, using the same criteria.

Bimodal populations were consistently found in mud and sand fractions in both Groups A and B for Mn, V and Ti. Bimodal populations were also present for both mud and sand fractions for Cu and Zr in Group A and for Fe and Cr in Group B.

b) Elemental Correlations

With only five values for each element in Group A, significant correlations require that r=0.96, at the 0.005 significance level. Fe, Mn and Zn are significantly intercorrelated (Fe:Mn r=0.996, Fe:Zn r=0.98, Mn:Zn r=0.97). One other strong correlation is found between Ti:Cr (r=0.97).

In Group B correlations in the mud fractions are strongest between Zr, V and Ti (Table 13). Good correlations are found between pairs such as Fe:Mn, Fe:V, Cu:Sn, Cu:Zn, but do not hold up well between otherwise paired elements. Co correlates well with Fe, Mn, V, Ti and

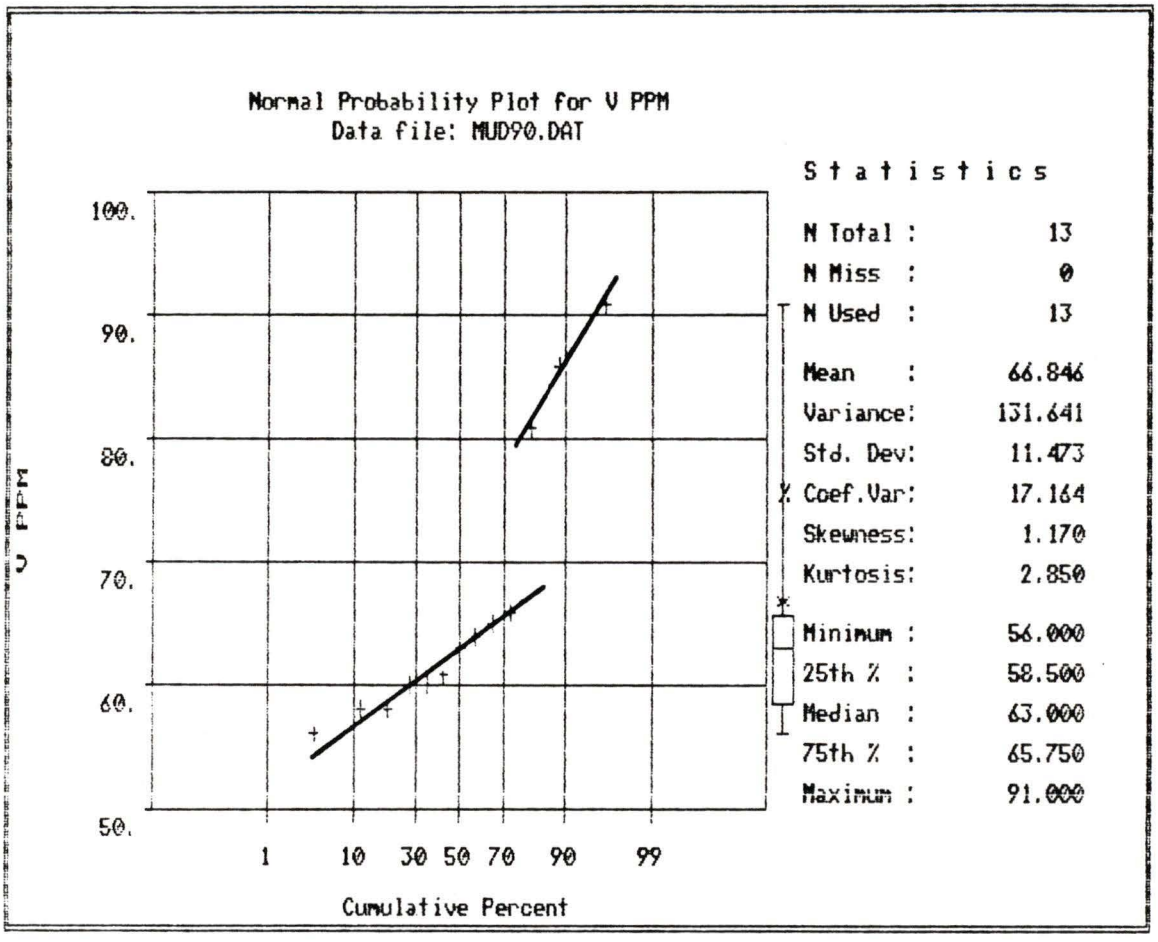

Figure 76. Probability plot of offshore V concentrations in mud (<0.063 mm) from 13 samples, 1990 (Group B).

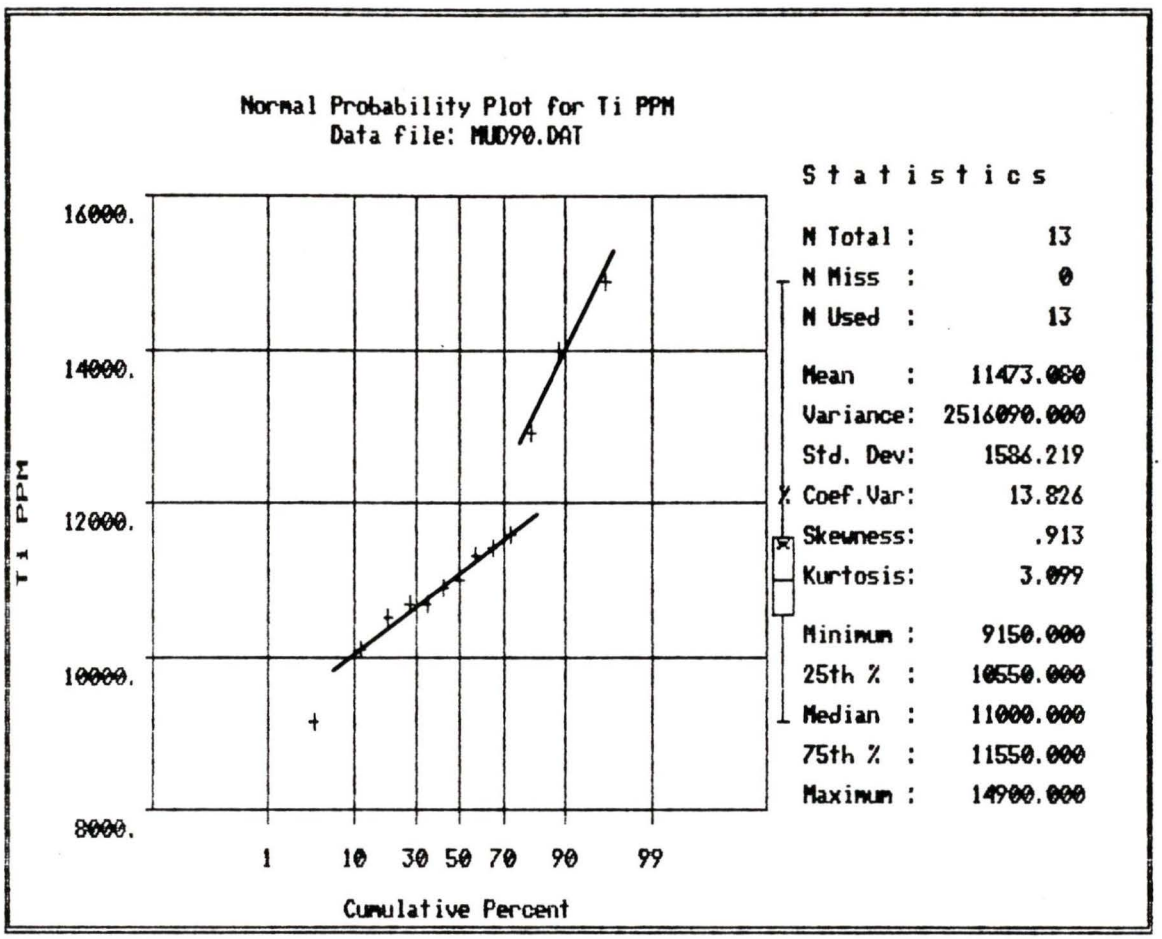

Figure 77. Probability plot of offshore Ti concentrations in mud (<0.063 mm) from 13 samples, 1990 (Group B).

TABLE 13. CORRELATION MATRIX, OFFSHORE MUD - 1990 (*Group B*)

	Co	Cu	Fe	Mn	Ni	Pb	V	Zn	Sn	Ti	Zr	Cr
Co	0	0.35	0.75	0.75	0.80	0.19	0.79	0.31	-0.10	0.74	0.50	-0.22
Cu		0	0.37	0.34	0.60	0.45	0.42	0.71	0.87	0.57	0.62	0.60
Fe			0	0.82	0.56	0.36	0.88	0.52	0.02	0.64	0.38	-0.38
Mn				0	0.46	0.60	0.58	0.52	0.10	0.38	0.06	-0.26
Ni					0	0.12	0.67	0.51	0.15	0.70	0.60	0.26
Pb						0	0.12	0.35	0.50	0.08	-0.01	-0.12
V							0	0.38	0.03	0.86	0.71	-0.36
Zn								0	0.62	0.25	0.18	0.42
Sn									0	0.20	0.34	0.61
Ti										0	0.90	-0.04
Zr											0	0.16
Cr												0

Values for correlation coefficient "r" derived from 13 samples for each element except Sn and Cr, with 12 samples each. The critical values of "r", for the 0.005 level of significance, are r=0.69 (for 13 samples) and r=0.71 (for 12 samples).

Ni, but there is no intercorrelation among these five elements.

Comparing sand and mud fraction correlations from Group A, Fe, Ti and V are strongly correlated in the sand samples, while Fe, Zn and Mn are strongly correlated in the mud samples.

Comparing sand and mud fraction correlations from Group B, Fe, V, Ti, Mn, Ni and Co appear to extend their correlations into the mud fraction, although the strength of the latter appears to change for some elements (Tables 10 and 13). Strength of correlations in the sand fraction of Group B was supported by the presence of the Sandcut Beach offshore transect samples (with intercorrelated anomalous elemental values) not represented in the mud samples.

c) Other Correlations

Mud samples from Group B indicate three logged elements which show significant negative correlations with depth; Co (r=-0.91), Mn (r=-0.73) and Ni (r=-0.71).

iii) Beach Sand Geochemistry

The sand fraction from beaches were submitted for analyses in both years. Significant geographic differences distinguish the two sample sets. Group A (1989) samples represent only the eastern shoreline from east Sooke Bay to Sandcut Beach. Group B (1990) samples represent the entire coastal zone from western Sooke Bay to Botanical Beach, near San Juan Point in the northwest (Figure 43).

Only three samples from Group B were taken from beaches adjacent to shoreline underlain by the metamorphic rocks of the Leech River Complex. One of these three samples was taken at Sombrio Beach proximal to the unconformable contact with the Metchosin Volcanics. The remaining 39 sample sites occur along shorelines underlain by the volcanics or Sooke Gabbro.

a) Univariate Statistics

Analyses for 17 elements were run on 24 beach samples in Group A (Table 14), and 22 elements were run on 18 beach samples from Group B (Table 15).

In both groups concentrations of Mo, Cd and Se were either not above detection limits (Appendix C), including Pd, Pt, Ag and Hg (B), or insufficient data for statistical analysis were available, including Pb, Sn, Sb and Bi in (B).

Trace Au values in three samples from Group B were obtained from Sandcut Beach (Table 15).

Again, anomalous sample concentrations from the Sandcut area to Point No Point represent local enrichment above background populations. Copper is the only element which had highest concentrations consistently found at Sandcut Beach in both Groups A and B (Figures 78 and 79). Values from both groups show a low background level, several enriched samples and finally three anomalous concentrations from Sandcut Beach.

In Group A, Pb, Sn and Hg were the other elements for

TABLE 14. BEACH SAND GEOCHEMISTRY - 1989
(*Group A*, 24 samples)

	Samples > det.	$\bar{X}$	s	skew-ness	kurt-osis	Min.	Median	Max.
Au ppb	NR	-	-	-	-	-	-	-
Pd ppb	NR	-	-	-	-	-	-	-
Pt ppb	NR	-	-	-	-	-	-	-
Co ppm	NR	-	-	-	-	-	-	-
Cu ppm	24	48.2	24.1	2.0	5.8	27.0	39.0	118.0
Fe %	24	2.3	0.3	-0.1	3.0	1.6	2.4	3.0
Mn ppm	24	494.2	75.6	0.1	2.2	353.0	485.5	625.0
Mo ppm	24	2.9	0.3	-3.0	10.1	2.0	3.0	3.0
Ni ppm	NR	-	-	-	-	-	-	-
Pb ppm	24	52.1	8.5	2.3	9.5	40.0	50.0	84.0
V ppm	24	211.7	30.2	-0.5	4.1	134.0	216.5	273.0
Zn ppm	24	40.3	7.5	1.6	6.8	28.0	38.0	66.0
Ag ppm	24	0.8	0.1	0.2	2.6	0.6	0.8	1.1
Cd ppm	0	-	-	-	-	-	-	-
Se ppm	0	-	-	-	-	-	-	-
Sn ppm	21	11.8	3.7	3.6	15.7	10.0	11.0	27.0
Hg ppb	24	36.9	109.4	4.6	22.0	5.0	15.0	550.0
Sb ppm	23	15.4	3.7	-0.7	2.6	7.0	16.0	20.0
Bi ppm	16	7.4	4.3	1.6	5.9	2.0	6.5	20.0
Ti ppm	24	5191.7	604.3	0.7	2.8	4300.0	5150.0	6600.0
Zr ppm	24	105.6	21.5	0.8	3.4	74.0	103.0	162.0
Cr ppm	24	115.1	21.2	1.3	3.9	93.0	108.0	175.0

NR = not run for that element in 1989.

TABLE 15. BEACH SAND GEOCHEMISTRY - 1990
(*Group B*, 18 samples)

	Samples > det.	$\bar{X}$	s	skew-ness	kurt-osis	Min.	Median	Max.
Au ppb	3*	9.3	1.2	-0.7	1.5	8.0	10.0	10.0
Pd ppb	0*	-	-	-	-	-	-	-
Pt ppb	0*	-	-	-	-	-	-	-
Co ppm	18	10.8	7.2	1.6	4.1	4.0	8.0	28.0
Cu ppm	18	89.6	135.0	1.6	3.9	10.0	23.5	391.0
Fe %	18	2.7	1.0	0.9	3.1	1.3	2.4	4.8
Mn ppm	18	370.6	164.6	1.0	3.1	175.0	322.5	775.0
Mo ppm	3	1.0	0.0	0.0	0.0	1.0	1.0	1.0
Ni ppm	18	19.8	5.1	0.4	3.5	9.0	19.0	30.0
Pb ppm	17	4.1	2.1	0.6	2.3	2.0	4.0	8.0
V ppm	18	76.3	33.1	0.6	2.4	30.0	68.0	142.0
Zn ppm	18	35.7	11.6	0.7	3.4	16.0	33.0	64.0
Ag ppm	0	-	-	-	-	-	-	-
Cd ppm	0	-	-	-	-	-	-	-
Se ppm	4	0.5	0.2	-0.3	1.6	0.2	0.5	0.7
Sn ppm	2	2.0	0.0	0.0	0.0	2.0	2.0	2.0
Hg ppb	18	28.3	9.9	1.9	7.0	20.0	30.0	60.0
Sb ppm	18	0.2	0.1	2.5	7.1	0.2	0.2	0.4
Bi ppm	2	0.1	0.0	0.0	0.0	0.1	0.1	0.1
Ti ppm	18	8155.6	3476.9	0.3	1.9	2550.0	7875.0	13700.0
Zr ppm	18	97.6	29.4	0.8	3.3	50.0	87.0	165.0
Cr ppm	18	202.8	68.3	1.1	4.2	110.0	195.0	385.0

* Only 3 samples assayed for Au, Pd and Pt in 1990.

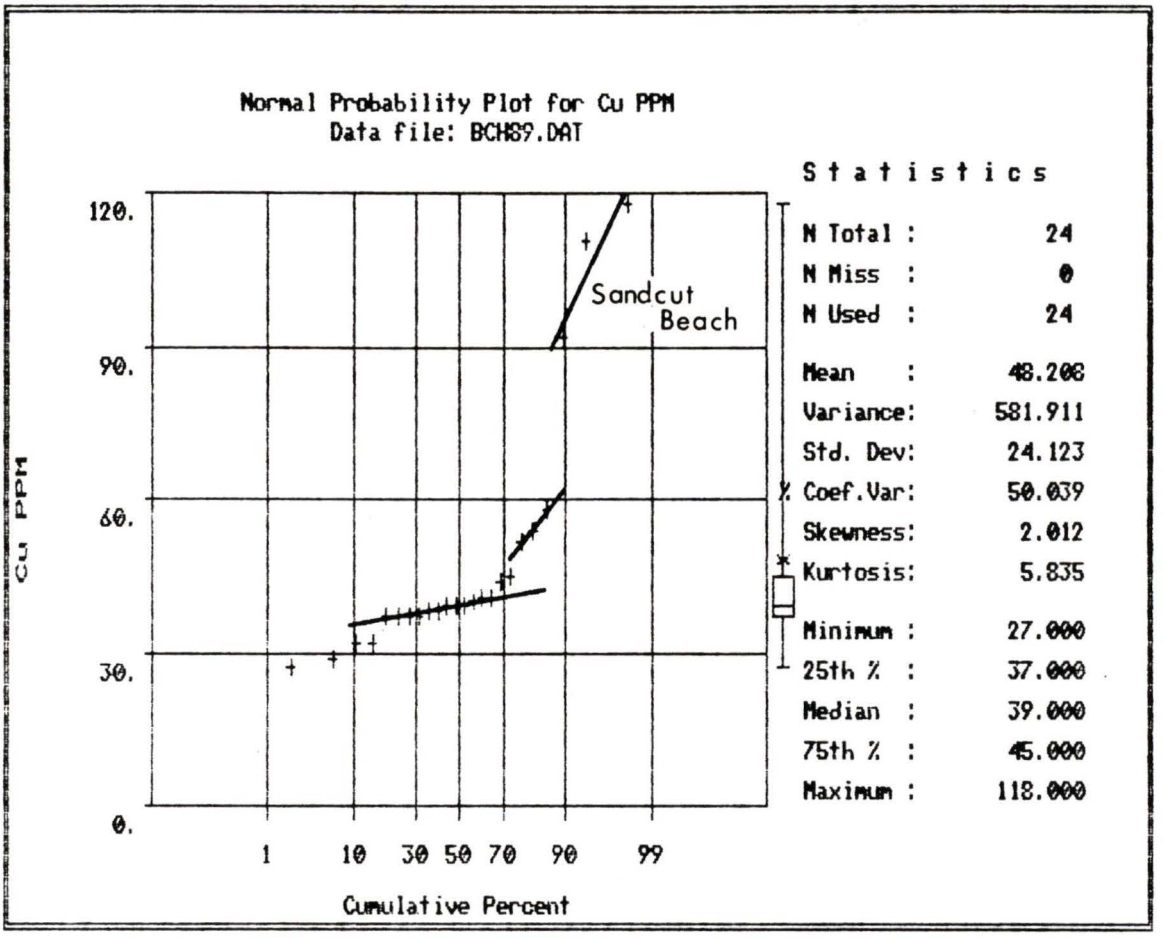

Figure 78. Probability plot of Cu concentrations in beach sands, 1989 (Group A). Highest values derive from Sandcut Beach.

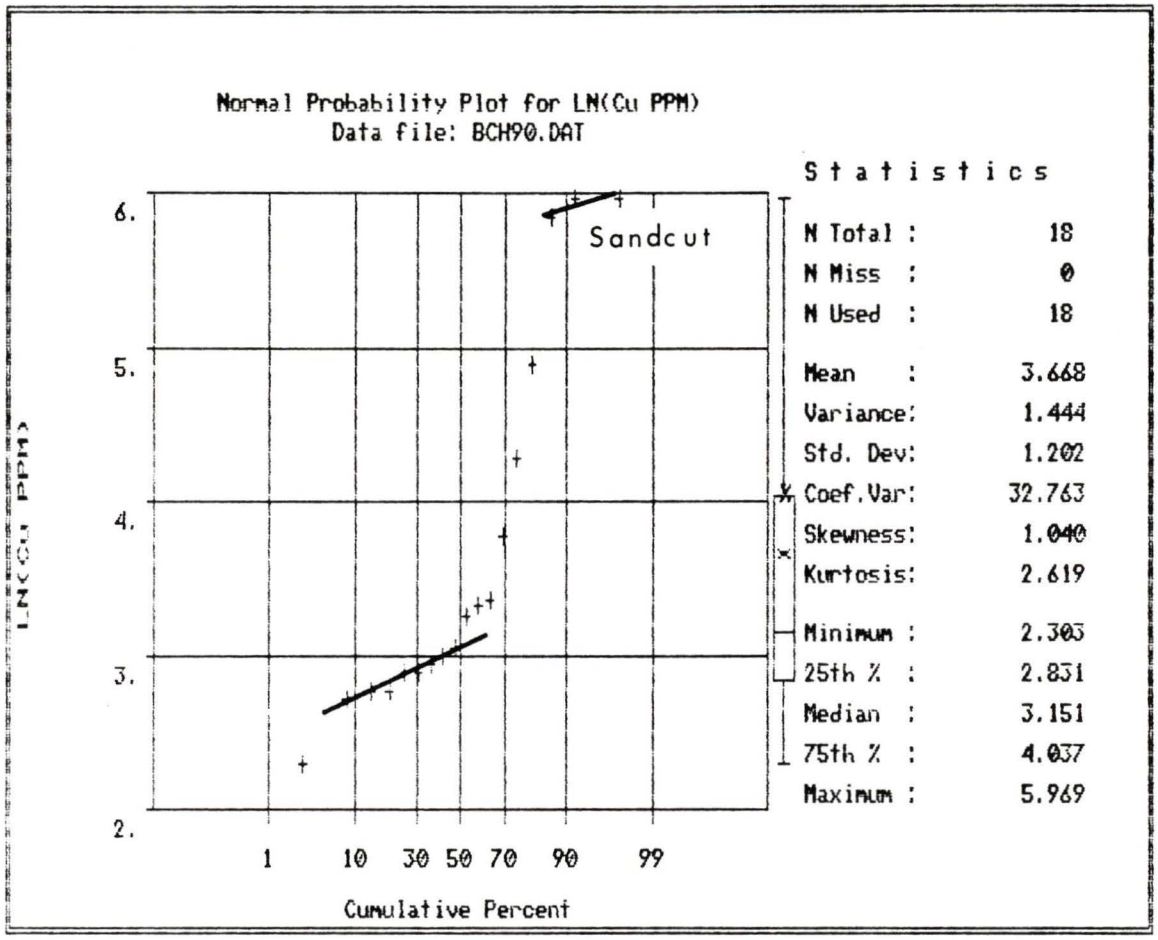

Figure 79. Probability plot of Cu concentrations (logged) in beach sands, 1990 (Group B). Highest values derive from Sandcut Beach.

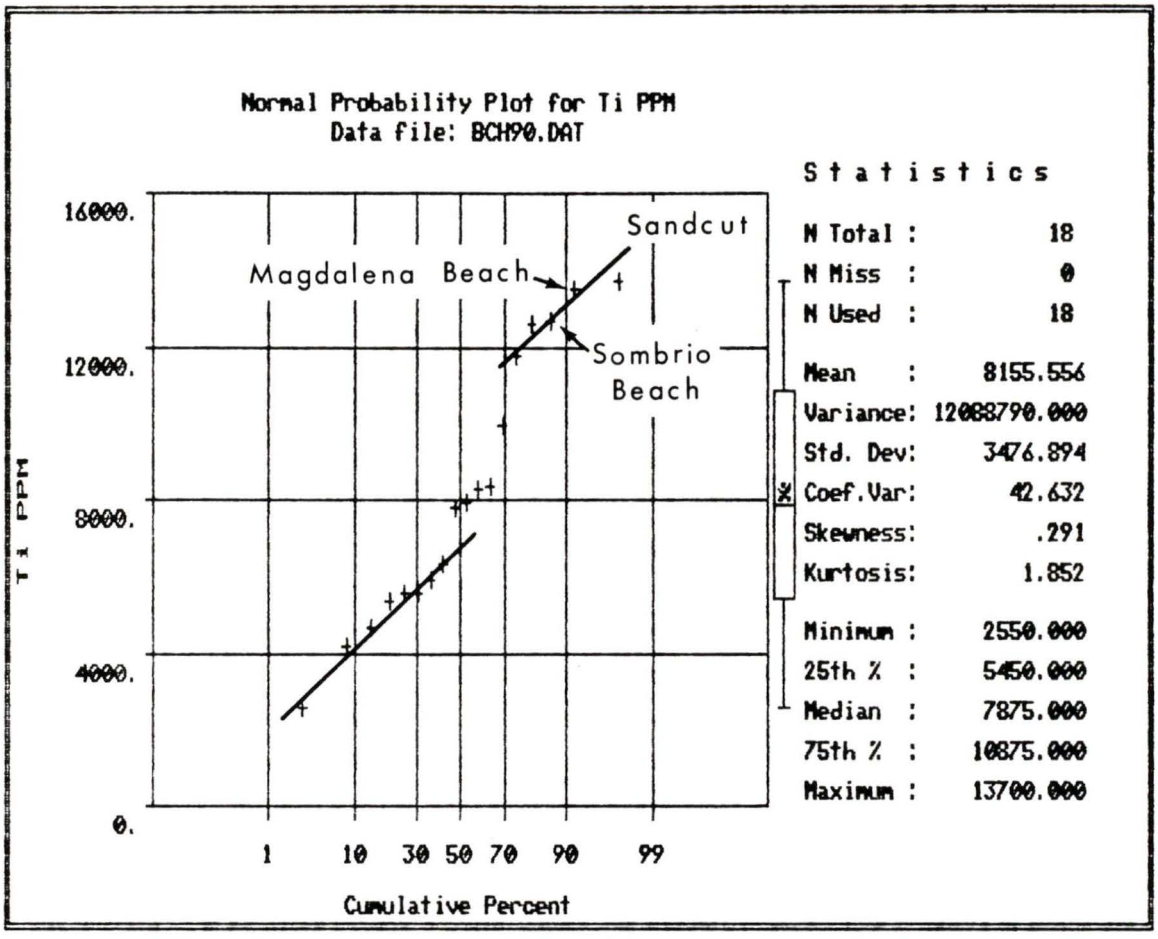

Figure 80. Probability plot of Ti concentrations in beach sands, 1990 (Group B). Highest values are found in the three samples from Sandcut Beach along with a sample from each of Magdalena and Sombrio Beaches.

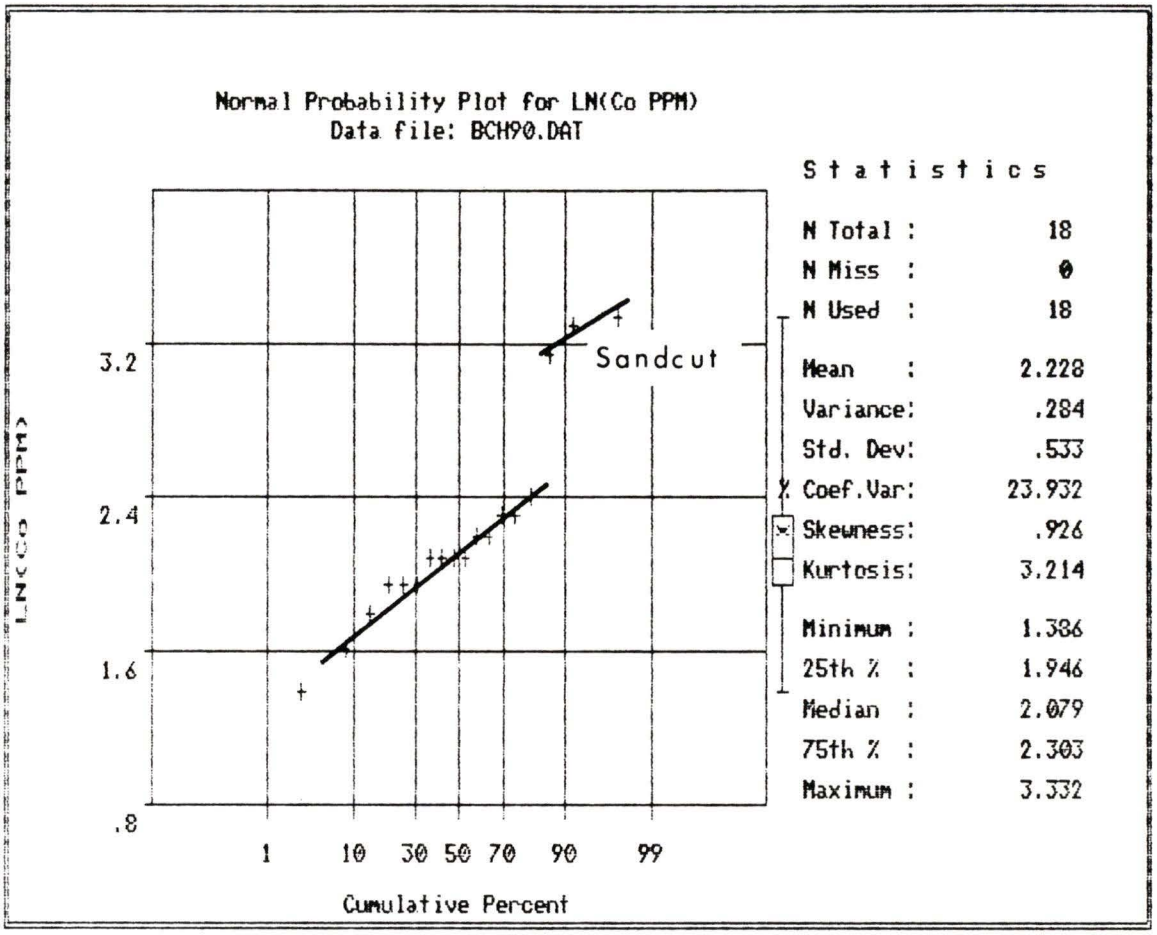

Figure 81. Probability plot of Co concentrations (logged) in beach sands, 1990 (Group B). Highest values derive from Sandcut Beach.

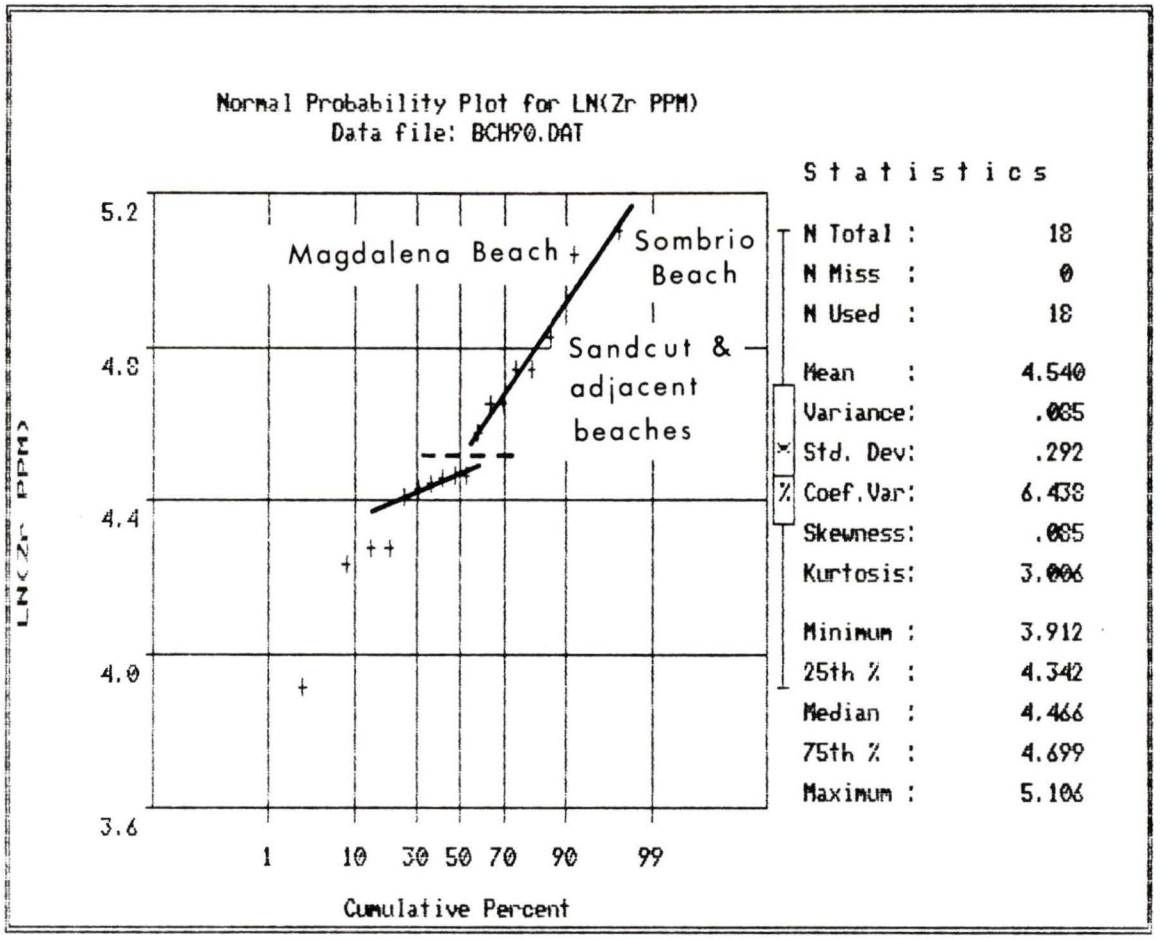

Figure 82. Probability plot of Zr concentrations (logged) in beach sands, 1990 (Group B). Highest values were obtained from samples at Sombrio and Magdalena Beaches, followed by samples from Sandcut and adjacent beaches.

which Sandcut Beach had the highest values.

Enriched populations in Group A were otherwise largely formed by a single Sandcut Beach sample along with samples from west Sooke Bay, Orveas Bay and French Beach. This occurred for Fe, Mn, Hg, Sb, Ti and Cr.

In Group B however, in addition to Cu, three samples from Sandcut Beach have anomalously high concentrations of Co, Fe, Mn, Ni, V and Ti. One sample from Sombrio Beach and the sample from Magdalena Beach, both with high heavy mineral contents, grouped with the Sandcut Beach samples for the above elements (e.g. Ti, Figure 80), except Co (Figure 81).

Variation in sample distribution between Group A and Group B account for variations observed between elemental populations. For example, in Group A, Fe forms a single normal population, whereas in Group B at least three modal groups occur. Such contrasts are also found for Mn and V.

In both groups Ti concentrations have polymodal distributions (e.g. Figure 80). However, in Group A minor enrichment of Ti concentrations occur in several samples from disparate geographic locales, producing the impression of a second population. This also occurs for Cr and Zr in both groups, and for Zn in Group A, and for Sb in Group B.

Zirconium concentrations were highest in Group B at Sombrio Beach and Magdalena Beach, followed by Sandcut Beach (Figure 82).

b) Elemental Correlations

Correlation matrices were calculated for beach samples from Groups A and B (Tables 16 and 17).

In Group A few strong correlations were found (Table 16). Fe, V and Ti show some correlation, but only Fe:V is very strong. Other significant correlations include Ti:Mn and Sn:Pb.

In contrast with Group A, many significant correlations were seen between elements in Group B (Table 17). The strength of these correlations are somewhat related to the effect of the anomalously high concentrations at Sandcut Beach, as discussed earlier.

Consistent correlations occur between Co, Cu, Fe, Ni, V and Ti (Table 17). A second grouping includes Mn, V, Ti and with less strength, Zr. A third grouping contains Zr, V, Ti and a negative correlation with Cr, showing a decrease in Cr for similar increases in the former elements. A fourth grouping shows good correlations between Fe, Mn and Ni.

These correlations are probably enhanced by their tendency to increase with sample heavy mineral content, discussed below. Zn was not correlated with heavy mineral percent and is not correlated to the above groups. Cr decreases with increasing heavy mineral percent and with decreases in all other elements.

TABLE 16. CORRELATION MATRIX, BEACH SAND - 1989 (*Group A*)

	Cu	Fe	Mn	Pb	V	Zn	Sn	Sb	Bi	Ti	Zr	Cr
Cu	0	0.58	0.58	0.38	0.28	0.34	0.28	0.42	-0.36	0.44	-0.30	-0.07
Fe		0	0.60	0.31	0.88	0.42	0.13	0.66	0.32	0.68	0.30	-0.31
Mn			0	0.25	0.54	0.46	0.33	0.16	-0.04	0.72	-0.12	0.20
Pb				0	0.16	0.08	0.89	0.54	-0.07	0.10	-0.14	-0.30
V					0	0.27	0.04	0.55	0.65	0.63	0.45	-0.39
Zn						0	0.03	0.14	-0.24	0.29	0.06	0.03
Sn							0	0.28	0.18	0.17	-0.13	-0.18
Sb								0	0.03	0.14	0.28	-0.64
Bi									0	0.44	0.64	-0.22
Ti										0	0.12	0.14
Zr											0	-0.32
Cr												0

Values for correlation coefficient "r" derived from 24 samples for each element except Sn, Sb and Bi, with 21, 23 and 16 samples respectively. The critical values of "r" for the 0.005 level of significance, are; r=0.52 (for 24 samples), r=0.53 (for 23 samples), r=0.55 (for 21 samples) and r=0.63 (for 16 samples).

TABLE 17. CORRELATION MATRIX, BEACH SAND - 1990 (*Group B*)

	Co	Cu	Fe	Mn	Ni	V	Zn	Ti	Zr	Cr
Co	0	0.98	0.94	0.60	0.90	0.88	0.55	0.72	0.27	-0.58
Cu		0	0.87	0.48	0.81	0.79	0.52	0.63	0.19	-0.52
Fe			0	0.77	0.95	0.96	0.64	0.85	0.48	-0.65
Mn				0	0.74	0.83	0.38	0.91	0.79	-0.60
Ni					0	0.92	0.58	0.81	0.43	-0.59
V						0	0.46	0.94	0.66	-0.79
Zn							0	0.30	-0.01	-0.02
Ti								0	0.84	-0.78
Zr									0	-0.69
Cr										0

Values for correlation coefficient "r" derived from 18 samples for each element, with critical value of r=0.59 for the 0.005 level of significance.

TABLE 18. RIVER SAND FRACTION* GEOCHEMISTRY - 1990 (*Group B*)

		SOMBRIO RIVER		**LOSS CREEK**		**JORDAN RIVER**		**MUIR CREEK**	
		Bar Head	Mid-Bar	Bar Head	Mid-Bar	Bar Head	Mid-Bar	Bar Head	Mid-Bar
Au	ppb	2	NR	<2	NR	<2	NR	<2	NR
Pd	ppb	<2	NR	2	NR	<2	NR	2	NR
Pt	ppb	<5	NR	<5	NR	<5	NR	<5	NR
Co	ppm	9	7	17	13	28	16	20	19
Cu	ppm	22	28	68	61	554	259	64	68
Fe	%	2.85	2.82	4.24	3.82	4.38	3.62	4.00	4.77
Mn	ppm	770	645	1300	635	845	440	640	620
Mo	ppm	<1	<1	<1	<1	<1	<1	<1	<1
Ni	ppm	19	19	43	40	36	29	35	38
Pb	ppm	8	32	44	58	46	16	136	24
V	ppm	73	72	114	103	149	107	129	143
Zn	ppm	44	42	54	52	68	60	52	60
Ag	ppm	<0.2	<0.2	<0.2	<0.2	<0.2	<0.2	<0.2	<0.2
Cd	ppm	<0.1	<0.1	<0.1	<0.1	<0.1	<0.1	<0.1	<0.1
Se	ppm	<0.2	<0.2	<0.2	<0.2	0.2	<0.2	0.2	<0.2
Sn	ppm	<2	<2	<2	4	2	2	<2	3
Hg	ppb	20	30	20	20	20	20	20	20
Sb	ppm	0.4	0.2	0.2	0.2	0.4	0.2	0.2	0.2
Bi	ppm	<0.1	0.1	<0.1	<0.1	<0.1	<0.1	<0.1	<0.1
Ti	ppm	6900	7100	11100	11400	15200	11800	10900	13300
Zr	ppm	105	105	100	105	115	100	99	125
Cr	ppm	230	196	210	220	132	130	174	170

* = sand fraction here is material < 1 mm and > 0.063 mm.
NR = assays not performed for those samples.

TABLE 19. RIVER MUD FRACTION GEOCHEMISTRY - 1990
(*Group B*)

	Sombrio River	Loss Creek	Jordan River	Muir Creek
Au ppb	30	32	20	4
Pd ppb	<2	4	4	<2
Pt ppb	<5	<5	<5	<5
Co ppm	19	73	37	21
Cu ppm	214	3510	469	224
Fe %	3.80	5.02	6.28	3.90
Mn ppm	685	790	1350	735
Mo ppm	1	1	<1	<1
Ni ppm	32	75	58	48
Pb ppm	112	166	164	70
V ppm	105	137	197	117
Zn ppm	90	196	122	72
Ag ppm	<0.2	0.5	<0.2	<0.2
Cd ppm	<0.1	0.6	<0.1	<0.1
Se ppm	<0.2	1.2	<0.2	<0.2
Sn ppm	10	15	20	7
Hg ppb	90	70	50	40
Sb ppm	0.4	3.0	0.4	0.4
Bi ppm	<0.1	<0.1	<0.1	<0.1
Ti ppm	11400	12400	16100	13700
Zr ppm	205	125	125	185
Cr ppm	130	132	114	158

Mud samples from head bar and mid-bar sites were combined for analysis from each river.

c) Other Correlations

Good correlations between increasing heavy mineral content and various elements in Group A, were only found for Cu (r=0.86) and Bi (r=-0.89). This suggests Bi is not found in the heavy fraction of sediments, and may be occurring as traces in vein quartz (Berry and Mason, 1959).

For samples in Group B, eight elements have good correlations with weight percent of heavy minerals:

Ti	r=0.95	Mn	r=0.86	Cu	r=0.79
V	r=0.92	Co	r=0.84	Zr	r=0.71
Fe	r=0.89	Ni	r=0.82		

Zn values obtained for Group B decreased significantly eastward (r=-0.65).

iv) River Geochemistry

The sand fraction of river samples was analysed for both the head of the river bar and mid-bar sites (Table 18). Mud fractions from both sites were combined for analysis from each river (Table 19).

Sand fraction of river samples returned no values from assays for Au, Pd and Pt (Table 18). Geochemistry revealed none or few values above the detection limit for Mo, Ag, Cd, Se, Sn and Bi. Hg and Sb concentrations were of limited range above the detection limit of the analytical technique.

For the remaining 11 elements Jordan River has the consistently highest concentration for seven elements, Co, Cu, Fe, V, Ti, Zn and Zr, while having the lowest concentration of Cr. Sombrio River has the lowest

concentrations for the above elements (except Zr and including Pb), with the highest concentrations of Cr.

Two-thirds of sample concentrations have higher values for the bar-head sample than from material taken midway down the side of the bar for all eleven elements.

Analysis of mud fractions from the four rivers returned no or limited concentrations for Pd, Pt, Mo, Ag, Cd, Se, Sb and Bi (Table 19).

In contrast to the sand fraction, mud values were highest at Loss Creek and Jordan River. Concentrations were highest at Jordan River for Fe, Mn, V, Sn and Ti, while Cr was again lowest. Loss Creek has generally highest values for Au, Co, Cu, Ni, Pb and Zn. Lowest values were shared between the other two rivers with Sombrio River having the lowest concentrations for Co, Cu, Fe, Mn, Ni, V and Ti.

Comparing river mud concentrations to the river sand concentrations, the former are higher for twelve elements, with Mn values generally comparable, and Cr being highest in the sand fraction.

v) Comparing Geochemistry: From River, Beach to Offshore

Comparison is made between sand analysed from beach and offshore environments for Group A, and river, beach and offshore environments for Group B.

Comparison of sand concentrations for 17 elements in the offshore and beach sample sets for Group A, indicate all elements except Cr have higher mean concentrations in beach

sands than offshore sands (Tables 7 and 14). Cr in the offshore has a slightly higher mean concentration.

Four elements found to be anomalous in both environments (beach and offshore) are Fe, Ti, V and Mn (A) (Tables 7 and 14). Concentrations in beach sands for these four elements are more than two standard deviations above offshore means.

In contrast to the results for Group A, comparison of mean concentration of 19 elements for sands from the beach and offshore in Group B show comparable values (Tables 8 and 15). Standard deviations are of similar magnitude, with the means of these two sets being within one standard deviation. The similarity of results may reflect the better representation of the entire coastline for beach samples in Group B.

Strong correlations in offshore samples for Group A are present for Fe, Ti and V followed by slightly lower correlations with Mn (Table 9). These correlations are repeated in the beach sand for Fe, Ti and V (Table 16). The beach sand correlations are only slightly lower and Mn is not well correlated.

Strong correlations in offshore sand sample concentrations in (B) between Co, Cu, Fe, Ti and V followed with slightly lower correlations with Mn and Ni, are mirrored in the beach results except for Mn which is less highly correlated with the other elements (Tables 10 and

17). Zn and Fe beach correlations had lower values.

Comparing river sand values and offshore sand mean values from (B), the former had distinctly higher concentrations for most elements (Tables 18 and 8); for example Co, Cu, Fe, Mn, Ni, Pb, V, Zn and Ti. Higher river concentrations may be the result of their finer grain-size range (<1 mm). Values for Zr and Cr are comparable from both environments. These generalisations are made excluding isolated anomalous values, particularly for Cu.

Comparing river sand concentrations with mean beach sand levels for (B), again, river values are consistently higher for the nine elements listed above, plus Zr (Tables 18 and 15). Again, Cr values are comparable from both sample sets, and comparisons are made excluding isolated anomalous values, such as occurs with Cu.

Comparing river mud values with offshore mud values (Tables 12 and 19), the former are higher for ten elements which have a range above detection level in the offshore, Co, Cu, Fe, Mn, Ni, Pb, V, Zn, Ti and Cr. Comparable levels are found for Sn and Hg in both environments, and only Zr has higher concentrations in offshore muds.

VII. DISCUSSION

1. Surficial Geology

The nearshore surficial geology of northern Juan de Fuca Strait is described in terms of sediment textural parameters and morphological features. Results indicate that the sediments are immature (Folk, 1974) based on sorting and mineral composition. While winnowing of sediments is evident on shallow terraces (boulder fields), most sediment sorting is moderate to very poor, and abrading of sediment grains is relatively minor. Significant amounts of lithic fragments in both heavy and light sediment fractions indicate a low degree of abrasion. Similarly, heavy minerals present in nearshore sands are predominantly metastable and generally angular to subangular.

Textural and mineralogic evidence suggests that the source of modern sediments is a mixture of glacial materials and erosion of adjacent or underlying bedrock. McLaren (1983) concluded that the largest source for nearshore sediments in the area was from eroding Quaternary sediments in coastal deposits. The patchwork distribution of marine surficial sediment units (Figure 8) and low levels of sorting would strongly support this conclusion.

Several findings from this study suggest that locally the Quaternary materials are being substantially diluted by river influx representing coastal lithologies. In addition, minor *in situ* weathering of the underlying sandstone of the

Sooke Formation may be contributing sediments locally. For example, distribution of grain size modes shows distinct differences from east to west. East from China Beach to Sooke Bay the modal grain size may be characterised as fine sand (2.00 to 3.00 phi) (Figure 16) derived from adjacent volcanic rocks by rivers and coastal erosion. Samples obtained from the mouths of Jordan River and Muir Creek have modes of fine grained sand, and the relatively fine sediment influx can be seen in the contoured mean grain size values extending offshore from Jordan River (Figure 9).

Coarser-grained, but softer, metamorphic rocks northwest of Loss Creek are the source for a medium to coarse grained (0 to 2.00 phi) modal group (Figure 17) found entering the coastal waters from both Loss Creek and Sombrio River (Figure 14). These coarser sediments remain in the shallower terrace areas and are transported eastward from Loss Creek in the nearshore. Finer volcanic sediments tend to blanket the southeast to all depths, while the river material in the northwest is being sorted and winnowed as it moves offshore, creating a general decrease in grain size with distance from shore.

Mineralogy from the four river samples suggests different river sediment loads (Figure 38), but examination of the offshore mineralogy (Figure 36) failed to reveal distinct heavy mineral provinces related to each river. Reworked coastal Quaternary materials and the dominant east-

northeast longshore transport, initially recognised by McLaren (1983), contribute significantly to the mineral diversity along the eastern beaches and thereby obscuring any expected heavy mineral distributions based on the mineral composition of river sediments.

Net sediment transport appears to be to the east in nearshore waters generally less than 30 m depth (McLaren, 1983) as suggested by mean grain size distribution east of Mystic Beach where an offshore bar of coarser material is forming east of the headland. Similar gently sloping beaches at Sandcut and French Beach show an offshore area of coarser sand with decreasing grain size both shoreward and towards deeper water. This is a wave-induced phenomenon due to the movement of sediments on and offshore as well as parallel to the shoreline, in longshore currents (Thomson, 1981). Heavy minerals which increase shoreward at Sandcut Beach are associated with the increasingly finer mean grain size. Sediment coarsens again near shore and in the swash zone while heavy mineral percentages diminish in the most shoreward sample of the transect.

Other evidence of net eastward littoral transport is the shallow tongue of sediment extending from the mouth of Jordan River observed in mean grain-size data (Figure 9). Eastward transport is also observed in the concentrations of heavy minerals at Sandcut Beach (Figure 23) which form a plume extending eastward from Desolation Point. This can

also be seen in the Ti percent distribution (Figure 73).

A third modal group provides evidence of yet another probable source of sediments, the Sooke Formation, which has been eroded to form coastal bluffs and an extensive intertidal platform. Fine to very fine sand (2.50 to 3.25 phi) (Figures 16 and 17) is found in the statistical groupings separating both northwestern and eastern sediment modes. A sample believed to be from eroded *in situ* Sooke Formation, obtained at the mouth of Sombrio River, and two other samples from suspected similar sites fall into the fine to very fine sand category (Figure 20). Bream (1987) describes the modal grain size of the Sooke Formation as fine-grained sandstone.

Many similarities exist between the Sooke Formation sandstones and modern nearshore surficial sediments. Sooke Formation sandstones are lithic arenites which are texturally immature, descriptions which can be applied to the adjacent modern sediments. Provenance for the Tertiary sediments is largely the Metchosin basalt, followed by other lithologies present on Vancouver Island (Bream, 1987). Similarities in the heavy mineralogy occur between common blue-green hornblende and significant volumes of lithic grains. Epidote constitutes a large proportion of the accessory minerals in the sandstones, followed by clinozoisite and zoisite, staurolite, pumpellyite and lesser pyroxene, with rare garnet and zircon. In the Sooke

Formation the most common opaque mineral is pyrite (as a cement, detrital grain or alteration product) not magnetite-ilmenite as in the modern marine sediments. Pyrite occurs in a variety of forms, from cubic crystals to framboidal masses (Bream, 1987).

A high quantity of pyrite (59.9%), occurs largely as framboids, in the winnowed sample from off the mouth of Sombrio River, further supporting the view that the sample is from eroded *in situ* Sooke Formation rocks.

The Sooke Formation differs from the modern sediments mainly in degree of sorting. The Tertiary sandstones are mostly well- to moderately well-sorted. These rocks were deposited in a high-energy wave-dominated shallow marine environment (Bream, 1987), similar to their setting today.

At present the sandstones of the Sooke Formation are undergoing chemical erosion (Harper, 1981), inevitably contributing sediments to the littoral sediment regime. The volume of sediment being contributed probably remains small, as Harper (1981) considers erosion of the Sooke Formation to be less than 20 cm per year.

The source of other nearshore sediments are more obvious. Surficial sediments from sites at the mouths of Loss Creek and Jordan River are described as sand (Figure 8) and probably represent river sediment with a mixture of coastal and migrating nearshore sediments, particularly at Jordan River.

Samples off the mouths of Sombrio River and Muir Creek are classified as gravely-muddy sand (gmS) (Figure 8). These samples are from embayments bordered by extensive shoreline bluffs and intertidal platforms of the Sooke Formation. Large areas of the nearshore off the mouths of Sombrio River and Muir Creek are mapped as gmS and represent two zones of the seafloor which contain poorly sorted fine to very-fine sand with mud in shallow, high-energy waters. The probable extension of sandstone platforms from shore coincident with a poorly sorted sand facies, gmS, may indicate areas where the Sooke Formation is exposed and eroding on the seafloor. Alternatively, underlying or proximal sources of mud and coarse-grained material, such as depressions or pockets of moraine, may supply such poorly-sorted sediments.

Sooke Formation is believed to be extensively exposed in the shallow waters from Sombrio River to beyond Sombrio Point where grab sampling was not successful, presumably due to exposed bedrock or boulders (as at the dive site). Parallel channels eroded into the sandstone platform at shallow water depths were observed below Loss Creek and at the northwestern edge of the study area. Their orientation suggests they may be surge channels. Harper (1981) notes numerous surge channels cut into the Carmanah Group intertidal platforms along the coast northwest of Port San Juan. There is no evidence to indicate whether the

submarine channels within the study area were originally subaerially exposed, or if they have been eroded under present marine conditions.

Deglaciation of Vashon ice (Fraser Glaciation) with retreat following downwasting and thinning resulted in marine penetration beyond the eastern end of Juan de Fuca Strait by 13 000 years BP (Clague *et al.*, 1982). Glacial or post-glacial sediments which may exist on the nearshore terraces or form part of such terraces are poorly documented. Thinly veneered morainal material in waters shallower than 100 m depth south of Sombrio Point, and observed in the sub-bottom around Otter Point, Sooke Bay and Port San Juan, may correspond to the grey glaciomarine sediments identified in vibro-cores from depths of 80 m in Sooke Bay (K.W. Conway, unpub. rep., 1989) and unit C glaciomarine grey clay of Linden and Schurer (1988) traced from Royal Roads to the entrance of the strait.

No evidence of former strand lines or the existence of submerged beaches was observed in this study. Although the shallow terraces are delineated by scarps with largely gentle slopes from 10 to 30 m, to greatest depths of 70 m, they do not show a build-up of beach material or high-energy erosion. A gradual increase in gravel towards the edge of shallow terraces is visible in the side-scan records and can be recognized in the distribution of surficial sediment in relation to ridge positions (Figures 8 and 21). This

increase in gravel is likely due to gravity and gentle slope processes which include the gullying south of Magdalena Point (Figure 21).

The study area extends approximately 60 km along the northern shore of Juan de Fuca Strait and probably includes the transition between the complex history of sea level change in the Victoria area and that of continual emergence along the west coast of Vancouver Island during the Holocene. Although no sign of lower sea level stand was recognized in the surficial mapping, there is evidence from Conway (unpub. rep., 1989) and Linden and Schurer (1988) that a lowered sea level may have occurred at least as far west as Sooke and Orveas Bays before transgression to present sea levels during the Holocene.

The existence of a relict channel extending from the mouth of Muir Creek to the edge of the submarine terrace, suggests subaerial exposure at some time in the past. Two vibro-cores in Orveas Bay show evidence of possible lower sea levels at the end of the Wisconsinan glaciation (K.W. Conway, unpub. rep., 1989). These cores have not been dated, and provide conflicting information when compared to the presence of abandoned marine scarps in backshore areas of Sooke Bay, Sandcut and China Beaches, and recently raised strandlines at French Beach and Port San Juan (Harper, 1980) and other onshore evidence of emergence (Riddihough, 1982; Clague *et al.*, 1982).

Most evidence supports emergence during the Holocene, at least east of Sheringham Point, as most of the vibrocores with possible intertidal horizons are in Sooke or Orveas Bay (K.W. Conway, unpub. rep., 1989). However, resolution of pre- or early Holocene sea levels along northern Juan de Fuca Strait is not at present possible as this study did not extend into the platform at depth, and therefore little more can be deduced about the history of the shallow terraces beneath the modern surface sediments.

The configuration of the nearshore terraces is likely the result of glacial scouring by ice sheets during the Pleistocene. As sediments on the terraces have not been directly dated the only evidence against the erosion of the terraces during the most recent ice advance is the constant scarp angle of 106^{o} which is at variance with the ice flow recorded during the Vashon maximum, which was initially south-southwest into the strait, and 116^{o} along the strait during resurgence (Alley and Chatwin, 1979). No obvious structural orientations from the underlying lithologies account for the terrace angles of 106^{o}.

Continued erosion of terrestrial Quaternary deposits during the last 10 000 years and discharge of coastal rivers and streams have contributed new material to the nearshore strait. Tidal currents and their scouring and winnowing effects have modified the surficial sediment distribution.

As a result of continued winnowing, sediments

containing appreciable amounts of mud are found mainly in mid-depths (below 30 m) associated with northwest facing slopes and areas of topographic lows, away from the prevailing current direction from the east. For material finer than 2 mm sorting decreases with depth, or distance from shore, and with a decrease in grain size. This poorly sorted muddy-sand accumulates at the base of the terrace slopes as the current sweeps the terraces. Glacial moraine once covered the terraces, now boulder fields and gravel units occur over the shallow floor of the nearshore west of Sheringham Point where the strong ebbing current combines with greater exposure to Pacific waves entering the strait.

The same tidal current energy which has scoured the surface free of most fine sediments, such as near Sombrio River, has contributed to the creation and movement of flow-transverse dunes. These dunes (small to large) appear to intermittently migrate west-northwest along the base of the terrace slopes in the eastern part of the study area, and on shallow terraces and along gentler slopes to the west. Confused bedforms may result from backeddies found in eastern shallow embayments such as Sooke Bay (Thomson, 1981), or may be induced by storm conditions which approach from the northwest causing movement of sediment in shallow areas against the prevailing flow.

Dive sites at the mouth of Sombrio River and Loss Creek found few fines and the surficial sediment

distribution (Figure 8) suggests relatively little material is being contributed to the strait from these two rivers. To the east there are increased fines substantiated by dive samples at the mouths of Jordan River and Muir Creek. In the former, only the tops of boulders are exposed above the sediment; the influx of material is moderate and may be largely limited to the adjacent shelf, as has been discussed earlier. At Muir Creek the sediment influx is substantially greater. The terrace floor is composed of muddy sand with little coarse material observed. Muir Creek continues to drain a basin which includes large deposits of Quaternary material and the Sooke Formation. The relict channel off Muir Creek is being slowly buried by sands, while the submarine pinnacle southwest of Muir Creek is being slowly buried as well, by sediment derived from the north-northeast.

The greatest modern source of sediments to the northern strait is from the San Juan and Gordon Rivers through Port San Juan. Principal component analysis strongly separated the sample from the mouth of Port San Juan as representing a distinctly different assemblage of minerals from that found along the northern strait. The latter sediments are largely muddy sands which coincide with the younger diachronous sand unit of Anderson (1968) which blankets the central strait. Anderson (1968) noted that this unit is thickest towards the north off Port San Juan

and Otter Point (west of Muir Creek). As a possible result of unconsolidated sediment build-up, channels extending southwest from Point San Juan have been scoured in the terrace substrate and evidence of debris flow fans are found beyond them at 90 m depth.

2. Heavy Minerals & Geochemistry

Heavy mineral percentages and geochemistry along the northern strait indicate that elemental background levels are found in the sediments out to 100 m depth, and areas of localised enrichment occur nearshore by river mouths and isolated beaches. Sandcut Beach, east of Jordan River, appears to host the greatest zone of enriched heavy minerals and elements both in beach profile samples and along transect samples out to 800 m from shore. The greater Jordan River area displays similar, although less intense, concentrations.

Mean weight percent of heavy minerals in the offshore (excluding 4 highest values) is 6.0%. This concentration is high compared to normal marine sands, 0.1%-0.5% (Folk, 1974). Contrast is supplied by studies of heavy minerals in waters of similar depths, above 100 m, such as the Chukchi Sea, Alaska (0.05%) (Luepke and Escowitz, 1989), and southern Beaufort Sea (0.1%-5.0%) (Costaschuk, 1980). Carter (1970) found 2.7% heavy minerals in the sands of Barkley Sound and 1.2% from sands of the adjacent continental shelf.

Sediments along northern Juan de Fuca Strait are considered immature. In the Chukchi Sea, mineral variety and overall immaturity has been noted (Luepke and Escowitz, 1989), while in the southern Beaufort Sea the sediments are considered mature with some limited influx from less-mature sources (Costaschuk, 1980). In both locations source rocks are sediments of Paleozoic, Mesozoic and Cenozoic age (Luepke and Escowitz, 1989; Costaschuk, 1980).

The abundance of ultrastable minerals are commonly used as one indication of sediment maturity. Such minerals are rare in the study area in part due to limited localised sources. X-ray diffraction results (Table 3) illustrate the mineral immaturity, with a single listing of rutile in the deepest sample analysed, at 87 m.

Beach samples outside the greater Jordan River area had a mean heavy mineral content of 11.0%, nearly twice the offshore value. In contrast, Carter (1970) combined beach and river sands in Barkley Sound for 3.2% heavy mineral content.

High heavy mineral values in both beach and offshore environments are most likely due to the proximity of the Metchosin Igneous Complex. Contrasts in river percent heavy mineral content between lower values at Sombrio River and the three eastern rivers emphasize the higher heavy mineral content in the Metchosin rocks. The latter supply significant quantities of amphibole, pyroxene and accessory

heavy minerals such as magnetite and ilmenite (Clapp 1912) to the local sediment. Erosion and transport of Quaternary sediments and Sooke Formation sandstones may contribute to heavy mineral content where hydraulic sorting has occurred such as on beaches, but could have the effect of diluting basaltic and gabbroic minerals if little such sorting is occurring.

In the offshore, magnetite represented 0.6% of the sand fraction, 8.7% of the heavy mineral residue. In the southern Beaufort Sea, although a mean value is not given, weight percent of magnetite ranges from trace values nearshore to greater than 16% in pockets and at depth (Costaschuk, 1980). Values greater than 4% dominate the shelf area. Costaschuk (1980) considers these values anomalous and tentatively interpreted them as largely authigenic. Magnetite in Barkley Sound has a mean of 0.5%, similar to the present study, and 0.2% on the continental shelf adjacent to Barkley Sound (Carter, 1970).

Magnetite from samples at Sandcut Beach and Point No Point resulted in a mean of 2.2%, 7.1% of the heavy mineral fraction. These values are substantially higher than those found offshore. Lower values were found for river and beach magnetite in Barkley Sound of 0.8% (Carter, 1970). Local enrichment of magnetite appears to occur along this shoreline. Magnetite is a common accessory mineral in the adjacent basalts and gabbros and was estimated by Clapp

(1917) as forming up to 10% of the rock locally.

Magnetite forms many placer beaches on Vancouver Island, including Florencia Bay along the west coast where magnetite contents reach 4.2% of beach sands (Holland and Nasmith, 1958). Bream (1987) did not find magnetite to be a common mineral in the Sooke Formation, but locally it formed placers, such as those exposed in bluffs at French Beach.

X-ray diffraction results and optical identification of heavy minerals resulted in comparable mineralogy, with a few important exceptions (Tables 3 and 17). XRD analyses are of the whole sand fraction whereas optical mineral identification was of the narrow sand fraction of 0.125-0.090 mm. Since mineralogy is a function of grain size, the narrow size fraction may not truly represent relative mineral abundances in the sand. The largest difference is in the low abundance of augite relative to XRD results. Augite may occur as coarser grains, or may be contained in lithic fragments, or both. Examination of limited samples of larger size fractions indicate that lithic fragments increase in abundance with size.

Mineralogy offshore and along the five eastern beaches largely reflects the basalts and gabbros which dominate the eastern two-thirds of the shoreline. Insufficient fine material, even at Sombrio beach, prevented more representative sampling of sediments adjacent to the metamorphic rocks in the northwest. For this reason the

considerable pink garnet found in relict stream samples near Sombrio River (Urlich *et al.*, 1984), and recorded elsewhere (Clapp, 1912), are not observed in such abundance in the present samples.

French Beach has the most highly sorted beach material within the study area. It has the lowest shape-fractionation index, and therefore has the highest hydraulic sorting. The sample from this beach contained 18.5% heavy minerals, 97.4% of which were in the very fine sand fraction. The highest garnet and second highest staurolite concentrations were found here. Development of the beach is discussed by McLaren *et al.* (1983). They suggest that the beach presently represents a closed sediment system as a result of on-offshore sediment cycling and localised seasonal reversals in drift direction (Harper, 1980). Thus the long term reworking and sorting of sediments may explain the relatively mature mineral composition. Reworking of backshore relict dunes and Quaternary bluffs could have supplied the minerals garnet and staurolite.

Geochemistry in the offshore, excluding the area off Jordan River, revealed mostly low trace metal values (Tables 4 and 5). The same can be said of the beach geochemistry (Tables 11 and 12). A few elements, Cu, Mn, Zr, Cr and V, occur in slightly elevated amounts while Ti concentrations are significantly higher than background. Increased concentrations of Fe, Ti, V, Cu, Mn, and to a lesser extent

Ni and Co, are inter-correlated both in the offshore and on beaches (Tables 6, 7, 13 and 14). Beach correlations tended to be more variable, a result of more localised influences.

Gold found at the mouth of Jordan River (100 ppb) probably represents a recent flood from the river. The vertical mobility of Au in fine sand suggests it would not have resided in surface sediments in a dynamic environment for any extended period.

Ti concentrations in sands within the study area rarely occur below 3000 ppm (0.3%) (Tables 4 and 5). General background values for Ti on the British Columbia coast are near 3000 ppm (T. Pedersen, pers. comm., 1990). Contours for both geochemical analytical sample sets suggest Ti is elevated near river mouths and in beach samples (Figure 73) in a similar pattern to the heavy mineral concentration in sand (Figure 23), particularly in the greater Jordan River area. Distributions of concentrations from sample sets for both years indicate a relative increase in offshore Ti values in sands to the east of the boundary with the Metchosin basalts and gabbros.

Trace metal concentrations were consistently higher in mud than in sand fractions, with the distinct exception of Cr. Although Cr displayed enrichment in the Jordan River and Sandcut nearshore areas, similar to Cu, Fe, Mn, V, and Ti, correlation with these elements appears to be lacking, except in the Group A offshore mud correlation with Ti,

which is notably based on a limited sample set (5). Cr has negative correlations with Zr, V, Ti and percent heavy mineral content in beach sands. The source of Cr in the mud and sand samples may originate from two minerals. Since enrichment in the Jordan River area coincides with other elements it is probable that trace Cr is bound in the magnetite found in the placer, discussed below. In addition to the above, minor green garnet (uvarovite, $Ca_3Cr_2(SiO_4)_3$) was identified in the sample from Loss Creek and offshore Sombrio Point. Cr from garnet may explain the presence of higher values in sands due to their resistence to mechanical abrasion (lack of cleavage and relative hardness). This possible source may originate from the Leech River Complex as the highest Cr concentrations obtained in river sands and muds were found at Sombrio River and Loss Creek.

Bimodal populations in both muds and sands were found for Mn, V and Ti for both samples sets (two years). Correlations between elements in sands were similar to those found in muds analysed in 1990. This was not the case for the sands or muds analysed in 1989, related probably to the smaller number of the mud samples (5) decreasing the probability of attaining a representative sample.

Zirconium showed a consistent increase in concentration with decrease in grain size, suggesting a possible association with clays. Zircons were found to be rare in this study, as in the Sooke Formation (Bream, 1987).

Local sources for zircon are limited (muscovite pegmatite intrusion). The possible glacial derivation of zircons from the coast mountains presents an alternative source.

3. Sandcut Placer - Jordan River Area

Geochemistry and analysis of heavy minerals has revealed placer formation along Sandcut Beach and in shallow waters out to 800 m from shore (Figure 83). Elevated heavy mineral content associated with the Sandcut placer may extend east along shore as far as the sands of western Point No Point. Formation of the placer is linked to mine tailings dumped at tidewater near the town of Jordan River to the west.

Evidence of the placer is found in all geochemical and mineralogical analyses. Greatest concentrations found in the placer occurred offshore at 200 m along the transect (42.4% heavy minerals, 1.33% Ti), and at the northwestern end of Sandcut Beach (45.9% heavy minerals, 1.37% Ti) (Figure 83).

The source of the heavy minerals was from the tailings pipes of the Sunro mine near Jordan River. Tailings from the tidewater and submarine tailing pipes, up to 1974, appear to have included grains of sufficient size to supply the heavy minerals to Sandcut Beach. A sample taken in 1989 from eastern Outfall Bay (Figure 83) had a low heavy mineral content (6.5%) and low associated elemental levels. Jordan River also had the highest concentration of heavy minerals

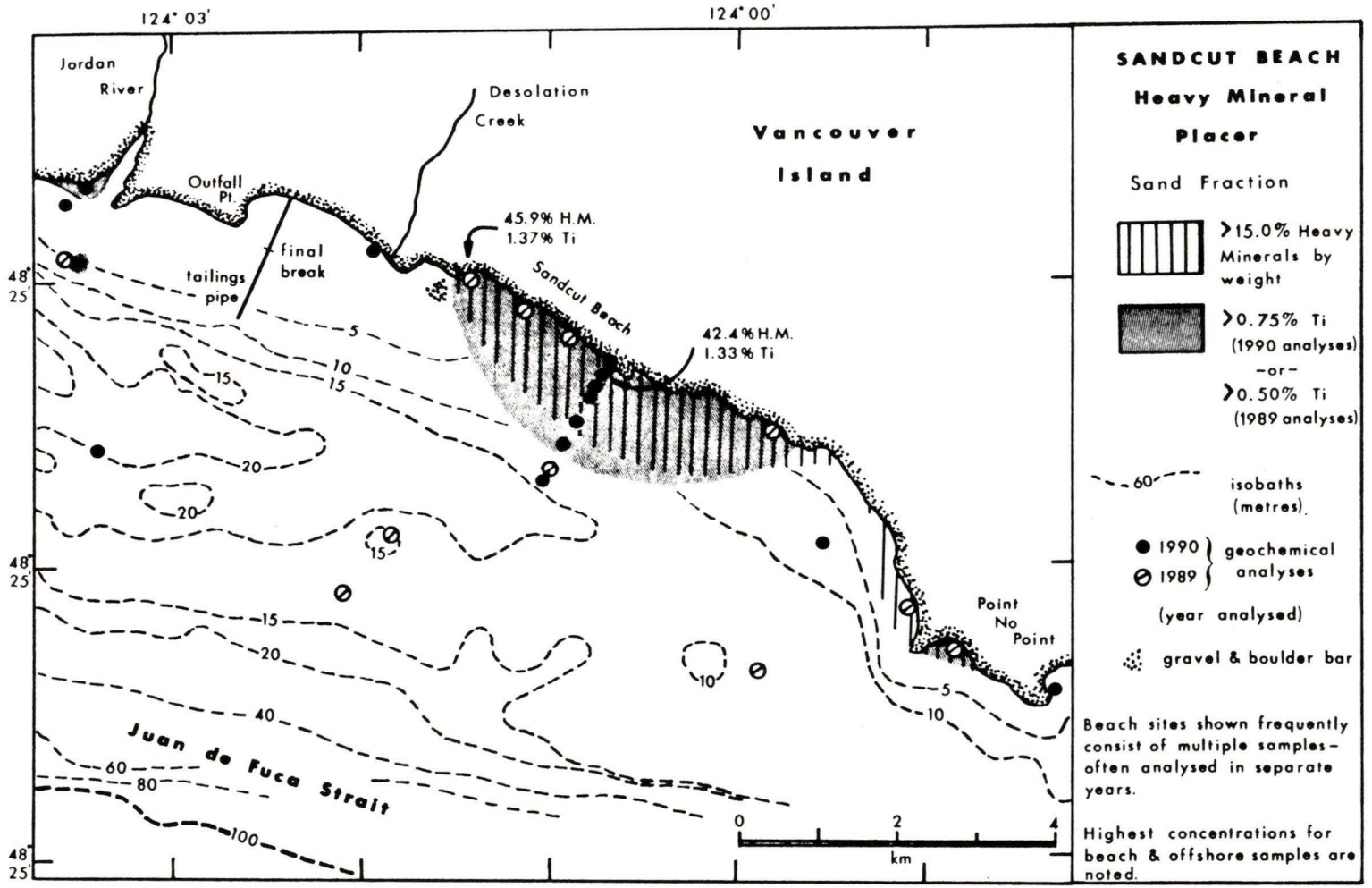

Figure 83. A heavy mineral placer is located along Sandcut Beach and extends offshore, on southwestern Vancouver Island. Ti% is contoured for 1989 (Group A) and 1990 (Group B).

of the four rivers, 25.0% (Figure 23). This sample site was subsequently found to be located below the old mine portal, accessed by a dumped pad, which was on the eastern cliff of the river. Mud concentrations from this site were the highest values obtained in this study for Fe, V and Ti.

Heavy gangue minerals available from the outfall would consist mainly of hornblende and may contain minor pyroxene (augite), epidote and accessory minerals such as magnetite and ilmenite (Clapp 1917, 1912 and Muller, 1977). However, magnetite content of sands offshore at Sandcut Beach are not at enriched levels (Figure 34). Higher concentrations of magnetite occur elsewhere in the Jordan River area (Figure 33). Slightly higher concentrations of magnetite are found for the whole Jordan River area most likely due to proximity to another source such as the inland Sooke gabbroic rocks, which contain significant amounts of magnetite (Clapp and Cooke, 1917).

Offshore sand near Sandcut Beach is moderately- to well-sorted with samples containing high heavy mineral percentages also having the lowest shape-fractionation indices, suggesting that little relative abrasion of minerals has occurred. Hydraulic-fractionation index values indicate that poor heavy mineral density sorting occurred for these samples. It appears then that samples at Sandcut Beach have experienced limited hydraulic reworking. For example, both indices for the Jordan River sample showed

that minerals there had already experienced more abrasion and sorting by density than was found at Sandcut Beach. The heavy mineral concentrations at Sandcut Beach, therefore, result from eastward transport from Outfall Bay and perhaps earlier from Outfall Point. Seasonal variations in wave approach may produce minor seasonal reversals in alongshore drift directions (Harper, 1980), but dispersal of sands westward may be slowed to some extent by the presence of a gravel and boulder intertidal bar southeast of Desolation Point (Figure 83).

While monitoring the mine effluent effects on the marine ecology, Ellis and Goddard (1975) considered that Cu levels in the sediments above 200 ppm would indicate an enriched population, and above 300 ppm would be considered the result of contamination. Three transect sand values of Cu and three beach values at Sandcut fall above 300 ppm (Figures 45 and 78).

The enrichment of Ti (Figures 52, 53, 73 and 80) is a result of concentrations of ilmenite or titanomagnetite found as accessory minerals in the tailings gangue. High concentrations of Ti in sands must be derived from grain size fractions larger or smaller than the size examined optically, which had limited opaques (Tables 17 and 18). Grains must therefore be larger than 0.125 mm or smaller than 0.090 mm, but above 0.063 mm, sieve size for mud. High mud values in Jordan River support the finer fraction as the

principal source. However, grain-size analysis of the sample with highest offshore Ti value has insignificant very fine grain-size material. The size range of effluent sands from the tailing pipes indicates minerals could be available in either size group. Other Ti-bearing minerals were rare in this study.

Strong positive correlations between Fe, Ti, Cr, Mn and V may be due to mineral composition. Magnetite, Fe_3O_4, may have atoms of Fe substituted by atoms of Mn, Ti, Cr or V (Berry and Mason, 1959). Elevated Ni values may be associated with pentlandite $(Fe, Ni)_9S_8$ which was reported at the Jordan River prospect by Stevenson (1951). Cobalt may substitute for Fe or Ni in the latter (Berry and Mason, 1959).

A possible alternative source of Ni and Mn should be noted from the mill. Grinding of ore was performed by a rod mill followed by ball mills. Ni was present in the liners used in the ball mills and manganese liners were used in the rod mills. Significant wear occurred in these units (Billingsley, 1965). Much of the discharge may have remained with the concentrate, but some could have been released in the tailings.

VIII. Conclusions

1. Nearshore sediments along northern Juan de Fuca Strait consist of relict glacial gravel and boulders shallower than 80 m depth, with medium to fine sand. Below 80 m a muddy sand veneer covers a sediment wedge which thickens into the strait.

2. The modern sediments derive from reworked glacial material, erosion of a coastal sandstone unit, and river influx reflecting the adjacent lithologies.

3. Sediments less than 2 mm in size are texturally and mineralogically immature.

4. For sediments less than 2 mm in size, sediment mean and modal grain sizes have little or no relation to depth. Sediment sorting is moderate to very poor and decreases with depth and a decrease in grain size.

5. Relatively minor amounts of sediment are being deposited along the northern strait at present, with maximum influx from Port San Juan and Orveas Bay.

6. Prevailing tidal currents, ocean swell and wind-induced waves are reworking the sparse sediments by winnowing and constructing bedforms such as dunes and oscillation ripples.

7. Background weight percent of heavy minerals along the northern strait is comparatively high; over twice the concentration of heavy minerals found in sands of Barkley Sound, and five times higher than sands of the continental shelf northwest of the mouth of the strait. Greatest source

of heavy minerals is most likely the basalts and gabbros of the Metchosin Igneous Complex.

8. Heavy mineralogy along the northern strait consists predominantly of amphiboles (hornblende), epidote and lithic fragments. Magnetite/ilmenite are the predominant opaque minerals.

9. Twenty-one elements show low background values in mud and sand samples from beaches and various depths offshore. Only Ti showed significantly high background values.

10. A heavy mineral and geochemical enrichment for Cu, Fe, Mn, V, Ti and Cr occurs between China Beach and Sheringham Point.

11. A placer of high heavy mineral concentrations (>15%) and high Ti values (>0.75%) is identified at Sandcut Beach and offshore as far as 800 m. Other elements are associated with this enrichment. Source of the placer is believed to be from former mine tailings dumped at, or below tide-water.

12. Formation of shallow marine or beach placers along northern Juan de Fuca Strait could be supported by the dynamic nature of the wind and wave regimes, and the heavy mineral character of the coastal lithologies. The textural and mineralogical immaturity of the sediments along the shallow coastal terraces suggest that, in general, insufficient hydraulic sorting can have occurred. However, individual pocket beaches may experience sufficient seasonal recycling to create localised heavy mineral placers.

REFERENCES

Alley, N.F. 1974. Terrain mapping and Quaternary geology, southern Vancouver Island, British Columbia. Geological Survey of Canada, Report of Activities, Part B, Paper 74-1, pp 209-211.

Alley, N.F. and Chatwin, S.C. 1979. Late Pleistocene history and geomorphology, southwestern Vancouver Island, B.C. Canadian Journal of Earth Science, 16:1645-1657.

Amos, C.L. and King, E.L. 1984. Bedforms of the Canadian eastern seaboard: a comparison with global occurrences. Marine Geology, 57:167-208.

Anderson, F.E. 1968. Seaward terminus of the Vashon Continental Glacier in the Strait of Juan de Fuca. Marine Geology, 6:419-438.

Annual Report 1964. Province of British Columbia, Energy Mines and Petroleum Resources, Report of Minister, pp 169, 294.

Armstrong, J.E. and Clague, J.J. 1977. Two major Wisconsin lithostratigraphic units in southwest British Columbia. Canadian Journal of Earth Science, 14:1471-1480.

Ashley, G.M. 1990. Classification of large-scale subaqueous bedforms: a new look at an old problem. Journal of Sedimentary Petrology, 60:160-172.

Bagnold, R.A. 1954. Experiments on a gravity free dispersion of large solid spheres in a Newtonian fluid under stress. Proceedings of the Royal Society (London) Series A, 225:49-63.

Barker, M.L. 1974. Water resources and related land uses Strait of Georgia-Puget Sound basin. Department of Environmental Geography, Paper 56, 55 p.

Barrie, J.V. 1978. Heavy Mineral Distribution in Bottom Sediments of the Bristol Channel. M.Sc. Thesis, University of Wales. Unpubl. manu.

Barrie, J.V. 1981. Hydrodynamic factors controlling the distribution of heavy minerals (Bristol Channel). Estuarine, Coastal and Shelf Science, 12:609-619.

Barrie, J.V. 1991. Contemporary and relict titaniferous sand facies on the western Canadian continental shelf.

Continental Shelf Research, 11:67-79.

Barrie, J.V. and Luternauer, J.L. 1986. Titaniferous placers on the central continental shelf off western Canada. Geological Survey of Canada, Current Research, Part B, Paper 86-1B, pp 849-852.

Barrie, J.V., Emory-Moore, M., Luternauer, J.L. and Bornhold, B.D. 1988. Origin of modern heavy mineral deposits, northern British Columbia continental shelf. Marine Geology, 84:43-51.

Barrie, J.V. and Bornhold, B.D. 1989. Surficial geology of Hecate Strait, British Columbia continental shelf. Canadian Journal of Earth Science, 26:1241-1254.

Bates, R.L. and Jackson, J.A. 1984. Dictionary of Geological Terms. Anchor Press/Doubleday, 571 p.

Berry, L.G. and Mason, B. 1959. Mineralogy: Concepts, Descriptions, Determinations. W.H. Freeman and Co., 630 p.

Billingsley, J.R. 1965. Underground mining and milling at Cowichan Copper Co. Ltd. Canadian Mining and Metallurgical Bulletin, 58:297-303.

Bornhold, B.D. and Giresse, P. 1985. Glauconitic sediments on the continental shelf off Vancouver Island, British Columbia, Canada. Journal of Sedimentary Petrology, 55:653-664.

Bornhold, B.D. and Yorath, C.J. 1984. Surficial geology of the continental shelf, northwestern Vancouver Island. Marine Geology, 57:89-112.

Boyle, R.W. 1979. The geochemistry of gold and its deposits (together with a chapter on geochemical prospecting for the element). Geological Survey of Canada, Bulletin 280, 584 p.

Bream, S.E. 1987. Depositional Environment, Provenance, and Tectonic Setting of the Upper Oligocene Sooke Formation, Vancouver Island, B.C. M.Sc. Thesis, University of Western Washington, 228 p. Unpubl. manu.

Callahan, J. 1987. A nontoxic heavy liquid and inexpensive filters for separation of mineral grains. Journal of Sedimentary Petrology, 57:765-766.

Canadian Hydrographic Service. 1989. Canadian tide and

current tables. Canada Department of Fisheries and Oceans, Ottawa., 5, 84 p., and 6, 73 p.

Canadian Hydrographic Service. 1973. Unpublished current data from stations L111 and L112, Juan de Fuca Strait. Canada Department of Fisheries and Oceans, Ottawa.

Carter, L. 1973. Surficial sediments of Barkley Sound and the adjacent continental shelf, west coast Vancouver Island. Canadian Journal of Earth Science, 10:441-459.

Carter, L. 1970. Surficial Sediments of Barkley Sound and Adjacent Continental Shelf, Vancouver Island, B.C. Phd. Thesis, University of British Columbia, 189 p. Unpubl. manu.

Carver, R.E. 1971. Heavy-Mineral Separation. *In* Procedures in Sedimentary Petrology; R.E. Carver, ed.; Wiley-Interscience, pp 427-452.

Clark, I. 1979. Practical Geostatistics. Applied Science Publishers Ltd., London, England, 129 p.

Clague, J.J. 1977. Quadra sand: a study of the late Pleistocene geology and geomorphology of coastal southwest British Columbia. Geological Survey of Canada, Paper 77-17, 24 p.

Clague, J.J. 1981. Late Quaternary geology and geochronology of British Columbia. Part 2: Summary and discussion of radiocarbon-dated Quaternary history. Geological Survey of Canada, Paper 80-35, 41 p.

Clague, J.J. 1989. Late Quaternary sea level change and crustal deformation, southwestern British Columbia. Geological Survey of Canada, Current Research, Part E, Paper 89-1E, pp 233-236.

Clague, J.J., Harper, J.R., Hebda, R.J. and Howes, D.R. 1982. Late Quaternary sea-levels and coastal movements, coast British Columbia. Canadian Journal of Earth Science, 19:597-618.

Clapp, C.H. 1912. Southern Vancouver Island. Geological Survey of Canada, Memmoir 13, 208 p.

Clapp, C.H. and Cooke, H.C. 1917. Sooke and Duncan Map-Areas, Vancouver Island. Geological Survey of Canada, Memoir 96, 445 p.

Clifton, H.E. and Luepke, G. 1987. Heavy-mineral placer

deposits of the continental margin of Alaska and the Pacific coast states. *In* Geology and Resource Potential of the Continental Margin of Western North America and Adjacent Ocean Basins - Beaufort Sea to Baja California; Circum-Pacific Council for Energy and Mineral Resources, Earth Science Series, 6:691-738.

Cockbain, A.E. 1963. Distribution of sediments on the continental shelf off the southern British Columbia coast. Manuscript Report No. 15, Institute of Oceanography, University of British Columbia, 11 p.

Costaschuk, S.M. 1980. Heavy mineral analysis of southern Beaufort Sea sediments. Geological Survey of Canada, Current Research, Part A, Paper 80-1A, pp 241-252.

Currie, R.G. and Bornhold, B.D. 1983. The magnetic susceptibility of continental-shelf sediments, west coast Vancouver Island, Canada. Marine Geology, 51:115-127.

Davis, J.C. 1973. Statistics and Data Analysis in Geology; John Wiley and Sons, New York, 550 p.

Einstein, H.A. 1950. The bed-load function for sediment transportation in open-channel flows. U.S. Department of Agriculture, Soil Conservation Service, Technical Bulletin 1026, 78 p.

Ellis, D.V. 1980. Environmental consequences of breaks and interrupted construction at marine outfalls in British Columbia. Coastal Discharges, Institution of Civil Engineers, London, U.K., 123-126 p.

Ellis, D.V. and Goddard, J.C. 1975. Tailing disposal to the sea at the Jordan River Mine: an environmental case-history from pre-discharge to rehabilitation. Unpubl. consultants' report.

Ellis, D.V. and Popham, J.D. 1983. Accidental formation and subsequent disappearance of a contaminated beach: a case history of environmental management. *In* Sandy Beaches as Ecosystems; McLachlan, A. and Erasmus, T., eds.; Proceedings of First International Symposium on Sandy Beaches, Port Elizabeth, S.A., 17-21 Jan. 1982. Junk Publishers, The Hague, 757 p.

Emery, K.O. and Noakes, L.C. 1968. Economic placer deposits of the continental shelf. United Nations Economic Commission for Asia and the Far East Technical Bulletin, 1:95-111.

Fairchild, L.H. and Cowan, D.S. 1982. Structure, petrology, and tectonic history of the Leech River complex northwest of Victoria, Vancouver Island. Canadian Journal of Earth Science, 19:1817-1835.

Fletcher, W.K. 1981. Analytical Methods in Geochemical Prospecting. Elsevier Scientific Publishing Co., Amsterdam, 255 p.

Flores, R.M. and Shideler, G.L. 1978. Factors controlling heavy-mineral variations on the south Texas outer continental shelf, Gulf of Mexico. Journal of Sedimentary Petrology, 48:269-280.

Folk, R.L. 1974. Petrology of Sedimentary Rocks. Hemphill Publishing Co., 182 p.

Galehouse, J.S. 1971*a*. Sedimentation Analysis. *In* Procedures in Sedimentary Petrology; R.E. Carver, ed.; Wiley-Interscience, New York, pp 69-94.

Galehouse, J.S. 1971*b*. Point Counting. *In* Procedures in Sedimentary Petrology; R.E. Carver, ed.; Wiley-Interscience, New York, pp 385-407.

Gibbs, R.J., Matthews, M.D., and Link, D.A. 1971. The relationship between sphere size and settling velocity. Journal of Sedimentary Petrology, 41:7-18.

Grundy, W.D. 1988. Using the USGS STATPAC Programs: A Hands-On Course. The Computer Oriented Geological Society, Denver, Colorado, course notes from 23 May 1988.

Harper, J.R. 1980. Seasonal changes in beach morphology along the British Columbia coast. *In* The Proceedings of Canadian Coastal Conference, 1980, National Research Council of Canada, Burlington, Ontario, pp 136-150.

Harper, J.R. 1981. A marine landform inventory of the West Coast Trail, Pacific Rim National Park. Woodward-Clyde Consultants, Victoria, B.C., Contract Report No. WR 21-80.

Hein, F.J. 1989. Evaluation of petrographic and mineralogic analysis for marine placer sediments. Geological Survey of Canada, Open File 2141, 71 p.

Herlinveaux, R.H. and Tully, J.P. 1961. Some oceanographic features of Juan de Fuca Strait. Journal of the Fisheries Research Board Canada, 18:1027-1071.

Herzer, R.H. and Bornhold, B.D. 1982. Glaciation and post-glacial history of the continental shelf off southwestern Vancouver Island, British Columbia. Marine Geology, 48:285-319.

Holland, S.S. 1950. Placer gold production of British Columbia. British Columbia Department of Mines Bulletin 28, 89 p.

Holland, S.S. 1976. Landforms of British Columbia: A Physiographic Outline. British Columbia Department of Mines and Petroleum Resources Bulletin 48, 138 p.

Holland, S.S. and Nasmith, H.W. 1958. Investigation of beach sands. British Columbia Department of Mines Special Report, 8 p.

Howes, D.E. and Nasmith, H.W. 1983. Quaternary geology of southern Vancouver Island, Fieldtrip No. 11. *In* Fieldtrip Guidebook, Geological Association of Canada-Mineralogical Association of Canada Joint Annual General Meeting, 1983, 25 p.

Hubert, J.F. 1971. Analysis of heavy-mineral assemblages. *In* Procedures in Sedimentary Petrology; R.E. Carver, ed.; Wiley-Interscience, New York, pp 453-478.

Hyndman, R.D., Yorath,C.J., Clowes, R.M. and Davis, E.E. 1990. The northern Cascadia subduction zone at Vancouver Island: seismic structure and tectonic history. Canadian Journal of Earth Science, 27:313-329.

Ingram, R.L. 1971. Sieve analysis. *In* Procedures in Sedimentary Petrology; R.E. Carver, ed.; Wiley-Interscience, New York, pp 49-67.

Kelley, J.C. 1971. Mathematical analysis of point count data. *In* Procedures in Sedimentary Petrology; R.E. Carver, ed.; Wiley-Interscience, New York, pp 409-425.

Komar, P.D. and Miller, M.C. 1974. On the comparison between the threshold of sediment motion under waves and unidirectional currents with a discussion of the practical evaluation of the threshold. Journal of Sedimentary Petrology, 45:362-367.

Komar, P.D., Neudeck, R.H. and Kulm, L.D. 1972. Observations and significance of deep-water oscillatory ripple marks on the Oregon continental shelf. *In* Shelf Sediment Transport, Process and Pattern; D.J.P. Swift, D.B. Duane and O.H. Pilkey, eds.; Dowden, Huthinson and

Ross, Stroudsburg, Pa., pp 601-619.

Komar, P.D. and Wang, C. 1984. Processes of selective grain transport and the formation of placers on beaches. Journal of Geology, 92:637-655.

Lasmanis, R. 1988. Washington offshore mineral resources. Washington Geological Newsletter, 16:5-10.

Linden, R.H. and Schurer, P.J. 1988. Sediment characteristics and sea-level history of Royal Roads Anchorage, Victoria, British Columbia. Canadian Journal of Earth Science, 25:1800-1810.

Luepke, G. and Escowitz, E.C. 1989. Grain-size, heavy-mineral, and geochemical analyses of sediments from the Chukchi Sea, Alaska: U.S. Geological Survey Bulletin 1896, 12 p.

Marine Environmental Data Service. Department of Fisheries and Oceans, unpubl. manu. Waves recorded off Tofino, B.C., Stn. 103, June 26, 1970 to Aug. 21, 1976. File 103-3.

Massey, N.W.D. 1986. Metchosin Igneous Complex, southern Vancouver Island: Ophiolite stratigraphy developed in an emergent island setting. Geology, 14:602-605.

Mayers, I.R. and Bennett, L.C. 1973. Geology of the Strait of Juan de Fuca. Marine Geology, 15:89-117.

McLaren, P. 1983. Coastal sediments of the Strait of Juan de Fuca: implications for oil spills. Geological Survey of Canada, Current Research, Part A, Paper 83-1A, pp 241-244.

McLaren, P., Harper, J. and Hale, P. 1983. Coastal environments of southern Vancouver Island, Fieldtrip No. 7. *In* Fieldtrip Guidebook, Geological Association of Canada-Mineralogical Association of Canada Joint Annual General Meeting, 1983, 76 p.

Macleod, N.S., Tiffin, D.L., Snavely, P.D. and Currie, R.G. 1977. Geologic interpretation of magnetic and gravity anomalies in the Strait of Juan de Fuca, U.S.-Canada. Canadian Journal of Earth Science, 14:223-238.

MINFILE, 1988. Sunro Mine, Sunloch-Gabbro, Gabbro, MINFILE no. 092C 073; Ministry of Energy, Mines and Petroleum Resources, B.C., pp 220-221.

Muller, J.E. 1976. Cape Flattery Map-Area (92C), B.C. Geological Survey of Canada, Paper 76-1A, pp 107-112.

Muller, J.E. 1977. Metchosin Volcanics and Sooke Intrusions of southern Vancouver Island. Geological Survey of Canada, Report of Activities, Part A, Paper 77-1A, pp 287-294.

Muller, J.E. 1982. Geology of Nitinat Lake Map Area. Geological Survey of Canada, Open File 821.

Muller, J.E. 1983. Geology - Victoria Map Area, Vancouver Island and Gulf Islands. Geological Survey of Canada, Map 1553A.

Muller, J.E., Snavely, P.D. and Tabor, R.W. 1983. The Tertiary Olympic Terrane, southwest Vancouver Island and northwest Washington, Fieldtrip No. 12. *In* Fieldtrip Guidebook, Geological Association of Canada-Mineralogical Association of Canada Joint Annual General Meeting, 1983, 59 p.

Nicol, A.W. 1975. X-ray diffraction. *In* Physiochemical Methods of Mineral Analysis; A.W. Nicol, ed.; Plenum Press, New York, pp 249-320.

Offshore Survey & Positioning Services Ltd. (O.S.P.S.) 1985. Nearshore sedimentation and recent tectonics, Virago Sound, Northern Graham Island, report prepared for Dr. B.D. Bornhold, Geological Survey of Canada, Energy, Mines & Resources Canada.

Peterson, C.D., Gleeson, G.W. and Wetzel, N. 1987. Stratigraphic development, mineral sources and preservation of marine placers from Pleistocene terraces in southern Oregon, U.S.A. Sedimentary Geology, 53:203-229.

Peterson, C.D., Komar, P.D. and Scheidegger, K.F. 1986. Distribution, geometry, and origin of heavy mineral placer deposits on Oregon beaches. Journal of Sedimentary Petrology, 56:67-77.

Reimchen Urlich Geological Engineering. 1985. Report on compound water cyclone testing program for micron sized mineral recovery, Sombrio Point placer property. Unpubl. consultants' report.

Reports of the Minister of Mines, British Columbia: 1919, pp 161-162 ; 1968, pp 106.

Riddihough, R.P. 1982. Contemporary movements and tectonics on Canada's west coast: a discussion. Tectonophysics, 86:319-341.

Rubey, W.W. 1933. The size distribution of heavy minerals within a water-laid sandstone. Journal of Sedimentary Petrology, 3:3-29.

Rusmore, M.E. and Cowan, D.S. 1985. Jurassic-Cretaceous rock units along the southern edge of the Wrangellia terrane on Vancouver Island. Canadian Journal of Earth Science, 22:1223-1232.

Samson, J. 1984. An overview of coastal and marine gold placer occurrences in Nova Scotia and British Columbia. Canada Oil and Gas Lands Administration, Ocean Mining Division, Report 1984-3, 165 p.

Sarracino, L. and Forbes, T. 1981. Sedimentology laboratory manual. Unpubl. manu., Pacific Geoscience Centre, Geological Survey of Canada, 58 p.

Sheehan, L. 1989. Analysis of laboratory methods used for heavy mineral research. Co-op Work Term Report, Department of Geography, University of Victoria, 36 p.

Sinclair, A.J. 1981. Applications of Probability Graphs in Mineral Exploration. Special Volume No.4, The Association of Exploration Geochemists, 95 p.

Slingerland, R. 1984. Role of hydraulic sorting in the origin of fluvial placers. Jounal of Sedimentary Petrology, 54:137-150.

Smith, R.R. 1988. Procedure used for separation of heavy mineral grains from sandstone and siltstone samples from the Queen Charlotte Islands, B.C., using sodium polytungstate. Unpubl. report, Pacific Geoscience Centre, Geological Survey of Canada.

Stevenson, J.S. 1951. Sunloch and Gabbro. British Columbia Ministry of Mines Annual Report, 1950, pp A180-A194.

Swift, D.J.P. 1971. Grain Mounts. *In* Procedures in Sedimentary Petrology; R.E. Carver, ed.; Wiley-Interscience, New York, pp 499-510.

Till, R. 1974. Statistical Methods for the Earth Scientist-An Introduction. John Wiley & Sons, New York, 154 p.

Thomson, D.B., Wells, D.E. and Falkenberg, W.H. 1981. An introduction to hydrographic surveying, Lecture Notes No. 53, University of New Brunswick, Fredericton, New Brunswick, 242 p.

Thomson, R.E. 1981. Oceanography of the British Columbia Coast. Canada Special Publications of Fisheries and Aquatic Science 56, 291 p.

Urlich, C.M., Reimchen, T.H.F. and Bakker, E. 1984. Report on geological evaluation of Sombrio Point placer property. Reimchen Urlich Geological Engineering, British Columbia Geological Branch Assessment Report, 46 p.

Van Andel, T.H., 1964. Recent marine sediments of Gulf of California. *In* Marine Geology of the Gulf of California; T.H. van Andel and G.G. Shor, Jr., eds.; American Association of Petroleum Geologists Memoir 3, 408 p.

Van Andel, T.H. and Poole, D.M. 1960. Sources of recent sediments in the northern Gulf of Mexico, Journal of Sedimentary Petrology, 30:91-122.

Yorath, C.J., Bornhold, B.D. and Thomson, R.E. 1979. Oscillation ripples on the northeast Pacific continental shelf. Marine Geology, 31:45-58.

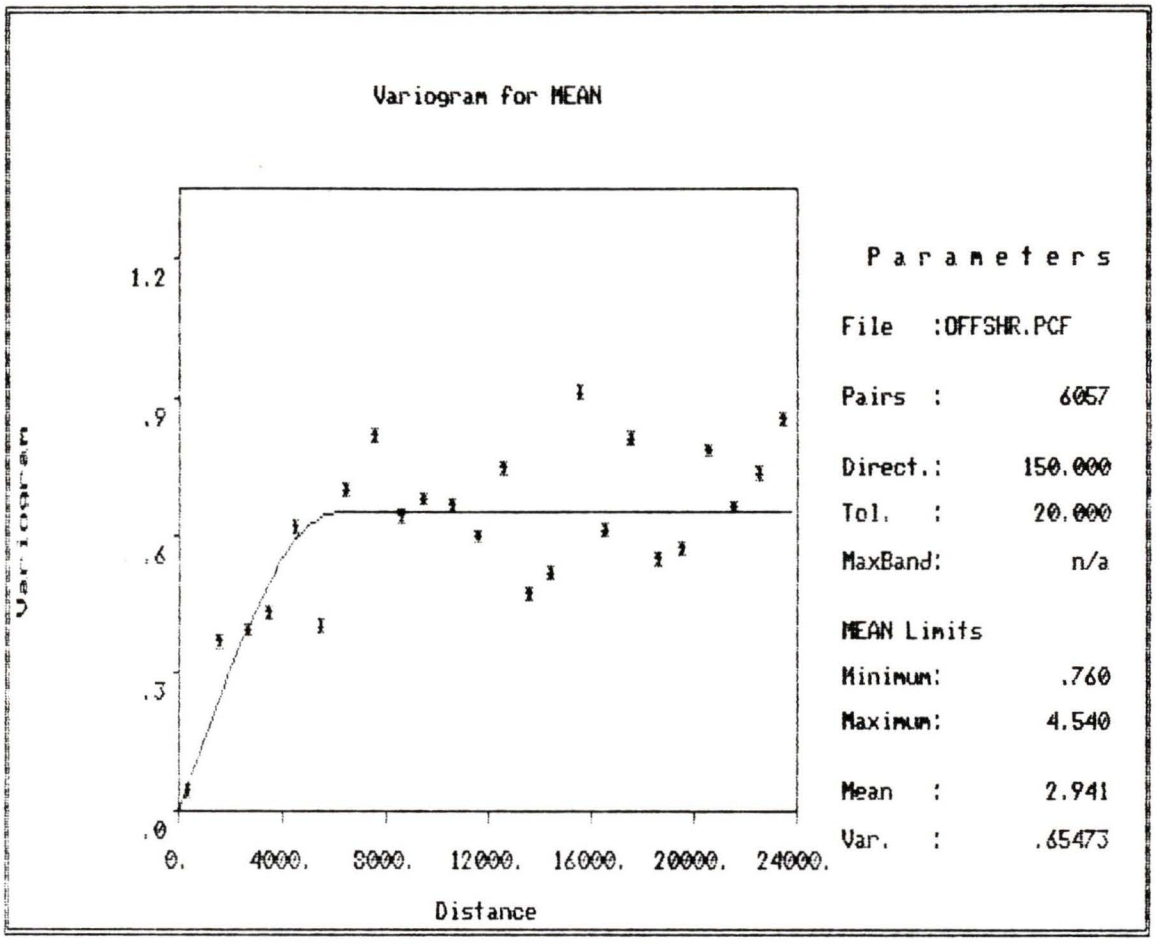

Variogram for grain-size means, oriented parallel to coast at 120°. Distance is shown in lags of 1000 m.

APPENDIX A

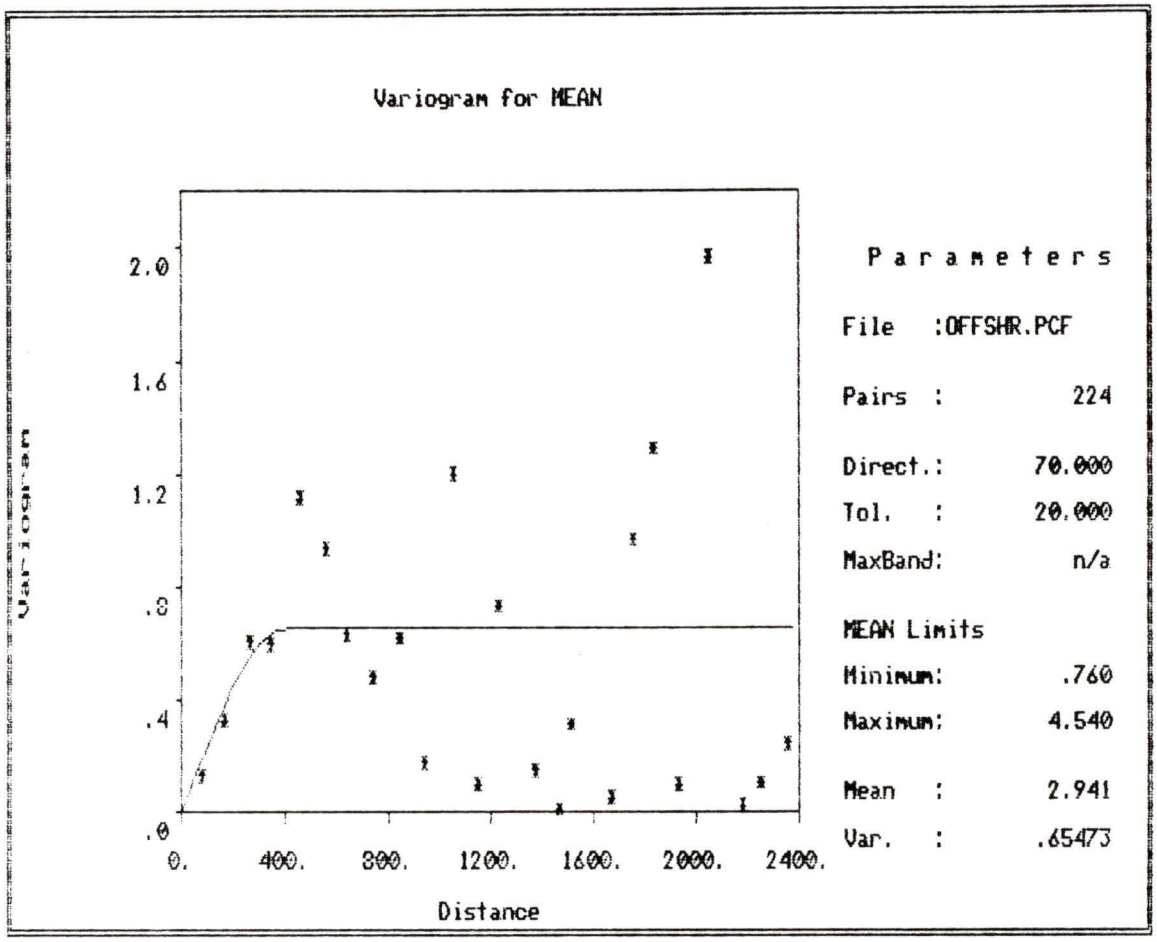

Variogram for grain-size means, oriented normal to coast at 200°. Distance is shown in lags of 100 m.

APPENDIX A

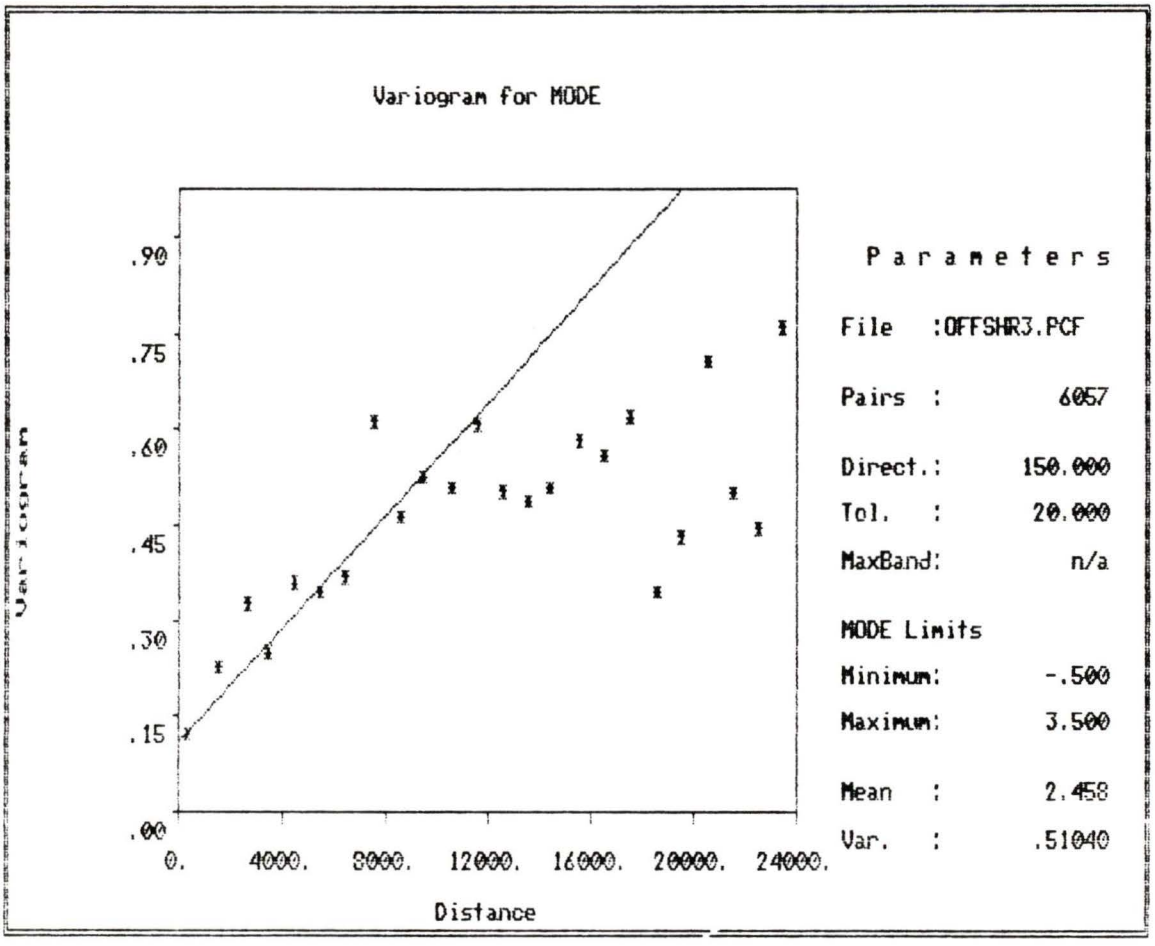

Variogram for grain-size modes, oriented parallel to coast at 120°. Distance is shown in lags of 1000 m.

APPENDIX A

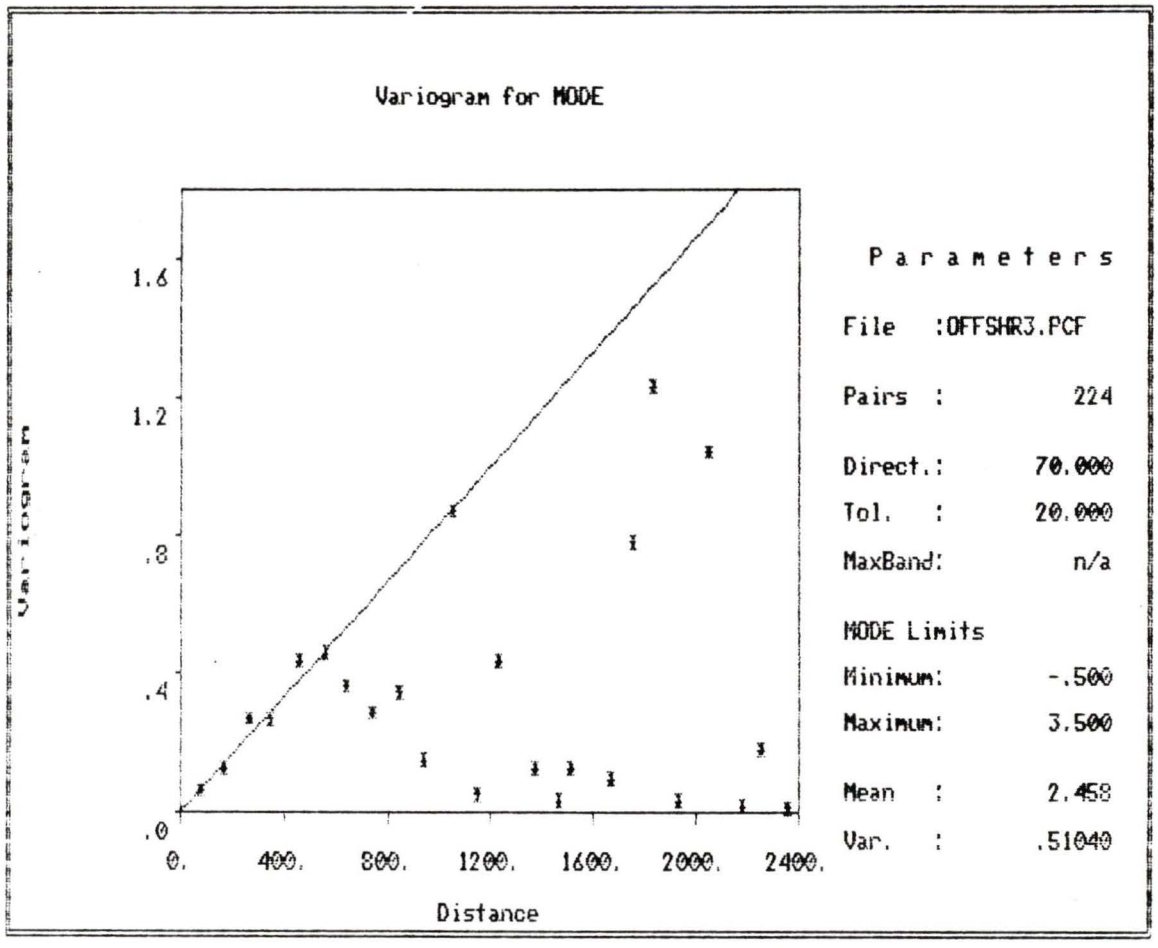

Variogram for grain-size modes, oriented normal to coast at 200°. Distance is shown in lags of 100 m.

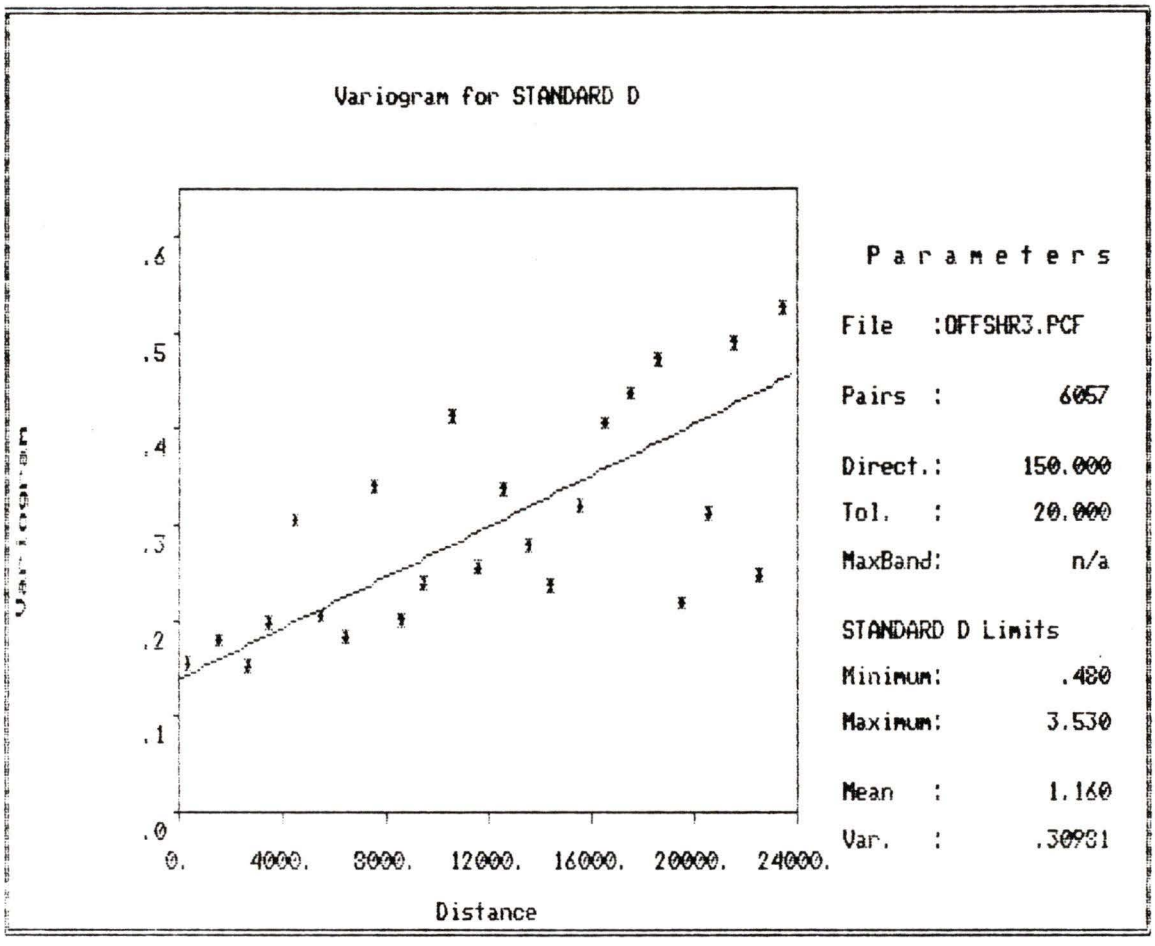

Variogram for grain-size sorting values (standard deviation), oriented parallel to coast at 120°. Distance is shown in lags of 1000 m.

APPENDIX A

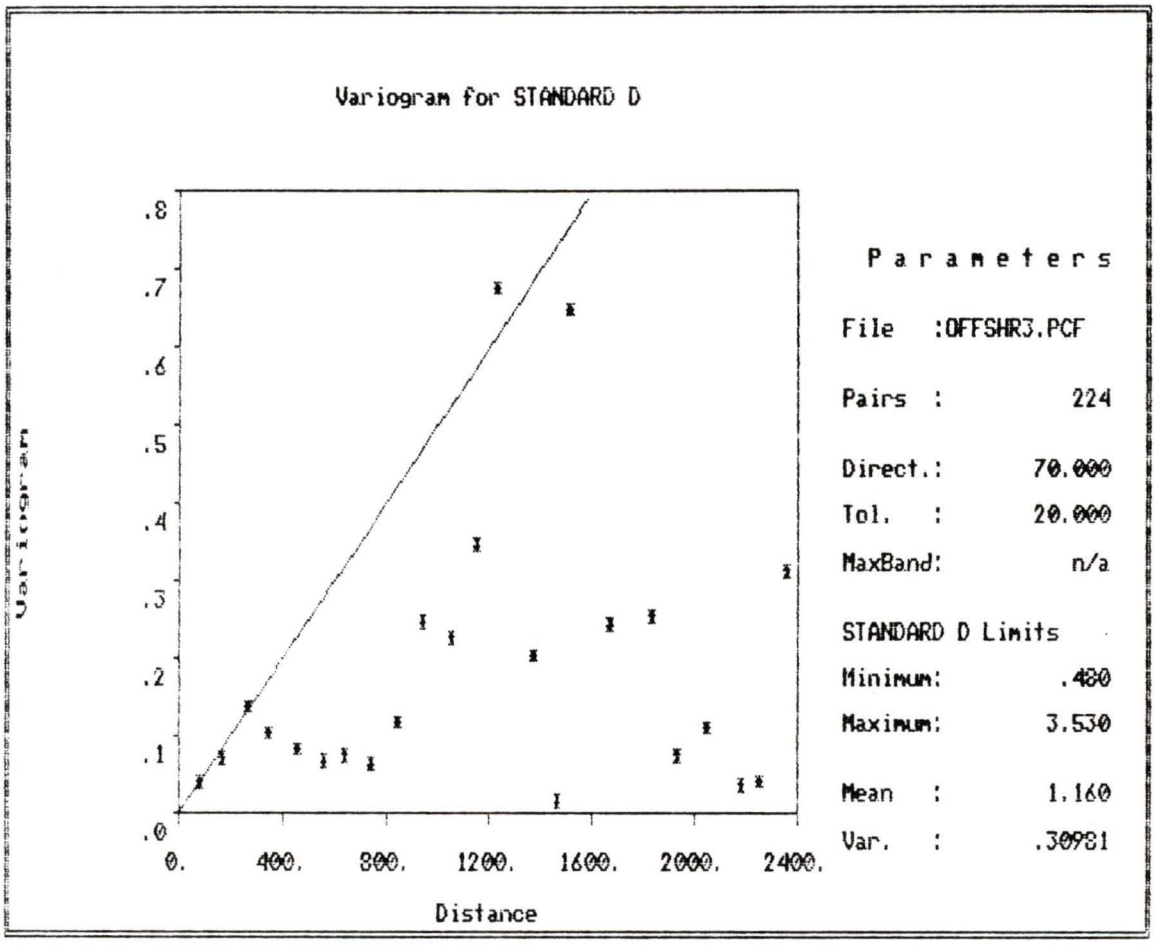

Variogram for grain-size sorting values (standard deviation), oriented normal to coast at 200°. Distance is shown in lags of 100 m.

APPENDIX B

HEAVY MINERAL DESCRIPTIONS

Transparent Minerals

Hornblende: blue-green
Crystals are angular to subrounded, elongated, with vitreous cleavage surfaces. Occaisionally other minerals are attached, with the most frequent being blue-black metallic minerals.

olive-green
yellow brown
green
green-brown
pale-green

All pleochroic to blue-green.

Hornblende: brown-green
Crystals are angular to sub-rounded, elongated, with dull to vitreous cleavage surfaces.

olive-green
yellow-brown
brown-green

Pyroxene
Crystals of augite are generally equant, with hypersthene-enstatite elongate. Surfaces are vitreous, occaisionally rough and irregular due to cleavage. Rare bronzite is observed.

pale brown
pale olive-brown
grey-green

Epidote
Crystals occur as equant transparent euhedra to rounded transluscent mottled grains. They occur in medium to small sizes, are vitreous or may have dull polished surfaces. Occaisionally dark metallic minerals are attached.

bright yellow-green
dull yellow-green
mottled colors-dark green, green, yellow, white

Clinozoisite & Zoisite
Crystals are angular to subrounded, often elongated, with vitreous surfaces. Occaisional crystal clusters occur.

clear	pale green
pale pink	red
yellow	

Staurolite
Crystals were observed large to small in size, usually slightly elongated. They commonly are poikilitic, have conchoidal fractures, appear vitreous and have frequent inclusions.

pale to deep straw yellow

Garnet
Crystals are large to medium in size, very angular to rounded, with vitreous lustre and conchoidal fractures. They are commonly clear with occaisional inclusions of other minerals, as well as frequent inclusions of disseminated pyrite.

clear	very pale pink
strong coral-pink	orange coral
yellow (rare)	green (rare)

Others
This grouping includes all minor transparent minerals; rutile, zircon, tourmaline, andalusite, apatite, sphene, chlorite, other amphiboles and unknowns.

Opaque Minerals

Magnetite-Ilmenite
These crystals are uniformly medium in size, equant with a metallic lustre. Frequent euhedral crystals were observed. Occaisionally hematite, quartz or another mineral was attached.

blue-black

Pyrite
Pyrite is only observed, in significant volume, in one grain mount (SR89-D1) where it most commonly occurs as framboids

with an irregular or rough metallic lustre. Crystals are large to small in size, almost exclusively occurring with quartz attached. Occaisional euhedral crystals were also observed. (Included under Lithic Fragments).

yellow-silver

Lithic Fragments
These appear as rounded grains with dull surfaces and irregular edges, grading from transluscent to opaque. They have a mottled appearance, with green, grey and black being the main colors. This grouping may include altered minerals. For the purposes of percentage groupings this assemblage also encompassed miscellaneous minor opaques (hematite, leucoxene, pyrite) and unidentified opaques.

APPENDIX C

GEOCHEMISTRY DETECTION LIMITS

	1989		1990	
	det. limit	Analytic Technique	det. limit	Analytic Technique
Au ppb	5 ppb	Fire-Assay-AA	2 ppb	Fire-Assay-ICP-AFS
Pd ppb	2 ppb	Fire-Assay	2 ppb	Fire-Assay-ICP-AFS
Pt ppb	15 ppb	Fire-Assay	5 ppb	Fire-Assay-ICP-AFS
Co ppm	NR		1 ppm	ICP-AES
Cu ppm	1 ppm	ICP	1 ppm	ICP-AES
Fe %	0.05 %	ICP	0.01 %	ICP-AES
Mn ppm	1 ppm	ICP	5 ppm	ICP-AES
Mo ppm	1 ppm	ICP	1 ppm	ICP-AES
Ni ppm	NR		1 ppm	ICP-AES
Pb ppm	5 ppm	ICP	5 ppm	ICP-AES
V ppm	1 ppm	ICP	1 ppm	ICP-AES
Zn ppm	1 ppm	ICP	2 ppm	ICP-AES
Ag ppm	0.5 ppm	ICP	0.2 ppm	HNO_3-aqua regia digest, AAS-BKGD CORR
Cd ppm	1 ppm	ICP	0.1 ppm	HNO_3-aqua regia digest, AAS-BKGD CORR
Se ppm	5 ppm	ICP	0.2 ppm	HCl-$KClO_3$ digest, AAS-BKGD CORR
Sn ppm	10 ppm	ICP	2 ppm	NH_4I sublimation, AAS
Hg ppb	5 ppb	HNO_3-HCl, cold vapour AA	10 ppb	HNO_3-HCl digest, AAS-flameless
Sb ppm	5 ppm	ICP	0.2 ppm	HCl-$KClO_3$ digest, AAS-BKGD CORR
Bi ppm	2 ppm	ICP	0.1 ppm	HCl-$KClO_3$ digest, AAS-BKGD CORR
Ti %/ppm	0.01 %	ICP	100 ppm	XRF
Zr ppm	1 ppm	ICP	5 ppm	XRF
Cr ppm	1 ppm	ICP	2 ppm	$HClO_4$-HNO_3-HF digest, AAS

1989: Unless noted otherwise above, samples had "multi-acid digest".

1990: Unless noted otherwise above, samples had nitric-aqua regia digestion, plus special organic extraction.

Sample	Latitude		Longitude		depth	%H.M.	SedX	sorting
JF17-100	48	21.97	123	45.63	5	10.76	2.07	1.31
JF17-200	48	21.94	123	45.67	6	*	2.34	0.88
JF17-300	48	21.91	123	45.72	8	*	3.71	0.81
JF17-400	48	21.89	123	45.76	10	*	3.75	1.22
JF17-500	48	21.86	123	45.81	12	*	3.61	1.17
JF17-600	48	21.83	123	45.85	14	*	3.42	1.13
JF17-700	48	21.80	123	45.90	14	1.15	3.62	1.12
JF17-800	48	21.77	123	45.95	14	*	3.95	1.14
JF17-900	48	21.74	123	45.99	14	*	3.63	1.07
JF17-1000	48	21.71	123	46.04	14	*	3.63	1.10
JF17-1100	48	21.69	123	46.08	14	*	3.64	1.07
JF17-1200	48	21.66	123	46.13	14	*	3.60	1.07
JF17-1300	48	21.63	123	46.18	15	*	3.57	1.05
JF17-1400	48	21.60	123	46.22	16	*	3.72	1.07
JF17-1500	48	21.57	123	46.27	18	1.89	3.67	1.07
JF21-100	48	21.57	123	48.09	5	*	3.49	1.98
JF21-200	48	21.51	123	48.08	12	2.65	3.52	1.11
JF21-300	48	21.46	123	48.06	19	*	3.16	1.32
JF23-100	48	21.87	123	49.84	7	17.82	2.65	0.50
JF23-200	48	21.84	123	49.89	15	*	2.71	0.78
JF23-300	48	21.80	123	49.93	23	3.04	3.11	0.96
JF32-150	48	23.37	123	56.66	5	10.41	2.84	0.48
JF32-200	48	23.36	123	56.68	5	*	2.99	0.60
JF32-300	48	23.34	123	56.73	6	*	3.00	0.55
JF32-400	48	23.33	123	56.78	6	*	3.08	0.63
JF32-500	48	23.31	123	56.83	6	*	3.16	0.61
JF32-600	48	23.29	123	56.88	6	*	3.12	0.61
JF32-700	48	23.27	123	56.94	6	4.25	3.25	0.63
JF32-800	48	23.25	123	56.99	6	*	3.21	0.61
JF32-900	48	23.23	123	57.04	6	*	3.01	0.67
JF32-1000	48	23.22	123	57.09	7	*	3.01	0.69
JF32-1100	48	23.20	123	57.14	7	*	2.95	0.59
JF32-1200	48	23.18	123	57.19	9	*	2.89	0.67
JF32-1300	48	23.16	123	57.24	10	*	2.68	0.51
JF32-1400	48	23.14	123	57.29	13	*	2.66	0.56
JF32-1500	48	23.12	123	57.34	17	12.86	2.68	0.58
JF38-100	48	24.71	124	00.68	5	28.18	2.26	0.50
JF38-200	48	24.66	124	00.72	5	42.35	3.03	0.54
JF38-300	48	24.62	124	00.75	5	35.54	3.20	0.57
JF38-400	48	24.58	124	00.78	8	27.93	3.25	0.63
JF38-500	48	24.54	124	00.82	8	15.39	3.66	0.79
JF38-600	48	24.49	124	00.85	9	13.54	3.19	0.81
JF38-700	48	24.45	124	00.88	11	7.48	3.21	0.72
JF38-800	48	24.41	124	00.92	14	9.89	2.95	0.80
JF38-900	48	24.37	124	00.95	17	8.69	2.60	0.63
JF38-1000	48	24.32	124	00.98	18	7.60	2.26	0.99
JF38-1100	48	24.28	124	01.02	20	7.78	2.33	1.13
JF44-150	48	25.93	124	05.48	5	11.51	2.39	0.69
JF44-200	48	25.91	124	05.50	5	13.77	2.78	0.63
JF44-300	48	25.88	124	05.54	5	8.52	3.22	0.79
JF44-400	48	25.84	124	05.59	5	4.80	3.96	1.05

Sample	Latitude		Longitude		depth	%H.M.	SedX	sorting
JF44-500	48	25.81	124	05.63	6	3.04	4.02	1.03
JF44-600	48	25.77	124	05.67	7	11.68	2.51	1.22
JF44-700	48	25.74	124	05.71	9	5.47	1.73	1.74
JF44-800	48	25.70	124	05.75	10	5.64	1.12	1.10
JF44-900	48	25.67	124	05.79	10	8.17	1.16	1.04
JF44-1000	48	25.63	124	05.83	10	6.91	1.15	1.13
JF44-1100	48	25.60	124	05.87	10	7.94	1.62	0.54
JF44-1200	48	25.56	124	05.92	10	8.16	2.09	1.35
JF44-1300	48	25.53	124	05.96	12	9.06	2.05	0.97
JF44-1400	48	25.49	124	06.00	12	5.57	2.31	1.08
JF44-1500	48	25.46	124	06.04	14	6.58	2.54	0.92
JR81-66	48	25.38	124	04.89	20	5.35	2.64	1.24
JR81-67	48	24.95	124	05.21	31	2.98	3.05	2.28
JR81-68	48	24.22	124	05.50	27	4.69	2.81	1.50
JR81-69	48	24.12	124	05.78	60	4.11	3.21	1.27
JR81-76	48	23.52	124	03.88	65	*	2.70	2.23
JR81-77	48	24.03	124	03.88	20	*	2.37	1.04
JR81-78	48	24.63	124	03.73	22	*	*	*
JR81-80	48	25.03	124	03.50	8	6.46	2.26	0.57
JR81-81	48	25.03	124	03.50	8	8.71	2.41	0.61
JR81-82	48	25.19	124	03.50	6	7.29	2.46	0.68
JR81-83	48	25.22	124	03.50	4	6.80	1.78	0.62
JR81-84	48	25.22	124	03.50	2	*	1.81	1.37
JR81-85	48	25.42	124	04.90	12	7.77	2.42	0.86
JR81-86	48	25.52	124	04.90	11	1.92	2.30	0.51
JR81-87	48	25.57	124	04.82	10	7.86	2.06	0.64
JR81-88	48	25.58	124	04.82	7	11.55	2.39	0.87
JR81-93	48	24.08	124	01.80	21	8.02	2.49	0.98
JR81-94	48	23.88	124	02.04	35	10.15	1.72	1.17
JR81-102	48	23.63	123	59.90	11	7.47	1.76	1.07
JR81-103	48	24.08	123	59.58	11	7.80	2.47	0.77
JF-B15-4	48	23.74	123	58.86	5	19.36	2.85	0.64
TUL88A-01	48	29.76	124	23.49	87	1.23	4.24	2.02
TUL88A-02	48	29.83	124	20.56	42	*	2.28	1.01
TUL88A-03	48	29.10	124	19.86	33	*	*	*
TUL88A-04	48	28.36	124	19.37	41	2.82	2.79	1.48
TUL88A-05	48	27.93	124	16.82	23	3.97	1.55	1.70
TUL88A-06	48	27.48	124	14.78	15	3.71	1.46	0.52
TUL88A-07	48	26.53	124	13.83	20	*	*	*
TUL88A-08	48	26.48	124	14.29	43	8.98	2.71	1.57
TUL88A-09	48	26.92	124	14.60	22	3.96	1.61	0.59
TUL88A-10	48	26.98	124	13.87	17	2.96	2.43	3.05
TUL88A-11	48	27.12	124	13.77	18	5.95	1.98	1.12
TUL88A-12	48	25.34	124	09.38	66	1.69	4.54	2.20
TUL88A-13	48	22.73	123	58.49	65	7.39	3.69	2.35
JR89-D1	48	25.02	124	03.44	9	9.67	2.29	1.25
MC89-D1	48	22.68	123	51.90	6	16.08	2.43	1.69
LC89-D1	48	28.70	124	16.41	9	14.40	0.76	0.56
SR89-D1	48	29.92	124	18.20	11	7.51	3.32	3.53
PAR89A-15	48	31.08	124	29.32	97	1.25	4.41	2.62
PAR89A-18	48	31.69	124	28.98	49	2.89	3.35	0.86

Sample	Latitude		Longitude		depth	%H.M.	SedX	sorting
PAR89A-19	48	31.93	124	28.61	32	2.79	3.33	1.54
PAR89A-20	48	30.78	124	26.56	78	2.73	3.50	1.07
PAR89A-21	48	31.02	124	26.42	41	1.27	2.68	1.32
PAR89A-22	48	31.17	124	26.43	26	1.09	3.18	1.33
PAR89A-24	48	30.29	124	24.76	79	*	4.08	0.88
PAR89A-27	48	30.76	124	24.36	27	3.08	0.98	1.36
PAR89A-29	48	30.15	124	22.09	52	*	3.11	1.37
PAR89A-30	48	30.22	124	21.94	35	*	2.07	0.99
PAR89A-32	48	28.63	124	21.42	87	0.77	4.20	0.82
PAR89A-33	48	28.90	124	21.13	66	*	3.92	0.81
PAR89A-34	48	29.51	124	20.76	47	*	2.23	1.38
PAR89A-35	48	30.16	124	20.53	34	6.59	1.63	1.46
PAR89A-37	48	29.74	124	18.83	17	5.00	2.54	2.12
PAR89A-38	48	29.12	124	20.06	35	4.74	3.33	3.23
PAR89A-39	48	29.33	124	18.70	21	*	*	*
PAR89A-40	48	28.54	124	18.85	25	2.56	3.13	1.80
PAR89A-41	48	28.71	124	17.67	26	2.68	3.72	1.70
PAR89A-42	48	28.81	124	17.38	20	3.79	2.01	1.55
PAR89A-45	48	27.17	124	17.98	78	*	3.44	2.47
PAR89A-47	48	27.43	124	17.24	47	6.01	2.80	1.63
PAR89A-48	48	28.26	124	17.70	24	4.33	3.76	1.78
PAR89A-51	48	26.47	124	15.91	36	9.44	2.50	1.73
PAR89A-52	48	27.54	124	15.83	15	5.42	2.01	1.28
PAR89A-54	48	26.01	124	13.85	84	*	4.25	0.83
PAR89A-56	48	26.39	124	13.50	28	2.98	3.42	1.25
PAR89A-57	48	26.55	124	13.38	12	2.01	3.64	1.35
PAR89A-58	48	26.94	124	12.97	19	7.57	1.69	1.14
PAR89A-59	48	25.80	124	11.63	77	1.21	4.15	0.86
PAR89A-60	48	25.99	124	11.47	14	3.19	3.30	1.60
PAR89A-61	48	25.71	124	11.16	71	1.90	4.24	0.90
PAR89A-62	48	25.51	124	09.63	71	*	4.29	0.90
PAR89A-63	48	25.67	124	09.69	31	*	3.85	1.04
PAR89A-64	48	25.70	124	09.82	25	2.09	3.69	1.10
PAR89A-65	48	25.72	124	09.85	17	1.81	3.64	1.26
PAR89A-66	48	24.45	124	08.66	101	1.41	3.80	1.04
PAR89A-67	48	24.82	124	08.45	74	4.03	3.68	1.24
PAR89A-68	48	25.22	124	08.38	60	2.41	3.67	0.87
PAR89A-69	48	25.61	124	08.47	36	2.27	3.54	1.16
PAR89A-70	48	25.66	124	08.57	25	3.63	3.21	1.35
PAR89A-71	48	24.51	124	07.14	50	5.12	2.51	1.01
PAR89A-73	48	24.36	124	03.31	20	3.26	1.95	1.30
PAR89A-74	48	23.04	123	59.68	54	2.34	3.31	1.07
PAR89A-75	48	23.18	123	59.67	12	4.96	2.25	1.27
PAR89A-76	48	22.16	123	53.95	61	*	3.68	1.45
PAR89A-77	48	22.21	123	53.95	48	1.80	3.94	1.05
PAR89A-78	48	22.50	123	54.16	34	3.37	3.83	1.00
PAR89A-79	48	22.09	123	52.83	68	2.80	4.37	2.31
PAR89A-80	48	22.18	123	52.77	48	3.26	3.77	1.20
PAR89A-81	48	22.22	123	52.70	27	10.89	2.48	1.75
PAR89A-83	48	21.08	123	47.20	67	5.91	4.36	2.59
PAR89A-85	48	21.42	123	46.53	33	*	4.07	0.93

Sample	Sed	Mode	Yr.	ppb:Au	Pd	Pt	ppm:Co	Cu	Fe%	Mn	Mo	Ni
JF17-100	1.25		*	*	*	*	*	*	*	*	*	*
JF17-200	2.25		*	*	*	*	*	*	*	*	*	*
JF17-300	3.25		*	*	*	*	*	*	*	*	*	*
JF17-400	2.50		*	*	*	*	*	*	*	*	*	*
JF17-500	2.50		*	*	*	*	*	*	*	*	*	*
JF17-600	2.50		*	*	*	*	*	*	*	*	*	*
JF17-700	2.50		*	*	*	*	*	*	*	*	*	*
JF17-800	2.50		*	*	*	*	*	*	*	*	*	*
JF17-900	2.75		*	*	*	*	*	*	*	*	*	*
JF17-1000	2.75		*	*	*	*	*	*	*	*	*	*
JF17-1100	2.75		*	*	*	*	*	*	*	*	*	*
JF17-1200	2.75		*	*	*	*	*	*	*	*	*	*
JF17-1300	2.75		*	*	*	*	*	*	*	*	*	*
JF17-1400	2.75		89	*	*	*	*	28	1.37	179	3	*
JF17-1500	2.75		*	*	*	*	*	*	*	*	*	*
JF21-100	-0.50		89	*	*	*	*	39	2.03	383	3	*
JF21-200	2.75		*	*	*	*	*	*	*	*	*	*
JF21-300	2.75		*	*	*	*	*	*	*	*	*	*
JF23-100	2.75		*	*	*	*	*	*	*	*	*	*
JF23-200	2.50		*	*	*	*	*	*	*	*	*	*
JF23-300	2.75		*	*	*	*	*	*	*	*	*	*
JF32-150	2.75		*	*	*	*	*	*	*	*	*	*
JF32-200	2.75		*	*	*	*	*	*	*	*	*	*
JF32-300	3.00		*	*	*	*	*	*	*	*	*	*
JF32-400	3.00		*	*	*	*	*	*	*	*	*	*
JF32-500	3.00		*	*	*	*	*	*	*	*	*	*
JF32-600	3.00		*	*	*	*	*	*	*	*	*	*
JF32-700	3.00		*	*	*	*	*	*	*	*	*	*
JF32-800	3.00		*	*	*	*	*	*	*	*	*	*
JF32-900	2.75		*	*	*	*	*	*	*	*	*	*
JF32-1000	2.75		*	*	*	*	*	*	*	*	*	*
JF32-1100	2.75		*	*	*	*	*	*	*	*	*	*
JF32-1200	2.75		*	*	*	*	*	*	*	*	*	*
JF32-1300	2.25		*	*	*	*	*	*	*	*	*	*
JF32-1400	2.50		*	*	*	*	*	*	*	*	*	*
JF32-1500	2.50		89	*	*	*	*	30	1.51	376	3	*
JF38-100	2.50		90	6	-2	-5	22	357	4.02	510	-1	25
JF38-200	3.00		90	*	*	*	30	470	4.54	460	1	33
JF38-300	3.00		90	*	*	*	23	352	4.37	460	1	30
JF38-400	3.25		90	*	*	*	19	256	4.20	460	1	28
JF38-500	3.25		*	*	*	*	*	*	*	*	*	*
JF38-600	2.75		90	*	*	*	13	106	3.29	340	1	22
JF38-700	3.00		*	*	*	*	*	*	*	*	*	*
JF38-800	2.75		90	*	*	*	12	115	3.08	375	1	25
JF38-900	2.50		*	*	*	*	*	*	*	*	*	*
JF38-1000	2.00		89	*	*	*	*	25	1.45	302	3	*
JF38-1100	2.00		90	*	*	*	8	64	2.38	315	-1	24
JF44-150	2.50		90	*	*	*	10	68	2.31	285	1	23
JF44-200	2.75		89	*	*	*	*	31	1.77	471	3	*
JF44-300	3.00		*	*	*	*	*	*	*	*	*	*
JF44-400	3.00		*	*	*	*	*	*	*	*	*	*

Sample	Sed	Mode	Yr.	ppb:Au	Pd	Pt	ppm:Co	Cu	Fe%	Mn	Mo	Ni
JF44-500	3.00		*	*	*	*	*	*	*	*	*	*
JF44-600	2.75		*	*	*	*	*	*	*	*	*	*
JF44-700	2.50		*	*	*	*	*	*	*	*	*	*
JF44-800	1.50		*	*	*	*	*	*	*	*	*	*
JF44-900	1.50		*	*	*	*	*	*	*	*	*	*
JF44-1000	1.50		90	*	*	*	9	22	2.56	400	-1	20
JF44-1100	1.75		*	*	*	*	*	*	*	*	*	*
JF44-1200	2.00		*	*	*	*	*	*	*	*	*	*
JF44-1300	2.25		89	*	*	*	*	27	1.52	337	3	*
JF44-1400	2.25		89	*	*	*	*	26	1.49	313	3	*
JF44-1500	2.25		*	*	*	*	*	*	*	*	*	*
JR81-66	2.50		89	*	*	*	*	19	1.18	239	3	*
JR81-67	2.00		90	*	*	*	8	63	2.36	245	-1	22
JR81-68	2.50		90	*	*	*	7	20	2.02	245	-1	17
JR81-69	2.50		90	*	*	*	7	77	2.10	225	-1	16
JR81-76	2.00		*	*	*	*	*	*	*	*	*	*
JR81-77	2.50		*	*	*	*	*	*	*	*	*	*
JR81-78	*		*	*	*	*	*	*	*	*	*	*
JR81-80	2.50		*	*	*	*	*	*	*	*	*	*
JR81-81	2.50		89	*	*	*	*	41	1.65	394	3	*
JR81-82	2.50		*	*	*	*	*	*	*	*	*	*
JR81-83	2.00		90	*	*	*	9	85	2.24	295	-1	20
JR81-84	2.00		*	*	*	*	*	*	*	*	*	*
JR81-85	2.50		89	*	*	*	*	29	1.60	380	3	*
JR81-86	2.50		*	*	*	*	*	*	*	*	*	*
JR81-87	2.00		*	*	*	*	*	*	*	*	*	*
JR81-88	2.00		*	*	*	*	*	*	*	*	*	*
JR81-93	2.50		89	*	*	*	*	20	1.27	272	3	*
JR81-94	2.00		89	*	*	*	*	26	1.84	470	3	*
JR81-102	2.00		89	*	*	*	*	26	1.69	350	3	*
JR81-103	2.50		90	*	*	*	7	44	2.11	260	-1	18
JF-B15-4	3.00		*	*	*	*	*	*	*	*	*	*
TUL88A-01	3.50		89	-5	5	20	*	20	1.35	155	3	*
TUL88A-02	1.75		*	*	*	*	*	*	*	*	*	*
TUL88A-03	*		*	*	*	*	*	*	*	*	*	*
TUL88A-04	2.25		89	-5	2	-15	*	105	1.11	201	2	*
TUL88A-05	0.25		*	*	*	*	*	*	*	*	*	*
TUL88A-06	1.50		89	-5	2	30	*	18	1.07	230	3	*
TUL88A-07	*		*	*	*	*	*	*	*	*	*	*
TUL88A-08	2.50		89	-5	2	20	*	22	1.33	257	3	*
TUL88A-09	1.75		89	-5	2	20	*	18	1.02	220	1	*
TUL88A-10	1.75		89	-5	8	-15	*	26	1.36	265	1	*
TUL88A-11	2.00		89	5	2	20	*	21	1.33	258	3	*
TUL88A-12	3.50		89	-5	2	30	*	24	1.44	220	3	*
TUL88A-13	2.50		89	-5	2	-15	*	23	1.42	206	3	*
JR89-D1	2.00		90	100	-2	-5	10	63	2.59	370	-1	22
MC89-D1	2.75		90	-2	-2	-5	11	34	2.90	390	-1	22
LC89-D1	0.75		90	-2	-2	-5	15	42	3.62	495	-1	37
SR89-D1	1.00		90	-2	-2	-5	7	30	2.50	490	-1	15
PAR89A-15	3.00		*	*	*	*	*	*	*	*	*	*
PAR89A-18	3.00		*	*	*	*	*	*	*	*	*	*

Sample	Sed	Mode	Yr.	ppb:Au	Pd	Pt	ppm:Co	Cu	Fe%	Mn	Mo	Ni
PAR89A-19	2.75		90	*	*	*	7	35	2.35	305	-1	12
PAR89A-20	3.00		*	*	*	*	*	*	*	*	*	*
PAR89A-21	3.00		*	*	*	*	*	*	*	*	*	*
PAR89A-22	3.00		90	*	*	*	6	20	1.85	205	-1	11
PAR89A-24	3.25		*	*	*	*	*	*	*	*	*	*
PAR89A-27	0.75		*	*	*	*	*	*	*	*	*	*
PAR89A-29	2.00		*	*	*	*	*	*	*	*	*	*
PAR89A-30	2.00		*	*	*	*	*	*	*	*	*	*
PAR89A-32	3.50		*	*	*	*	*	*	*	*	*	*
PAR89A-33	3.25		*	*	*	*	*	*	*	*	*	*
PAR89A-34	1.25		*	*	*	*	*	*	*	*	*	*
PAR89A-35	0.75		90	*	*	*	7	10	2.38	325	-1	13
PAR89A-37	0.50		*	*	*	*	*	*	*	*	*	*
PAR89A-38	1.25		90	*	*	*	6	28	1.97	240	-1	15
PAR89A-39	*		*	*	*	*	*	*	*	*	*	*
PAR89A-40	1.50		*	*	*	*	*	*	*	*	*	*
PAR89A-41	2.00		*	*	*	*	*	*	*	*	*	*
PAR89A-42	1.50		*	*	*	*	*	*	*	*	*	*
PAR89A-45	2.00		*	*	*	*	*	*	*	*	*	*
PAR89A-47	2.00		*	*	*	*	*	*	*	*	*	*
PAR89A-48	2.00		*	*	*	*	*	*	*	*	*	*
PAR89A-51	1.75		*	*	*	*	*	*	*	*	*	*
PAR89A-52	1.50		*	*	*	*	*	*	*	*	*	*
PAR89A-54	3.50		*	*	*	*	*	*	*	*	*	*
PAR89A-56	2.50		*	*	*	*	*	*	*	*	*	*
PAR89A-57	3.25		*	*	*	*	*	*	*	*	*	*
PAR89A-58	1.50		*	*	*	*	*	*	*	*	*	*
PAR89A-59	3.50		*	*	*	*	*	*	*	*	*	*
PAR89A-60	3.50		*	*	*	*	*	*	*	*	*	*
PAR89A-61	3.25		*	*	*	*	*	*	*	*	*	*
PAR89A-62	3.25		*	*	*	*	*	*	*	*	*	*
PAR89A-63	3.25		*	*	*	*	*	*	*	*	*	*
PAR89A-64	3.25		*	*	*	*	*	*	*	*	*	*
PAR89A-65	3.25		*	*	*	*	*	*	*	*	*	*
PAR89A-66	3.00		90	*	*	*	7	20	2.58	205	-1	18
PAR89A-67	3.25		*	*	*	*	*	*	*	*	*	*
PAR89A-68	3.25		*	*	*	*	*	*	*	*	*	*
PAR89A-69	3.25		*	*	*	*	*	*	*	*	*	*
PAR89A-70	2.00		*	*	*	*	*	*	*	*	*	*
PAR89A-71	2.25		*	*	*	*	*	*	*	*	*	*
PAR89A-73	1.75		90	*	*	*	6	12	2.05	275	-1	18
PAR89A-74	2.50		*	*	*	*	*	*	*	*	*	*
PAR89A-75	2.25		*	*	*	*	*	*	*	*	*	*
PAR89A-76	3.25		*	*	*	*	*	*	*	*	*	*
PAR89A-77	3.25		*	*	*	*	*	*	*	*	*	*
PAR89A-78	3.00		90	*	*	*	7	30	2.51	230	-1	18
PAR89A-79	3.25		90	*	*	*	7	29	2.47	210	-1	17
PAR89A-80	3.25		*	*	*	*	*	*	*	*	*	*
PAR89A-81	1.25		90	*	*	*	8	32	2.38	290	-1	17
PAR89A-83	3.25		90	*	*	*	7	51	2.17	215	-1	15
PAR89A-85	3.25		*	*	*	*	*	*	*	*	*	*

Sample ppm:	Pb	V	Zn	Ag	Cd	Se	Sn	Hg	Sb	Bi
JF17-100	*	*	*	*	*	*	*	*	*	*
JF17-200	*	*	*	*	*	*	*	*	*	*
JF17-300	*	*	*	*	*	*	*	*	*	*
JF17-400	*	*	*	*	*	*	*	*	*	*
JF17-500	*	*	*	*	*	*	*	*	*	*
JF17-600	*	*	*	*	*	*	*	*	*	*
JF17-700	*	*	*	*	*	*	*	*	*	*
JF17-800	*	*	*	*	*	*	*	*	*	*
JF17-900	*	*	*	*	*	*	*	*	*	*
JF17-1000	*	*	*	*	*	*	*	*	*	*
JF17-1100	*	*	*	*	*	*	*	*	*	*
JF17-1200	*	*	*	*	*	*	*	*	*	*
JF17-1300	*	*	*	*	*	*	*	*	*	*
JF17-1400	50	87	38	0.6	-1	-5	-10	35	8	-2
JF17-1500	*	*	*	*	*	*	*	*	*	*
JF21-100	52	169	40	0.8	-1	-5	10	40	18	-2
JF21-200	*	*	*	*	*	*	*	*	*	*
JF21-300	*	*	*	*	*	*	*	*	*	*
JF23-100	*	*	*	*	*	*	*	*	*	*
JF23-200	*	*	*	*	*	*	*	*	*	*
JF23-300	*	*	*	*	*	*	*	*	*	*
JF32-150	*	*	*	*	*	*	*	*	*	*
JF32-200	*	*	*	*	*	*	*	*	*	*
JF32-300	*	*	*	*	*	*	*	*	*	*
JF32-400	*	*	*	*	*	*	*	*	*	*
JF32-500	*	*	*	*	*	*	*	*	*	*
JF32-600	*	*	*	*	*	*	*	*	*	*
JF32-700	*	*	*	*	*	*	*	*	*	*
JF32-800	*	*	*	*	*	*	*	*	*	*
JF32-900	*	*	*	*	*	*	*	*	*	*
JF32-1000	*	*	*	*	*	*	*	*	*	*
JF32-1100	*	*	*	*	*	*	*	*	*	*
JF32-1200	*	*	*	*	*	*	*	*	*	*
JF32-1300	*	*	*	*	*	*	*	*	*	*
JF32-1400	*	*	*	*	*	*	*	*	*	*
JF32-1500	50	114	33	0.7	-1	-5	10	20	13	-2
JF38-100	8	120	46	-0.2	-0.1	0.3	11	20	-0.2	-0.1
JF38-200	8	115	58	-0.2	-0.1	0.6	4	30	-0.2	-0.1
JF38-300	8	110	52	-0.2	-0.1	0.8	-2	30	0.2	-0.1
JF38-400	4	107	50	-0.2	-0.1	0.2	-2	20	-0.2	-0.1
JF38-500	*	*	*	*	*	*	*	*	*	*
JF38-600	4	77	48	-0.2	-0.1	-0.2	-2	30	-0.2	-0.1
JF38-700	*	*	*	*	*	*	*	*	*	*
JF38-800	6	78	54	-0.2	-0.1	-0.2	-2	30	0.2	-0.1
JF38-900	*	*	*	*	*	*	*	*	*	*
JF38-1000	49	114	26	0.8	-1	-5	10	20	12	-2
JF38-1100	6	60	54	-0.2	-0.1	-0.2	3	30	0.2	-0.1
JF44-150	6	60	36	-0.2	-0.1	-0.2	-2	20	0.2	-0.1
JF44-200	50	127	39	0.8	-1	-5	10	20	15	-2
JF44-300	*	*	*	*	*	*	*	*	*	*
JF44-400	*	*	*	*	*	*	*	*	*	*

Sample ppm:	Pb	V	Zn	Ag	Cd	Se	Sn	Hg	Sb	Bi
JF44-500	*	*	*	*	*	*	*	*	*	*
JF44-600	*	*	*	*	*	*	*	*	*	*
JF44-700	*	*	*	*	*	*	*	*	*	*
JF44-800	*	*	*	*	*	*	*	*	*	*
JF44-900	*	*	*	*	*	*	*	*	*	*
JF44-1000	10	78	36	-0.2	-0.1	-0.2	7	20	0.2	-0.1
JF44-1100	*	*	*	*	*	*	*	*	*	*
JF44-1200	*	*	*	*	*	*	*	*	*	*
JF44-1300	50	129	30	0.8	-1	-5	11	20	14	-2
JF44-1400	45	124	29	0.6	-1	-5	-10	15	10	-2
JF44-1500	*	*	*	*	*	*	*	*	*	*
JR81-66	43	94	23	0.5	-1	-5	-10	20	6	-2
JR81-67	6	50	46	-0.2	-0.1	-0.2	2	30	0.2	-0.1
JR81-68	4	51	32	-0.2	-0.1	0.2	-2	20	0.4	0.1
JR81-69	10	45	36	-0.2	-0.1	-0.2	2	30	0.2	-0.1
JR81-76	*	*	*	*	*	*	*	*	*	*
JR81-77	*	*	*	*	*	*	*	*	*	*
JR81-78	*	*	*	*	*	*	*	*	*	*
JR81-80	*	*	*	*	*	*	*	*	*	*
JR81-81	45	125	32	0.7	-1	12	-10	15	11	-2
JR81-82	*	*	*	*	*	*	*	*	*	*
JR81-83	2	59	32	-0.2	-0.1	-0.2	-2	20	0.2	-0.1
JR81-84	*	*	*	*	*	*	*	*	*	*
JR81-85	49	132	31	0.9	-1	-5	-10	20	11	-2
JR81-86	*	*	*	*	*	*	*	*	*	*
JR81-87	*	*	*	*	*	*	*	*	*	*
JR81-88	*	*	*	*	*	*	*	*	*	*
JR81-93	45	104	25	0.6	-1	-5	-10	20	6	-2
JR81-94	48	134	30	0.8	-1	-5	10	20	12	-2
JR81-102	47	134	30	0.7	-1	-5	-10	20	14	-2
JR81-103	2	55	30	-0.2	-0.1	-0.2	-2	20	0.2	-0.1
JF-B15-4	*	*	*	*	*	*	*	*	*	*
TUL88A-01	52	78	35	0.7	-1	-5	-10	35	13	-2
TUL88A-02	*	*	*	*	*	*	*	*	*	*
TUL88A-03	*	*	*	*	*	*	*	*	*	*
TUL88A-04	46	80	47	0.5	-1	-5	-10	25	-5	-2
TUL88A-05	*	*	*	*	*	*	*	*	*	*
TUL88A-06	45	81	24	0.5	-1	-5	-10	15	-5	-2
TUL88A-07	*	*	*	*	*	*	*	*	*	*
TUL88A-08	44	104	26	0.6	-1	-5	-10	25	-5	-2
TUL88A-09	43	74	24	0.5	-1	-5	-10	30	-5	-2
TUL88A-10	47	111	35	0.7	-1	-5	-10	20	-5	-2
TUL88A-11	47	102	29	0.6	-1	-5	-10	15	6	-2
TUL88A-12	54	100	34	0.7	-1	-5	-10	40	14	-2
TUL88A-13	56	105	34	0.8	-1	-5	-10	15	16	-2
JR89-D1	36	74	40	-0.2	-0.1	0.2	2	20	0.2	-0.1
MC89-D1	18	91	38	-0.2	-0.1	-0.2	-2	20	0.2	-0.1
LC89-D1	8	106	52	-0.2	-0.1	-0.2	2	20	0.4	-0.1
SR89-D1	38	63	38	-0.2	-0.1	-0.2	-2	20	0.2	-0.1
PAR89A-15	*	*	*	*	*	*	*	*	*	*
PAR89A-18	*	*	*	*	*	*	*	*	*	*

Sample ppm:	Pb	V	Zn	Ag	Cd	Se	Sn	Hg	Sb	Bi
PAR89A-19	52	52	44	-0.2	-0.1	-0.2	10	40	-0.2	-0.1
PAR89A-20	*	*	*	*	*	*	*	*	*	*
PAR89A-21	*	*	*	*	*	*	*	*	*	*
PAR89A-22	6	35	38	-0.2	-0.1	-0.2	-2	60	0.2	-0.1
PAR89A-24	*	*	*	*	*	*	*	*	*	*
PAR89A-27	*	*	*	*	*	*	*	*	*	*
PAR89A-29	*	*	*	*	*	*	*	*	*	*
PAR89A-30	*	*	*	*	*	*	*	*	*	*
PAR89A-32	*	*	*	*	*	*	*	*	*	*
PAR89A-33	*	*	*	*	*	*	*	*	*	*
PAR89A-34	*	*	*	*	*	*	*	*	*	*
PAR89A-35	4	57	36	-0.2	-0.1	-0.2	-2	50	0.2	-0.1
PAR89A-37	*	*	*	*	*	*	*	*	*	*
PAR89A-38	26	47	34	-0.2	-0.1	-0.2	2	30	0.2	0.1
PAR89A-39	*	*	*	*	*	*	*	*	*	*
PAR89A-40	*	*	*	*	*	*	*	*	*	*
PAR89A-41	*	*	*	*	*	*	*	*	*	*
PAR89A-42	*	*	*	*	*	*	*	*	*	*
PAR89A-45	*	*	*	*	*	*	*	*	*	*
PAR89A-47	*	*	*	*	*	*	*	*	*	*
PAR89A-48	*	*	*	*	*	*	*	*	*	*
PAR89A-51	*	*	*	*	*	*	*	*	*	*
PAR89A-52	*	*	*	*	*	*	*	*	*	*
PAR89A-54	*	*	*	*	*	*	*	*	*	*
PAR89A-56	*	*	*	*	*	*	*	*	*	*
PAR89A-57	*	*	*	*	*	*	*	*	*	*
PAR89A-58	*	*	*	*	*	*	*	*	*	*
PAR89A-59	*	*	*	*	*	*	*	*	*	*
PAR89A-60	*	*	*	*	*	*	*	*	*	*
PAR89A-61	*	*	*	*	*	*	*	*	*	*
PAR89A-62	*	*	*	*	*	*	*	*	*	*
PAR89A-63	*	*	*	*	*	*	*	*	*	*
PAR89A-64	*	*	*	*	*	*	*	*	*	*
PAR89A-65	*	*	*	*	*	*	*	*	*	*
PAR89A-66	30	44	48	-0.2	-0.1	-0.2	-2	40	0.2	-0.1
PAR89A-67	*	*	*	*	*	*	*	*	*	*
PAR89A-68	*	*	*	*	*	*	*	*	*	*
PAR89A-69	*	*	*	*	*	*	*	*	*	*
PAR89A-70	*	*	*	*	*	*	*	*	*	*
PAR89A-71	*	*	*	*	*	*	*	*	*	*
PAR89A-73	10	53	30	-0.2	-0.1	-0.2	-2	30	0.2	-0.1
PAR89A-74	*	*	*	*	*	*	*	*	*	*
PAR89A-75	*	*	*	*	*	*	*	*	*	*
PAR89A-76	*	*	*	*	*	*	*	*	*	*
PAR89A-77	*	*	*	*	*	*	*	*	*	*
PAR89A-78	24	47	44	-0.2	-0.1	-0.2	6	40	0.2	-0.1
PAR89A-79	14	43	46	-0.2	-0.1	-0.2	-2	40	0.2	-0.1
PAR89A-80	*	*	*	*	*	*	*	*	*	*
PAR89A-81	76	65	36	-0.2	-0.1	-0.2	9	30	0.2	-0.1
PAR89A-83	18	46	38	-0.2	-0.1	-0.2	5	40	0.2	-0.1
PAR89A-85	*	*	*	*	*	*	*	*	*	*

Sample	ppm:Ti	Zr	Cr	% Magnetite
JF17-100	*	*	*	*
JF17-200	*	*	*	*
JF17-300	*	*	*	*
JF17-400	*	*	*	*
JF17-500	*	*	*	*
JF17-600	*	*	*	*
JF17-700	*	*	*	*
JF17-800	*	*	*	*
JF17-900	*	*	*	*
JF17-1000	*	*	*	*
JF17-1100	*	*	*	*
JF17-1200	*	*	*	*
JF17-1300	*	*	*	*
JF17-1400	2700	118	74	*
JF17-1500	*	*	*	*
JF21-100	4300	110	83	*
JF21-200	*	*	*	*
JF21-300	*	*	*	*
JF23-100	*	*	*	*
JF23-200	*	*	*	*
JF23-300	*	*	*	*
JF32-150	*	*	*	*
JF32-200	*	*	*	*
JF32-300	*	*	*	*
JF32-400	*	*	*	*
JF32-500	*	*	*	*
JF32-600	*	*	*	*
JF32-700	*	*	*	*
JF32-800	*	*	*	*
JF32-900	*	*	*	*
JF32-1000	*	*	*	*
JF32-1100	*	*	*	*
JF32-1200	*	*	*	*
JF32-1300	*	*	*	*
JF32-1400	*	*	*	*
JF32-1500	3600	81	121	*
JF38-100	10300	91	162	0.65
JF38-200	13300	100	128	1.18
JF38-300	12200	110	172	0.80
JF38-400	11500	120	200	0.80
JF38-500	*	*	*	0.62
JF38-600	9250	120	220	0.60
JF38-700	*	*	*	0.40
JF38-800	8350	140	280	0.67
JF38-900	*	*	*	0.53
JF38-1000	3600	72	162	0.88
JF38-1100	6150	125	300	*
JF44-150	5350	78	290	0.69
JF44-200	4500	77	132	1.29
JF44-300	*	*	*	0.57
JF44-400	*	*	*	0.14

Sample	ppm:Ti	Zr	Cr	% Magnetite
JF44-500	*	*	*	0.29
JF44-600	*	*	*	*
JF44-700	*	*	*	0.32
JF44-800	*	*	*	0.30
JF44-900	*	*	*	0.34
JF44-1000	8350	125	176	0.54
JF44-1100	*	*	*	0.73
JF44-1200	*	*	*	0.97
JF44-1300	3700	75	143	1.42
JF44-1400	3400	77	145	0.70
JF44-1500	*	*	*	0.89
JR81-66	2700	65	145	0.65
JR81-67	5600	105	156	0.34
JR81-68	6000	120	200	0.25
JR81-69	5550	105	180	0.33
JR81-76	*	*	*	*
JR81-77	*	*	*	*
JR81-78	*	*	*	*
JR81-80	*	*	*	0.58
JR81-81	4000	73	180	0.84
JR81-82	*	*	*	0.69
JR81-83	6600	80	230	0.50
JR81-84	*	*	*	*
JR81-85	4300	83	149	1.18
JR81-86	*	*	*	0.15
JR81-87	*	*	*	0.55
JR81-88	*	*	*	1.17
JR81-93	2900	67	166	1.13
JR81-94	4500	80	199	1.25
JR81-102	3700	81	173	0.84
JR81-103	6800	105	215	*
JF-B15-4	*	*	*	0.46
TUL88A-01	2800	101	85	0.10
TUL88A-02	*	*	*	*
TUL88A-03	*	*	*	*
TUL88A-04	2500	66	68	0.30
TUL88A-05	*	*	*	0.56
TUL88A-06	2200	75	99	0.53
TUL88A-07	*	*	*	*
TUL88A-08	3300	86	115	*
TUL88A-09	2200	82	72	0.60
TUL88A-10	2800	80	117	0.34
TUL88A-11	2900	82	83	1.04
TUL88A-12	3400	94	82	0.12
TUL88A-13	3600	105	57	0.60
JR89-D1	7450	115	184	*
MC89-D1	10100	145	180	*
LC89-D1	9700	96	156	*
SR89-D1	5000	91	182	*
PAR89A-15	*	*	*	*
PAR89A-18	*	*	*	*

Sample	ppm:Ti	Zr	Cr	% Magnetite
PAR89A-19	5750	105	168	*
PAR89A-20	*	*	*	*
PAR89A-21	*	*	*	*
PAR89A-22	4250	110	146	*
PAR89A-24	*	*	*	*
PAR89A-27	*	*	*	*
PAR89A-29	*	*	*	*
PAR89A-30	*	*	*	*
PAR89A-32	*	*	*	*
PAR89A-33	*	*	*	*
PAR89A-34	*	*	*	*
PAR89A-35	6100	110	184	*
PAR89A-37	*	*	*	*
PAR89A-38	4900	105	134	*
PAR89A-39	*	*	*	*
PAR89A-40	*	*	*	*
PAR89A-41	*	*	*	*
PAR89A-42	*	*	*	*
PAR89A-45	*	*	*	*
PAR89A-47	*	*	*	*
PAR89A-48	*	*	*	*
PAR89A-51	*	*	*	*
PAR89A-52	*	*	*	*
PAR89A-54	*	*	*	*
PAR89A-56	*	*	*	*
PAR89A-57	*	*	*	*
PAR89A-58	*	*	*	*
PAR89A-59	*	*	*	*
PAR89A-60	*	*	*	*
PAR89A-61	*	*	*	*
PAR89A-62	*	*	*	*
PAR89A-63	*	*	*	*
PAR89A-64	*	*	*	*
PAR89A-65	*	*	*	*
PAR89A-66	6600	110	210	*
PAR89A-67	*	*	*	*
PAR89A-68	*	*	*	*
PAR89A-69	*	*	*	*
PAR89A-70	*	*	*	*
PAR89A-71	*	*	*	*
PAR89A-73	6050	110	200	*
PAR89A-74	*	*	*	*
PAR89A-75	*	*	*	*
PAR89A-76	*	*	*	*
PAR89A-77	*	*	*	*
PAR89A-78	6700	115	182	*
PAR89A-79	6200	105	172	*
PAR89A-80	*	*	*	*
PAR89A-81	8300	105	164	*
PAR89A-83	6350	125	205	*
PAR89A-85	*	*	*	*

Sample	Latitude	Longitude	%H.M.	Yr.	ppb:Au/Pd/Pt		
JF-B1-1	48 21.80	123 47.87	*	89	*	*	*
JF-B1-3	48 21.80	123 47.87	12.29	89	*	*	*
JF-B2-3	48 21.77	123 48.13	*	89	*	*	*
JF-B3-2	48 21.34	123 49.35	10.00	n/a			
JF-B4-1	48 21.94	123 49.80	15.63	89	*	*	*
JF-B5-1	48 22.20	123 50.00	*	89	*	*	*
JF-B5-2B	48 22.20	123 50.00	*	89	*	*	*
JF-B5-3	48 22.20	123 50.00	*	89	*	*	*
JF-B5-5	48 22.20	123 50.00	*	89	*	*	*
JF-B6-2	48 22.40	123 50.59	*	89	*	*	*
JF-B7-3	48 22.75	123 51.53	18.01	89	*	*	*
JF-B8-3	48 22.78	123 52.07	16.33	89	*	*	*
JF-B8-6	48 22.78	123 52.07	*	89	*	*	*
JF-B11-1	48 22.95	123 53.02	*	89	*	*	*
JF-B11-2	48 22.95	123 53.02	*	89	*	*	*
JF-B11-4	48 22.95	123 53.02	6.33	89	*	*	*
JF-B12-2	48 23.39	123 56.53	18.49	89	*	*	*
JF-B12-3	48 23.39	123 56.53	*	89	*	*	*
JF-B13-1	48 23.55	123 56.65	*	89	*	*	*
JF-B14-1	48 23.75	123 56.86	9.94	n/a			
JF-B14-2	48 23.75	123 56.86	13.18	89	*	*	*
JF-B14-3	48 23.75	123 56.86	8.91	n/a			
JF-B15-1	48 23.74	123 58.86	26.12	89	*	*	*
JF-B15-2	48 23.74	123 58.86	26.23	n/a			
JF-B15-3	48 23.74	123 58.86	17.93	n/a			
JF-B16-1	48 23.87	123 59.07	28.26	89	*	*	*
JF-B16-2	48 23.87	123 59.07	27.26	n/a			
JF-B16-3	48 23.87	123 59.07	17.22	n/a			
JF-B16-4	48 23.87	123 59.07	28.95	n/a			
JF-B17-1	48 24.83	124 00.83	31.16	89	*	*	*
JF-B17-2	48 24.83	124 00.83	27.40	n/a			
JF-B17-3	48 24.83	124 00.83	36.35	90	10	-2	-5
JF-P1-1	48 24.92	124 01.11	34.17	89	*	*	*
JF-P1-2	48 24.92	124 01.11	30.85	n/a			
JF-P1-3	48 24.92	124 01.11	39.97	90	8	-2	-5
JF-B18-1	48 25.03	124 01.42	24.46	n/a			
JF-B18-2	48 25.03	124 01.42	40.40	89	*	*	*
JF-B18-3	48 25.03	124 01.42	45.87	90	10	-2	-5
BG89-03	48 31.55	124 26.45	0.88	90	*	*	*
SB89-01	48 29.97	124 17.97	4.53	90	*	*	*
SB89-04	48 29.59	124 17.60	27.99	90	*	*	*
MAB89-01	48 26.95	124 09.45	36.73	90	*	*	*
MB89-02	48 26.39	124 07.08	9.24	90	*	*	*
CB89-02	48 26.10	124 05.73	12.26	90	*	*	*
CB89-08	48 25.44	124 04.27	10.67	90	*	*	*
JR89-01	48 25.34	124 03.41	9.20	90	*	*	*
JR89-02	48 25.12	124 01.87	6.46	90	*	*	*
PNP89-01	48 24.49	123 59.83	24.37	90	*	*	*
CRB89-01	48 23.59	123 58.38	11.69	90	*	*	*
FLB89-01	48 22.92	123 55.80	5.04	90	*	*	*
KC89-01	48 22.94	123 53.64	6.62	90	*	*	*

Sample	Latitude	Longitude	%H.M.	Yr.	ppb:Au/Pd/Pt		
SG89-01	48 22.51	123 51.12	15.81	90	*	*	*
SO89-03	48 21.68	123 45.17	6.63	90	*	*	*

Sample	ppm:Co	Cu	Fe%	Mn	Mo	Ni	Pb	V	Zn	Ag	Cd
JF-B1-1	*	52	3.03	561	3	*	55	273	43	0.9	-1
JF-B1-3	*	44	2.67	491	3	*	50	265	37	0.7	-1
JF-B2-3	*	41	2.39	440	3	*	49	218	35	0.6	-1
JF-B4-1	*	41	2.62	508	3	*	53	236	37	0.8	-1
JF-B5-1	*	39	2.42	449	3	*	51	226	37	0.7	-1
JF-B5-2B	*	37	2.44	592	3	*	47	219	43	0.7	-1
JF-B5-3	*	37	2.42	468	3	*	52	234	38	0.9	-1
JF-B5-5	*	37	2.36	445	3	*	54	220	38	0.8	-1
JF-B6-2	*	38	1.97	379	2	*	44	172	35	0.7	-1
JF-B7-3	*	40	2.41	489	3	*	47	206	66	0.8	-1
JF-B8-3	*	39	2.22	529	3	*	49	215	38	1.1	-1
JF-B8-6	*	37	2.16	481	3	*	50	193	51	0.9	-1
JF-B11-1	*	39	2.34	467	3	*	63	205	38	0.9	-1
JF-B11-2	*	32	1.89	398	3	*	52	152	32	0.9	-1
JF-B11-4	*	27	1.61	353	2	*	47	134	28	0.9	-1
JF-B12-2	*	29	2.06	625	3	*	40	211	38	0.8	-1
JF-B12-3	*	45	2.57	482	3	*	50	229	43	0.8	-1
JF-B13-1	*	54	2.15	532	3	*	48	200	45	0.7	-1
JF-B14-2	*	32	1.96	444	3	*	45	191	33	0.7	-1
JF-B15-1	*	58	2.34	568	3	*	84	210	42	0.9	-1
JF-B16-1	*	38	2.15	401	3	*	52	204	36	0.9	-1
JF-B17-1	*	111	2.64	595	3	*	61	221	44	1.0	-1
JF-B17-3	23	345	4.01	475	-1	26	2	116	46	-0.2	-0.1
JF-P1-1	*	92	2.62	539	3	*	50	228	44	0.8	-1
JF-P1-3	27	390	4.64	565	-1	30	4	137	50	-0.2	-0.1
JF-B18-2	*	118	2.86	625	3	*	58	219	47	1.0	-1
JF-B18-3	28	391	4.82	595	-1	30	4	142	52	-0.2	-0.1
BG89-03	5	10	2.04	215	1	15	6	30	64	-0.2	-0.1
SB89-01	7	15	2.52	385	-1	18	2	63	38	-0.2	-0.1
SB89-04	9	26	3.33	580	-1	23	-2	115	38	-0.2	-0.1
MAB89-01	9	20	2.91	775	-1	21	2	92	32	-0.2	-0.1
MB89-02	8	16	2.09	290	-1	19	4	57	30	-0.2	-0.1
CB89-02	8	21	2.36	305	-1	19	4	66	32	-0.2	-0.1
CB89-08	10	28	2.75	340	-1	20	4	80	38	-0.2	-0.1
JR89-01	10	29	2.76	365	1	21	2	82	38	-0.2	-0.1
JR89-02	8	44	2.21	270	-1	19	2	58	30	-0.2	-0.1
PNP89-01	11	134	2.96	365	1	19	8	84	34	-0.2	-0.1
CRB89-01	8	73	2.17	245	-1	17	6	53	26	-0.2	-0.1
FLB89-01	6	16	1.66	205	-1	17	4	40	22	-0.2	-0.1
KC89-01	7	18	1.84	230	-1	17	6	50	28	-0.2	-0.1
SG89-01	7	18	2.21	290	-1	17	2	70	28	-0.2	-0.1
SO89-03	4	19	1.27	175	-1	9	8	38	16	-0.2	-0.1

Sample ppm:Se		Sn	Hg	Sb	Bi	Ti	Zr	Cr	%Mag.
JF-B1-1	-5	13	15	19	20	6600	140	114	*
JF-B1-3	-5	11	15	17	10	5800	121	98	*
JF-B2-3	-5	10	15	15	8	5000	118	97	*
JF-B4-1	-5	11	15	19	8	5500	112	104	*
JF-B5-1	-5	10	15	16	4	4600	100	112	*
JF-B5-2B	-5	10	15	12	7	5200	97	124	*
JF-B5-3	-5	10	10	16	7	5000	101	104	*
JF-B5-5	-5	11	15	18	11	4700	162	117	*
JF-B6-2	-5	-10	15	-5	-2	4300	125	96	*
JF-B7-3	-5	10	10	12	6	5000	119	119	*
JF-B8-3	-5	12	10	11	11	6200	106	107	*
JF-B8-6	-5	10	10	15	4	5100	80	139	*
JF-B11-1	-5	12	20	19	6	4700	106	97	*
JF-B11-2	-5	10	15	12	-2	4500	83	144	*
JF-B11-4	-5	-10	15	7	-2	4800	81	152	*
JF-B12-2	-5	10	10	8	-2	5600	105	175	*
JF-B12-3	-5	11	5	20	5	5500	140	98	*
JF-B13-1	-5	11	30	17	-2	5200	106	108	*
JF-B14-2	-5	-10	15	14	-2	4500	91	108	*
JF-B15-1	-5	27	20	18	-2	5200	94	101	2.94
JF-B15-2									2.54
JF-B15-3									0.38
JF-B16-1	-5	11	15	18	-2	4500	95	93	3.91
JF-B16-2									2.97
JF-B16-3									0.43
JF-B16-4									1.10
JF-B17-1	-5	12	10	20	4	5300	74	100	2.28
JF-B17-2									1.80
JF-B17-3	0.4	-2	30	0.2	-0.1	11800	105	110	1.07
JF-P1-1	-5	12	20	13	5	5500	99	110	3.80
JF-P1-2									2.43
JF-P1-3	0.7	2	20	0.2	-0.1	12600	105	136	2.05
JF-B18-2	-5	14	550	19	2	6300	80	145	2.81
JF-B18-3	0.6	2	20	0.2	-0.1	13700	115	148	1.84
BG89-03	-0.2	-2	60	0.2	-0.1	2550	50	385	*
SB89-01	-0.2	-2	30	0.2	0.1	5550	86	192	*
SB89-04	-0.2	-2	20	0.2	-0.1	12700	165	124	*
MAB89-01	-0.2	-2	20	0.2	0.1	13500	155	194	*
MB89-02	-0.2	-2	30	0.4	-0.1	6350	85	220	*
CB89-02	-0.2	-2	40	0.2	-0.1	7950	97	225	*
CB89-08	-0.2	-2	30	0.2	-0.1	8350	87	196	*
JR89-01	-0.2	-2	20	0.2	-0.1	7800	84	168	*
JR89-02	-0.2	-2	20	0.2	-0.1	5950	82	200	*
PNP89-01	-0.2	-2	30	0.2	-0.1	9950	115	152	*
CRB89-01	-0.2	-2	30	0.2	-0.1	5600	72	260	*
FLB89-01	0.2	-2	30	0.4	-0.1	4150	69	320	*
KC89-01	-0.2	-2	30	0.2	-0.1	5350	72	240	*
SG89-01	-0.2	-2	20	0.2	-0.1	8300	125	180	*
SO89-03	-0.2	-2	30	0.2	-0.1	4650	87	200	*

APPENDIX D *Offshore Muds* 300

Sample	Yr.	ppb:Au	Pd	Pt	ppm:Co	Cu	Fe%	Mn	Mo	Ni	Pb	V
TUL88A-01	89	-5	5	20	*	55	1.82	240	3	*	64	135
TUL88A-08	89	-5	2	20	*	62	1.79	218	4	*	70	119
TUL88A-10	89	-5	2	20	*	59	2.16	402	4	*	69	142
TUL88A-12	89	-5	-2	15	*	50	1.75	211	4	*	70	121
TUL88A-13	89	-5	2	20	*	44	1.69	193	4	*	73	124
JR89-D1	90	*	*	*	12	173	3.71	315	1	27	40	91
MC89-D1	90	4	-2	-5	11	120	3.38	270	-1	25	46	86
SR89-D1	90	-2	-2	-5	10	77	3.48	350	-1	20	86	66
PAR89A-19	90	*	*	*	8	166	3.54	280	1	19	62	81
PAR89A-22	90	*	*	*	9	120	3.06	260	1	21	30	65
PAR89A-35	90	*	*	*	8	54	2.79	245	-1	19	34	58
PAR89A-38	90	*	*	*	8	219	2.81	250	1	22	68	56
PAR89A-66	90	*	*	*	7	65	2.89	225	-1	19	30	60
PAR89A-73	90	*	*	*	8	124	3.03	250	-1	23	44	61
PAR89A-78	90	*	*	*	8	47	2.80	220	-1	18	22	58
PAR89A-79	90	*	*	*	8	72	3.17	245	-1	21	26	63
PAR89A-81	90	*	*	*	8	116	3.08	250	1	21	80	64
PAR89A-83	90	*	*	*	7	56	2.93	215	-1	18	30	60

Sample	ppm:Zn	Ag	Cd	Se	Sn	Hg	Sb	Bi	Ti	Zr	Cr
TUL88A-01	54	0.9	-1	-5	12	45	21	-2	5300	122	67
TUL88A-08	58	0.9	-1	-5	11	85	17	-2	4600	146	53
TUL88A-10	75	0.6	-1	-5	11	50	19	-2	4400	117	41
TUL88A-12	52	0.9	-1	-5	11	20	21	-2	4900	130	57
TUL88A-13	50	0.9	-1	-5	11	30	19	-2	4500	124	47
JR89-D1	90	-0.2	-0.1	0.4	8	50	0.8	-0.1	14900	330	*
MC89-D1	78	-0.2	-0.1	-0.2	6	70	0.6	-0.1	14000	370	62
SR89-D1	84	-0.2	-0.1	0.2	6	80	1.0	0.1	10100	145	40
PAR89A-19	94	-0.2	-0.1	-0.2	14	90	0.4	-0.1	12900	305	94
PAR89A-22	90	-0.2	-0.1	-0.2	11	70	0.4	-0.1	11000	245	196
PAR89A-35	72	-0.2	-0.1	-0.2	6	70	0.2	-0.1	10900	210	92
PAR89A-38	86	-0.2	0.3	-0.2	18	60	0.8	-0.1	11600	290	232
PAR89A-66	76	-0.2	-0.1	-0.2	5	60	0.4	-0.1	9150	195	86
PAR89A-73	98	-0.2	0.3	0.2	10	80	0.4	-0.1	10500	210	136
PAR89A-78	66	-0.2	-0.1	-0.2	3	60	0.4	-0.1	11300	245	84
PAR89A-79	80	-0.2	-0.1	-0.2	3	50	0.4	-0.1	10700	215	146
PAR89A-81	78	-0.2	-0.1	-0.2	10	50	0.6	-0.1	11400	250	90
PAR89A-83	68	-0.2	-0.1	-0.2	-2	60	0.6	-0.1	10700	225	86

CAPTIONS FOR FIGURES ENCLOSED IN BACK POCKET

Figure 2. Bathymetry of northernwestern Juan de Fuca Strait, contoured from hydrographic chart field sheets Nos. 1156L and 1190L, Canadian Hydrographic Service. Isobaths are in metres.

Figure 5. Sample distribution and sample source, within study area, northern Juan de Fuca Strait. Samples total 234, with 150 samples from the offshore seabed and 84 taken along adjacent beaches and above high tide marks on four rivers.

Figure 6. Four geophysical survey track lines in January 1988 and three survey lines in March 1989. Information obtained includes sidescan swaths and sub-bottom profiles.

Figure 8. Surficial sediment distribution within the study area, northern Juan de Fuca Strait. Sediments are classified using a modified scheme after Folk (1974).

Figure 9. Distribution of mean grain size of surficial sediments, northern Juan de Fuca Strait. Contours are in phi units. Gravel is excluded from the grain size averages.

Figure 14. Distribution of modal grain size of surficial sediments, northern Juan de Fuca Strait. Contours are in phi units. Gravel is excluded from the grain size averages.

Figure 18. Distribution of sediment sorting (standard deviation), northern Juan de Fuca Strait. Contours are in phi units. Gravel is excluded from the grain size averages.

Figure 21. Surficial features found on the nearshore seabed, northern Juan de Fuca Strait. Directional and speed data from the two moored current stations are shown in Figure 4.

Figure 23. Distribution of heavy mineral contents by weight percent, northern Juan de Fuca Strait and southwestern Vancouver Island. Percentages for the four streams are listed as bar-head/side-of-bar.

Figure 31. Location of samples used in mineral analyses (X-ray diffraction and heavy mineral counts), northern Juan de Fuca Strait. West to east line indicates order of offshore mineral-type histograms (Figure 36).

Figure 43. Distribution of geochemistry sample sites, northern Juan de Fuca Strait and southwestern Vancouver Island. The two sample sets from 1989 (Group A) and 1990 (Group B) are distinguished, and samples with both sand and mud fractions analysed are shown. Multi-sample beach profiles had individual samples analysed in separate years at Sandcut Beach.

Figure 73. Geographic distribution of Ti% in sand fraction of offshore, beach and river samples, northern Juan de Fuca Strait and southwestern Vancouver Island. Concentrations are contoured by years - 1989 (Group A) and 1990 (Group B). River concentrations are listed as bar-head/side-of-bar.

VITA

Surname:Kilby Given Names:Caleen Elaine

Place of Birth:Detroit, Michigan Date of Birth:June 1, 1955

Educational Institutions Attended:

Whitman College	1973 to 1975
University of Alberta	1975 to 1978
University of Victoria	1987 to 1991

Degrees Awarded:

B.Sc. (General)	University of Alberta	1977
Certificate of Specialization in Geology	University of Alberta	1978

PARTIAL COPYRIGHT LICENSE

I hereby grant the right to lend my thesis to users of the University of Victoria Library, and to make single copies only for such users or in response to a request from the Library of any other university, or similar institution, on its behalf or for one of its users. I further agree that permission for extensive copying of this thesis for scholarly purposes may be granted by me or a member of the University designated by me. It is understood that copying or publication of this thesis for financial gain shall not be allowed without my written permission.

Title of Thesis: Nearshore Surficial Geology, Heavy Minerals and Geochemistry, Northern Juan de Fuca Strait

Author [redacted]

CALEEN ELAINE KILBY

6 August 1991

FIGURE 43.

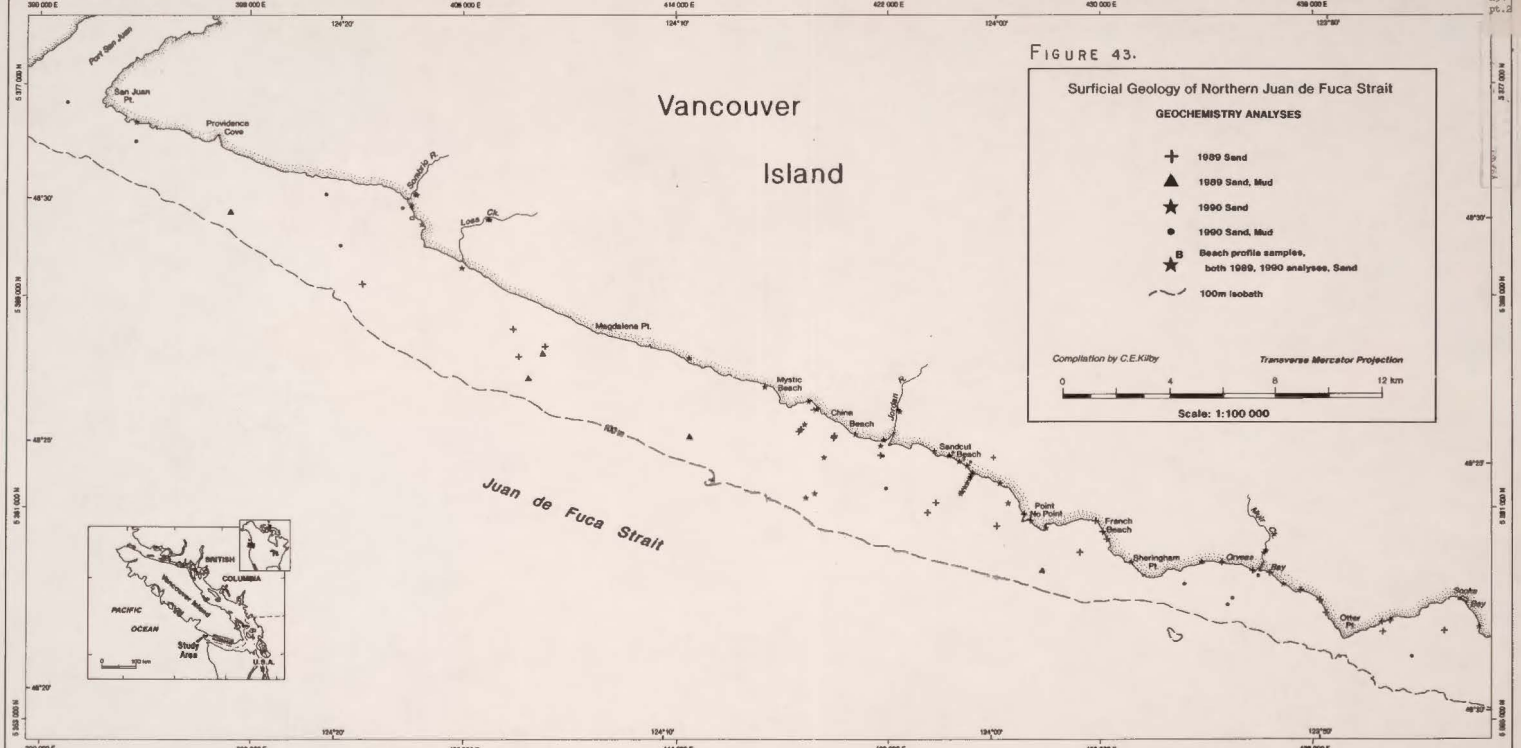

FIGURE 5.

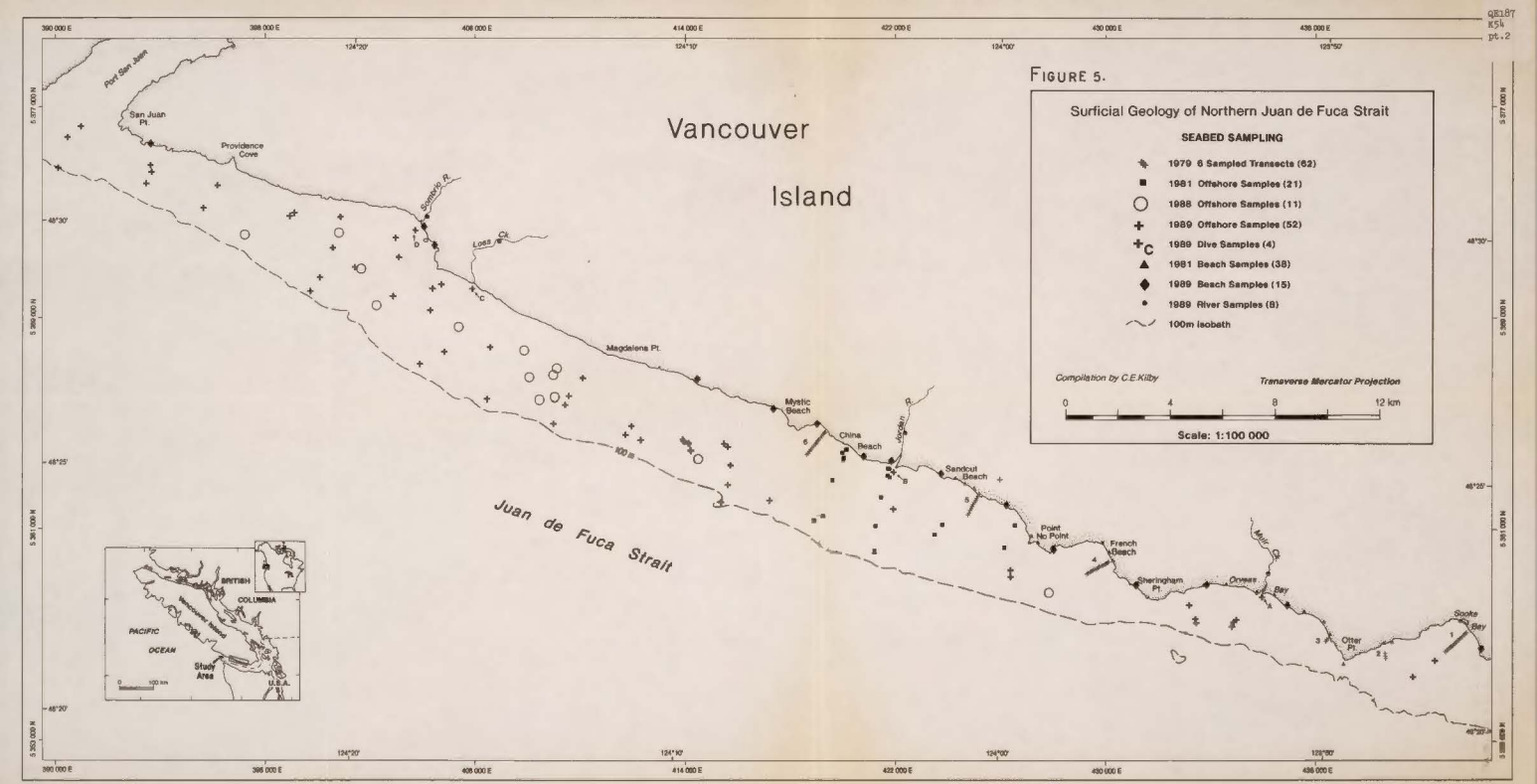

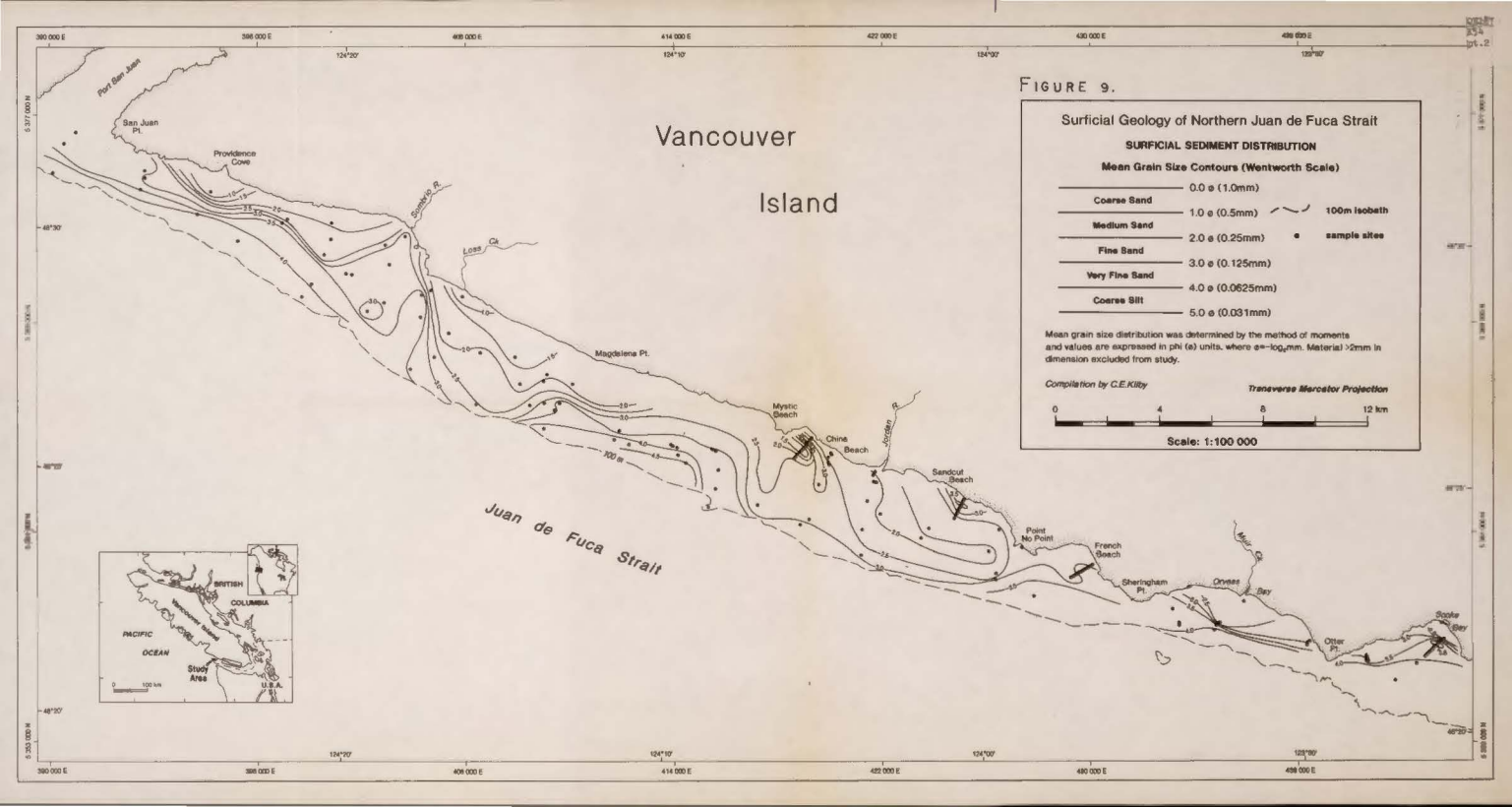
Vancouver
Island
Juan de Fuca Strait
Port San Juan
San Juan Pt.
Providence Cove
Sombrio R.
Loss Ck
Magdelena Pt.
Mystic Beach
China Beach
Jordan R.
Sandcut Beach
Point No Point
French Beach
Sheringham Pt.
Miller Ck
Orveas Bay
Otter Pt.
Stoke Bay
BRITISH COLUMBIA
PACIFIC OCEAN
Study Area
U.S.A.
Surficial Geology of Northern Juan de Fuca Strait
SURFICIAL SEDIMENT DISTRIBUTION
Mean Grain Size Contours (Wentworth Scale)
Coarse Sand
Medium Sand
Fine Sand
Very Fine Sand
Coarse Silt
0.0 ø (1.0mm)
1.0 ø (0.5mm)
2.0 ø (0.25mm)
3.0 ø (0.125mm)
4.0 ø (0.0625mm)
5.0 ø (0.031mm)
100m isobath
sample sites
Mean grain size distribution was determined by the method of moments and values are expressed in phi (ø) units, where ø=-log2mm. Material >2mm in dimension excluded from study.
Compilation by C.E.Kilby
Transverse Mercator Projection
0 4 8 12 km
Scale: 1:100 000

FIGURE 9.

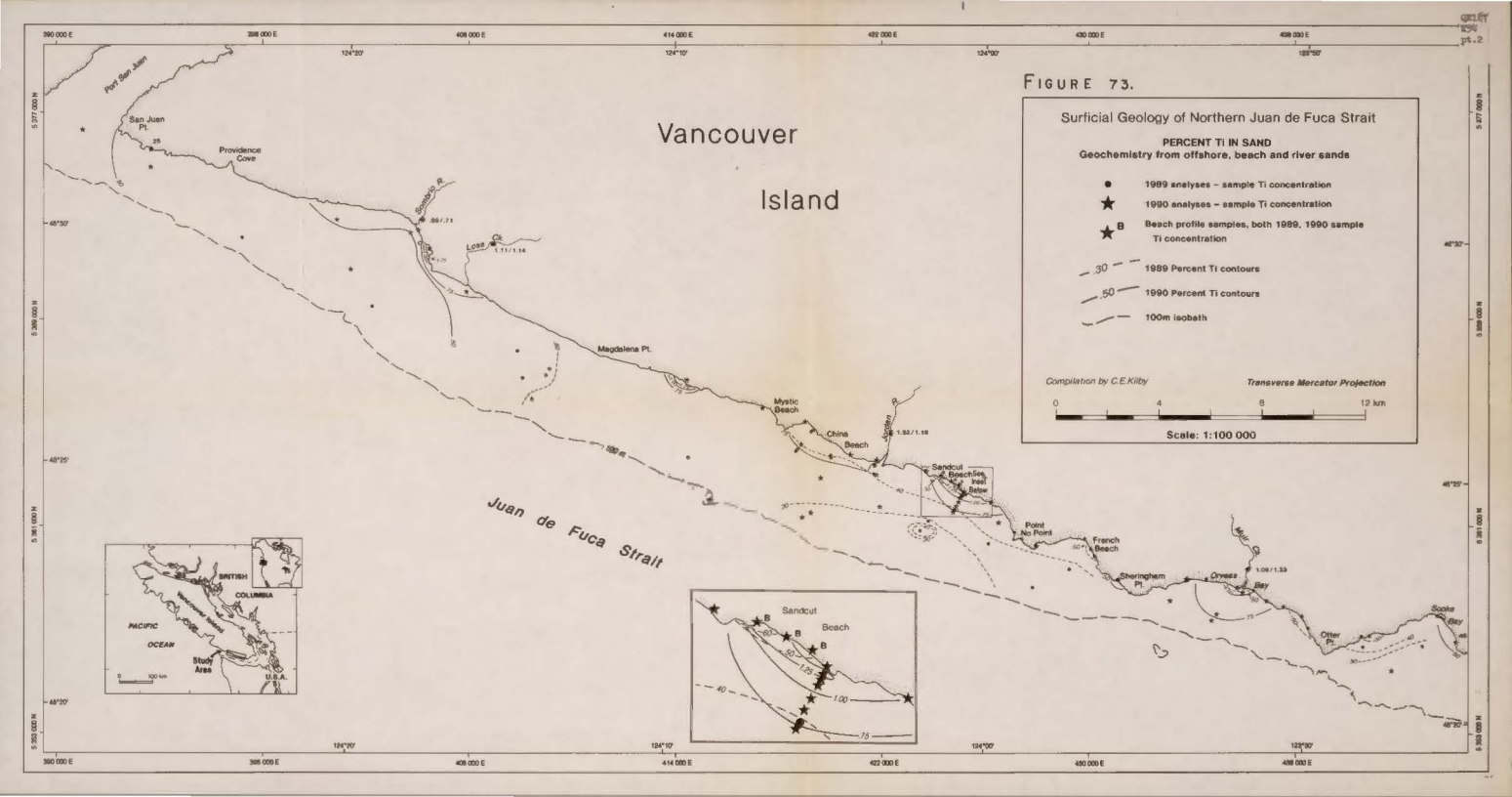
FIGURE 73.
Surficial Geology of Northern Juan de Fuca Strait
PERCENT Ti IN SAND
Geochemistry from offshore, beach and river sands
1989 analyses – sample Ti concentration
1990 analyses – sample Ti concentration
B Beach profile samples, both 1989, 1990 sample Ti concentration
30 1989 Percent Ti contours
50 1990 Percent Ti contours
100m isobath
Compilation by C.E.Kilby
Transverse Mercator Projection
0 4 8 12 km
Scale: 1:100 000
Vancouver Island
Juan de Fuca Strait
Port San Juan
San Juan Pt.
Providence Cove
Sombrio R.
Loss Cr.
Magdalena Pt.
Mystic Beach
China Beach
Jordan R.
Sandcut Beach
Point No Point
French Beach
Sheringham Pt.
Otter Pt.
Sooke Bay
Study Area
BRITISH COLUMBIA
PACIFIC OCEAN
U.S.A.
Sandcut Beach

FIGURE 18.

FIGURE 6.

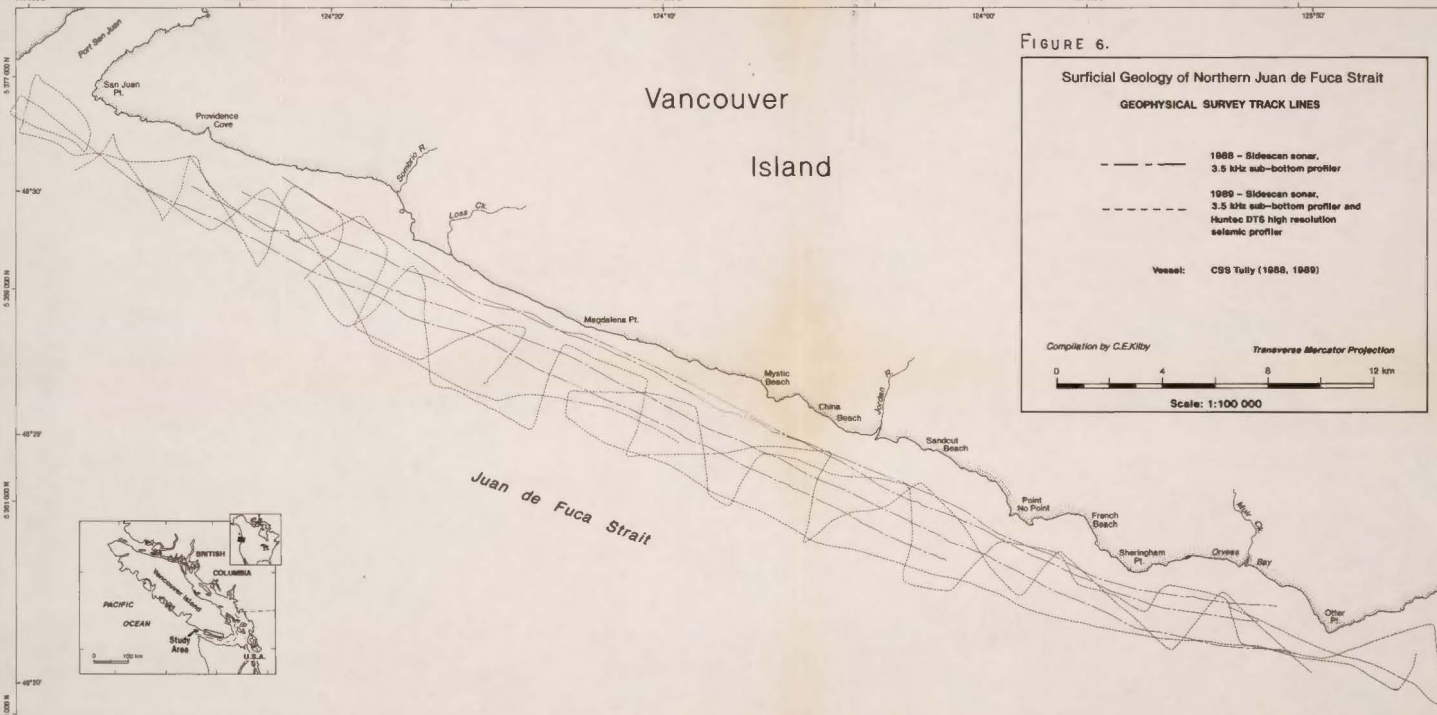

FIGURE 31.

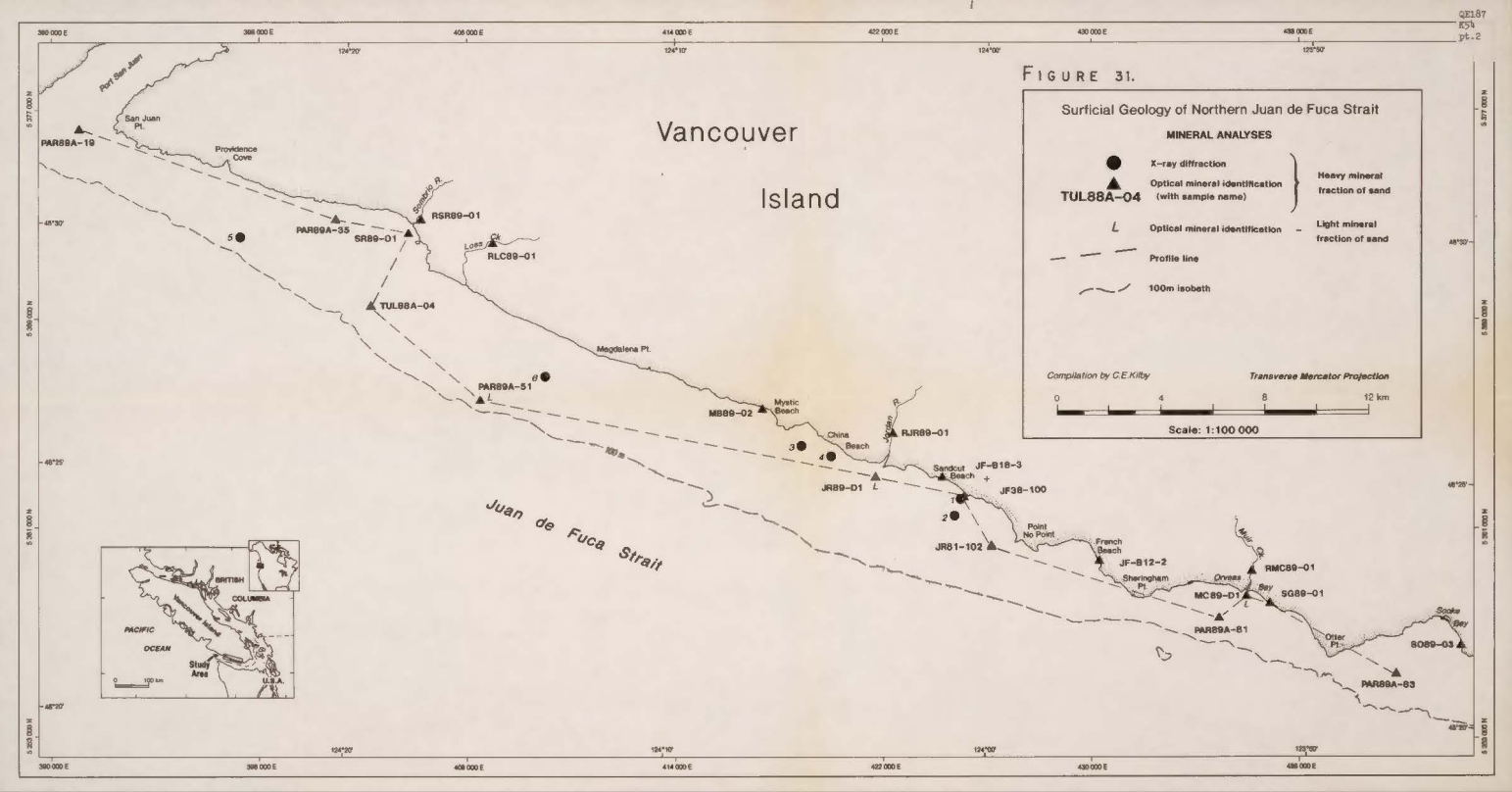

FIGURE 14.

Surficial Geology of Northern Juan de Fuca Strait

SURFICIAL SEDIMENT DISTRIBUTION

Mode Grain Size Contours (Wentworth Scale)

	0.0 ø (1.0mm)	
Coarse Sand		
	1.0 ø (0.5mm)	100m isobath
Medium Sand		
	2.0 ø (0.25mm)	sample sites
Fine Sand		
	3.0 ø (0.125mm)	
Very Fine Sand		
	4.0 ø (0.0625mm)	

Mean grain size distribution was determined by the method of moments and values are expressed in phi (ø) units, where $ø = -\log_2$ mm. Material >2mm in dimension excluded from study.

Compiled by C.E.Kilby

Transverse Mercator Projection

0 4 8 12 km

Scale: 1:100 000

FIGURE 23.

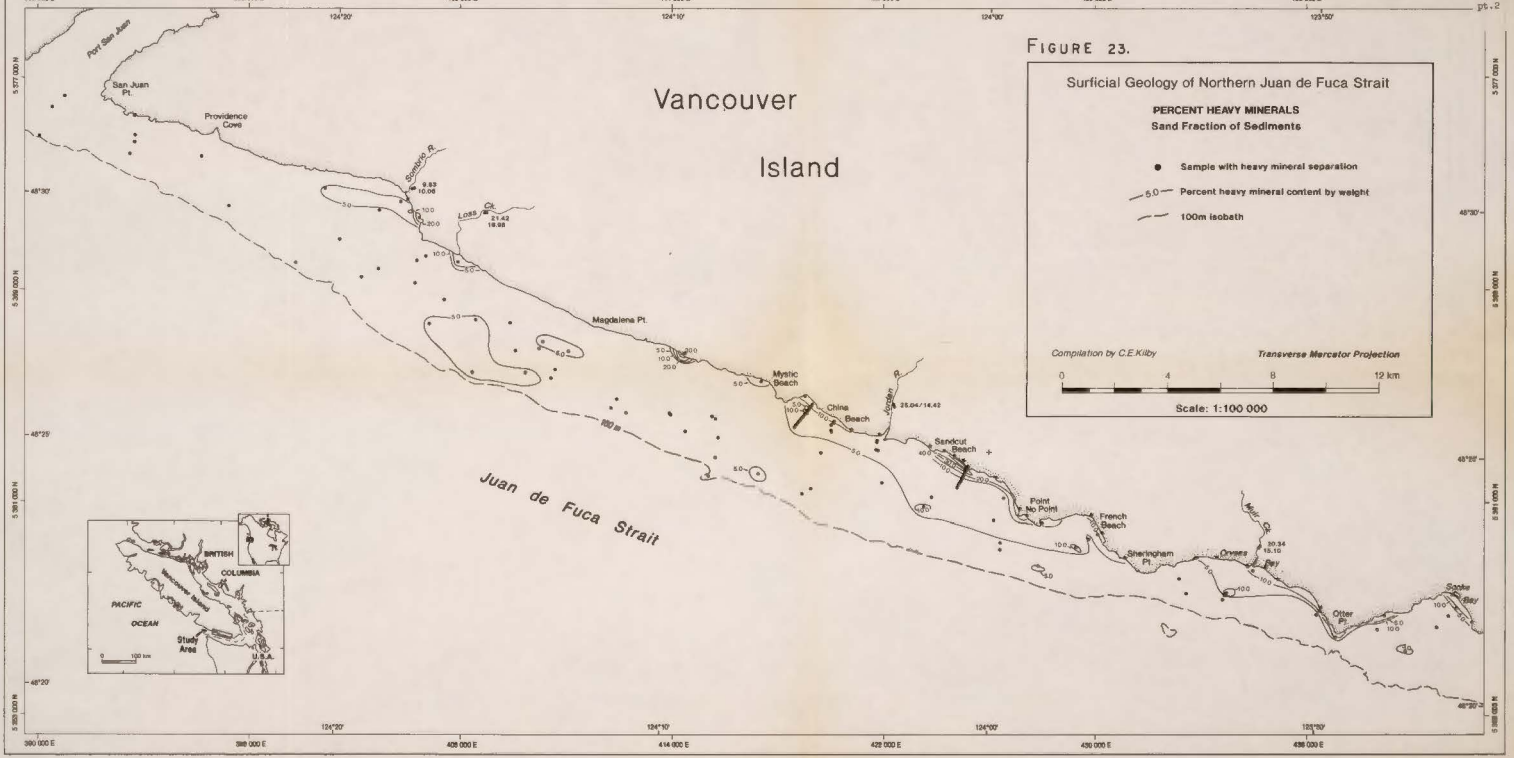

Figure 8.

Surficial Geology of Northern Juan de Fuca Strait

SURFICIAL SEDIMENT DISTRIBUTION

Grain Size Fields

Based on a Modified Folk Ternary Classification and Sidescan Sonar Coverage

Bedrock

sample site

100 m isobath

NS = no sediment

Compilation by C.E. Kilby

Transverse Mercator Projection

Scale 1:50 000


FIGURE 2.
Northern Juan de Fuca Strait
BATHYMETRY
Depth in Metres
Based on Canadian Hydrographic Service Field Sheets Nos. 1190-L and 1156-L
Compilation by C.E.Kilby
Transverse Mercator Projection
Scale 1:50 000
Vancouver Island
Port San Juan
San Juan Pt.
Providence Cove
Sombrio R.
Loss Ck
Magdalena Pt.
Mystic Beach
China Beach
Jordan R.
Sandcut Beach
Point No Point
French Beach
Sheringham Pt.
Orveas Bay
Muir Ck
Juan de Fuca Strait
100 m
BRITISH COLUMBIA
Vancouver Island
PACIFIC OCEAN
Study Area
U.S.A.
390 000 E
406 000 E
414 000 E
422 000 E
430 000 E
124°20'
124°10'
124°00'
48°30'
48°25'
48°20'
5 377 000 N
5 369 000 N
5 361 000 N
5 353 000 N

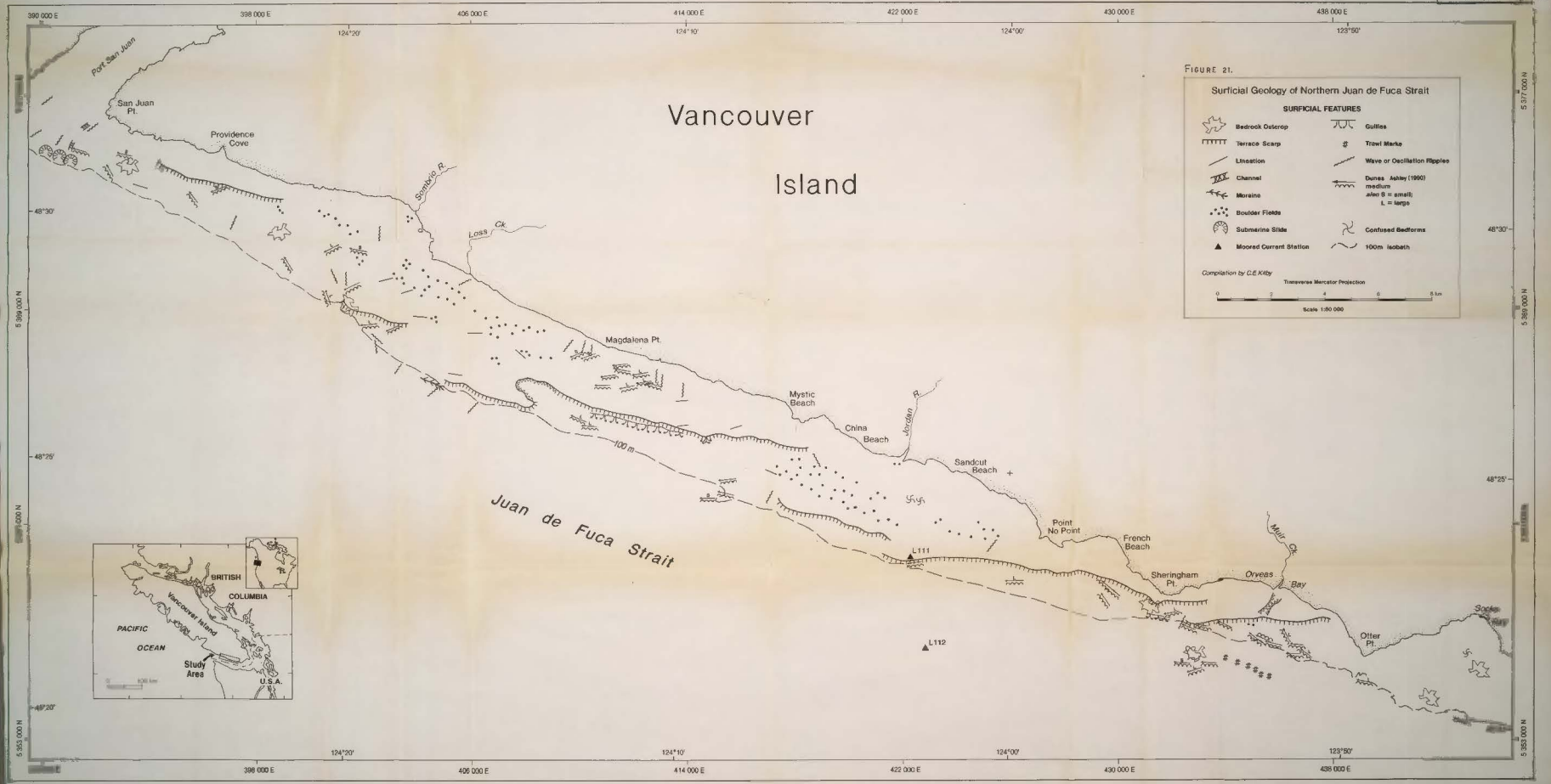

FIGURE 21.

Surficial Geology of Northern Juan de Fuca Strait

SURFICIAL FEATURES

- Bedrock Outcrop
- Terrace Scarp
- Lineation
- Channel
- Moraine
- Boulder Fields
- Submarine Slide
- Moored Current Station
- Gullies
- Trawl Marks
- Wave or Oscillation Ripples
- Dunes Ashley (1990) medium also S = small; L = large
- Confused Bedforms
- 100m Isobath

Compilation by C.E.Kilby

Transverse Mercator Projection

0 2 4 6 8 km

Scale 1:50 000